UNIVERSITAT POLITÈCNICA DE CATALUNYA

DEPARTMENT OF GEOTECHNICAL ENGINEERING AND GEO-SCIENCES

Anomalous Dynamics of Darcy Flow and Diffusion Through Heterogeneous Media

Ph.D THESIS

Supervisors:

Marco Dentz

Jesus Carrera

Anna Russian

Barcelona, 2013

Acknowledgements

This thesis was funded by the European Commission through FP7 projects ITN project, IMVUL project (Grant Agreement 212298). I had the opportunity to travel and have successful interactions with several scientists internationally.

Abstract

This thesis studies diffusion phenomena in heterogeneous media, which includes Darcy flow and diffusive solute transport in geological media. Natural media are heterogeneous at different scales, which induces complexity in diffusion phenomena. The work is centered on the integration of the effects of heterogeneity on Darcy flow and solute diffusion into large scale models. The quantification of the effects of heterogeneity in diffusion phenomena is highly important for a large number of problems such as diffusion and reaction of chemicals and radionuclides in low permeability media, which is essential in subsurface hazardous waste storage problems, CO2 sequestration performance and groundwater management. In a stochastic framework we quantify the effects of heterogeneity in large scale models considering two interrelated strategies that can be called 'coefficient approach', which deals with the derivation of effective coefficients to insert in equivalent homogeneous models, and dynamic approach', which deals with the upscaling of the local scale equations and the derivation of large scale formulations which can differ from their local counterparts. Whenever a diffusion process cannot be described in terms of effective coefficient, that behaviour is named anomalous or non-Fickian. Anomalous diffusion behaviours observed experimentally are frequently modelled by effective theories such as fractional diffusion equations, continuous time random walks. One limitation of these models is that often they are rather phenomenological and the relation to the local scale heterogeneity and dynamics may not be clear. In the dynamic approach we derive large scale descriptions that can explain anomalous behaviour and link it with a description of the local scale medium heterogeneity. To this end, we upscale the local scale governing equations using different methods depending on the type of medium heterogeneity. For moderately heterogeneous media we upscale flow equation by stochastic averaging. Starting from the classical flow equation at local scale determined by Darcy's law, we derive an upscaled non-local effective formulation. The non-local effective formulation is compared with its local counterpart by considering the head response for a pulse injection. Numerically, we solve flow and diffusion in heterogeneous media using particle tracking methods. While classical random walk particle tracking is an efficient numerical tool to solve for diffusion problems in moderately heterogeneous media, strong medium contrasts, as encountered in fractured media, render this method inefficient. For highly heterogeneous

media efficiency of classical random walk can be increased by the use of the time domain random walk (TDRW) method. We rigorously derive the equivalence of the TDRW algorithm and the diffusion equation and we extend the classical TDRW method to solve diffusion problem in a heterogeneous medium with multi-rate mass transfer properties. Moreover we use the TDRW method in connection with a stochastic model for the heterogeneity in order to upscale heterogeneous diffusion processes. For a certain class of heterogeneity, the upscaled dynamics obey a CTRW. Analytically we upscale diffusion in highly heterogeneous media by using a multicontinuum representation of the media. Using volume and ensemble averaging we derive a multicontinuum model that can explain anomalous diffusion behavior and link it with a suitable local scale description of the medium heterogeneity. Finally, we integrate the multicontinuum model derived in the context of aquifer modelling. We derive a multicontinuum catchment model that can explain anomalous behavior observed in the aquifer dynamics at basin scale. We identify the physical mechanisms that induce anomalous behaviour and we determine the time scales that control its temporal evolution.

Resumen

Esta tesis estudia fenómenos de difusión, entre los que se incluyen el flujo a la escala de Darcy y la difusión molecular de solutos, en medios geológicos. Estos medios son heterogéneos a diferentes escalas, lo que induce complejidad en el fenómeno. El trabajo se centra en la integración de los efectos de heterogeneidad en el flujo de Darcy y la difusión de solutos en modelos a gran escala. La cuantificación de los efectos de la heterogeneidad sobre los fenómenos de difusión es importante para un gran número de problemas que abarcan desde la cuantificación de la recarga de acuíferos o la interpretación de ensayos de bombeo, hasta como la difusión de sustancias químicas, necesario por ejemplo para problemas de almacenamiento de residuos en el subsuelo, o la evaluación de reacciones químicas controladas por mezcla, como las que tienen lugar en problemas de almacenamiento geológico de CO2. Adoptamos un marco estocástico para cuantificar los efectos de la heterogeneidad en los modelos a gran escala considerando dos estrategias relacionadas entre sí: la de coeficientes efectivos y la dinámica. La primera consiste en la derivación de coeficientes efectivos para insertarlos en ecuaciones equivalente a un modelo homogéneo, pero aplicadas a gran escala. En el "enfoque dinámico", se realiza el opera el cambio de escala, de manera que las formulaciones a gran escala que se derivan pueden presentar una estructura diferente a las de escala local. Cuando un proceso de difusión no puede ser descrito en términos de coeficiente efectivo, este comportamiento se denomina anómalo o no-Fickiano. Los comportamientos anómalos de difusión observados experimentalmente se modelan habitualmente usando modelos fractales o modelos de caminos aleatorios. Una de las limitaciones de estos modelos es que tradicionalmente proceden de descripciones fenomenológicas, de manera que la relación con la heterogeneidad a escala local no es clara, lo que les resta capacidad predictiva. En el enfoque dinámico derivamos descripciones a gran escala que pueden explicar el comportamiento anómalo y vincularlo con una descripción de la heterogeneidad a escala local. Para este fin, usamos diferentes métodos, dependiendo del tipo de heterogeneidad del medio. Cuando es moderada, obtenemos ecuaciones de flujo a gran escala utilizando el promedio estocástico. A partir de la ecuación de flujo clásico a escala local, obtenemos una formulación efectiva no local. La formulación eficaz, no-local, se compara con su correspondiente local. Numéricamente, se resuelve el flujo y la difusión en medios heterogéneos utilizando métodos de

caminos aleatorios de partículas. Los métodos de caminos aleatorios clásicos son métodos eficientes para medios poco heterogéneos. Para medios muy heterogeneos es más eficiente aplicar el método de caminos aleatorios en el dominio temporal (conocido por sus siglas en inglés, TDRW). En este trabajo derivamos la equivalencia entre el algoritmo del TDRW y la ecuación de difusión y extendemos el método clásico del TDRW para resolver la difusión en un medio heterogéneo con mecanismos complejos de atrape múltiple. Además, utilizamos el método TDRW para obtener una formulación a gran escala. Para una determinada clase de heterogeneidad, la dinámica observada a larga escala se puede describir con un CTRW. Analíticamente derivamos la formulacion a gran escala para la difusión en muy heterogéneos mediante una representación multicontinua de los medios. Aplicando el promedio espacial y el promedio conjunto (entre realizaciones estocásticas) derivamos un modelo multicontinuo que explica el comportamiento anómalo de difusión y lo vincula con heterogeneidad local del medio. Por último, integramos el modelo multicontinuo en el contexto de la modelación de acuíferos. Derivamos un modelo de acuífero que explica el comportamiento anómalo observado en la dinámica a escala de cuenca. Se identifican los mecanismos físicos que inducen comportamiento anómalo y se determinan las escalas de tiempo que lo controlan.

Contents

Chapter 1

Introduction

This thesis studies diffusion phenomena in heterogeneous media. It comprises the understanding and quantification of Darcy flow in heterogeneous aquifer and diffusion of a solute in low permeability media.

Darcy's law has been derived empirically from experimental observation and it states that the water flux is linearly proportional to the head loss through the hydraulic conductivity. Diffusion of a solute is described by Fick's law. For the Fick's law the diffusive flux is related to the gradient of the concentration by the diffusion coefficient. Mathematically, both Darcy's law and Fick's law are equivalent to the Fourier's law, which, as first, states that the flux is linearly proportional to a potential loss [*Fourier*, 1822; *Carslaw and Jaeger*, 1947]. At the same epoch, formally equivalent formulations have been discovered in electricity, with Ohm's law, that relates electricity current to the gradient of electrical potential through electrical conductivity and for the elasticity, with the Hooke's law that relates mechanical stress to the gradient of displacements through the elasticity modulus [*Sanchez-Villa et al.*, 2006].

The different physical phenomena differ in the range of variability of the parameters that control the flux in function of the potential loss such as thermal or hydraulic conductivity, elasticity modulus, for example. Thermal conductivity varies at most by one or two orders of magnitude in different materials, while hydraulic conductivity can vary by orders of magnitude even in apparently homogeneous media [*Warren and Root*, 1963].

The quantification of the effects of heterogeneity in diffusion phenomena is fundamental for a large number of problems such as diffusion and reaction of chemicals and radionuclides in low permeability media, which is essential in subsurface hazardous waste storage problems, [*Wittebroodt et al.*, 2008], efficient management of groundwater resources, control of seawater

intrusion [*Diersch and Kolditz*, 2002], contamination problems for predicting situations related to water quality [*Duffy and Lee*, 1992], risk assessment, or CO_2 sequestration performance [*Metz et al.*, 2005]. Importance of diffusion in heterogeneous low conductivity material has been further investigated in relation to transport in highly heterogeneous media such as fracture formations that are characterized by diffusion of solutes in low permeability regions [*Warren and Root*, 1963; *Carrera et al.*, 1998; *Dykhne et al.*, 2005; *Gouze et al.*, 2008a].

Geological materials are highly heterogeneous in terms of physical and chemical properties, which occur at different scales, as illustrated in Figure 1.1. Figure 1.1 illustrates from left to right, images of heterogeneous media characterized by heterogeneity ranging from kilometer scale, to micron scale. Heterogeneity induces complexity and for this reasons, it is

Figure 1.1: *Example of heterogeneity at different scale. From the left: fracture granite formation at km scale, fracture granite formation at m scale, sample of granite at cm scale, X-ray microtomography of Majorca limestone (Courtesy of Philippe Gouze, CNRS Montpellier).*

fundamental to integrate the impact of heterogeneity into large scale models.

The spatially variable nature of hydraulic parameters and diffusive parameters in heterogeneous media has lead to the use of stochastic approaches to quantify their impact on the large scale behavior. Stochastic modeling is used as a tool to describe and quantify in a systematic manner the impact of spatial variability observed at small scales into an effective large scale behaviour, plus a way to compute the uncertainty associated with a given prediction [*Freeze*, 1975]. In a stochastic framework an heterogeneous medium is seen as a realization of an ensemble of all possible medium realizations with the same statistical properties and the spatially varying parameters are modeled as stochastic random fields. The large scale properties are derived by averaging the local scale properties over the ensemble of all medium realizations [*Gutjahr et al.*, 1978].

The systematic investigation of the impact of spatial heterogeneity on large scale behaviour can be addressed by two interrelated strategies, which can be called coefficients approach and dynamic approach. The coefficient approach quantifies the effect of heterogeneity in terms of effective coefficients such as effective hydraulic coefficients for flow and effective diffusivity for diffusion. The behavior on larger scales is described by equivalent homogeneous models

with large-scale parameters. The dynamics approach deals with the upscaling of the local scale equations and the derivation of large scale equation which may be different from the local scale description.

Traditionally, the coefficient approach has been used to characterize the heterogeneity impact on the large scale behavior in terms of effective parameters, such as effective hydraulic conductivities [*Sanchez-Villa et al.*, 2006] for flow and effective diffusivities for solute diffusion [*Pabitra*, 2004; *Dean et al.*, 2007]. The evaluation of an effective hydraulic conductivity has been subject of numerous studies since the 1960s, when Matheron found that the effective conductivity is bounded by the arithmetic mean K_A and the harmonic mean K_H of the point values conductivities [*Matheron*, 1967]. Matheron derived that in $d = 1$ dimension the effective conductivity is given by the harmonic mean of the point values conductivities, for $d = 2$ dimension by the geometric mean and for $d = 3$ he conjectured that the effective conductivity is given by: $K_G e^{\sigma^2/6}$ where K_G represents the geometric average of the local conductivities, σ^2 is the variance of the natural logarithm of the conductivity field [*Matheron*, 1967]. The first compact expression for the effective conductivity K_{eff} in stationary isotropic conductivity field for any d dimensional media has been [*Gutjahr et al.*, 1978]: $K_{eff} = K_G \left[1 + \left(\frac{1}{2} - \frac{1}{d}\right)\sigma^2\right]$. This dependency on the spatial dimension can be physically understood by the fact that as the number of space dimensions increases, the flow avoids more easily the low permeability regions, and thus the medium is more conductive. Exhaustive reviews of the results obtained for the effective conductivity since the studies of Matheron, are given in *Renard and de Marsily* [1997] and *Sanchez-Villa et al.* [2006]. In the literature, the problem of flow in heterogeneous media has been addressed principally with the effective coefficient approach, while the problem of solute diffusion has been addressed frequently in terms of effective coefficients [*Pabitra*, 2004; *Dean et al.*, 2007] as well as in terms of modified dynamic equations such as fractional diffusion equations and continuous time random walks [*Metzler and Klafter*, 2000]. One of the shortcomings of such effective theories is that often they are rather phenomenological and the relation to the local scale heterogeneity and dynamics may not be clear.

In fact, experimental and theoretical observations demonstrated that large scale descriptions in terms of effective coefficient could be not enough to the catch the complexity of Darcy flow and solute diffusion in heterogeneous media. Theoretically, the general applicability of an effective hydraulic conductivity in the flow equation is put in discussion by the work of *Indelman and Rubin* [1996] and successively by *Tartakovsky and Neuman* [1998a], who derived a non-local effective equation both in time and space. Anomalous diffusion dynamic in disor-

dered media has been widely discussed in [*Bouchaud and Georges*, 1990; *Carrera*, 1993; *Havlin and Ben-Avraham*, 2002a; *Dykhne et al.*, 2005; *Dvoretskaya and Kondratenko*, 2009]. Experimentally, it has been shown that the coefficient approach is not sufficient to model many observed phenomena. For flow, the temporal evolution of the hydraulic head at a fixed position is termed drawdown. Pumping test in heterogeneous media have evidenced that heterogeneity causes tailing in drawdown curves and scale dependence in diffusion parameters [*Sanchez Vila et al.*, 1996; *Schulze-Makuch, D., Douglas, A. Carlson, Douglas, S. Cherkauer, Malik*, 1999; *Rovey and Cherkauer*, 1995]. Tailing is defined as late time behaviour in the drawdown curves that can not be reproduced by the classical models. Pumping tests conducted in natural media often produce anomalous drawdown curves. For a homogeneous medium, the late time slope of the drawdown curve should evolve as $t^{-\beta}$, with $\beta = 1 - d/2$, and d the Euclidean dimension of the flow problem. However the experimental evidences suggest flow dimensions smaller than 2 in planar aquifers or less than 3 in apparently $d = 3$ dimensional fields [*Le Borgne*, 2004; *Le Borgne and Gouze*, 2008]. Similarly, tracer tests in strongly heterogeneous media, have evidenced tailing in breakthrough curves [*Cortis*, 2004; *Le Borgne and Gouze*, 2008; *Gouze et al.*, 2008a; *Willmann et al.*, 2008], and scale dependency in diffusion parameters for advection-diffusion problems [*Neuman*, 1990; *Gelhar et al.*, 1992]. These kind of behaviors may be traced back to diffusion in low-permeability medium subregions that lead to solute retardation. Thus, for the understanding of such phenomena it is necessary to quantify diffusion phenomena in heterogeneous media [*Gouze et al.*, 2008a]. Furthermore, the quantification of anomalous diffusion-limited reaction rates in heterogeneous environments depends on the quantification of the first arrival times of a reactant at a target [*Condamin et al.*, 2007].

Anomalous drawdown has been modeled by fractional [*Barker*, 1988; *Acuna and Yortsos*, 1995] and multi-fractional [*de Dreuzy et al.*, 2010, 2004; *Lods and Gouze*, 2008] flow models. One limit of this kind of models is the importance of the choice of fractal dimension d, which is not directly related to the spatial organization of hydraulic parameters and it can vary depending on type of field test performed and on the boundary and initial conditions (e.g. [*Little and Bloomfield*, 2010; *Zhang*, 2004]). For these reasons interpretation of multi-fractal models is rather difficult [*Tessier et al.*, 1996] and their utility in predictability is limited [*Labat et al.*, 2002].

Anomalous (non-Fickian) diffusion has been successfully modeled by CTRW model e.g. [*Metzler and Klafter*, 2000; *Cortis*, 2004; *Berkowitz et al.*, 2006; *Sanchez-Villa et al.*, 2006; *Gouze et al.*, 2008b], multi rate mass transfer (MRMT) models e.g. [*Harvey and Gorelick*, 1995; *Carrera et al.*,

1998; *Haggerty and Gorelick*, 1995; *Lods*, 2004] and delayed diffusion models [*Dentz and Tartakovsky*, 2006]. The equivalence between CTRW models and MRMT models has been demonstrated by *Dentz and Berkowitz* [2003]. MRMT model and time-fractional model (e.g. [*Schumer*, 2003]) can be seen as particular cases of CTRW [*Dentz and Tartakovsky*, 2006]. These model attribute the anomalous behavior phenomenologically to a distribution of typical transport time scales (residence time distribution for MRMT, and waiting time distribution in CTRW) that are due to subscale medium heterogeneity.

Tailing in drawdown and breakthrough curves is ubiquitous phenomenon for Darcy flow and diffusion in heterogeneous media and its ubiquity suggests that tailing must reflect something of a fundamental nature [*Willmann et al.*, 2008]. The challenge consists in linking the large scale effective description with the local scale physical processes and heterogeneity distribution.

In this thesis we investigate flow and diffusion in heterogeneous media, considering both the coefficient and the dynamic approach. We use different upscaling methods in order to link the anomalous behaviour with a description of the heterogeneity.

In the second chapter we upscale flow in heterogeneous media in a stochastic approach. In a stochastic approach we model spatially variable conductivity as a random function. Starting from a local scale description we use stochastic averaging to derive an upscaled flow formulation in terms of effective parameters and equations.

In this context, perturbation theory in the fluctuations of hydraulic conductivity has frequently been used to compute effective parameters in heterogeneous media [*Drummond and Hogan*, 1987; *Dagan*, 1993; *Renard and de Marsily*, 1997; *Kitanidis*, 1990; *Keller*, 2001; *Neuweiler et al.*, 2001; *Teodorovich*, 2002]. *Gutjahr et al.* [1978] proposed a compact expression for effective hydraulic conductivity in d spatial dimensions that has been tested rigorously by Dagan using small perturbations up to order σ^4 [*Dagan*, 1993], with σ^2 the variance of the hydraulic conductivity fluctuations. Also non-perturbative methods such as selfconsistent resummations and renomalization theory have been used to determine the effective coefficients [*Dean et al.*, 2007]. Although a lot of attention has been dedicated to the study of effective parameters through perturbation theory, most of the work has been done for steady state. The transient problem, has been firstly addressed by *Alonso and Krizek* [1974] and *Freeze* [1975] for $d = 1$ dimensional flow and with a negligible correlation distance.

In the dynamic approach, *Indelman and Abramovich* [1994] and successively *Tartakovsky and Neuman* [1998b] upscaled local flow equation using ensemble average and derived non-local

formulations for $d = 1$ and $d = 3$ dimensional media. We extend the work of *Tartakovsky and Neuman* [1998a] by deriving upscaled non-local equations for any d spatial dimension in a compact formulation. Moreover, we derive jointly large scale coefficients and upscaled equations and we discuss the diffusion behaviour for a pulse injection comparing the local and the non-local formulation. By localization of the non-local formulations, we obtain time dependent effective coefficients, which asymptotically tend to the well known values for effective conductivity [*Sanchez-Villa et al.*, 2006].

The results in Chapter 2 are valid for moderately heterogeneous media. Geological media, such as fractured formations, however, may be highly heterogeneous. Thus, the results obtained in Chapter 2 are only of limited applicability. Strong medium heterogeneous represent a problem both for analytical as well as numerical solution methods. While classical random walk particle tracking is an efficient numerical tool to solve for diffusion problems in heterogeneous media, strong medium contrasts, as encountered in fractured and composite media, render this method inefficient. Chapter 3 is dedicated to diffusion in strongly heterogeneous and pixelized media from a random walk perspective. As pointed out above, highly heterogeneous media and sharp interfaces in the distribution of heterogeneity make the use of classical RW methods inefficient [*McCarthy*, 1993; *Delay et al.*, 2005]. Classical RW method can be very costly because it may require a fine time-discretization in order to ensure that a particle, in its random trajectory, samples all the heterogeneity [*Delay et al.*, 2002]. *McCarthy* [1993] pointed out that classical RW could be very inefficient because particles can spend a lot of computational time moving in low diffusivity zones. Efficiency of classical random walk can be increased by the use of the time domain random walk (TDRW) method to solve diffusion in disordered media. TDRW method was first introduced by McCarthy [*McCarthy*, 1993], used by Banton for simulating non-reactive solute transport in $d = 1$ dimensional porous media [*Banton et al.*, 1997], by Noetinger for the upscaling of fluid flow in fracture rocks [*Noetinger and Estebenet*, 2000] and further developed by Delay and Bodin [*Delay et al.*, 2002; *Reimus and James*, 2002; *Bodin et al.*, 2003; *Delay et al.*, 2005]. The TDRW method is closely related to the CTRW [*Dentz and Berkowitz*, 2003]. Strictly speaking CTRW describes particles movement as a random walk in space and in time [*Dentz and Tartakovsky*, 2006]. As we said before, CTRW has been successfully used to model anomalous, non-Fickian, transport in geological formations [*Berkowitz et al.*, 2006; *Cortis*, 2004; *Gouze et al.*, 2008b] and even transient flow problem [*Cortis and Knudby*, 2006]. The equivalence between large scale averaging theory and the CTRW has been object of the work of *Noetinger, B.Estebenet and Quintard* [2001].

In literature we have not found a rigorous derivation of the equivalence between the TDRW and the flow equation. This however is necessary to adapt the TDRW approach to more complex transport scenarios that include advection, reaction and trapping mechanisms. In the first part of Chapter 3 we present a rigorous derivation of the TDRW algorithm demonstrating its equivalence with the diffusion equation and showing that TDRW is a particular case of a CTRW, or rather an inhomogeneous CTRW. Moreover we extend the TDRW method to solve diffusion problem in a heterogeneous medium with multi-rate mass transfer properties using a statistical representation of the medium.

In the second part of Chapter 3 we use the TDRW method in connection with a stochastic model for the heterogeneity in order to upscale heterogeneous diffusion processes. For a certain class of heterogeneity, the upscaled dynamics obey a CTRW.

In Chapter 3, we studied an efficient random walk method to quantify diffusion processes in heterogeneous media. Chapter 4 considers a multicontinuum representation of a highly heterogeneous medium, in order to derive the equations that govern large diffusion phenomena. Using volume and ensemble averaging we derive a multicontinuum model that can explain anomalous diffusion behavior and link it with a suitable local scale description of the medium heterogeneity.

Double and multi permeability/porosity model have been used in hydrology since the pioneering 'double-porosity' model of *Barenblatt et al.* [1960]. The double porosity of Barenblatt and the large number of double-permeability/porosity models have been developed successively (e.g. [*Warren and Root*, 1963; *Dykhuizen*, 1987; *Peters and Klavetter*, 1988; *Dykhuizen*, 1990; *Bai et al.*, 1993]) represent the medium as an overlapping of two regions characterized by strongly different diffusion parameters, that are thus called as 'mobile' and 'immobile' regions. The mobile and immobile continua exchange solute mass by linear mass transfer. These models assume that the mobile and immobile zones are in quasi-equilibrium and mass transfer is modeled as a first order process. Contrary to the above mentioned models, we consider non-equilibrium in the immobile zone and we derive a multicontinuum model which can explain anomalous pre-asymptotic and asymptotic behaviour and link the anomalous scaling with a description of heterogeneity.

In the last chapter we focus on the problem of modeling the dynamic of an aquifer at basin scale. The dynamic response of a catchment to any recharge process is highly important for groundwater management. Modeling aquifer dynamic is a challenging problem due to the variety of physical processes involved and the limited information available on hydraulic

parameters, aquifer properties and geometry [*Scanlon et al.*, 2002]. Classical recharge models, as the linear reservoir model and the linear Dupuit model, assume that the aquifer is homogeneous [*Gelhar*, 1974]. Aquifers are in general spatial heterogeneous, which gives rise to a distribution of residence times in the system [*Fiori et al.*, 2009], and thus to a behavior that cannot be captured by the classical aquifer. In fact, experimental studies on time series of hydrological records have evidenced that classical models cannot explain some behaviors observed in the aquifer discharge and head responses to recharge [e.g., *Zhang and Yang*, 2010; *Labat et al.*, 2002; *Zhang*, 2004; *Molenat et al.*, 1999, 2000; *Jiménez-Martínez et al.*, 2012].

Anomalous behavior is frequently modeled with multi-fractal approaches [e.g., *Turcotte and Greene*, 1993; *Tessier et al.*, 1996; *Kantelhardt et al.*, 2003; *Labat et al.*, 2011]. A limitation of these models is that the fractal dimension is not directly linked to the spatial organization of the aquifer, and it can vary depending on the experimental conditions used to determine it [e.g., *Little and Bloomfield*, 2010]. Thus, in Chapter 5, we account for spatial the heterogeneity of the aquifer by modeling the catchment as a multicontinuum medium. We use the theory developed in Chapter 4 to derive a multicontinuum catchment model which can explain anomalous behavior and which can, in principle, be parametrized by a suitable description of the local scale medium heterogeneity.

Chapter 2

Averaged Flow Equation

2.1 Introduction

Flow in heterogeneous media is qualitative and quantitatively different from flow in homogeneous media [*Indelman and Rubin*, 1996; *Noetinger, B.Estebenet and Quintard*, 2001; *Keller*, 2001]. The systematic investigation of the impact of spatial heterogeneity on the effective behavior of flow can be addressed by two interrelated strategies, which can be called coefficients approach and dynamic approach. The coefficient approach quantifies flow in terms of effective coefficients such as effective hydraulic coefficients to insert in the classical flow equation. Effective hydraulic conductivity is commonly requested by numerical models, widely used in groundwater management, as single effective parameter to consider in the flow equation and model flow in any d dimensional heterogeneous media. The dynamics approach deals with the up-scaling of the local scale equation in heterogeneous media. Stochastic average provides a systematic way to quantify the impact of heterogeneity on flow through heterogeneous media and the derived effective equation is linked to a statistical description of heterogeneity. In this chapter we use stochastic methods to determine effective flow coefficient and to obtain an effective upscaled equation for flow in heterogeneous media characterized by spatially varying hydraulic conductivity. Within a stochastic approach, a spatially varying hydraulic conductivity in a heterogeneous medium is assumed to be one realization chosen from an ensemble of conductivity fields. Here we model variable hydraulic conductivity as random function and the mean behaviour for the hydraulic head, also modeled as a random function, is obtained considering ensemble average. Starting from a local problem we derive effective equation that is non local both in time and in space. Non locality implies that a description of flow in heterogeneous media in terms of effective coefficient could be not enough to catch

the effects of the heterogeneity on the head response. It is well known that averaging flow in heterogeneous media leads to a non-local equation. The challenge consists in linking the effective equation and a description of heterogeneity. We use a formalism similar to that of *Indelman and Rubin* [1996] or *Tartakovsky and Neuman* [1998b], who derived non-local effective flow equation in time and space, using ensemble averaging. The non local nature of flow in heterogeneous media has been highlighted by *Hu and Cushman* [1994] who consider non locality of Darcy's law for unsaturated flow. Differently from the previous works, we solve the effective non-local equation for $d = 1, 2$ and 3 spatial dimension in Laplace space and we discuss the head response for a pulse injection comparing the non-local formulations and the classical one. *Tartakovsky and Neuman* [1998b] noticed that the effect of non-locality is more pronounced in one dimension that in three, but didn't give an explanation to the observation. Here we investigate this aspect and we explain why the effect of non-locality decreases as the dimensionality of the problem increases. By localization we derive effective coefficients from the non-local formulations, which asymptotically tend to the well known values of effective conductivity in heterogeneous media. Thus we demonstrate that effective conductivity computed in terms of spatial moments for a pulse injection in an infinitive medium is equivalent to the effective conductivity classically defined for a constant head gradient in a bounded domain.

2.2 Stochastic Average

2.2.1 Stochastic Model

We consider flow in heterogeneous media characterized by spatially varying hydraulic conductivity. Considering that specific storativity $s(\mathbf{x})$ is usually less variable that hydraulic conductivity $K(\mathbf{x})$, e.g. *Indelman and Rubin* [1996], for simplicity we take $s(\mathbf{x}) = s$ constant and we set it equal to unity. In this case the flow equation can be written as:

$$\frac{\partial h(\mathbf{x}, t)}{\partial t} - \nabla \cdot [K(\mathbf{x}) \nabla h(\mathbf{x}, t)] = 0 \tag{2.1}$$

where $\mathbf{x} = (x_1, ..., x_d)^T$ with d spatial dimension. In a stochastic framework the spatially varying hydraulic conductivity is modeled as a spatial random field. On the base of geostatistical studies hydraulic conductivity is frequently considered lognormal distributed [*Law*, 1944]. Log-normal model implies a smooth distribution of conductivities about the mean value and

avoids the unphysical situation of negative conductivity. Here we model $K(\mathbf{x})$ as a multi log-normal stationary random function with isotropic correlation function. We express $K(\mathbf{x})$ in term of the log-hydraulic conductivity $f(\mathbf{x})$:

$$K(\mathbf{x}) = e^{f(\mathbf{x})} \tag{2.2}$$

where $f(\mathbf{x})$ is a multi-Gaussian random field. We decompose the random variable $f(\mathbf{x})$ and $K(\mathbf{x})$ into their ensemble values $\overline{f}$, $\overline{K}$ and randomly fluctuation parts $f'(\mathbf{x}) = f(\mathbf{x}) - \overline{f}$ and $K'(\mathbf{x}) = K(\mathbf{x}) - \overline{K}$, whose mean are zero by definition. The overbar in the following denotes the ensemble average or rather the average over all the realization of the random field. Notice that the mean conductivity $\overline{K}$ does not depend on $\mathbf{x}$ because of stationarity of the random field. The fluctuating part of the log-conductivity is described by the following multivariate joint distribution:

$$p[f'(\mathbf{x}_1), ..., f'(\mathbf{x}_N)] = \frac{e^{-\frac{1}{2}\sum_{i,j=1}^{N} f'(\mathbf{x}_i)\, \mathbf{C}_f'^{-1}(\mathbf{x}_i - \mathbf{x}_j)\, f'(\mathbf{x}_j)}}{\sqrt{(2\pi)^N \det \mathbf{C}_f'}}. \tag{2.3}$$

with $\mathbf{C_f}$ is the covariance matrix and N the number of spatial positions considered in random field. Considering (2.2) hydraulic conductivity can be expressed in terms of the fluctuations $f'(\mathbf{x})$ as:

$$K(\mathbf{x}) = K_G\, e^{f'(\mathbf{x})} \tag{2.4}$$

where $K_G = e^{\overline{f}}$ is the geometric mean of $K(\mathbf{x})$. The ensemble mean $\overline{K}$ is given by:

$$\overline{K} = K_G\, e^{\sigma^2/2} \tag{2.5}$$

where σ^2 is the variance of the random variable $f(\mathbf{x})$ that, as said before, we chose Gaussian distributed. Considering (2.5) the deviation $K'(\mathbf{x})$ from the averaged $\overline{K}$, can be approximated as:

$$K'(\mathbf{x}) \simeq K_G \left[f'(\mathbf{x}) - \frac{\sigma^2}{2} \right]. \tag{2.6}$$

Therefore, up to order σ^2, the covariance function of the fluctuating part of the hydraulic conductivity $C(\mathbf{x} - \mathbf{x}') = \overline{K'(\mathbf{x})K'(\mathbf{x}')}$ can be approximated in function of $C_f(\mathbf{x} - \mathbf{x}') = \overline{f'(\mathbf{x})f'(\mathbf{x}')}$ by:

$$C(\mathbf{x} - \mathbf{x}') \simeq K_G^2\, C_f(\mathbf{x} - \mathbf{x}'). \tag{2.7}$$

Note that the translational invariance of the random field implies that the correlation of the fluctuation around the mean value of K at two points depends only on their distance. Considering that $f'(\mathbf{x})$ is multi Gaussian, stochastically, it is fully characterized by its correlation function. In the following we consider a Gaussian correlation structure for $f'(\mathbf{x})$. Consequently the covariance function for $K'(\mathbf{x})$ reads:

$$C(\mathbf{x}-\mathbf{x}') \simeq K_G^2\,\sigma^2 e^{-\sum_{i=1}^{d}(x_i-x_i')^2/(2l_i^2)} \tag{2.8}$$

where l_i, $i = 1,..d$ is the correlation length of the random field $f'(\mathbf{x})$. The correlation length denotes the typical scale of the spatial fluctuations of the medium. Correlation of $f'(\mathbf{x})$ drop to zero exponentially fast on length scale larger than l. For simplicity we choose l_i invariant for any directions $l_i = l$.

Notice that the stochasticity of $K(\mathbf{x})$ is mapped on $h(\mathbf{x},t)$ by the flow equation (2.1). We decompose the hydraulic head in its ensemble mean and a randomly fluctuating part $h(\mathbf{x},t) = \overline{h}(\mathbf{x},t) + h'(\mathbf{x},t)$, the same as we did with the hydraulic conductivity. The aim is to find an effective equation for $\overline{h}(\mathbf{x},t)$, which represents the mean behaviour of the hydraulic head in an heterogeneous medium.

2.2.2 Averaged Flow Equation

In this section we upscale flow in heterogeneous media characterized by a spatially varying hydraulic conductivity with a stochastic approach and we obtain an effective non-local formulation for the mean behaviour of the hydraulic head in a heterogeneous medium. As discussed above, we model hydraulic conductivity and hydraulic head as multivariate random fields and we decompose them into their ensemble values, $\overline{K}(\mathbf{x})$ and $\overline{h}(\mathbf{x},t)$ plus random fluctuations about their ensemble values, $K'(\mathbf{x}) = K(\mathbf{x}) - \overline{K}$ and $h'(\mathbf{x},t) = \overline{h}(\mathbf{x},t) - \overline{h}(\mathbf{x},t)$, whose means are zero by definition. Note that the ensemble value of hydraulic conductivity is constant in space because we consider $K(\mathbf{x})$ as a stationary random field. Here the objective is to find an effective equation for the expected value of the hydraulic head $\overline{h}(\mathbf{x},t)$, that represents the mean behaviour of the hydraulic head taking into account the random conductivity field $K(\mathbf{x})$. We consider the unknown random variables:

$$\begin{aligned} h(\mathbf{x},t) &= \overline{h}(\mathbf{x},t) + h'(\mathbf{x},t), & \overline{h'(\mathbf{x},t)} &= 0 \\ K(\mathbf{x}) &= \overline{K} + K'(\mathbf{x}), & \overline{K'(\mathbf{x})} &= 0 \end{aligned} \tag{2.9}$$

and we substitute them into the flow equation (2.1):

$$\left[\frac{\partial \overline{h}}{\partial t} + \frac{\partial h'}{\partial t}\right] = \nabla \cdot \overline{K}\ \nabla \overline{h} + \nabla \cdot \overline{K}\ \nabla h' + \nabla \cdot K'\ \nabla \overline{h} + \nabla \cdot K'\ \nabla h' \tag{2.10}$$

that we average stochastically. Considering that the expected value of the fluctuating terms are zero, we get:

$$\frac{\partial \overline{h}}{\partial t} = \nabla \cdot \overline{K}\ \nabla \overline{h} + \overline{\nabla \cdot K'\ \nabla h'}. \tag{2.11}$$

This is a closure problem because the averaged equation for the averaged $\overline{h}$ still depends on the fluctuating term h'.

In order to find an equation for h' in terms of $\overline{h}$ and close the problem, we subtract equation (2.11) from equation (2.10) to obtain:

$$\frac{\partial h'}{\partial t} = \nabla \cdot (\overline{K}\ \nabla h') + \nabla \cdot K'\ \nabla \overline{h} + \nabla \cdot (K'\ \nabla h' - \overline{K'\ \nabla h'}). \tag{2.12}$$

This is again a closure problem because the equation for h' depends on $\nabla h'$. We consider a perturbative closure and we disregard the term $K'\ \nabla h' - \overline{K'\ \nabla h'}$ and assume that its mean square value is far smaller than those of other terms in (2.12):

$$\overline{[K'\nabla h' - \overline{K'\nabla h'}]^2} \ll \max\{(K\overline{\nabla h'})^2, (K\nabla \overline{h})^2\} \tag{2.13}$$

This is a reasonable assumption for low variance of $K(\mathbf{x})$ because it is a difference between second order terms in the fluctuation of K and h. Thus we obtain the following equation for h':

$$\frac{\partial h'}{\partial t} - \nabla \cdot (\overline{K}\ \nabla h') = \nabla \cdot K'\ \nabla \overline{h}, \tag{2.14}$$

which can be solved by the Green's function method [*Beck et al.*, 1992]. The Green's function $g(\mathbf{x}, t|\mathbf{x}', \tau)$ for the problem expressed in (2.14) satisfies the following equation:

$$\frac{\partial\ g(\mathbf{x}, t|\mathbf{x}', \tau)}{\partial t} - \nabla \cdot [\overline{K}\ \nabla g(\mathbf{x}, t|\mathbf{x}', \tau)] = 0 \tag{2.15}$$

with $g(\mathbf{x}, t = \tau|\mathbf{x}', \tau) = \delta(\mathbf{x} - \mathbf{x}')$, and natural boundaries conditions, that means that $g(\mathbf{x}, t|\mathbf{x}', \tau)$ goes to zero for $\mathbf{x}$ to infinity. Notice that this implies that g depends only on the difference $\mathbf{x} - \mathbf{x}'$ and $t - \tau$, so that $g(\mathbf{x}, t|\mathbf{x}', \tau) = g(\mathbf{x} - \mathbf{x}', t - \tau)$. Solving (2.14) using the Green's function method, we multiply both sides of (2.14) times $g(\mathbf{x} - \mathbf{x}', t - \tau)$, we integrate it over all space

and from 0 to t in $d\tau$ and we obtain the following integral expression for h':

$$h'(\mathbf{x},t) = \int_0^t d\tau \int_{-\infty}^{\infty} d\mathbf{x}' \; [\nabla' \cdot K' \nabla' \overline{h}(\mathbf{x},t)] \; g(\mathbf{x}-\mathbf{x}', t-\tau). \tag{2.16}$$

We substitute (2.16) in (2.11) and we obtain a closed equation for $\overline{h}(\mathbf{x},t)$:

$$\frac{\partial \overline{h}(\mathbf{x},t)}{\partial t} = \nabla \cdot \overline{K} \nabla \overline{h}(\mathbf{x},t) + \nabla \cdot \int_0^t d\tau \int_{\infty}^{\infty} d\mathbf{x}' \; [\nabla' \cdot \overline{K'(\mathbf{x}) K'(\mathbf{x}')} \nabla' \overline{h}(\mathbf{x}',\tau)] \; \nabla \; g(\mathbf{x}-\mathbf{x}', t-\tau). \tag{2.17}$$

Considering that $\nabla g(\mathbf{x}-\mathbf{x}', t-\tau) = -\nabla' g(\mathbf{x}-\mathbf{x}', t-\tau)$ and the covariance function $C(\mathbf{x}-\mathbf{x}') = \overline{K'(\mathbf{x}) K'(\mathbf{x}')}$ given in (2.8), we obtain:

$$\frac{\partial \overline{h}(\mathbf{x},t)}{\partial t} = \nabla \cdot \overline{K} \, \nabla \overline{h}(\mathbf{x},t) - \nabla \cdot \int_0^t d\tau \int_{-\infty}^{\infty} d\mathbf{x}' \; \left[\nabla' \cdot C(\mathbf{x}-\mathbf{x}') \nabla' \overline{h}(\mathbf{x}',\tau)\right] \; \nabla' g(\mathbf{x}-\mathbf{x}', t-\tau). \tag{2.18}$$

Using Green's identity and then shifting the variables according to $\mathbf{x}' \rightarrow \mathbf{x}-\mathbf{x}'$ we finally obtain the integro partial-differential equation for $\overline{h}(\mathbf{x},t)$:

$$\frac{\partial \overline{h}(\mathbf{x},t)}{\partial t} = \overline{K} \; \nabla^2 \overline{h}(\mathbf{x},t) + \nabla \cdot \int_0^t d\tau \int_{-\infty}^{\infty} d\mathbf{x}' \; \boldsymbol{\mathcal{K}}(\mathbf{x}',\tau) \; \nabla \; \overline{h}(\mathbf{x}-\mathbf{x}', t-\tau) \tag{2.19}$$

where $\boldsymbol{\mathcal{K}}$ denotes the d dimensional tensor

$$\boldsymbol{\mathcal{K}}(\mathbf{x}',\tau) = C(\mathbf{x}') \; \nabla' \otimes \nabla' g(\mathbf{x}',\tau) \tag{2.20}$$

with ∇' is referred to $\mathbf{x}'$ and $\otimes$ indicates the tensor product, that reads $[\nabla \otimes \nabla]_{ij} = \partial/(\partial x_i \partial x_j)$. Equation (2.19) is an effective equation for the expected value of the hydraulic head $\overline{h}(\mathbf{x},t)$ for a random conductivity field $K = K(\mathbf{x})$. The effective equation obtained is non-local both in time and space and consists of a convolution of the gradient of the expected value of the hydraulic head $\nabla \overline{h}$ and a kernel $\boldsymbol{\mathcal{K}}$, that can be considered as a memory term. Spatial and temporal non locality imply that head at a given time t in a given position $\mathbf{x}$, depends on the head at the previous times $\tau < t$ in different positions $\mathbf{x}'$. This dependency is governed by the kernel given in (2.24), which encapsulates the heterogeneity of the conductivity field, that we considered multi-log normal so that can be stochastically depicted by the covariance function $C(\mathbf{x}-\mathbf{x}')$. Notice that (2.19) can also be derived using perturbation theory as shown

in Appendix A.1 in a more systematic way. Equation (2.19) can be re-written as:

$$\frac{\partial \overline{h}(\mathbf{x},t)}{\partial t} = -\nabla \cdot \mathbf{q}(\mathbf{x},t) \tag{2.21}$$

where we introduced a time and space dependent volumetric flux of water $\mathbf{q}(\mathbf{x},t)$:

$$\mathbf{q}(\mathbf{x},t) = -\left[\overline{K}\,\nabla\overline{h}(\mathbf{x},t) + \int_0^t d\tau \int_{-\infty}^{\infty} d\mathbf{y}\; \mathcal{K}(\mathbf{x}',\tau)\;\nabla\overline{h}(\mathbf{x}-\mathbf{x}',t-\tau)\right]. \tag{2.22}$$

Analogously to *Tartakovsky and Neuman* [1998a] we highlight that the flux $\mathbf{q}(\mathbf{x},t)$ in an heterogeneous media is non-local both in time and in space, depending on the flux at previous times and in different positions.

Localization in space. If $\boldsymbol{\mathcal{K}}(\mathbf{x}',\tau)$ is sharply peaked about zero and $\nabla\overline{h}(\mathbf{x}-\mathbf{x}',t-\tau)$ is smooth (as it is, because $\overline{h}$ is the expected value) we can localize $\overline{h}(\mathbf{x}-\mathbf{x}',t-\tau)$ in $(\mathbf{x},t)$ and get rid of the convolution product. In order to evaluate the kernel we consider the Green's function g solution of the problem expressed in (2.15), that for any d spatial dimension reads:

$$g(\mathbf{x},t) = \frac{1}{(4\pi\overline{K}t)^{d/2}}\, e^{-\frac{\mathbf{x}^2}{4\overline{K}t}} \tag{2.23}$$

and therefore, considering the expression for the covariance given in (2.8), the kernel $\boldsymbol{\mathcal{K}}(\mathbf{x},t)$ for any d dimension is given by:

$$\mathcal{K}_{ij} = \left[\frac{x_i x_j}{4(K_G t)^2} - \frac{\delta_{ij}}{2K_G t}\right] \frac{1}{(4\pi K_G t)^{d/2}}\, e^{-\frac{\mathbf{x}^2}{4K_G t}} C(\mathbf{x}-\mathbf{x}'). \tag{2.24}$$

Notice that in (2.24) we consider K_G instead of $\overline{K}$ as in (2.23) in order to have a consistent formulation up to σ^2 order of approximation. From the expression for the kernel (2.24), we see that $\boldsymbol{\mathcal{K}}(\mathbf{x},t)$ is peaked about $\mathbf{x}=0$ because of the covariance function $C(\mathbf{x})$ given in (2.8) that multiplies the expression. This is illustrated in figure 2.1 for the $d=1$ case. Under these conditions, we can localize (2.19), expanding $\overline{h}(\mathbf{x}-\mathbf{x}',t-\tau)$ about $\mathbf{x}=\mathbf{0}$ and considering only the zero order term:

$$\overline{h}(\mathbf{x}-\mathbf{x}',t-t') = \overline{h}(\mathbf{x},t) + \mathbf{x}'\cdot\nabla\overline{h}(\mathbf{x},t-t') + \frac{1}{2}\mathbf{x}'\cdot\nabla\otimes\nabla\overline{h}(\mathbf{x},t-t')\cdot\mathbf{x}' + ... \tag{2.25}$$

We take into account only the zeroth oreder term. At large distance the gradient of the average $\overline{h}(\mathbf{x},t)$ can be expected to be small. Inserting this expression into (2.19), we obtain a non-local

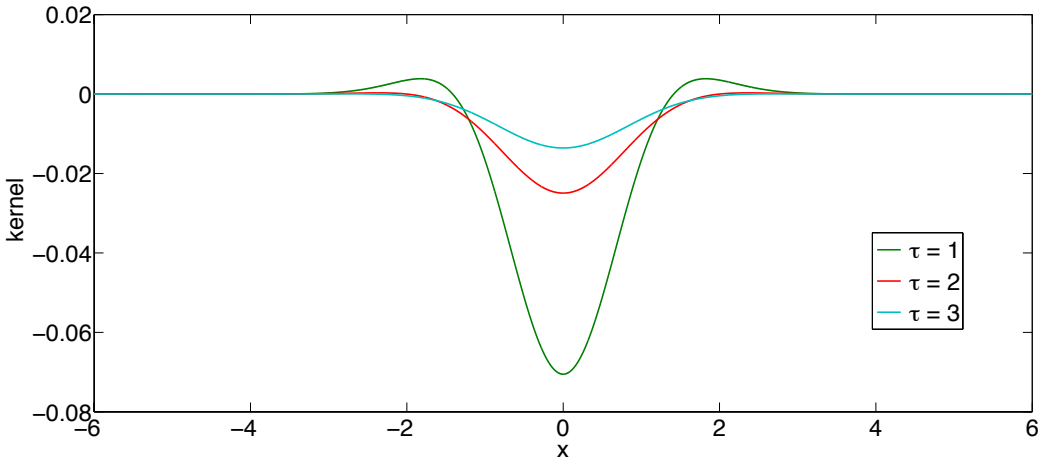

Figure 2.1: *Kernel $\mathcal{K}(x,\tau)$ given in* (2.24) *plotted in function of x for different τ.*

expression for $\overline{h}(\mathbf{x},t)$ only in time:

$$\frac{\partial \overline{h}(\mathbf{x},t)}{\partial t} = \overline{K}\ \nabla^2 \overline{h}(\mathbf{x},t) + \nabla \cdot \int_0^t d\tau\ \boldsymbol{\mathcal{K}_L}(\tau)\ \nabla\ \overline{h}(\mathbf{x},t-\tau) \tag{2.26}$$

where $\boldsymbol{\mathcal{K}_L}(t)$ is given by the space integral of the kernel:

$$\mathcal{K}_{L_{ij}}(t) = \int d\mathbf{x}\ \mathcal{K}_{ij}(\mathbf{x},t) \tag{2.27}$$

Inserting (2.24) into (2.27) and executing the integral, we obtain:

$$\mathcal{K}_{L_{ij}}(t) = \delta_{ij}\mathcal{K}_L(t) = -\frac{\sigma^2 K_G^2}{\tau_K}\left(1 - 2\frac{t}{\tau_K}\right)^{-\frac{d}{2}-1} \tag{2.28}$$

where $\tau_K = \ell^2/K_G$ for $i = 1,..d$. The characteristic time τ_K represents the typical timescale of the problem and we discuss it in the following. Note that in the following we leave out the tensorial notation considering that, for symmetry, $\mathcal{K}_{L,ij}(t) = 0$ for $i \neq j$ and $\mathcal{K}_{L,ij}(t) = \mathcal{K}_L(t)$ for $i = 1,..d$.

Localization in time. The kernel $\mathcal{K}_L(t)$ decreases to zero as $t^{-d/2-1}$ for times $t \gg \tau_K$. In this regime we can localize equation (2.26) respect to time to obtain:

$$\frac{\partial \overline{h}(\mathbf{x},t)}{\partial t} = K_e(t)\ \nabla^2 \overline{h}(\mathbf{x},t) \tag{2.29}$$

where $K_e(t)$ is defined by:

$$K_e(t) = \overline{K} + \int_0^\infty d\tau \; \mathcal{K}_L(\tau) \tag{2.30}$$

Equation (2.29) is a flow equation with a time dependent effective hydraulic conductivity given by localization in space and in time of the non-local equation (2.19). Solution for the flow equation with a time dependent conductivity is given in the appendix. In the next section we discuss the effective hydraulic conductivity.

2.2.3 Effective Hydraulic Conductivity

Effective conductivity for heterogeneous media is defined for steady state problem. Therefore, analogously to the classical definition of effective conductivity we take the hydraulic head gradient constant $\nabla\overline{h}(\mathbf{x}, t) = \mathbf{J}$ and in this case, equation (2.22) reduces to:

$$\mathbf{q} = -\left[\overline{K}\,\mathbf{J} + \int_0^\infty d\tau \int_{-\infty}^\infty d\mathbf{x}' \; \mathcal{K}(\mathbf{x}', \tau)\; \mathbf{J}\right]. \tag{2.31}$$

As the head gradient is constant, we do not have anymore a convolution between the kernel and the gradient, the flow turns to be local, and the effective conductivity K_{eff}, as classically defined is the limit for time to infinity of the localized kernel $\mathcal{K}(\mathbf{y}, \tau)$:

$$K_{eff} = \overline{K} + \int_0^\infty dt' \int_{-\infty}^\infty d\mathbf{x}' \; \mathcal{K}(\mathbf{x}', t') = \lim_{t\to\infty} K_e(t) \tag{2.32}$$

with $K_e(t)$ defined in (2.30). In the literature of diffusion in disorder media, effective conductivity K_{eff} is defined in terms of the second moment of the scalar quantity which diffuses for a pulse injection into an infinite medium [*Dean et al.*, 2007]:

$$K_{eff} = \frac{1}{2}\frac{\partial}{\partial t}\int d\mathbf{x} \; x_i^2 h(\mathbf{x}, t) \tag{2.33}$$

with $h(\mathbf{x}, t = 0) = \delta(\mathbf{x})$. This corresponds to the diffusion of a solute in a infinite media evolving from a point injection as input. In this case $K_e(t)$ corresponds to a time dependent diffusion coefficient. Here $K_e(t)$ describes dispersion of pressure pulse over time. It can also be seen as an effective time dependent hydraulic conductivity in a localized version of the flow equation (2.29). From the definition (2.30) and (2.28) we obtain the following explicit

expression for $K_e(t)$ in d spatial dimension:

$$K_e(t) = K_{eff} + \frac{\sigma^2 K_G}{d}\left(1 + 2\frac{t}{\tau_K}\right)^{-\frac{d}{2}} \tag{2.34}$$

with K_{eff} given by the well known asymptotic values for the effective conductivity in d spatial dimension [*Gutjahr et al.*, 1978].

$$K_{eff} = \begin{cases} K_G\left(1 - \dfrac{\sigma^2}{2}\right), & d = 1 \\ K_G, & d = 2 \\ K_G\left(1 + \dfrac{\sigma^2}{6}\right), & d = 3 \end{cases} \tag{2.35}$$

Notice that (2.34) is a perturbative approximation of the effective conductivity up to first order in σ^2. Higher order can be derived using perturbation expansion of h presented in Appendix. In particular, in $d = 1$, K_{eff} is the perturbative approximation of the harmonic mean up to order σ^2. Note that $K_e(t)$ converges to its asymptotic value K_{eff} for times $t \gg \tau_K$. Thus the local model (2.29), is well characterized by $K_e(t) = K_{eff}$ in the regime where it is valid so that is becomes:

$$\frac{\partial \overline{h}(\mathbf{x}, t)}{\partial t} = K_{eff}\, \nabla^2 \overline{h}(\mathbf{x}, t) \tag{2.36}$$

For times $t \gg \tau_K$, (2.34) reads:

$$K_e(t) = K_{eff} + \frac{\sigma^2 K_G}{d} 2^{-\frac{d}{2}} \left(\frac{t}{\tau_K}\right)^{-\frac{d}{2}}. \tag{2.37}$$

Equation (2.37) evidence how fast the effective conductivity tends to its asymptotic value for any d spatial dimension. For $d = 1$, $K_e(t)$ tends to its corresponding K_{eff} as $t^{-1/2}$, for $d = 2$ as t^{-1} and in $d = 3$ as $t^{-3/2}$. In the following we consider the flow problem in 1, 2 and 3 dimensions, we compute the head response for the local and the non-local problem and we show that $K_e(t)$ is consistent with time dependent effective conductivity obtained using perturbation's methods in terms of spatial moment of the hydraulic head defined in (2.34) derived in the appendix.

2.3 Effective behaviour

In the following we discuss the temporal evolution of the effective conductivity and we evaluate the head response for a pulse injection for $d = 1, 2$ and 3 spatial dimension.

2.3.1 Temporal Evolution of Effective Hydraulic Conductivity

In figure 2.2 we display the temporal evolution of $K_e(t/\tau_K)$ defined in (2.34) for $d = 1, 2$ and 3 spatial dimensions.

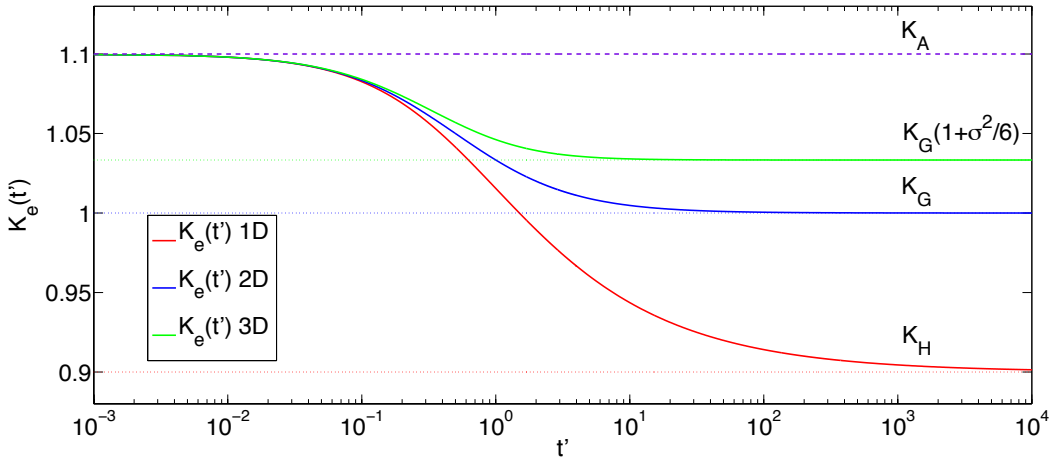

Figure 2.2: *Effective conductivity $K_e(t')$, plotted in function of the dimensionless time $t' = t/\tau_K$ with $\tau_k = \ell^2/K_G$, for d =1,2 and 3 dimensional media.*

As illustrated in the figure 2.2, $K_e(t)$ is bounded by the arithmetic mean of the local conductivity, for time to zero, and the harmonic mean for larger times. All the $K_e(t)$ for any d dimension are equal to the arithmetic mean for time to zero and decrease in time to the correspondent well known asymptotic values of K_{eff} for $d = 1$, 2 and 3 dimensional media. The evolution of the effective hydraulic conductivity depends on the dimensionality of the space. The characteristic timescale is given by τ_K, which indicates the typical time for the dispersion of a pression pulse over a correlation length ℓ of the medium.

Time dependent effective conductivity $K_e(t)$ tends to its corresponding asymptotic value depending on the dimensionality $d = 1, 2, 3$ of the problem as $t^{-d/2}$. This indicates that with increasing dimension, heterogeneity is sampled with increasing efficiency. This can be understood by the fact that in $d = 2$ and $d = 3$ there are more directions available. Therefore the system samples in the same time a larger part of the medium heterogeneity for larger dimension. Notice that $K_e(t)$ also describes the diffusion of a solute evolving from a point

source in a infinite medium. As said in section 2.2.3, this problem is equivalent to a random walk in a heterogeneous media, where the mean number of distinct sites visited by a random walker goes with the square of step number n, $\sqrt{n}$ in $d = 1$, according to $n/\sqrt{n}$ in $d = 2$ and as n in $d = 3$ [*Weiss*, 1994]. This quantifies the fact the heterogeneity is sampled faster with increasing dimension. We will use this notion on distinct number of sites visited also in Chapter 4.

2.3.2 Drawdown

The mean hydraulic head satisfies equation (2.26), which, for $\mathcal{K}_{L,ij} = \delta_{ij}\mathcal{K}_L(t)$ as given in equation (2.28), reduces to:

$$\frac{\partial \overline{h}(\mathbf{x},t)}{\partial t} = \overline{K}\,\nabla^2\overline{h}(\mathbf{x},t) + \int_0^t d\tau\; \mathcal{K}_L(\tau)\,\nabla^2\overline{h}(\mathbf{x},t-\tau). \tag{2.38}$$

We consider here an initial boundary value problem that mimics a slug test. Notice that this corresponds to diffusion of a solute evolving from a point injection. The initial condition is $\overline{h}(\mathbf{x}, t = 0) = \delta(\mathbf{x})$. As boundaries condition we consider that the averaged head is zero at infinity. Equation (2.38) can be solved analytically in Laplace space. Laplace transform of (2.38) gives:

$$\lambda\,\overline{h}^*(\mathbf{x},\lambda) - [\overline{K} + \mathcal{K}_L^*(\lambda)]\,\nabla^2\overline{h}^*(\mathbf{x},\lambda) = \delta(\mathbf{x}) \tag{2.39}$$

In order to solve the previous non-local equation we consider the local diffusion equation:

$$\frac{\partial c(\mathbf{x},t)}{\partial t} - D\nabla^2 c(\mathbf{x},t) = 0. \tag{2.40}$$

The solution of (2.40), for pulse injection as initial condition and natural boundaries conditions, is well known and it is given by the Gaussian distribution:

$$c(\mathbf{x},t) = \frac{1}{(4\pi D t)^{d/2}}\, e^{-\frac{\mathbf{x}^2}{4Dt}} \tag{2.41}$$

with d spatial dimension. Notice that the Laplace transform of (2.40) with $c(\mathbf{x}, t = 0) = \delta(\mathbf{x})$ is given by:

$$\lambda\, c^*(\mathbf{x},\lambda) - D\nabla^2 c(\mathbf{x},\lambda) = \delta(\mathbf{x}). \tag{2.42}$$

Thus, comparing (2.42) and (2.39) we find that the solution for $\overline{h}^*(\mathbf{x},\lambda)$ can be expressed in terms of the Laplace transform of (2.41) by substituting $D = \overline{K} + \mathcal{K}_L^*(\lambda)$.

In the following we discuss the behaviours of the drawdown curves, this mean the temporal evolution of $\overline{h}(\mathbf{x}, t)$ for a fixed position in space. Hydraulic head for d =1, 2 and 3 spatial dimensions is computed analytically in Laplace space in terms of the Laplace transform of (2.41) by substituting $D = \overline{K} + \mathcal{K}_L^*(\lambda)$ for and the time behaviour is determined by numerical Laplace inversion of $\overline{h}^*(\mathbf{x}, \lambda)$ using a Matlab routine based on the Hoog algorithm [*Hollenbeck*, 1998].

Drawdown in $d = 1$ dimension. Considering the Laplace transform of (2.41) for $d = 1$ the solution for the mean hydraulic head reads:

$$\overline{h}^*(x, \lambda) = \frac{1}{\sqrt{4\left[\overline{K} + \mathcal{K}_L^*(\lambda)\right]\lambda}}\, e^{-\sqrt{\frac{\lambda}{\overline{K}+\mathcal{K}_L^*(\lambda)}}\,|x|} \tag{2.43}$$

and $\mathcal{K}_L^*(\lambda)$, given by the Laplace transform of (2.28) for $d = 1$, is:

$$\mathcal{K}_L^*(\lambda) = K_G\sigma^2\left[1 - \sqrt{\pi}\sqrt{\frac{l^2\,\lambda}{2\,K_G}}\; e^{\frac{l^2\lambda}{2\overline{K}}}\;\operatorname{erfc}\left(\sqrt{\frac{l^2\,\lambda}{2\,K_G}}\right)\right] \tag{2.44}$$

where $\operatorname{erfc}(\cdot)$ indicates the complementary error function defined as:

$$\operatorname{erfc}(x) = \frac{2}{\sqrt{\pi}}\int_x^\infty e^{-t^2}dt. \tag{2.45}$$

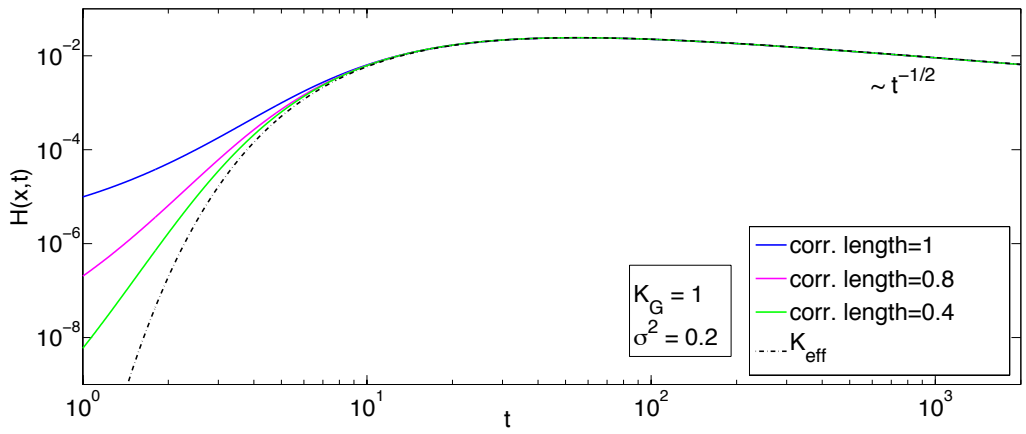

Figure 2.3: *Drawdown curves for $d = 1$ dimensional media. Log-normal distributed hydraulic conductivity with geometric mean $K_G = 1m/day$, variance of $\log K$ $\sigma^2 = 0.2$, distance observation point $= 10m$. Drawdown curves for different correlation length of $\log K$: $l = (1, 0.8, 0.4)m$ compared with an equivalent homogeneous representation with $K_{eff} = K_H$.*

Figure 2.3 shows drawdown curves in $d = 1$ dimension for variable correlation lengths of $l = 0.4m$, $l = 0.8m$ and $l = 1m$. We display the solution of the non-local equation (solid lines) and the local asymptotic equation (dash line). We observe that asymptotically drawdown curves scale as $t^{-1/2}$ as in the homogeneous case, but the drawdowns obtained for the non-local equation arrives earlier than the equivalent homogeneous one. This behaviour can be explained by the fact that the evolution of $\overline{h}(x,t)$ in the non-local case is influenced by the values of conductivity at small times. In average conductivity at small time is given by the arithmetic mean K_A which is larger than the value of the asymptotic effective conductivity: $K_A \geqslant K_{eff}$. We furthermore observe that the drawdown curves arrive earlier with increasing correlation length. For increasing l the length over which the pressure pulse is exposed to an approximately constant local K value increases. Thus, in average, at small time the pressure pulse is exposed to an equivalent conductivity higher than its asymptotic value for a large time. This is also expressed by the evaluation of $K_e(t)$ shows in figure 2.2. As shown in Figure 2.2 the evolution of $K_e(t)$ is governed by the characteristic time scale $\tau_K = l^2/K_G$. For increasing l, τ_K increases and $K_e(t)$ is, at the same time larger than for a smaller correlation length. This explains the earlier arrivals of drawdown for large correlation length.

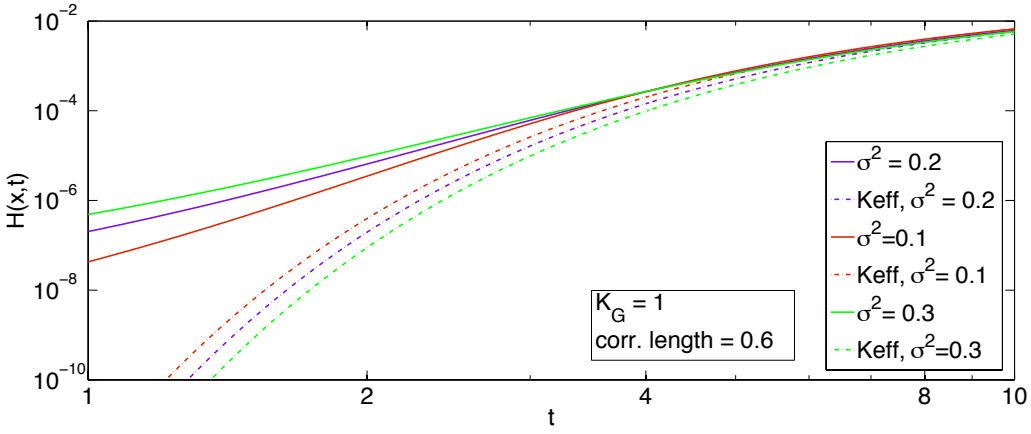

Figure 2.4: *Drawdown curves for 1 dimensional media. Log-normal distributed hydraulic conductivity with geometric mean* $K_G = 1m/day$, *correlation length of* $\log K$: $l = 0.5m$, *distance observation point* $= 10m$. *Drawdown curves for different variance of* $\log K$: $\sigma^2 = 0.1, 0.2, 0.3$ *compared with an equivalent homogeneous representation with* $K_{eff} = K_H$.

In Figure 2.4 we display drawdown curves for the non-local (solid) and the local asymptotic (dash) models for variable log-conductivity variance. We observe that for the non-local model, the drawdown arrive earlier with increasing heterogeneity, while for the effective asymptotic formulation, the opposite holds. As noticed above, the non-local model is influenced by the

average conductivity at early times, which is larger that its asymptotic value. The arithmetic mean $K_A = e^{\sigma^2/2}$ increases with σ^2 and consequently we have earlier arrival times. The local asymptotic model is dominated by the harmonic mean $K_H = e^{-\sigma^2/2}$, which decreases with increasing σ^2.

Drawdown in $d = 2$ dimension Considering $d = 2$ dimensional media, the hydraulic head given by Laplace transform of (2.41), is:

$$\overline{h}^*(\mathbf{x}, \lambda) = \frac{1}{2\,\pi\,[\overline{K} + \mathcal{K}_L^*(\lambda)]}\ \mathsf{K}_0\left(\sqrt{\frac{\mathbf{x}^2\lambda}{\overline{K} + \mathcal{K}_L^*(\lambda)}}\right) \tag{2.46}$$

where $\mathsf{K}_0(\cdot)$ indicates the modified Bessel function of second kind of order zero and the kernel $\mathcal{K}_L^*(\lambda)$, from Laplace transform of (2.28) for $d = 2$, is:

$$\mathcal{K}_L^*(\lambda) = -\frac{K_G\sigma^2}{2}\left[1 - \frac{l^2\lambda}{2K_G}\, e^{\frac{l^2\lambda}{2K_G}}\ \mathrm{Ei}\left(\frac{l^2\lambda}{2K_G}\right)\right] \tag{2.47}$$

where $\mathrm{Ei}(\cdot)$ indicates the exponential integral function defined as:

$$\mathrm{Ei}(x) = \int_x^\infty \frac{e^{-t}}{t}dt, \qquad x > 0. \tag{2.48}$$

In figure 2.5 we compare the drawdown computed considering the non-local formulation (solid lines) with $\sigma^2 = (0.1, 0.2, 0.3)m$ with the local asymptotic formulation with $K_{eff} = K_G$ (dash line). As illustrated in (2.5) the late time behaviour of drawdown with the non local

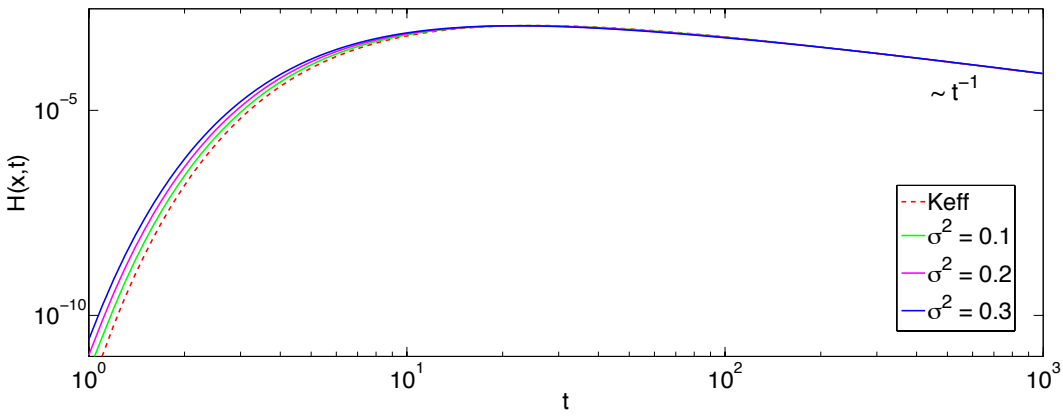

Figure 2.5: *Drawdown curves for 2 dimensional problem. Conformal distributed hydraulic conductivity with geometric mean $K_G = 1m/day$, distance observation point $= 10m$, correlation length of $\log K$: $l = 2m$. Non-local formulation compared with a classical local one with $K_{eff} = K_G$.*

formulation scales in time as t^{-1} as for the homogeneous case and for small variance the non-local formulation tends to the homogeneous one, but, increasing the variance we get earlier arrival times as in the $d = 1$ dimensional case. Notice that for $d = 2$ dimensional case, differently that from $d = 1$, the effective conductivity K_{eff} does not depend on the variance. In figure 2.6 we compare drawdown curves obtained with the non-local formulation (solid lines) and for the equivalent homogeneous one (dash lines) for different correlation lengths $l = 0.2, 0.5, 10)m$. As for the $d = 1$ case, we observe that varying the correlation length, the curves differ from the local formulation. For small correlation length the curves obtained with the non local formulation tend to the ones obtained using K_G, but increasing the correlation length we get earlier arrival time. Drawdown curves for the non-local formulation at early time can be about one order of magnitude higher respect the homogeneous effective one. The explanation is the same that for the $d = 1$ problem. Local effective description is dominated by $K_{eff} = K_G$, while in the non-local formulation, at early times the pressure pulse depends on the values of conductivity close to the arithmetic mean and $K_A \geqslant K_G$.

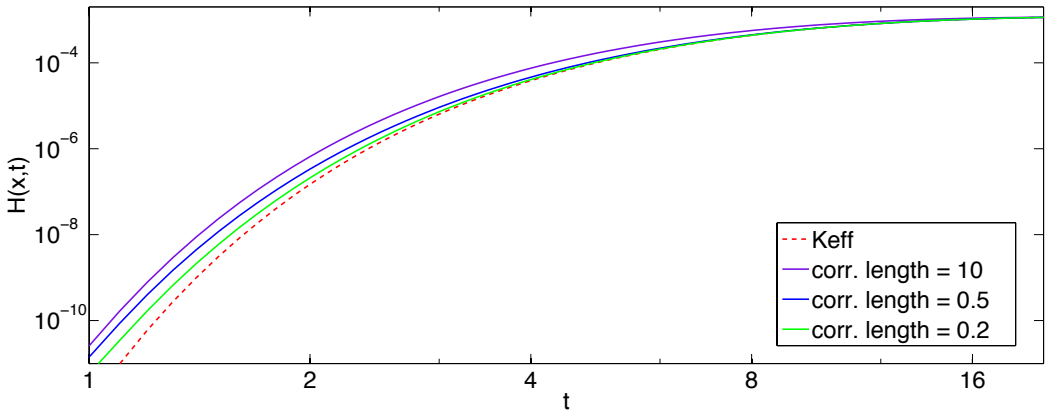

Figure 2.6: *Drawdown curves for 2 dimensional problem. Log normal distributed hydraulic conductivity with geometric mean* $K_G = 1m/day$*, distance observation point* $= 10m$*, variance of* $\log K$*:* $\sigma^2 = 0.3$*. Non-local formulation compared with a classical local one with* $K_{eff} = K_G$*.*

Drawdown in $d = 3$ dimension For $d = 3$ spatial dimension, the Laplace transform of (2.41) gives:

$$\overline{h}^*(\mathbf{x}, \lambda) = \frac{1}{4\pi} \frac{1}{[\overline{K} + \mathcal{K}_L^*(\lambda)]\mathbf{x}} e^{-\sqrt{\frac{\lambda}{[\overline{K}+\mathcal{K}_L^*(\lambda)]}}\,\mathbf{x}} \tag{2.49}$$

with the kernel $\mathcal{K}_L^*(\lambda)$ given by:

$$\mathcal{K}_L^*(\lambda) = -K_G\sigma^2\frac{1}{3}\left[1 - 2\frac{l^2\lambda}{2K_G} + 2\sqrt{\pi}\left(\frac{l^2\lambda}{2K_G}\right)^{\frac{3}{2}} e^{\frac{l^2\lambda}{2K}}\,\mathrm{erfc}\left(\sqrt{\frac{l^2\lambda}{2K_G}}\right)\right]. \tag{2.50}$$

In figure 2.7 we compare the drawdown for the non local formulation given in (2.49) for

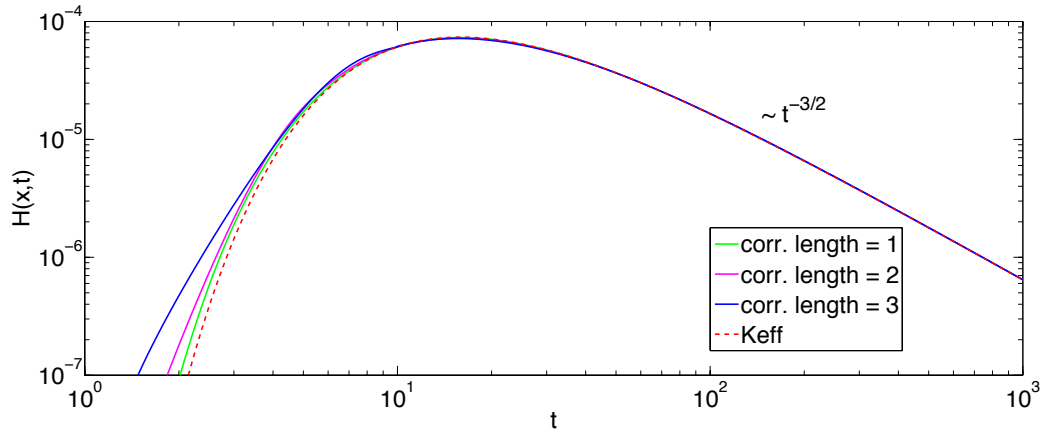

Figure 2.7: *Drawdown curves in a 3 dimensional media for different correlation lengths of* $\log K$*:* $l = (1,2,3)m$ *indicated in the figure. Log-normal distributed hydraulic conductivity with geometric mean* $K_G = 1m/day$*, variance of* $\log K$ $\sigma^2 = 0.3$*, distance observation point* $= 10m$*. Non-local formulation (continuous lines) compared with a classical local one (dash line) with* $K_{eff} = K_G(1+\sigma^2/6)$*.*

different correlation lengths of the log conductivity field $l = (1,2,3)m$ (solid lines) with the local classical formulation with an effective conductivity given by $K_{eff} = K_G(1+\sigma^2/6)$ (dash line). At late times the curves coincide and hydraulic heads scale asymptotically as $t^{-3/2}$, but at early times the ones obtained with the non-local formulation arrive before that the one obtained with the classical K_{eff}. In figure 2.8 we compare the effect of different variance $\sigma^2 = (0.05, 0.1, 0.2)m$ at early time in the drawdown curves for the non-local formulation (solid lines) and the classical one with $K_{eff} = K_G(1+\sigma^2/6)$ (dash line). Higher variances imply earlier arrival times. For small variance non local formulation tends to the classical one, but increasing the variance, the drawdown curves of non-local formulation at early times are about one order of magnitude higher than the classical ones. Notice that for $d = 1$ we had the opposite effect: higher σ^2 gives smaller K_{eff} while in $d = 2$ K_{eff} is independent from the variance. Increasing the variance we obtain earlier arrival times both for the non-local and the asymptotic description, but the effect is more remarkable in the non-local formulation. This can be explained by the fact that K_{eff} is an averaged value for the hydraulic conductivity in asymptotic regime, where all the heterogeneity is sampled. Differently the non-local formu-

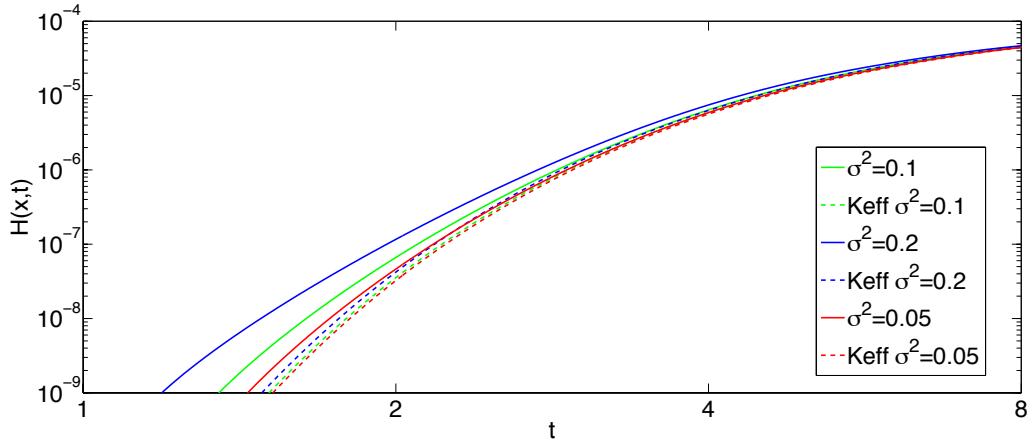

Figure 2.8: *Drawdown curves in a 3 dimensional media for early times. Log-normal distributed hydraulic conductivity with geometric mean* $K_G = 1m/day$*, variance of* $\log K$ $\sigma^2 = 0.05, 0.1, 0.2$*, distance observation point=* $20m$*, correlation length of* $\log K$*:* $l = 3m$*. Non-local formulation compared with a classical local one with* $K_{eff} = K_G(1 + \sigma^2/6)$*.*

lation takes into account the possibility that the pressure pulse reaches the observation point without sampling all the heterogeneity, but 'choosing' only the higher conductivity regions.

2.4 Conclusions

In this chapter we used a stochastic method to upscale flow in heterogeneous media characterized by a spatially varying hydraulic conductivity and a constant storativity. In a stochastic framework we modeled spatially varying hydraulic conductivity as multi-lognormal random field and we derived an effective equation for the ensemble mean value of the hydraulic head. The effective equation derived is non local. Non-locality is expressed by the convolution of the gradient of the mean hydraulic head with a kernel that takes into account a statistical description of the heterogeneity of the conductivity field. Heterogeneity brings non-locality both in time and in space in the flow problem an it implies that a description in terms of effective coefficient is not enough to fully characterize flow in heterogeneous media. We demonstrate the the well known values for the effective conductivity in $d = 1, 2$ and 3 dimensional media can be obtained by localization of the effective equation derived. Localizing both in space and in space the non local formulation derive we obtain a time dependent effective coefficient and its asymptotic limit for $d = 1, 2$ and 3 spatial dimension reduces into the well known value for effective conductivity in heterogeneous media. We show that effective conductivity computed in terms of spatial moments for a pulse injection in an infinitive medium is equivalent to the effective conductivity classically defined for a constant head gradient in a bounded domain.

Considering localization in space of the effective equation derived, we solved the non-local in time formulation in Laplace space and we discussed the hydraulic response for a pulse injection in a $d = 1, 2$ and 3 spatial dimension. We compared the drawdown curves obtained with the non-local formulation and with the classical local formulation and the well known values for the effective conductivity K_{eff} in d dimensions [*Sanchez-Villa et al.*, 2006]. Asymptotically the non-local formulation and the classical description coincide, but in the transient regime the classical description underestimates earlier arrival times. Indeed the effective values of K_{eff} is defined for steady state condition, when all the heterogeneity is sampled. Non-local formulation gives earlier arrival times and the effect increases as the variance and the correlation length of the hydraulic conductivity field increase. Higher correlation length implies longer transitional regime, which, in turns, implies higher underestimation of the earlier arrival times using a local model. Correct estimation of early arrival times is highly important in particular in groundwater vulnerability problem. The effect of underestimation of early arrival times is less remarkable for increasing spatial dimension. This is due to the fact that efficiency in the sampling of heterogeneity depends on the dimensionality of the problem: increasing spatial dimension, heterogeneity is sampled with increasing efficiency and therefore steady state condition is reached earlier. It implies that increasing the dimensionality of the problem the local description with K_{eff} became earlier an effective description of the heterogeneous problem. The efficiency in the sampling of the heterogeneity can be quantified in a particle tracking framework, as we discuss in the following chapter dedicated to particle tracking method. Considering a random walk, the efficiency in the sampling of heterogeneity is given by the probability for a random walker to explore new sites, which increases with increasing spatial dimension [*Weiss*, 1994]. This is reflected also on the temporal evolution of the effective time dependent hydraulic conductivity $K_e(t)$ computed by localization of the kernel of the non-local equation in function of the spatial dimension d. $K_e(t)$ tends to the well known values of the hydraulic conductivity for any d dimension as $t^{-1/2}$ for $d = 1$, as t^{-1} in $d = 2$ and according to $t^{-3/2}$ in $d = 3$.

Chapter 3

Diffusion in Heterogeneous Media: a Random Walk Perspective

[I]

3.1 Introduction

In this chapter we study diffusion in heterogeneous media characterized by spatially varying diffusion properties using random walk. Diffusion in heterogeneous media is a ubiquitous process in nature that describes a range of different physical phenomena [*Haus and Kehr*, 1987; *Havlin and Ben-Avraham*, 2002b; *Dean et al.*, 2007] including chemical transport in low permeability media such as clays and granites [*Delay et al.*, 2002] and in general in immobile regions of a heterogeneous porous medium [*Gouze et al.*, 2008b], Darcian fluid flow through heterogeneous media, heat transport and electric current through a conductor [*King*, 1987; *Drummond and Hogan*, 1987; *McCarthy*, 1993], as well as diffusion in biological systems [*Codling et al.*, 2008]. The present work is motivated through the diffusion of chemicals in heterogeneous low permeability media that are characterized by spatially varying diffusion properties. The concentration $c(\mathbf{x}, t)$ of a dissolved chemical satisfies the diffusion equation

$$R(\mathbf{x})\frac{\partial c(\mathbf{x}, t)}{\partial t} = \nabla \cdot [D(\mathbf{x})\nabla c(\mathbf{x}, t)]\,, \tag{3.1}$$

[I]The first part of this chapter has been published in the paper *Diffusion and Trapping in Heterogeneous Media: An Inhomogeneous Continuous Time Random Walk Approach*, Dentz M., P. Gouze, A. Russian, J. Dweik, F. Delay; Advances in Water Resources Advances in Water Resources 49 (2012) 13-22.

in which $D(\mathbf{x})$ the diffusion coefficient and $R(\mathbf{x})$ is a random retardation coefficient. Notice that for diffusion of a non-reactive solute $R(\mathbf{x}) = \phi(\mathbf{x})$ with $\phi(\mathbf{x})$ porosity. For diffusion under linear equilibrium sorption-desorption reaction: $R(\mathbf{x}) = \{[1 - \phi(\mathbf{x})]k_d(\mathbf{x}) + \phi(\mathbf{x})\}$ where k_d is the distribution coefficient that relates the mobile and the adsorbed concentration. For the case of the flow of an incompressible fluid through a porous medium, $c(\mathbf{x}, t)$ represents hydraulic head, $R(\mathbf{x}) = S(\mathbf{x})$ is the specific storativity and $D(\mathbf{x})$the hydraulic conductivity. The diffusion equation (3.1) for heterogeneous media does not have a general closed form solution and is often approached analytically using perturbation methods [*Drummond and Hogan*, 1987; *King*, 1987; *Dean et al.*, 2007], and numerically using finite difference, finite element or finite volume methods [*Patankar*, 1980; *Crank*, 1975]. In this paper, we focus on numerical approaches based on random walk particle tracking [*Kinzelbach*, 1987; *Drummond and Hogan*, 1987]. This numerical method is based on the fact that equation (3.1) is equivalent to the Langevin equation [e.g., *Gouze et al.*, 2008b]

$$\frac{d\mathbf{x}(t)}{dt} = \frac{\nabla D[\mathbf{x}(t)]}{R[\mathbf{x}(t)]} + \sqrt{2\frac{D[\mathbf{x}(t)]}{R[\mathbf{x}(t)]}}\xi(t), \tag{3.2}$$

in which $\mathbf{x}(t)$ describes the trajectories of the 'solute' particles that constitute the concentration distribution $c(\mathbf{x}, t)$. In fact, $c(\mathbf{x}, t)$ is expressed in terms of the particle trajectory as [*Risken*, 1996]

$$c(\mathbf{x}, t) = \frac{1}{R(\mathbf{x})} \langle \delta[\mathbf{x} - \mathbf{x}(t)] \rangle , \tag{3.3}$$

in which $\delta(\mathbf{x})$ denotes the d-dimensional Dirac delta-distribution.

The numerical solution of the Langevin equation (3.2) can be very costly because the heterogeneous diffusion properties may require a fine time-discretization in order to ensure that a particle actually 'sees' the spatial variability [e.g., *James and Chrysikolpoulos*, 2001; *Delay et al.*, 2002]. There may be inaccuracies because in some regions of the medium with little variability a coarse discretization is sufficient while in regions with high variability a fine time discretization is required [*James and Chrysikolpoulos*, 2001]. Also, as pointed out by McCarthy [*McCarthy*, 1993] in regions of small diffusivity a particle may have to wait at a given site for a large number of simulation steps, which is inefficient. Furthermore, for pixelized maps of heterogeneous media as obtained by X-ray micro-tomography (XMT) [*Delay et al.*, 2002; *Gouze et al.*, 2008b], see Figure 3.1, diffusion properties are spatially discontinuous, which makes the use

of Eq. (3.2) complicated because it relies on the calculation of the gradient of the diffusion coefficient $D(\mathbf{x})$ (see for example [*Delay et al.*, 2005]). Therefore, there is a need for random walk scheme that can handle this kind of problems. The time domain random walk (TDRW) approach represents an alternative to the classical random walk (RW) framework. In Section 4.2 we present a rigorous derivation of the TDRW algorithm and a demonstration its equivalence to the diffusion equation. Furthermore, we extend the TDRW to solve diffusion problem in a heterogeneous medium with multi-rate mass transfer properties using a statistical representation of the medium.

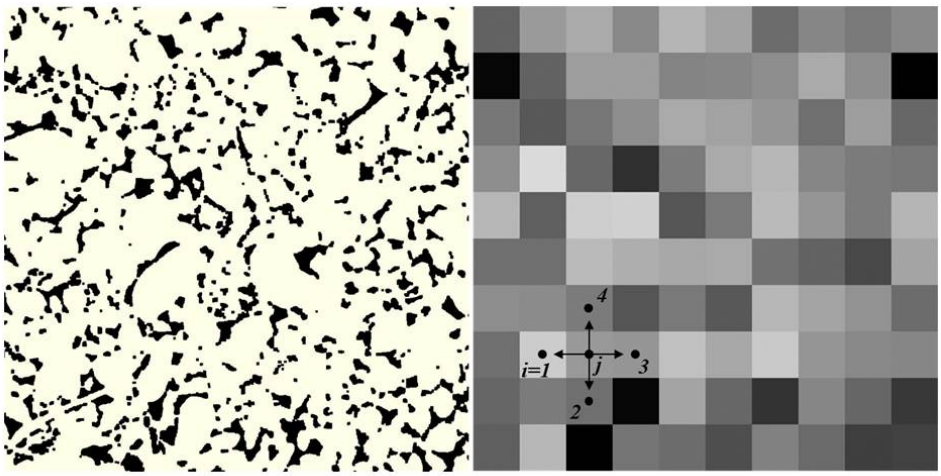

Figure 3.1: *Left: Numerical cross-section of a connected pore cluster obtained from a $d = 3$ dimensional XMT image (5 mm $\times$ 5 mm limestone sample), the black color indicates pore space. Right: Equivalent upscaled porosity map. The arrows indicate possible particle transitions to nearest neighbors.*

Heterogeneity brings complexity in diffusion problems, which, in turn, induces uncertainty and anomalous behaviour [*Havlin and Ben-Avraham*, 2002b; *Bouchaud and Georges*, 1990]. There are many model that describe non-Fickian/anomalous diffusion phenomena, like CTRW [*Berkowitz et al.*, 2006; *Metzler and Klafter*, 2000], delayed-diffusion models [*Dentz and Tartakovsky*, 2006], MRMT models [*Haggerty and Gorelick*, 1995; *Carrera et al.*, 1998] fractional diffusion models [*Metzler and Klafter*, 2000]. Oftentimes these approaches are not linked to the heterogeneity distribution, which puts a limitation on their predictive capability. Stochas-

tic modeling provides a systematic way to quantify the heterogeneity impact on diffusion in heterogeneous media, see also Chapter 3. In section 4.3 we discuss the upscaling of diffusion in a $d = 3$ spatial dimension medium characterized by varying $R(\mathbf{x})$ and constant $D(\mathbf{x}) = D$. Using a stochastic modeling approach we derive an explicit non-local diffusion equation for the average particle density.

3.2 Time Domain Random Walk

As pointed out in the introduction, numerical solution of Langevin equation can be very costly, here we present a particle scheme that relies on spatial increments, whose absolute values are deterministic, combined with random time increment [*McCarthy*, 1993; *Banton et al.*, 1997; *Noetinger and Estebenet*, 2000; *James and Chrysikolpoulos*, 2001; *Delay et al.*, 2002; *Reimus and James*, 2002]. That is, at each random walk step the particle moves a given distance (which can be given by the pixel size of the discretized medium representation, for example) in a random direction, whose probability is calculated from the diffusion properties of the medium. The time for the step is random, which reflects the stochastic nature of the diffusion process. There has been in fact a certain ambiguity on how to model the distribution of transition time. In [*McCarthy*, 1993], *Noetinger and Estebenet* [2000] and *Delay et al.* [2002], for example, an exponential transition time distribution is employed, while *James and Chrysikolpoulos* [2001] and *Delay and Bodin* [2001] use a log-normal transition time distribution. Ref. [*Reimus and James*, 2002] identifies the transition time with the first-passage time to cross a certain distance by diffusion. The different variants of this methodology have been called continuous time random walk (CTRW) on random media [*McCarthy*, 1993; *Noetinger and Estebenet*, 2000] and time-domain random walk (TDRW) [*Banton et al.*, 1997; *James and Chrysikolpoulos*, 2001]. In the different aforementioned applications, TDRW method has been used for the determination of effective diffusivity [*Delay et al.*, 2002], effective hydraulic and electrical conductivity [*McCarthy*, 1993], for the upscaling of fluid flow in fractured rocks [*Noetinger and Estebenet*, 2000] and for the efficient simulation of chemical transport in fracture networks [*Delay and Bodin*, 2001; *Bodin et al.*, 2003].

The TDRW method is closely related to the continuous time random walk (CTRW) framework [*Montroll and Weiss*, 1965; *Scher and Lax*, 1973]. A CTRW describes the stochastic movement of particles as random walk in space and time. The CTRW approach has been used for the modeling of electron transport in disordered media *Scher and Lax* [1973], diffusion in

turbulence [*Zumofen and Klafter*, 1993], chemical transport in heterogeneous porous media, to name but a few, see also the exhaustive review paper by Berkowitz et al. *Berkowitz et al.* [2006]. It has been used successfully to model anomalous transport features in fluctuating environments. In this context it can be seen as an average transport framework that is based on the observation that, when looking at average Lagrangian transport dynamics, particles may need different times to cross the same distance, due to heterogeneous medium properties. Effective particle dynamics can be described as a CTRW. This is the reason why CTRW is often referred to as an ensemble averaged transport model. Strictly speaking, it is a model that describes particle movements as a random walk in space and time coordinates. As pointed out above, McCarthy [*McCarthy*, 1993] and Noetinger and Estebenet [*Noetinger and Estebenet*, 2000] refer to TDRW as a CTRW method because the time increment is random. The papers on TDRW, we reviewed above, propose a TDRW algorithm as an efficient solution methodology for the heterogeneous diffusion equation. However, in none of these papers, have we found a demonstration of the formal equivalence of the TDRW algorithm and the diffusion equation, as it exists for the equivalence of the diffusion equation (3.1) and the Langevin equation (3.2).

3.2.1 Theoretical Development

The solution of the diffusion equation in a classical RW scheme based on equation (3.2) can be very costly. In this section we present an efficient particle tracking scheme to solve flow in heterogeneous media.

In this section, we first consider a continuous time random walk (CTRW) [*Montroll and Weiss*, 1965; *Scher and Lax*, 1973; *Berkowitz et al.*, 2006] on an inhomogeneous spatial lattice, which is characterized by non-stationary spatial transition probabilities and space-dependent transition time distribution [*Berkowitz et al.*, 2002; *Goychuk*, 2004; *Chechkin et al.*, 2005]. We then show that the inhomogeneous CTRW with an exponential transition time distribution solves the discrete equations that describe diffusion in heterogeneous media. This demonstrates the equivalence of the time-domain random walk (TDRW) scheme, which was developed for the solution of heterogeneous diffusion problems [*McCarthy*, 1993; *Noetinger and Estebenet*, 2000; *Delay et al.*, 2002], and CTRW. Based on these results, we discuss an extension of the TDRW method for heterogeneous diffusion in combination with heterogeneous trapping properties.

3.2.1.1 Spatially Inhomogeneous CTRW

We consider a spatially inhomogeneous continuous time random walk (CTRW) [e.g., *Montroll and Weiss*, 1965; *Scher and Lax*, 1973] on a lattice defined by the following set of recursion equations

$$\mathbf{x}_i(n+1) = \mathbf{x}_j(n) + \boldsymbol{\xi}_{ij}, \qquad t_{n+1} = t_n + \theta_j, \tag{3.4}$$

where the position of lattice point j is denoted by $\mathbf{x}_j$. The probability for a spatial transition ξ_{ij} between points j and i (i.e. from j to i) is given by w_{ij}, the probability density of the random time increment θ_j depends on the position of the particle at step n. Its distribution is given by the transition time density $\psi_j(t)$. Equation (3.4) describes an inhomogeneous CTRW because the probabilities w_{ij} and $\psi_j(t)$ for spatial and temporal particle transitions depend on the particle positions within the lattice.

The particle density $g_i(t)$ at point i is defined by

$$g_i(t) = \left\langle \Delta[\mathbf{x}_i - \mathbf{x}_j(t)] \right\rangle. \tag{3.5}$$

The angular brackets denote the average over all particles that are launched in the random walk (3.4) and the function $\Delta[\mathbf{x}_i - \mathbf{x}_j(t)]$ is 1 if $\mathbf{x}_j(t) = \mathbf{x}_i$ and zero otherwise. The random walk (3.4) describes time as a stochastic process. The number of steps needed to reach time t is counted by the renewal process $n_t = \max(n|t_n \leq t)$. The number density $g_i(t)$ then reads in terms of the space-time particle trajectories (3.4) as

$$g_i(t) = \left\langle \Delta[\mathbf{x}_i - \mathbf{x}_j(n_t)] \right\rangle. \tag{3.6}$$

This expression can be expanded as

$$g_i(t) = \sum_{n=0}^{\infty} \left\langle \Delta[\mathbf{x}_i - \mathbf{x}_j(n)] \delta_{n,n_t} \right\rangle. \tag{3.7}$$

The statement $n = n_t$ is equivalent to $0 \leq t - t_n < \theta_i$. This condition can be expressed by the product of two Heaviside functions $H(\cdot)$. Thus, we can write $g_i(t)$ as

$$g_i(t) = \sum_{n=0}^{\infty} \left\langle \Delta[\mathbf{x}_i - \mathbf{x}_j(n)]\, H[(\theta_i - (t-t')]\, H(t-t') \right\rangle. \tag{3.8}$$

By inserting a Dirac-delta, we obtain

$$g_i(t) = \sum_{n=0}^{\infty} \int_0^t dt' \left\langle \Delta[\mathbf{x}_i - \mathbf{x}_j(n)]\delta(t' - t_n) \right\rangle \left\langle H(\theta_j - (t - t') \right\rangle . \tag{3.9}$$

We could break the noise average because of the Markovianity of the process (3.4). Executing the second average explicitly and defining $R_i(t) = \sum_{n=0}^{\infty} \left\langle \Delta[\mathbf{x}_i - \mathbf{x}_j(n)]\delta(t - t_n) \right\rangle$, we obtain

$$g_i(t) = \int_0^t dt' \mathcal{A}_i(t') \int_{t-t'}^{\infty} d\tau \psi_i(\tau). \tag{3.10}$$

The $\mathcal{A}_i(t)$ describes the probability per time for the particle to just arrive at $\mathbf{x}_i$ at time t. From the Markovianity of the process (3.4) we obtain for $R_i(t)$ that

$$\mathcal{A}_i(t) = \rho_i \delta(t) + \sum_{[ik]} w_{ik} \int_0^t dt' \psi_k(t - t') \mathcal{A}_k(t'), \tag{3.11}$$

with $\rho_i = g_i(t = 0)$ the initial particle density at point $\mathbf{x}_i$. Notice that (3.11) is a Chapman-Kolmogorov type equation that describes the probability to just arrive at $\mathbf{x}_i$ at time t as the sum over all possible transitions from a position $\mathbf{x}_k$ to $\mathbf{x}_i$ of duration $t - t'$. The notation $\sum_{[ik]}$ indicates summation over nearest neighbors of pixel i. Combination of (5.32) and (3.11) in Laplace space gives for the Laplace transform of $g_i(t)$ the well known generalized Master equation [e.g., *Kenkre et al.*, 1973]

$$\lambda g_i^*(\lambda) = \rho_i + \sum_{[ik]} \frac{w_{ik} \lambda \psi_k^*(\lambda)}{1 - \psi_k^*(\lambda)} g_k^*(\lambda) - \frac{\lambda \psi_i^*(\lambda)}{1 - \psi_i^*(\lambda)} g_i^*(\lambda). \tag{3.12}$$

The Laplace transform is defined in *Abramowitz and Stegun* [1965]. Here and in the following, Laplace transformed quantities are marked by an asterisk, the Laplace variable is denoted by λ.

3.2.1.2 Equivalence with Heterogeneous Diffusion

In order to establish the equivalence between the inhomogeneous CTRW detailed in in the previous section and the heterogeneous diffusion equation (3.1), we consider the exponential transition time density [*Berkowitz et al.*, 2006]

$$\psi_j(t) = \tau_j^{-1} \exp(-t/\tau_j). \tag{3.13}$$

Inserting the Laplace transform of (4.7) into (3.12) gives

$$\lambda g_i^*(\lambda) = \rho_i + \sum_{[ij]} w_{ij}\tau_j^{-1} g_k^*(\lambda) - \tau_i^{-1} g_i^*(\lambda). \tag{3.14}$$

Transforming this equation back to real time, we obtain the Master equation

$$\frac{\partial g_i}{\partial t} = \sum_{[ij]} w_{ij}\tau_j^{-1} g_j - \tau_i^{-1} g_i. \tag{3.15}$$

We now define the transition probabilities w_{ij} and transition times τ_j as

$$w_{ij} = \frac{b'_{ij}}{\sum_{[jk]} b'_{kj}}, \qquad \tau_j = \frac{1}{\sum_{[kj]} b'_{kj}}, \tag{3.16}$$

where the b'_{ij} are defined below. By definition the w_{ij} fulfill the normalization condition $\sum_{[ji]} w_{ij} = 1$. Inserting these definitions into (3.15), we obtain

$$\frac{\partial g_i}{\partial t} = \sum_{[ij]} b'_{ij} g_j - \sum_{[ki]} b'_{ki} g_i. \tag{3.17}$$

Notice that for $b'_{ij} = b'_{ji}$, this equation describes diffusion on a lattice with symmetric barriers [e.g., *Bouchaud and Georges*, 1990].

To establish the equivalence of the Master equation (3.17) and the diffusion equation (3.1), we need to further specify the b'_{ij} in terms of the retardation coefficient and diffusion coefficients. Thus, we define now

$$b'_{ij} = \frac{b_{ij}}{V_j R_j}, \qquad b_{ij} = \frac{S_{ij}\hat{D}_{ij}}{\xi_{ij}}, \tag{3.18}$$

where V_j and R_j are volume and retardation coefficient of pixel j, respectively, S_{ij} denotes the surface area between pixels i and j and $\hat{D}_{ij}$ is an average diffusion coefficient between pixels i and j, see Section 3.2.2.1. Notice that the b_{ij} are symmetric by definition, while the b'_{ij} and thus the transition probabilities w_{ij} are in general not. Furthermore, we define the rescaled particle density

$$c_i = \frac{g_i}{V_i R_i}. \tag{3.19}$$

Inserting (5.14) and (3.19) into (3.17) gives

$$V_i R_i \frac{\partial c_i}{\partial t} = \sum_{[ij]} b_{ij} c_j - \sum_{[ij]} b_{ij} c_i. \tag{3.20}$$

This equation together with definition (5.14) of the b_{ij} corresponds to a finite volume discretization of (3.1) as outlined for example in *Delay et al.* [2002]. The quantity c_i is identified with the solute concentration in the fluid phase. Thus, in the limit $\xi_{ij} \to 0$, we obtain the heterogeneous diffusion equation (3.1). This establishes the equivalence between (3.1) and the CTRW scheme (3.4) for the transition probabilities w_{ij} and mean transition times τ_j defined as

$$w_{ij} = \frac{b_{ij}}{\sum_{[jk]} b_{kj}}, \qquad \tau_j = \frac{V_j R_j}{\sum_{[kj]} b_{kj}}, \tag{3.21}$$

where we used (5.14) in (3.16). Notice that the random walk algorithm based on (3.4) and (3.16) for the exponential $\psi_i(t)$ (4.7) is identical to the time domain random walk (TDRW) presented by *Delay et al.* [2002]. Delay et al. *Delay et al.* [2002] deduced the exponential transition time distribution (4.7) by interpreting (3.20) in terms of single particle transitions. This explicit demonstration, removes ambiguity with respect to the distribution of transition times.

3.2.1.3 Heterogeneous Diffusion With Multirate Mass Transfer (MRMT)

In the previous section we established the equivalence between the spatially discrete heterogeneous diffusion equation (3.1) and the inhomogeneous CTRW (3.4) with (4.7) and (3.21), or in other words, a TDRW. Here we consider the generalization of this framework to heterogeneous diffusion combined with multirate mass transfer (MRMT). The MRMT approach [e.g., *Haggerty and Gorelick*, 1995; *Carrera et al.*, 1998] describes transport in the presence of traps, or immobile zones, in which the solute can be immobilized for a certain amount of time. The trapping mechanisms may be chemical such as adsorption, or physical, such as very slow diffusion. It has been shown in Refs. [*Dentz and Berkowitz*, 2003] and [*Benson and Meerschaert*, 2009] that the CTRW and multirate mass transfer modeling approaches are equivalent under certain conditions. Thus, based on these results and on the observation that a TDRW describes an inhomogeneous CTRW, we develop in the following a TDRW approach that models particle transport in heterogeneous media under spatially varying diffusion and trapping properties.

As in the previous section, we start with the formulation of MRMT as an inhomogeneous CTRW. We then consider the corresponding generalized Master equation and establish the

equivalence to the spatially heterogeneous diffusion equation with spatially variable mass transfer. Linear multirate sorption-desorption and in general linear multirate mass transfer can be modeled in the framework of CTRW by introducing a trapping time distribution $p(t)$ [e.g., *Margolin et al.*, 2003]. The particle transition time then is given by the time spent in the mobile domain and the sum of trapping times during a transition. The transition time distribution $\psi(t)$ with traps then is given in terms of the transition time distribution $\psi_0(t)$ without traps as [*Margolin et al.*, 2003]

$$\psi^*(\lambda) = \psi_0^*\left(\lambda + \alpha\left[1 - p^*(\lambda)\right]\right), \tag{3.22}$$

in which α is the trapping frequency during a transition. Benson and Meerschaert *Benson and Meerschaert* [2009] studied the case for which the transition time without traps is exponentially distributed using random walk particle tracking. A similar approach was used by Delay and co-workers [*Delay and Bodin*, 2001; *Delay et al.*, 2008] to extend the TDRW method to account for matrix diffusion in the context of transport in fractured media.

Here, we consider the general case that the trapping time distribution $p_j(t)$ and trapping frequency α_j depend on position. Using the Laplace transform of the exponential distribution (4.7) for $\psi_0^*(t)$ in (3.22), we obtain for the $\psi_j(t)$ of heterogeneous diffusion and MRMT the expression

$$\psi_j^*(\lambda) = \frac{1}{1 + \lambda\tau_j + \alpha_j\tau_j[1 - p_j^*(\lambda)]}. \tag{3.23}$$

Inserting this explicit form in the generalized Master equation (3.12) gives

$$\begin{aligned}\lambda g_i^*(\lambda) = \rho_i + \sum_{[ik]} \frac{w_{ik}\lambda g_k^*(\lambda)}{\lambda\tau_k + \alpha_k\tau_k[1 - p_k^*(\lambda)]} \\ - \frac{\lambda g_i^*(\lambda)}{\lambda\tau_i + \alpha_i\tau_i[1 - p_i^*(\lambda)]}.\end{aligned} \tag{3.24}$$

In order to obtain the partial differential equation that governs transport under heterogeneous MRMT, we identify the w_{ik} in (3.24) with

$$w_{ik} = \frac{b_{ik}\tau_k}{V_k R_k}, \tag{3.25}$$

where we used (3.16) and (5.14). Furthermore, we set $g_i = R_i V_i c_i$, see (3.19). Thus, we can

rewrite (3.24) as

$$\lambda R_i V_i c_i^*(\lambda) = R_i V_i c_i(t=0) + \sum_{[ik]} b_{ik} \frac{\lambda c_k^*(\lambda)}{\lambda + \alpha_k[1 - p_k^*(\lambda)]} - \sum_{[ik]} b_{ik} \frac{\lambda c_i^*(\lambda)}{\lambda + \alpha_i[1 - p_i^*(\lambda)]} \tag{3.26}$$

As in the previous, we obtain in the limit $\xi_{ij} \to 0$ the spatially continuous equation

$$R(\mathbf{x})\lambda c^*(\mathbf{x},\lambda) - \nabla \cdot D(\mathbf{x})\nabla \mu^*(\mathbf{x},\lambda) c^*(\mathbf{x},\lambda) = R(\mathbf{x}) c(\mathbf{x}, t=0), \tag{3.27}$$

in which we defined the memory function

$$\mu^*(\mathbf{x},\lambda) = \frac{\lambda}{\lambda + \alpha(\mathbf{x})[1 - p^*(\mathbf{x},\lambda)]}. \tag{3.28}$$

In real time, we obtain from (3.27) by inverse Laplace transform the non-local heterogeneous diffusion problem

$$R(\mathbf{x}) \frac{\partial c(\mathbf{x},t)}{\partial t} = \nabla \cdot D(\mathbf{x}) \nabla \int_0^t dt' c(\mathbf{x},t') \mu(\mathbf{x}, t-t'). \tag{3.29}$$

This equation models heterogeneous diffusion together with heterogeneous multirate mass transfer. In this context, considering $R(\mathbf{x}) = \phi(\mathbf{x})$, with $\phi(\mathbf{x})$ porosity, the mobile solute concentration $c_m(\mathbf{x},t)$ is defined as [*Dentz and Berkowitz*, 2003]

$$c_m(\mathbf{x},t) = \int_0^t dt' c(\mathbf{x},t') \mu(\mathbf{x}, t-t'). \tag{3.30}$$

The porosity $\phi(\mathbf{x})$ now is divided into the mobile and immobile porosities, $\phi_m(\mathbf{x})$ and $\phi_{im}(\mathbf{x})$, respectively, such that $\phi(\mathbf{x})c(\mathbf{x},t) = \phi_m(\mathbf{x})c_m(\mathbf{x},t) + \phi_{im}(\mathbf{x})c_{im}(\mathbf{x},t)$. The immobile concentration is denoted by $c_{im}(\mathbf{x},t)$. We consider a scenario for which the solute is initially distributed in the mobile domain. Thus, by inserting the Laplace transform of (3.30) into (3.27) gives for the mobile concentration

$$\frac{\phi(\mathbf{x})}{\mu^*(\mathbf{x},\lambda)} \lambda c_m^*(\mathbf{x},\lambda) - \nabla \cdot D(\mathbf{x}) \nabla c_m^*(\mathbf{x},\lambda) = \phi_m(\mathbf{x}) c_m(\mathbf{x}, t=0), \tag{3.31}$$

where the right side reflects the fact that initially there is only solute in the mobile domain.

We now establish the relation between the memory function $\mu(\mathbf{x},t)$ and the transfer function $\varphi(\mathbf{x},t)$ given within the context of MRMT. The MRMT approach gives the following non-local transport equation for the mobile concentration [e.g., *Carrera et al.*, 1998; *Haggerty et al.*, 2000]

$$\phi_m(\mathbf{x})\frac{\partial c_m(\mathbf{x},t)}{\partial t} + \phi_{im}(\mathbf{x})\frac{\partial}{\partial t}\int_0^t dt'\,\varphi(\mathbf{x},t-t')c_m(\mathbf{x},t') = \nabla\cdot D(\mathbf{x})\nabla c_m(\mathbf{x},t). \tag{3.32}$$

The difference to the formulations given in Refs. *Carrera et al.* [1998]; *Haggerty et al.* [2000] are due to the non-zero initial condition employed here. The site-dependent transfer function $\varphi(\mathbf{x},t)$ encodes the details of the microscopic mass transfer mechanisms between the mobile and immobile regions [e.g., *Harvey and Gorelick*, 1995; *Dentz and Berkowitz*, 2003]. Comparing the Laplace transform of (3.32) with (3.31) gives the following relation between the memory function $\mu^*(\mathbf{x},\lambda)$ and the transfer function $\varphi^*(\mathbf{x},\lambda)$

$$\mu^*(\mathbf{x},\lambda) = \frac{\phi(\mathbf{x})}{\phi_m(\mathbf{x}) + \phi_{im}(\mathbf{x})\varphi^*(\mathbf{x},\lambda)}. \tag{3.33}$$

For the relation between the Laplace transforms of the transfer function, $\varphi^*(\mathbf{x},\lambda)$, and the trapping time distribution, $p^*(\mathbf{x},\lambda)$, we obtain by using (3.28)

$$\varphi^*(\mathbf{x},\lambda) = \frac{\phi(\mathbf{x})}{\phi_{im}(\mathbf{x})} - \frac{\phi_m(\mathbf{x})}{\phi_{im}(\mathbf{x})} + \frac{\alpha(\mathbf{x})\phi(\mathbf{x})}{\phi_{im}(\mathbf{x})\lambda}\left[1 - p^*(\mathbf{x},\lambda)\right]. \tag{3.34}$$

3.2.2 Model Setup and Numerical Implementation

We consider diffusion in the d-dimensional domain Ω with the $(d-1)$-dimensional boundaries B_Ω. In the following we use regular meshes in $d = 2$ and $d = 1$ spatial dimensions. Consequently the internodal distance is $\xi_{ij} = \xi$ is constant. Thus, the interfacial area S_{ij} between the pixels i and j is constant and given by $S = \xi^{d-1}$ and so is the volume of the pixel, $V_i = V = \xi^d$. The normalized transition probability w_{ij} from position j to position i is given by (5.14).

No flow boundary conditions are treated as a zero diffusion limit ($w_{ij} = 0$). Dirichlet boundary conditions at the inlet $B_\Omega^{in} \subset B_\Omega$ (constant concentration) are implemented as described in the following. The inlet B_Ω^{in} is formed by P_{in} pixels. At each of these pixels the concentration is constant, $c_i = c^{in}$ for $i = 1,\ldots,P_{in}$. Note that for $d = 1$ spatial dimension $P_{in} = 1$. In the numerical particle tracking simulations, however, we do not prescribe the

concentration at the inlet boundary, but the number of particles at each node. Therefore, we consider the number density g_i given by (3.19). Its values at the boundary nodes is given by $g_i^{in} = R_i V c^{in}$. Since the g_i are in general not normalized, we define now the normalized number density as

$$n_i = \frac{g_i}{\sum_{j=1}^{P_{in}} g_j^{in}} = \frac{R_i c_i}{c^{in} \sum_{j=1}^{P_{in}} R_j}. \tag{3.35}$$

This is the observable that we obtain from the TDRW simulations, namely n_i is equal to the number N_i of particles in the pixel normalized by the number of particles N on the boundary, $n_i = N_i/N$. Thus, the concentration c_i at pixel i is given in terms of the n_i as

$$c_i = n_i \frac{c^{in} \sum_{j=1}^{P_{in}} R_j}{R_i}. \tag{3.36}$$

The number N_i^{in} of particles at the boundary pixels then are given by

$$N_i^{in} = N \frac{R_i}{\sum_{j=1}^{P_{in}} R_j} \tag{3.37}$$

for $i = 1, \ldots, P_{in}$.

An absorbing boundary condition (zero concentration) at the outlet boundary $B_\Omega^{out} \subset \Omega$ is implemented by removing particles as they cross B_Ω^{out}. The outlet boundary is formed by P_{out} pixels. Note that $P_{out} = 1$ in $d = 1$ spatial dimension. The cumulative distribution of arrival times $F(t)$ at the outlet boundary then is given by

$$F(t) = \frac{1}{N} \sum_{j=1}^{P_{out}} N_j(t), \tag{3.38}$$

where $N_j(t)$ is the number of particles that have crossed the outlet boundary until time t. Correspondingly, the distribution density of arrival times, $f(t)$, is

$$f(t) = \frac{1}{N} \sum_{j=1}^{P_{out}} \frac{\Delta N_j(t)}{\Delta t}, \tag{3.39}$$

where $\Delta N_j(t)$ is the number of particles that crosses the outlet during the sampling interval $[t, t + \Delta t]$.

3.2.2.1 Interpixel Diffusion Coefficients

In Section 3.2.1.2, we left intentionally open how to choose the interpixel diffusion coefficients $\hat{D}_{ij}$. Frequently, it is determined as the harmonic average between the diffusion coefficient in adjacent pixels [e.g., *Delay et al.*, 2002]. Here we want to compare the performance of different choices for the interpixel diffusion coefficient.

To this end, we consider diffusion in a two-dimensional domain of length $L = 10^2\xi$ and width $d = 50\xi$. It is characterized by a spatially varying diffusion coefficient $D(\mathbf{x})$ and constant retardation $R(\mathbf{x}) = R = 1$. The heterogeneous domain is generated by assigning to each pixel in the domain randomly diffusion coefficients that are chosen independently, from a lognormal distribution characterized by the geometric average $D_G = 0.5$ and variance of $\ln D$ given by $\sigma^2_{\ln D} = 1$. We record the vertically averaged concentration close to the outlet at $x_1 = 90\xi$ and compare it to the analytical solution for the equivalent homogeneous problem. Specifically, we consider the case of an instantaneous solute pulse at the inlet boundary at $x_1 = 0$. The position vector here is $\mathbf{x} = (x_1, x_2)^T$.

It was shown by *Matheron* [1967] that the exact effective diffusion coefficient D^e for this setup is given by the geometric mean $D^e = D_G$ of the lognormally distributed $D(\mathbf{x})$. Thus, the equivalent homogeneous diffusion problem for $c(x_1, t) = d^{-1}\int_0^d dx_2 c(\mathbf{x}, t)$ is one-dimensional and characterized by the geometric mean diffusion coefficient D_G,

$$\frac{\partial c(x_1,t)}{\partial t} - D_G \frac{\partial^2 c(x_1,t)}{\partial x_1^2} = 0, \tag{3.40}$$

with the initial condition $c(x_1, t = 0) = 0$. The boundary condition at the outlet is $c(L, t) = 0$, the one at the inlet is $c(0, t) = j_0\delta(t)$. The solute flux j_0 is given by $j_0 = c_0\tau_p$ with c_0 the concentration on the inlet boundary and τ_p the pulse duration. The analytical solution for $c(x_1, t)$ then is given by [e.g., *Carslaw and Jaeger*, 1947]

$$c(x_1,t) = j_0 \frac{2D_G\pi}{L^2} \sum_{n=1}^{\infty} n \sin\left(\frac{n\pi x_1}{L}\right) \exp\left(-\frac{n^2 D_G \pi^2 t}{L^2}\right), \tag{3.41}$$

In the following $d = 2$ dimensional numerical simulations, we apply the concentration $c_0 = 1/\xi^2$. The pulse duration τ_p is given by the mean diffusion time over one pixel $\tau_p = \xi^2/(2D_G)$. Thus, we have $j_0 = 1/(2D_G)$. At the horizontal boundaries at $x_2 = 0$ and $x_2 = d$ no-flux boundary conditions are specified. The domain size is $L = 10$ m.

We compare this analytical solution for the exact average diffusion problem (3.40) to the

outcome of the corresponding TDRW simulations for two difference choices of the interpixel diffusion coefficient, namely (i) the harmonic mean and (ii) the geometric mean of the diffusion coefficients in adjacent pixels. The choice that yields the best comparison with the exact average solution will be employed in the following numerical simulations.

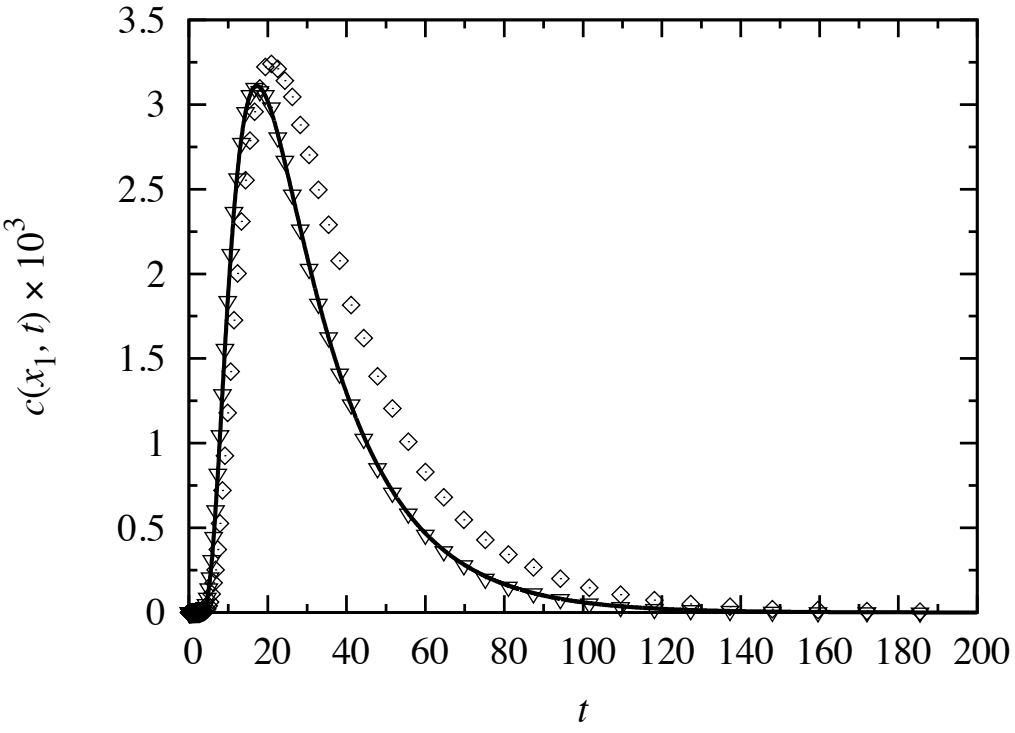

Figure 3.2: *Vertically averaged concentration at $x = 9$ m for diffusion in a heterogeneous medium characterized by a log-normally distributed diffusion coefficient. Comparison of the numerical solutions for interpixel diffusion coefficients given by the (squares) harmonic and (triangles) geometric mean, and the (solid line) analytical solution* (3.41) *with $D_G = 0.52\ m^2 s^{-1}$, and $L = 10$ m. The number of pixels used in the TDRW simulation in horizontal direction is 10^2 and in vertical direction* 50*. The simulations were performed using $N = 5 \times 10^8$ particles.*

Figure 3.2 displays the vertically averaged and normalized concentration $c_L(t)$ close to the outlet boundary at $L = 90\xi$ obtained from the TDRW simulation for the two different interpixel diffusion coefficients. It is compared to $c(x_1, t)$ for the equivalent homogeneous medium given by (3.41) with $D_G = 0.52$. We observe that the interpixel diffusion coefficient given by the geometric mean gives the best agreement with the analytical solution. Therefore, in the following $d = 2$ dimensional TDRW simulations we will employ the geometric mean for the interpixel diffusion coefficients

$$\hat{D}_{ij} = \sqrt{D_i D_j}. \tag{3.42}$$

Note that it is beyond the scope of the present paper to demonstrate that it is the best approximation for non-lognormal distributions or for three-dimensional transport. This issue is in fact not specific to the TDRW approach but concerns all discretized methods applied to heterogeneous diffusion problems.

For the $d = 1$ dimensional TDRW simulations presented in the following, the interpixel diffusion coefficient is given by the harmonic mean

$$\hat{D}_{ij} = D_H = 2\frac{D_i D_j}{D_i + D_j}. \tag{3.43}$$

The pulse duration τ_p is as above given by the mean diffusion time over one pixel $\tau_p = \xi^2/(2D_H)$, the boundary concentration, however, is $c_0 = 1/\xi$. Thus, for $d = 1$ we have $j_0 = \xi/(2D_H)$.

Also note that the setup considered here corresponds to a pulsed through diffusion test. Diffusion experiments (or through diffusion tests) are widely used for measuring the effective diffusion of low permeability porous media, such as manufactured cements or consolidated argillaceous formations considered as potential host rock for radioactive waste repositories [*Wittebroodt et al.*, 2008]. At the laboratory scale such experiments consist in applying a constant concentration gradient across a thin core of rock by maintaining constant concentration at the two edges (usually a zero concentration at the outlet) and recording the solute flux at the outlet [*Pabitra*, 2004].

3.2.2.2 Heterogeneous Diffusion

The heterogeneous diffusion problem (3.1) is solved using the random walk particle tracking scheme (3.4) with the transition time density (4.7) and the transition probabilities w_{ij} and the mean transition time τ_j given by (3.21). The transport time is updated for each particle transition according to

$$t_{n+1} = t_n + \theta_j, \qquad \theta_j = -\tau_j \ln(\eta_n), \tag{3.44}$$

where the random variable η_n is uniformly distributed in $[0, 1]$.

3.2.2.3 Diffusion with Multirate Mass Transfer

In Section 3.2.1.3, we showed that MRMT can be modeled in the TDRW context by introducing particle traps characterized by a given distribution of trapping times. The resulting TDRW-MRMT model is implemented following Ref. [*Benson and Meerschaert*, 2009]. First, we note that the transition time θ_j, which is distributed according to (4.7), measures the total time the particle is mobile. During this mobile time, the particle can get trapped at the constant rate α_j, see Section 3.2.1.3. The times the particle are mobile between trapping events is denoted by $\hat{\theta}_j$. Since trapping occurs at constant rate, $\hat{\theta}_j$ is exponentially distributed

$$p_{mj}(t) = \alpha_j \exp(-\alpha_j t). \tag{3.45}$$

The number of trapping events that actually occur during a mobile transition of time θ_j, n_{θ_j}, is the random number that fulfills

$$n_{\theta_j} = \max\left(n \left| \sum_{l=1}^{n} \hat{\theta}_{jl} \leq \theta_j < \sum_{l=1}^{n+1} \hat{\theta}_{jl} \right. \right). \tag{3.46}$$

It is a renewal process, and specifically, for the exponential distribution (3.45), it is a Poisson process. The distribution $p_n(n|\theta_j)$ of n_{θ_j} thus is given by the Poisson distribution

$$p_n(n|\theta_j) = \frac{(\alpha_j \theta_j)^n}{n!} \exp(-\alpha_j \theta_j). \tag{3.47}$$

The unconditional distribution of the number of trapping events at pixel j then is given by

$$p_{n_j}(n) = \int_0^\infty dt \psi_j(t) p_n(n|t) = \frac{n(\alpha_j \tau_j)^n}{(\alpha_j \tau_j + 1)^{n+1}}, \tag{3.48}$$

in which we used (4.7) for $\psi_j(t)$. Thus, the mean number of trapping events $\overline{n}_j$ at pixel j is given by $\overline{n}_j = \alpha_j \tau_j$. The overbar in the following denotes the noise average over all particles. The spatial average of the mean numbers of trapping events per pixel is $N_{\text{trap}} = \langle \overline{n}_j \rangle$. The spatial average over all pixels is denoted by angular brackets.

In general, the trapping rate α_j is spatially distributed and can be considered as a property of the heterogeneous medium. For the following analysis, we correlate the trapping rate to porosity $\phi(\mathbf{x})$ that we substitute instead of the generic retardation coefficient $R(\mathbf{x})$ and assume that the noise mean number of traps at pixel j is inversely proportional to porosity,

$\overline{n}_j = A\phi_j^{-1}$ with A a constant of proportionality. This relates the trapping rate α_j to porosity as $\alpha_j = A/(\phi_j\tau_j)$. Note also that the spatial average number of trapping events under this assumption is given by $N_{\text{trap}} = A/\phi_H$, where ϕ_H is the harmonic mean of porosity over all locations. Thus, we can express the proportionality constant A in terms of the average number of traps per pixel, N_{trap}, as $A = N_{\text{trap}}\phi_H$ and therefore set

$$\alpha_j = \frac{N_{\text{trap}}\phi_H}{\tau_j\phi_j}, \qquad \overline{n}_j = N_{\text{trap}}\frac{\phi_H}{\phi_j}. \tag{3.49}$$

We now can determine the total transition time, denoted by Θ_j. It is given by the sum of the total mobile time θ_j at pixel j and the sum over the trapping times, denoted here by ϑ_j,

$$\Theta_j = \theta_j + \sum_{l=1}^{n_{\theta_j}} \vartheta_{jl}, \tag{3.50}$$

where n_{θ_j} is given by (3.46). Note that the sum on the right hand side denotes a compound Poisson process. Time now is updated by

$$t_{n+1} = t_n + \Theta_j. \tag{3.51}$$

3.2.3 Numerical Simulations

As mentioned in the Introduction, there are many processes driven by diffusive transport in media displaying heterogeneous diffusion properties. Here, we focus on the diffusion of solute in porous media. Furthermore, in the following we will assume for simplicity that $D(\mathbf{x}) = \phi(\mathbf{x})D_0$ where D_0 is the coefficient for free diffusion in water. More general formulations such as $D(\mathbf{x}) = \phi(\mathbf{x})^n D_0$ as proposed by [*Gouze et al.*, 2008b] can be implemented easily, as well as the assumption that $\phi(\mathbf{x})$ and $D(\mathbf{x})$ are independent.

3.2.3.1 Heterogeneous Diffusion in Porous Media

We consider a scenario which corresponds to a pulse diffusion test which allows to deduce the distribution of residence times in a heterogeneous rock sample.

The transfer function $\varphi(t)$ for a low permeability rock sample is of central concern for transport modeling in the framework of multirate mass transfer, see Section 3.2.1.3. It is related to the distribution of residence times $p(t)$ through expression (3.34). For purely diffusive mass transfer between a mobile region and immobile regions, which in general is characterized by

heterogeneous diffusion properties, the transfer function $\varphi(t)$ encodes the fraction of rock matrix containing connected micro-porosity or inter-grain porosity as well as stagnant and trapped water [*Gouze et al.*, 2008b]. The transfer function integrates, by definition, all the information on the geometry and the heterogeneous diffusion properties of the immobile domain as well as its accessibility to tracer particles from the mobile domain (this means, the properties of the mobile-immobile interfacial area). Therefore, for a given value of D_0, the memory function can be considered as an intrinsic property of the rock characterizing its immobile fraction. Gouze et al. [*Gouze et al.*, 2008b] showed that the parameters necessary for characterizing diffusion in the 3D immobile domain, i.e., mainly the porosity distribution and the boundary geometry, can be extracted from X-ray microtomography.

By definition, the transfer function is related to the probability that a tracer particle entering the immobile zone at $t = 0$ remains in it until time t [*Haggerty et al.*, 2004], see also (3.34). Consequently, computing the memory function with the TDRW method consists in applying an instantaneous solute pulse at the mobile-immobile interface and record the residence time of the particles that enter the immobile domain. As the immobile domain geometry is very complex (both in terms of boundary conditions and diffusion coefficient variability within the immobile domain) computations in $d = 3$ spatial dimensions for pertinent representative elementary volumes (order of 10^6 voxels) are usually prohibitive using standard random walk methods with constant time increments. The TDRW method provides an efficient alternative. Two examples of computed memory functions are given in Figure 3.3. The first one concerns the memory function of a sphere of constant porosity for which the analytical solution is known [*Carrera et al.*, 1998]. In this case we obtain a memory function characterized by a power-law tail $\varphi(t) \propto t^{-\beta}$ with exponent $\beta = 1/2$. The second example calculates the memory function for a natural rock sample (limestone). Figure 3.3 illustrates the long-time tail of $\varphi(t)$ associated with the natural rock denoting the strong retention of the particles in the immobile domain triggered by the tortuosity and the variability of the diffusion paths. In this case we obtain a memory function with exponent $\beta = 1.1$.

3.2.3.2 Diffusion with Multirate Mass Transfer

Here we consider the diffusion model combined with multirate mass transfer as described in Sections 3.2.1.3 and 3.2.2.3. For computational simplicity, we consider a $d = 1$ dimensional

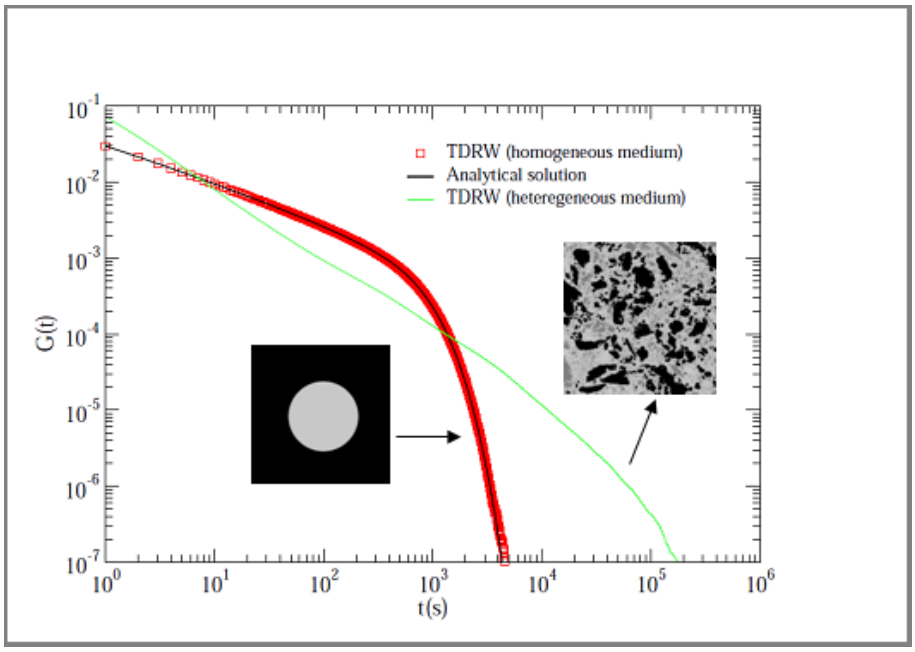

Figure 3.3: *Residence time distribution $\varphi(t)$ for a homogeneous sphere, and for a heterogeneous limestone sample as obtained from the TDRW simulation.*

setup. In the absence of traps, diffusion is described by

$$\phi(x)\frac{\partial c(x,t)}{\partial t} - \frac{\partial}{\partial x}\phi(x)D_0\frac{\partial}{\partial x}c(x,t) = 0. \tag{3.52}$$

The equivalent homogeneous model is given by

$$\phi_A\frac{\partial \bar{c}(x,t)}{\partial t} - \frac{\partial}{\partial x}\phi_H D_0\frac{\partial}{\partial x}\bar{c}(x,t) = 0, \tag{3.53}$$

see C.1.

The domain is initially solute free. We consider as boundary conditions a solute pulse at the inlet, $c(0,t) = j_0\delta(t)$, and zero concentration at the outlet at $x = L$, $c(L,t) = 0$.

The heterogeneous diffusion problem (3.52) is non-dimensionalized by setting $x = \tilde{x}L$, $t = \tilde{t}\tau_L$ and $c(x,t) = \tilde{c}(x/L, t/\tau_L)j_0/\tau_L$, where $\tau_L = L^2/D_0$. Thus, we obtain from (3.52)

$$\phi(\tilde{x})\frac{\partial \tilde{c}(\tilde{x},\tilde{t})}{\partial \tilde{t}} - \frac{\partial}{\partial \tilde{x}}\phi(\tilde{x})\frac{\partial}{\partial \tilde{x}}\tilde{c}(\tilde{x},\tilde{t}) = 0. \tag{3.54}$$

The non-dimensional inlet boundary condition is given by $\tilde{c}(\tilde{x} = 0, \tilde{t}) = \delta(\tilde{t})$. In the following, all quantities are non-dimensional, the tildes are omitted for simplicity of notation.

The mass transfer properties in the following are assumed to be uniform, that is, the

trapping time ϑ_j is independent of the pixel position, $\vartheta_j = \vartheta$, and therefore $p_j(t) = p(t)$. For illustration, we consider a (truncated) Pareto distribution for the trapping times, which can account for the occurrence of a broad distribution of heterogeneity length scales,

$$p(t) = \frac{\beta}{t_1[1-(t_1/t_2)^\beta]} \left(\frac{t}{t_1}\right)^{-1-\beta}, \qquad t_1 < t < t_2. \tag{3.55}$$

The median time scale t_1 is related to the smallest, the cut-off time t_2 to the largest heterogeneity feature. For this $d = 1$ dimensional scenario the transport equation (3.29) simplifies to

$$\phi(x)\frac{\partial c(x,t)}{\partial t} = \frac{\partial}{\partial x}\phi(x)\frac{\partial}{\partial x}\int_0^t dt' c(x,t')\mu(x,t-t'), \tag{3.56}$$

where the memory function $\mu(x,t)$ is given in Laplace space by, see (3.28),

$$\mu^*(x,\lambda) = \frac{\lambda}{\lambda + \alpha(x)[1-p^*(\lambda)]}. \tag{3.57}$$

The trapping rate $\alpha(x)$ depends on porosity as given by (3.49).

For the numerical simulations presented in the following, the domain is discretized into 10^2 pixels. For the simulations of heterogeneous diffusion, porosity values are assigned randomly to each pixel according to a truncated Gaussian distribution,

$$p_\phi(f) = A_\phi^{-1}\Theta(f-\phi_b)\Theta(\phi_t - f)\frac{\exp\left[-\frac{(f-\phi_A)}{2\sigma_\phi^2}\right]}{\sqrt{2\pi\sigma_\phi^2}}, \tag{3.58}$$

in which the normalization constant A_ϕ is given by

$$A_\phi = \int_{\phi_b}^{\phi_t} df \frac{\exp\left[-\frac{(f-\phi_A)}{2\sigma_\phi^2}\right]}{\sqrt{2\pi\sigma_\phi^2}}. \tag{3.59}$$

The lower cut-off of the porosity distribution is set to $\phi_b = 0.2$, the upper cut-off to $\phi_t = 0.8$. The standard deviation is set to $\sigma_\phi = 0.2$. The median time scale t_1 in (3.55) is set to $t_1 = 2.5 \times 10^{-3}$.

Figure (3.4) illustrates the evolution of concentration at $x_1 = 0.1$, $x_2 = 0.5$ and $x_3 = 0.9$ for the heterogeneous model without traps and the equivalent homogeneous model, which

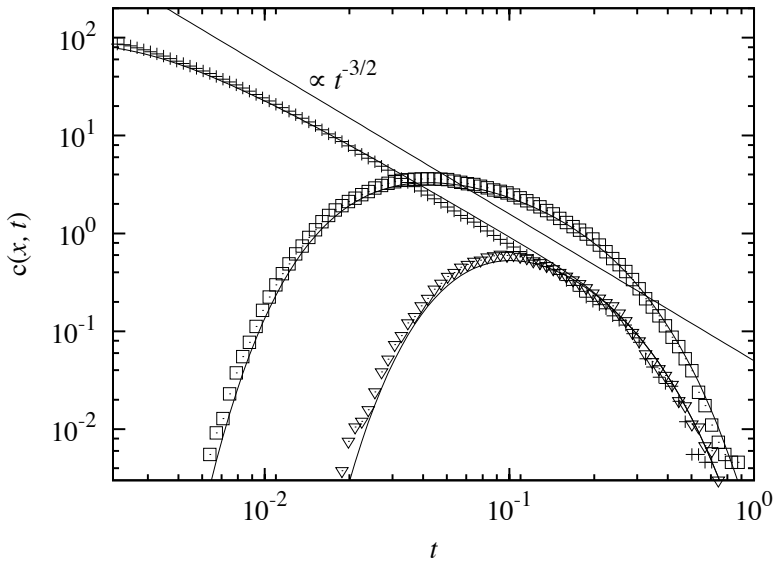

Figure 3.4: *Evolution of solute concentration in an heterogeneous $d = 1$ dimensional domain at three different observation points: $x = 0.1$ (crosses), $x = 0.5$ (squares), and $x = 0.9$ (triangles), compared with solution* (3.41) *of the equivalent homogeneous model* (3.53) *with $\phi_A = 0.48$ and $\phi_H = 0.43$.*

is characterized by the arithmetic and harmonic averages of the porosity values within the domain, see (3.53) and C.1. Close to the inlet boundary at x_1, we observe an intermediate time regime characterized by a power-law $c(x_1, t) \propto t^{-\gamma}$ with exponent $\gamma = 3/2$. This behavior is characteristic for diffusion in a homogeneous semi-infinite medium, which is a valid approximation far away from the outlet boundary. In fact, in the time regime $x^2 \ll t \ll 1$, the solution of (3.53) can be approximated by (see B.2)

$$c(x,t) = \frac{x \exp\left(-\frac{x^2\phi_A}{4\phi_H t}\right)}{\sqrt{4\pi\phi_A/\phi_H}\, t^{-3/2}}, \tag{3.60}$$

which gives the observed $t^{-3/2}$ behavior. The characteristic power-law can only be observed in the intermediate regime $x^2 \ll t \ll 1$. The lower bound denotes the typical non-dimensional diffusion time to arrive at x, while the upper bound, 1, is the non-dimensional diffusion time to the outlet boundary. Thus, at times larger than 1 particles leave the system at the absorbing boundary at $x = 1$ and the approximation of a semi-infinite medium does not hold anymore. This explains the breakdown of the power-law behavior, that is the cut-off, at time 1. For x_1, this regime is well developed. For increasing x, this regime shrinks and no power-law behavior is observable.

Figure 3.5 shows the evolution of the solute concentration $c(x_1, t)$ with time at $x_1 = 0.1$,

$x_2 = 0.2$ in the presence of traps ($N_{\text{Trap}} = 3$) with $\beta = 2/5$ in (3.55) and cut-off times of $t_2 = 1$, $t_2 = 10^3$, $t_2 = 10^7$, $t_2 = 10^{10}$ and $t_2 = \infty$. The peak times are shifted to significantly larger times compared to the case without traps. The time evolution of concentration is cut-off now at a scale t_c that is given by the trapping rate α, (3.49), and the mean trapping time $\bar{t}$, $t_c \approx \alpha \bar{t}$. The trapping rate α here is of the order of 10^4. This behavior is discussed in C.1 for an equivalent homogeneous case. For $t_2 = 1$, the mean trapping time $\bar{t} \approx 0.4$, and thus the cut-off time is of the order of $t_c \approx 10^3$. The cutoff time t_2 here is much smaller than t_c, $t_2 \ll t_c$. Thus, we can still observe the characteristic $t^{-3/2}$ behavior in the time regime $t_2 \ll t \ll t_c$ because in this regime, concentration behaves essentially like in the case without traps, but characterized by a renormalized diffusion coefficient, see B.2.

As t_2 increases, this behavior changes. The peak of $c(x,t)$ becomes wider and $c(x,t)$ decreases with a flatter slope. As long as the cut-off time is smaller than t_c, the evolution of $c(x,t)$ is essentially truncated at t_c.

In the case of a pure power-law, that is $t_2 = \infty$, a persistent power-law regime develops at asymptotically long times for $t \gg t_1 \alpha^{1/\beta}$, where α is the trapping rate, see B.2. In this regime $c(x,t)$ behaves as $c(x,t) \propto t^{-\beta}$. In the case of a finite truncation time t_2, an intermediate

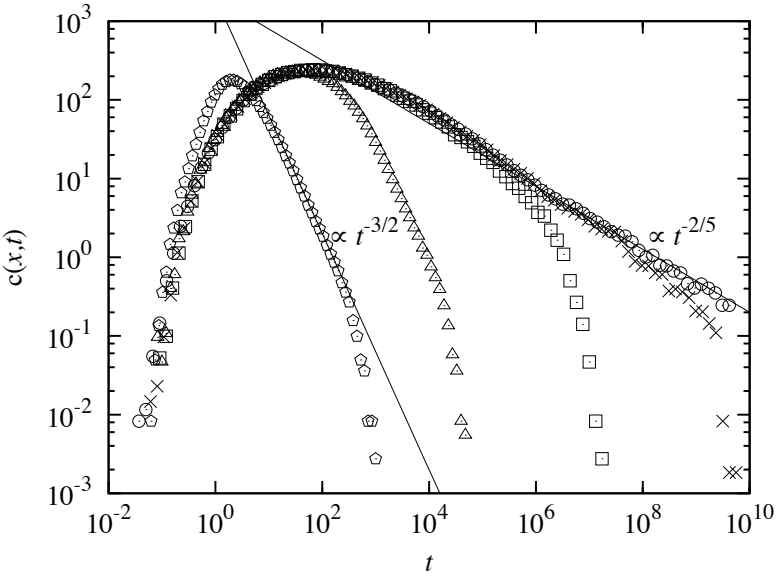

Figure 3.5: *Evolution of solute concentration in an heterogeneous $d = 1$ dimensional at $x = 0.1$ for the truncated power-law trapping time distribution* (3.55) *with $\beta = 0.4$ for cut-off times of (pentagons) $t_1 = 1$, (triangles) $t_1 = 10^3$, (squares) $t_1 = 10^7$, (crosses) $t_2 = 10^{10}$ and (circles) $t_2 = \infty$.*

power-law regime develops if $t_2 \gg t_1 \alpha^{1/\beta} \gg t_1$. For this scale order the power-law behavior $c(x,t) \propto t^{-\beta}$ can be observed in the regime $t_1 \alpha^{1/\beta} \ll t \ll t_2$. Concentration $c(x,t)$ is then

truncated at the cut-off scale t_2. These behaviors are discussed in more detail for an equivalent homogeneous medium in C.1.

3.2.4 Conclusions

TDRW is a computationally robust and efficient method to model diffusion in discretized heterogeneous media. It is specifically adapted to perform calculations on constant-size voxelized media such as 3D porosity images obtained by processing X-ray microtomography. The efficiency of the method is due to its intrinsic compliance with parallel computing and the few calculations required. Accordingly, TDRW has often been used for diffusion calculations during the last decade, replacing standard methods, such as finite differences, finite elements or random walk method based on constant time discretization. Nevertheless, to the best of our knowledge, its equivalence with spatially discretized heterogeneous diffusion equation has not been formally proved, albeit its ability to reproduce analytical solution for homogeneous cases has been broadly verified.

In this paper we demonstrated that the TDRW scheme, that is, the CTRW (3.4) characterized by the exponential transition time density (4.7) and the transition probabilities and mean transition times (3.21), is equivalent to the finite volume discretization of the heterogeneous diffusion equation (3.1). Based on this insight, we developed a TDRW particle scheme that models multiple trapping events (TDRW-MRMT), which can account for linear kinetic sorption-desorption reactions and solute trapping due to unresolved sub-scale heterogeneity. We provide an exact numerical algorithm for the implementation of the TDRW-MRMT based on CTRW theory. The TDRW approach is illustrated for the calculation of the residence time distribution in heterogeneous rocks. The TDRW-MRMT method is used to study diffusion in a bounded $d = 1$ dimensional medium in the presence of traps characterized by a truncated power-law trapping time distribution. We identify time regimes of anomalous behavior and discuss the truncation time of the evolution of the concentration distribution at an observation point in function of the cut-off time scale of the truncation power-law.

In summary, the presented developments provide a solid theoretical basis of the TDRW method and a novel TDRW-MRMT framework to account for the impact of subscale heterogeneities on diffusion behavior in heterogeneous media.

3.3 Average Diffusion in $d = 3$ Dimensional Heterogeneous Media

In the previous section we stated that discretized diffusion equation is equivalent to a TDRW and that TDRW represents an inhomogeneous CTRW. Here we use this framework in the context of a stochastic model in order to determine the large scale behaviour of diffusion in heterogeneous media. We consider diffusion in heterogeneous 3 dimensional medium which is characterized by a random retardation coefficient $R(\mathbf{x})$ and a constant diffusivity D. In this case equation (3.1) reduces to:

$$R(\mathbf{x})\,\frac{\partial c(\mathbf{x},t)}{\partial t} - \nabla \cdot D\nabla c(\mathbf{x},t) = 0 \tag{3.61}$$

and, similarly to the previous section, in order to use the TDRW derived in the previous section, we consider:

$$g(\mathbf{x},t) = c(\mathbf{x},t)R(\mathbf{x}). \tag{3.62}$$

This problem is motivated by upscaling of flow in heterogeneous media with variable storativity and for diffusion and reaction of radionuclides in low permeability media. From a theoretical point of view, we have a non-trivial spatially heterogeneous model, whose averaged behaviour can be assessed exactly using stochastic averaging. To date there are only few models for which this can be done.

The spatially varying retardation $R(\mathbf{x})$ is now modeled as a spatial random field. It is organized in voxel of length ℓ. Each voxel is assigned independently a random retardation coefficient from a distribution $p_R(r)$. Such medium can be seen as a large scale approximation of a correlated random field $R(\mathbf{x})$ on scale larger than the characteristic heterogeneity scale. Figure 3.1 shows a cross section of a realization of $R(\mathbf{x})$. This random retardation model is equivalent to the random trap model discussed in *Bouchaud and Georges* [1990]. This can be seen as follow. The discretized version of (3.61) is given by th Master equation (3.12) for constant D and $V_i = \ell^3$, where ℓ is the voxel size. Thus we obtain:

$$\frac{\partial g_i(t)}{\partial t} = \sum_{[ij]} \frac{1}{6}\frac{g_j(t)}{\tau_j} - \frac{g_i(t)}{\tau_i}. \tag{3.63}$$

This Master equation describes diffusion on a $d = 3$ dimensional cubic lattice with randomly

assigned trapping time τ_i at the vertexes. The trapping time is obtained from (3.16) as:

$$\tau_i = \frac{\ell^2 R_i}{6D} \tag{3.64}$$

The distribution is obtained from the distribution $p_R(r)$ of the retardation coefficient by mapping:

$$p_\tau(t) = \frac{6D}{\ell^2}\, p_R\left(\frac{6Dt}{\ell^2}\right). \tag{3.65}$$

Notice that the values of R_i in different pixels are uncorrelated so that the distribution of R_i can be statistically characterized by the single point pdf p_R.

This equation corresponds to the master equation for diffusion in a random trap model [*Bouchaud and Georges*, 1990] in a 3 dimensional cubic lattice. In such model each lattice site is considered as a trap, with a mean trapping time τ_i and the transition probability is constant. Here the trapping time is given by $\tau_i = \ell^2 R_i / D$, where ℓ is the pixel dimension, that we take constant, and the transition probability is equal to $1/6$.

A trap model for which the trapping time at a site is time invariant corresponds to "quenched" disorder, which differs from "annealed disorder" in which the properties of the lattice vary randomly in time. A CTRW describes a random walk in an " annealed disorder", where at each random step, space and time increment are chosen independently from the previous steps. In a "quenched disorder", the trapping time at a given site is the same for each visit of the site and it can induce correlation between the successive trapping times encountered. Whenever this correlation is relevant it induces a diffusion law which averaged behaviour is different from a CTRW. However the probability of return is related to the dimensionality of the problem. Weiss [*Weiss*, 1994] shows that asymptotically the number of new sites visited $S(n)$ by a random walker, in function of the number of steps n, depends on the dimensionality d of the problem:

$$S(n) \sim \begin{cases} \left(\dfrac{8n}{\pi}\right)^{1/2}, & d = 1, \\ \dfrac{\pi n}{\ln n}, & d = 2, \\ n, & d = 3 \end{cases} \tag{3.66}$$

In 3 dimensions the number of new sites visited increases linearly with the number of steps and therefore the problem of correlation in successive time increments is avoided and the average behaviour of a particle tracking in a quenched disorder for a trap model is the same

of a CTRW. Differently in 1 and 2 dimensional media, if the number of steps n goes to infinity, the sites are visited an infinitive number of times and different diffusion behaviours arise [*Weiss*, 1994; *Ben-Avraham and Havlin*, 2000].

3.3.1 Theoretical Development

The starting point of the upscaling procedure is equation (3.9) for $g_i(t)$. Considering ensemble average we obtain:

$$\overline{g}_i(t) = \sum_{n=0}^{\infty} \int_0^t dt' \overline{\langle \Delta[\mathbf{x}_i - \mathbf{x}_j(n)] \delta(t' - t_n) \rangle \langle H[\theta_j - (t - t')] \rangle} \tag{3.67}$$

where the overline indicates the ensemble average over all the possible realizations of the heterogeneous medium. Notice that we can split the disorder average for d dimension $d > 2$ where, as discussed in the introduction of this section, the number of distinct sites visited increases linearly with the number of steps and successive time increments are not correlated. For this reason θ_j and t_n are independent and we can split the disorder average:

$$\overline{g}_i(t) = \sum_{n=0}^{\infty} \int_0^t dt' \overline{\langle \Delta[\mathbf{x}_i - \mathbf{x}_j(n)] \delta(t' - t_n) \rangle} \ \overline{\langle H[\theta_j - (t - t')] \rangle} \tag{3.68}$$

Analogously to the previous section we can re-write (3.68) as

$$\overline{g}_i(t) = \int_0^t dt' \ \overline{\mathcal{A}_i}(t') \int_{t-t'}^{\infty} \overline{\psi}(\tau) \tag{3.69}$$

where

$$\overline{\psi}(\tau) = \int_0^{\infty} d\tau_R \, p_\tau(\tau_R) \frac{1}{\tau_R} e^{-\frac{\tau}{\tau_R}} \tag{3.70}$$

where τ_R is a mean transition time for a voxel with a given retardation coefficient R, that, considering the definition of the mean transition time derived in (3.16), with a constant diffusion coefficient in 3 dimensional media reads:

$$\tau_R = \frac{L^2 R}{6D} \tag{3.71}$$

and p_τ is the probability to have a given τ_R over the realizations, that in function of the distribution probability of R_i, that we call p_R, reads:

$$p_\tau(\tau_R) = \frac{6D}{L^2} \ p_R\left(\frac{6D\tau_R}{L^2}\right). \tag{3.72}$$

Notice that the values of R_i in different pixels are uncorrelated so that the distribution of R_i can be statistically characterized by the single point pdf p_R. From a continuous to a discrete description, R_i can be considered uncorrelated if the correlation lenght of the continuous coefficient $R(\mathbf{x})$ is of the order of magnitude of the pixel size ℓ. Similarly to (3.11) we can highlight the recursive character of $\mathcal{A}$ re-writing it as:

$$\overline{\mathcal{A}_i}(t) = \rho_i \delta(t) + \sum_{[ik]} \frac{1}{6} \int_0^t dt' \overline{\psi}_k(t-t') \overline{\mathcal{A}_k}(t'), \tag{3.73}$$

where $\rho_i = g_i$ at $t = 0$ is the initial particle density at point $\mathbf{x}_i$ and the factor $\frac{1}{6}$ is the transition probability $w_{i,j}$ given in (3.16) for a constant discretization $\xi_i = \ell$ of a 3 dimensional media with constant diffusion coefficient. Equation (3.69) indicates that the total number of particles $g_i(t)$, is given by the sum over all probabilities that a solute particle reaches the voxel i at some time t' and the transition to the next site takes more time than $t - t'$. Analogously to the previous section, we solve the problem in Laplace space , where (3.69), read:

$$\lambda \overline{g_i}^*(\lambda) = \rho_i + \sum_{[i,k]} \frac{1}{6} \frac{\lambda \overline{\psi}^*}{1 - \overline{\psi}^*} \overline{g}_k^* - \frac{\lambda \overline{\psi}^*}{1 - \overline{\psi}^*} \overline{g}_i^* \tag{3.74}$$

The quantity $\overline{g}_i(t)$ refers to the i-th position on the lattice and its value is representative for volume the i-th voxel. In the following we pass from a discrete to a continuous description of the particle density in order to obtain an upscaled formulation of $\overline{g}(\mathbf{x}, t)$ for an observation scale L larger than the resolution scale ℓ.

$$\overline{g}(\mathbf{x}, t) = \sum_i^{\infty} g_i(t) \ell^{-3} \prod_{d=1}^{3} H\left(\frac{\ell}{2} - |x_{1d} - x_d|\right) \tag{3.75}$$

where $H(\cdot)$ is the Heaviside function that is equal to 1 is its argument is larger than zero and zero otherwise. Considering the relation expressed in (3.75) for both g_i and ρ_i in (3.74), equation (3.74) can be written as:

$$\lambda \overline{g}^*(\mathbf{x}, \lambda) = \rho(\mathbf{x}) + \sum_{i=-\infty}^{\infty} \sum_{[i,k]} \frac{1}{6} M^*(\lambda)\, \overline{g}_k^*(\lambda) \ell^{-3} \prod_{d=1}^{3} H\left(\frac{\ell}{2} - |x_{1d} - x_d|\right) - M^*(\lambda) \overline{g}^*(\mathbf{x}, \lambda) \tag{3.76}$$

where we defined a memory function $M^*(\lambda)$ given by:

$$M^*(\lambda) = \frac{\lambda \overline{\psi}^* \tau_R}{1 - \overline{\psi}^*}. \tag{3.77}$$

In order to understand how to pass from the discrete $\overline{g}_k(t)$ to the continuous $\overline{g}(\mathbf{x},t)$ we consider the simpler problem in 1 dimension, where:

$$\overline{g}(x,t) = \frac{\ell}{2}\sum_{i=-\infty}^{\infty}[\overline{g}_{i-1}(t)+\overline{g}_{i+1}(t)]\,H(\ell/2-|x_i-x|) \tag{3.78}$$

that, considering the sampling propriety of the delta Dirac function, with $x' = x-\ell$, can be written as:

$$\overline{g}(x,t) = \frac{\ell}{2}\sum_{i=-\infty}^{\infty}\int dx'[\delta(x-x'+\ell)g_{i-1}(t)+\delta(x-x'-\ell)g_{i+1}(t)]\,H(\ell/2-|x_i-x'-\ell|) \tag{3.79}$$

and considering the change of variable $i-1=j$ it reads:

$$\overline{g}(x,t) = \frac{\ell}{2}\int dx'[\delta(x-x'+\ell)+\delta(x-x'-\ell)]\sum_{j=-\infty}^{\infty}g_j(t)\,H(\ell/2-|x_j-x'|). \tag{3.80}$$

Considering (3.75) for $d=1$ case, the summation in (3.80) is equal to:

$$\sum_{j=-\infty}^{\infty}g_j(t)\,H(\ell/2-|x_j-x'|) = \overline{g}(x',t) \tag{3.81}$$

and therefore (3.80) reads:

$$\overline{g}(x,t) = \frac{\ell}{2}\int dx'[\delta(x-x'+\ell)+\delta(x-x'-\ell)]\overline{g}(x',t) \tag{3.82}$$

The same procedure can be repeated in the $d=3$ case and (3.76) can be written as:

$$\lambda\overline{g}^*(\mathbf{x},\lambda) = \rho(\mathbf{x}) + \int d\mathbf{x}'\,\frac{1}{\tau}p(\mathbf{x}-\mathbf{x}')\,\overline{g}^*(\mathbf{x}')\,M^*(\lambda) - M^*(\lambda)\,\overline{g}^*(\mathbf{x},\lambda) \tag{3.83}$$

where the transition probability $p(\mathbf{x}-\mathbf{x}')$, considering 3 dimensional isotropic media, reads:

$$p(\mathbf{x}) = \frac{1}{6}\sum_{i=1}^{3}[\delta(x_i-\ell)+\delta(x_i+\ell)]\prod_{i\neq j}\delta(x_j). \tag{3.84}$$

Considering the inverse Laplace transform of (3.83) we obtain a non local equation in time domain:

$$\frac{\partial\overline{g}(\mathbf{x},t)}{\partial t} = \int_{-\infty}^{\infty}d\mathbf{x}'\,\frac{1}{\tau}\,p(\mathbf{x}')\int_0^{\infty}dt'\,M(t')\,\overline{g}(\mathbf{x}-\mathbf{x}',t-t') \;-\int_0^{\infty}dt'\,M(t')\,\overline{g}(\mathbf{x},t-t'). \tag{3.85}$$

Equation (3.85) is a non-local equation both in time and in space because the number of particle in $(\mathbf{x}, t)$ depends also on $(\mathbf{x}', t')$. In order to get rid of the convolution product between $\overline{g}(\mathbf{x} - \mathbf{x}')$ and $p(\mathbf{x}')$, we localize g for small $\mathbf{x}'$ using Taylor expansion till the second order approximation, and (3.85) reads:

$$\frac{\partial \overline{g}(\mathbf{x}, t)}{\partial t} = \int_0^\infty dt' \; M(t') \int_{-\infty}^\infty d\mathbf{x}' \; \frac{p(\mathbf{x}')}{\tau_R} \left[\mathbf{x}' \cdot \nabla \overline{g}(\mathbf{x}', t - t') + \frac{1}{2} \mathbf{x}' \cdot \nabla \otimes \nabla \overline{g}(\mathbf{x}, t - t') \cdot \mathbf{x}' \right]. \quad (3.86)$$

The first term in the space integral of (3.86) represents the first moment of the particle distribution and it is equal to zero for each component:

$$\int_{-\infty}^\infty dx_i' \; p(x_i') \; x_i' = 0, \quad (3.87)$$

while the second term is a tensor and the only non-zero terms, the diagonals terms, represent the second moments of the particles distribution:

$$\int_{-\infty}^\infty d\mathbf{x}' \;\; p(\mathbf{x}') \; x_i' x_j' = 0 \qquad i \neq j \quad (3.88)$$

and

$$\int_{-\infty}^\infty d\mathbf{x}' \;\; p(\mathbf{x}') \; x_i'^2 = \frac{1}{3} \ell^2 = 2D\tau_R. \quad (3.89)$$

Therefore, substituting the previous results in (3.85), we obtain an effective non-local equation for the total mean number of particles $\overline{g}(\mathbf{x}, t)$:

$$\frac{\partial \overline{g}(\mathbf{x}, t)}{\partial t} = \nabla \cdot D \int_0^\infty dt' \; M(t') \; \nabla \overline{g}(\mathbf{x}, t - t') \quad (3.90)$$

The effective equation obtained is non local in time and the dynamic of $\overline{g}(\mathbf{x}, t)$ is controlled by a memory function $M(t)$, which depends on the spatial distribution of the random retardation coefficient $R(\mathbf{x})$. In order to obtain an effective equation for the total mobile concentration $\overline{c}(\mathbf{x}, t)$, we consider the Laplace transform of (3.90) that reads:

$$\lambda \overline{g}^*(\mathbf{x}, \lambda) - \nabla \cdot D \, M^*(\lambda) \nabla \overline{g}^*(\mathbf{x}, \lambda) = \delta(\mathbf{x}) \quad (3.91)$$

and with the change of variable $\overline{g}^*(\mathbf{x},\lambda) = \overline{c}'^*(\mathbf{x},\lambda)/M^*(\lambda)$ we obtain:

$$\lambda \frac{1}{M^*(\lambda)} \overline{c}'^*(\mathbf{x},\lambda) - \nabla \cdot D\,\nabla \overline{c}'^*(\mathbf{x},\lambda) = \delta(\mathbf{x}) \tag{3.92}$$

that is analogous to the Laplace transform of (3.61), so that we identify $\overline{c}'^*(\mathbf{x},\lambda) \equiv \overline{c}^*(\mathbf{x},\lambda)$ and we get:

$$\overline{c}^*(\mathbf{x},\lambda) = M^*(\lambda)\,\overline{g}^*(\mathbf{x},\lambda), \quad \overline{R(\mathbf{x})c^*(\mathbf{x},\lambda)} = \varphi^*(\lambda)\,\overline{c}^*(\mathbf{x},\lambda) \tag{3.93}$$

where we defined:

$$\varphi^*(\lambda) = \frac{1}{M^*(\lambda)}. \tag{3.94}$$

Equivalently in time domain we have:

$$\overline{c}(\mathbf{x},t) = \int dt' M(t-t')\,\overline{g}(\mathbf{x},t'), \quad \overline{R(\mathbf{x})c(\mathbf{x},t)} = \int dt' \varphi(t-t')\overline{c}(\mathbf{x},t') \tag{3.95}$$

and the upscaled equation for the average concentration reads:

$$\frac{\partial}{\partial t} \int dt' \varphi(t-t')\overline{c} - D\nabla^2 \overline{c} = 0. \tag{3.96}$$

Equation (3.96) is an effective equation non-local in time, where the memory term, $\varphi(t-t')$, depends on the spatial distribution of the retardation coefficient $R(\mathbf{x})$. Notice that the upscaled formulation obtained is the same of the MRMT models [*Haggerty and Gorelick*, 1995; *Carrera et al.*, 1998] and Multicontinuum models (see Chapter 5). In MRMT models equation (3.96) represents the governing equation for the 'mobile' concentration and the memory term is given by the exchange of solute between mobile and immobile zones. Indeed considering (3.1) in the context of diffusion under linear sorption-desorption reaction, $c(\mathbf{x},t)$ refers to the dissolved solute. The total concentration $c_T(\mathbf{x},t)$, is given by the sum of the concentration of the dissolved solute and of the adsorbed one $c_{ad}(\mathbf{x},t) = k_d(\mathbf{x})c(\mathbf{x},t)$, where $k_d(\mathbf{x})$ is the distribution coefficient:

$$c_t(\mathbf{x},t) = \{[1-\phi(\mathbf{x})]k_d(\mathbf{x}) + \phi(\mathbf{x})\}c(\mathbf{x},t) = R(\mathbf{x})c(\mathbf{x},t). \tag{3.97}$$

and (3.96) is an upscaled equation for the concentration of a dissolved solute, or 'mobile' concentration.

3.3.2 Conclusions

In this section we used particle tracking method as analytical tool to upscale diffusion in a stochastic framework. We considered the problem of diffusion in a $d = 3$ dimensional medium characterized by a constant diffusivity and a random retardation coefficient. Using the TDRW derived in the previous section, we derived an upscaled non-local in time diffusion equation, where the memory function depends on the spatial distribution of the retardation coefficient. Considering the ubiquity of the diffusion process, this work is motivated by many real problems as diffusion and reaction of chemicals and radionuclides in low permeability media, fundamental in waste repository problems or for the upscaling of flow in media characterized by variable storativity. Although the condition of constant diffusivity and $d = 3$ could appear idealized, we point out that this problem represents a particular case of diffusion in heterogeneous media that can be rigorously described by a CTRW. A CTRW describes a RW in an "annealed" disorder [*Bouchaud and Georges*, 1990], which implies that successive time increments are completely uncorrelated. In the previous section we demonstrated that discretized diffusion equation in heterogeneous media corresponds to a TDRW, that, in principle, implies correlation. This difference implies that only particular cases of diffusion in disordered media can be rigorously upscaled by a CTRW. Because of this, we claim that the work of *Cortis and Knudby* [2006], who upscale flow in heterogeneous media characterized by spatially variable conductivity using CTRW is not rigorously corrected. Here we show that diffusion in constant diffusivity media can be mapped into trap model [*Bouchaud and Georges*, 1990], where transition probability and transition time are independent, but the fact that a site can be visited by the same random walker many times induces correlation in the time increments. Anyway the number of new sites visited in function of the number of steps, depends on the dimensionality of the problem [*Weiss*, 1994]. In a 1 and 2 dimensional media, asymptotically the number of new sites visited does not increase linearly with the number of step, the same site can be visited an infinite number of time and this induces correlation in the random time increments [*Weiss*, 1994]. Indeed in a d dimensional lattice with $d > 2$ the number of new sites visited increases linearly with the number of steps and it implies that we can upscale properly the diffusion problem described above and obtain an effective upscaled formulation.

Chapter 4

Anomalous Diffusion in Composite Media

[I]

We study diffusion in composite media characterized by strong contrasts in the diffusion properties. We consider layered geometries consisting of a highly conductive and a (heterogeneous) low conductivity layer. For a homogeneous low conductivity layer, diffusion is found to be sub-diffusive in an intermediate time regime. The mean square displacement scales as $t^{1/2}$ for times smaller than the typical diffusion time scale in the low conductivity layer. Asymptotically, diffusion is normal. For a heterogeneous low conductivity layer, the mean square displacement evolves subdiffusively as well. It behaves as t^{α} with $1/2 \leq \alpha \leq 1$. The exponent α is determined by the distribution of heterogeneous diffusion properties in the low-conductivity layer. Using spatial and stochastic averaging, we derive explicit non-local diffusion equations, whose kernels are determined by the heterogeneous diffusion properties of the low-conductivity layer. For power-law kernels, the obtained partial differential equations are equivalent to fractional diffusion models. The anomalous diffusion behavior is studied analytically in terms of the solutions of the non-local diffusion equations, as well as numerically by direct solution of the diffusion problem in the heterogeneous composite medium using an efficient inhomogeneous continuous time random walk (CTRW) method. We focus on the first-passage time distributions, the time evolution of the particle density, and the mean square displacement. This work sheds some new light on the heterogeneity mechanisms that may cause anomalous diffusion.

[I]This chapter is part of the paper *Anomalous Diffusion in Composite Media*, Russian A., M. Dentz and J. Carrera, to be submitted to Phys. Rev. E.

4.1 Introduction

Diffusion in heterogeneous environments is often found to be anomalous, this means, the mean squared displacement of a diffusing particle grows as t^{α}, with $\alpha \neq 1$ [*Bouchaud and Georges*, 1990; *Ben-Avraham and Havlin*, 2000; *Havlin and Ben-Avraham*, 2002a].

Diffusion in heterogeneous media is handled by most of the fields of science: in fluidodynamics and hydrology considering flow equation in porous and fractured media [*Delay et al.*, 2002; *Keller*, 2001; *Cortis and Knudby*, 2006; *Dykhuizen*, 1987], in thermodynamic considering heat equation [*Kaviany*, 1995] and in all the disciplines dealing with transport processes [*Dean et al.*, 2007; *Diersch and Kolditz*, 2002; *Drummond and Hogan*, 1987; *Haggerty and Gorelick*, 1995; *Noetinger*, 1994] like molecular and particle transport in biology [*Codling et al.*, 2008] or electric current through conductors in electrodynamics [*Dean et al.*, 2004; *King*, 1987]. Importance of diffusion in heterogeneous low conductivity material has been further investigated in relation to underground nuclear waste disposal [*Warren and Root*, 1963; *Dykhne et al.*, 2005; *Gouze et al.*, 2008a; *Carrera et al.*, 1998].

One distinguish in the diffusion processes in the different physical phenomena is the variability in diffusion parameters. In groundwater hydrology hydraulic conductivity can vary of order of magnitude even in apparently homogeneous media. Considering heat conduction, thermal conductivity usually varies at the most of one or two orders of magnitude in different materials [*Carslaw and Jaeger*, 1947].

Traditionally the approach is to characterize diffusion in heterogeneous media in terms of effective parameters, such as effective hydraulic conductivity or effective diffusivity. Exhaustive reviews of the results obtained for the effective conductivity since the studies of Matheron in the 1960s [*Matheron*, 1967], are given in [*Sanchez-Villa et al.*, 2006] and [*Renard and de Marsily*, 1997].

Nevertheless further experimental investigations demonstrate that large scale description in terms of effective conductivity is not sufficient to model some observed phenomena (e.g. tailing in drawdown curves [*Le Borgne*, 2004; *Le Borgne and Gouze*, 2008]) and scale dependence of diffusion parameters [*Sanchez Vila et al.*, 1996; *Schulze-Makuch, D., Douglas, A. Carlson, Douglas, S. Cherkauer, Malik*, 1999]. Actually these observations suggest that the large scale equations are different from their local counterparts and that a different large scale description is needed.

Anomalous diffusion and anomalous drawdowns are well modeled by fractional [*Barker*,

1988; *Acuna and Yortsos*, 1995] and multi-fractional [*de Dreuzy et al.*, 2010, 2004; *Lods and Gouze*, 2008] diffusion models. A limitation of these models is that the fractal dimension is not directly linked to the heterogeneity of the media, it can vary depending on the boundary and initial conditions (e.g. [*Little and Bloomfield*, 2010; *Zhang*, 2004]). For these reasons interpretation of multi-fractal models is rather difficult [*Tessier et al.*, 1996] and their utility for prediction is limited [*Labat et al.*, 2002].

CTRW has been successfully used to model non-Fickian transport in disordered media e.g. [*Berkowitz et al.*, 2006; *Cortis*, 2004; *Gouze et al.*, 2008b; *Sanchez-Villa et al.*, 2006; *Metzler and Klafter*, 2000] and transient flow [*Cortis and Knudby*, 2006]. The equivalence between large scale averaging theory and the CTRW has been object of the work of Noetinger et al. [*Noetinger, B.Estebenet and Quintard*, 2001] and the equivalence between CTRW and multi rate mass transfer (MRMT) models has been demonstrated by Dentz [*Dentz and Berkowitz*, 2003]. MRMT models have been widely used to model transport and flow problems in heterogeneous media e.g. [*Harvey and Gorelick*, 1995; *Carrera et al.*, 1998; *Haggerty and Gorelick*, 1995; *Lods*, 2004].

A particular CTRW in heterogeneous media, where the distribution of residence time depends by the location, is called time domain random walk (TDRW). This method has been first introduced by *McCarthy* [1993], used by Banton for simulating non-reactive solute transport in $d = 1$ dimensional porous media [*Banton et al.*, 1997], by Noetinger for the upscaling of fluid flow in fracture rocks [*Noetinger and Estebenet*, 2000], and further developed by Delay and Bodin [*Delay et al.*, 2002; *Bodin et al.*, 2003; *Delay et al.*, 2005].

We consider diffusion in composite media. In particular we consider a dual and a multi continuum model given in Figure 4.1. The dual continuum model is constituted by two homogeneous layers which represent the mobile region (where the scalar quantity diffuses faster) and the immobile region (where scalar quantity diffuses slower).

Since the pioneering 'double-porosity' model of Barenblatt [*Barenblatt et al.*, 1960] a large number of double-permeability/porosity models have been developed (e.g. [*Warren and Root*, 1963; *Dykhuizen*, 1987; *Peters and Klavetter*, 1988; *Dykhuizen*, 1990; *Bai et al.*, 1993]). These models assumes that both the mobile and the immobile zone are in quasi-equilibrium and mass transfer is modeled as a first order process. Among others, works considering a kinetic approach are derived using perturbations methods [*Zhang and Sun*, 2000], or homogenization method. Complete review of homogenized models for saturated conditions through a heterogeneous porous medium is given in [*Peszynska and Showalter*, 2007], while non-saturated conditions are considered in [*Lewandowska*, 2004; *Bertin et al.*, 2000].

We take into account non-equilibrium effects in the immobile zone, which give raise to anomalous behaviour and we derive temporally non-local governing equations.

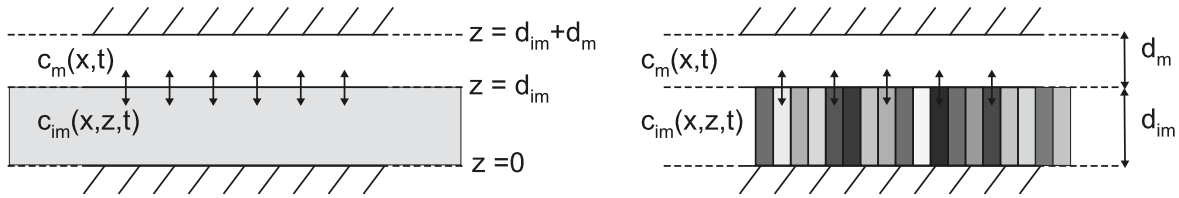

Figure 4.1: *On the left: dual continuum model, on the right: multi continuum model. Dual and multi continuum model are constituted by a 'mobile' layer of thickness d_m and an immobile one of thickness d_{im}. Vertical arrows between the two layers indicate mass exchange between the mobile and the immobile regions.*

In the following we introduce the problem of diffusion in heterogeneous media, the medium models taken into account and the numerical method used to test analytical solutions. In the third section we derive non-local governing equation for the up-scaled dual and the multi continuum model proposed. Successively we give the solutions for the model derived focusing on anomalous behaviour of mean square displacement, first passage time distribution and temporal evolution of the concentration and in the last section we focus on the anomalous behaviour we can obtain with the model derived. Analytical solutions are tested numerically. Main results are summed and discussed in the conclusions.

4.2 Diffusion in Heterogeneous Media

Diffusion of a scalar quantity $C(\mathbf{x}, t)$ in a heterogeneous medium is described by

$$R(\mathbf{x})\frac{\partial C(\mathbf{x}, t)}{\partial t} - \nabla \cdot [K(\mathbf{x})\nabla C(\mathbf{x}, t)] = 0. \tag{4.1}$$

In the context of diffusion of contaminants in low conductivity media, $R(\mathbf{x})$ can be related to the medium porosity $\phi(\mathbf{x})$ and linear equilibrium adsorption properties of the medium as $R(\mathbf{x}) = [1 - \phi(\mathbf{x})]k_d(\mathbf{x}) + \phi(\mathbf{x})$ with $k_d(\mathbf{x})$ the distribution coefficient, $C(\mathbf{x}, t)$ is the non-adsorbed contaminant concentration, and $K(\mathbf{x})$ the bulk diffusion coefficient. In the context of heat transport, $R(\mathbf{x})$ stands for heat capacity, $C(\mathbf{x}, t)$ temperature, and $K(\mathbf{x})$ thermal conductivity. For the description of Darcy-scale flow in heterogeneous porous media, $R(\mathbf{x})$ denotes specific storativity, $C(\mathbf{x}, t)$ hydraulic head and $K(\mathbf{x})$ hydraulic conductivity. This work is motivated through contaminant diffusion in low permeability media, and Darcy-scale flow by

heterogeneous porous media.

4.2.1 Random Walk Perspective

The diffusion equation (4.1) is equivalent to the Langevin equation [*Risken*, 1989]

$$\frac{d\mathbf{x}(t)}{dt} = \frac{\nabla K[\mathbf{x}(t)]}{R[\mathbf{x}(t)]} + \sqrt{2\frac{K[\mathbf{x}(t)]}{R[\mathbf{x}(t)]}}\xi(t), \tag{4.2}$$

where $\mathbf{x}(t)$ denotes the trajectory of a particle, $\xi(t)$ is a Gaussian white noise characterized by zero mean and $\langle xi(t')_i xi(t')_j \rangle = \delta(t-t')\,\delta_{ij}$.

The scalar $C(\mathbf{x},t)$ is expressed in terms of the particle trajectories $\mathbf{x}(t)$ as

$$C(\mathbf{x},t) = R(\mathbf{x})^{-1}\left\langle \delta[\mathbf{x}-\mathbf{x}(t)]\right\rangle, \tag{4.3}$$

where the angular brackets denote the noise average.

The cases of variable conductivity $K(\mathbf{x})$ and constant storativity $R(\mathbf{x}) = R$, on the one hand, and variable storativity $R(\mathbf{x})$ and constant conductivity $K(\mathbf{x}) = K$, on the other, can be mapped into the random barrier and random trap models, respectively [*Bouchaud and Georges*, 1990]. These models describe diffusion on random lattices. In the random barrier model, each link of the lattice acts as a symmetrical barrier. For diffusion in a finite domain, the equilibrium particle density is uniform and accumulation in low conductivity regions is avoided [*Bouchaud and Georges*, 1990]. In the random trap model each lattice site is considered a trap characterized by a random trapping time. In this model, the equilibrium distribution is proportional to the distribution of trapping times [*Bouchaud and Georges*, 1990].

4.2.2 Numerical Simulations

Diffusion properties are spatially discontinuous in the proposed models, which makes the use of (4.2) complicated because of the calculation of the gradient of the conductivity $\nabla K(\mathbf{x})$ [*Delay et al.*, 2005]. Therefore the method of choice is time domain random walk (TDRW), which relies on spatial increments, whose absolute values are deterministic, combined with random time increments [*McCarthy*, 1993; *Banton et al.*, 1997; *Delay et al.*, 2002]. We consider the TDRW scheme presented in *Dentz et al.* [2012]. The TDRW that describes the random walk

equivalent to eq. (4.1), used in the numerical simulations is:

$$\mathbf{x}_i(n+1) = \mathbf{x}_j(n) + \boldsymbol{\xi}_{ij}, \qquad t_{n+1} = t_n + \theta_j, \tag{4.4}$$

where the position of lattice point j is denoted by $\mathbf{x}_j$. The probability for a spatial transition ξ_{ij} between points j and i, w_{ij}, and the mean transition time τ_j are given by:

$$w_{ij} = \frac{b_{ij}}{\sum_{[ik]} b_{kj}}, \qquad \tau_j = \frac{A_j R_j}{\sum_{[kj]} b_{kj}}. \tag{4.5}$$

where A_j is the area of the pixel j, $\sum_{[ik]}$ indicates the sum over the nearest neighbours of pixel j and

$$b_{ij} = \frac{\Delta_{z,ij}(K)_{ij}}{\Delta_x}, \tag{4.6}$$

with $(K)_{ij}$ the harmonic mean of the conductivities of the two pixels i and j, $\Delta_{z,ij}$, the length of the interface between the pixel i and j, given by the vertical discretization of the domain, Δ_x the lag distance between the centres of the two pixels, or the horizontal discretization of the domain that we take constant, so that the area of the pixel j is given by $A_j = \Delta_x \Delta_{z,ij}$. According to [*Delay et al.*, 2002], we consider transition time exponentially distributed, and the transition time density reads:

$$\psi_{\theta_j}(\theta_j) = \tau_j^{-1} \exp(-\theta_j/\tau_j). \tag{4.7}$$

Details on the implementation of the numerical simulations are given in Appendix C.3.

4.2.3 Observables

4.2.3.1 Mean squared displacement

Diffusion in heterogeneous media can be characterized by the evolution of the mean-square displacement (MSD) $m_{ij}(t)$, which is defined by

$$m_{ij}(t) = \int d\mathbf{x}\, x_i x_j c(\mathbf{x}, t) = \langle x_i(t) x_j(t) \rangle. \tag{4.8}$$

For normal diffusion, $m_{ij}(t)$ evolves linearly in time $m_{ij}(t) \sim t$. For diffusion in disordered media this scaling is not valid in general, and it is often found that $m_{ij}(t) \sim t^\beta$ with $\beta \neq 1$ *Bouchaud and Georges* [1990]. For $0 < \beta < 1$ the behavior is termed sub-diffusive, for $\beta > 1$,

super-diffusive, and for $\beta = 2$ ballistic *Havlin and Ben-Avraham* [2002a]. Sub-diffusion in disordered media is typically attributed to trapping in particular regions like dead ends and bottlenecks that exist in the disordered structure.

4.2.3.2 First passage time distribution

Another quantity of interest is the first passage time distribution (FPTD) of a particle. The information provided by the FPTD is central in many application ranging from contaminant transport in geological media (solute breakthrough curves) *Berkowitz et al.* [2006], to the evaluation of reaction rates in diffusion limited reactions *Havlin and Ben-Avraham* [2002a], to name a few. The FPTD $f(\mathbf{x}, t)$ can be defined by the renewal equation *Hughes* [1995]

$$C(\mathbf{x}, t) = \delta(\mathbf{x})\delta(t) + \int_0^t dt' f(\mathbf{x}, t') C(\mathbf{x}, t|\mathbf{x}, t'), \tag{4.9}$$

where the propagator $C(\mathbf{x}, t|\mathbf{x}', t')$ solves the diffusion equation (4.1) for the initial condition $C(\mathbf{x}, t = t'|\mathbf{x}', t') = \delta(\mathbf{x} - \mathbf{x}')$. In a $d = 1$ dimensional homogeneous medium, the FPTD scales asymptotically as $f(x, t) \propto t^{-3/2}$.

4.2.3.3 Temporal evolution of the concentration

We will also consider the time evolution of $C(\mathbf{x}, t)$ at a given point in space, which in the context of Darcy flow in heterogeneous media is termed drawdown *Delleur* [1999]. The drawdown depends on the boundary and initial conditions. For an instantaneous point-like injection into a d-dimensional homogeneous medium, it scales asymptotically as $C(\mathbf{x}, t) \propto t^{-d/2}$.

4.3 Multicontinuum Model

4.3.1 Model Medium and Governing Equations

The heterogeneous model medium under consideration is a $d = 2$ dimensional composite medium that consists of a mobile, highly conductive layer and a (heterogeneous) immobile, low conductivity layer, as illustrated in Figure 4.1. For diffusion in this medium, equation (4.1) can be separated into an equation for the mobile region and one for the immobile region. The coordinate vector now and in the following denotes $\mathbf{x} = (x, z)^T$. Thus, for the mobile regions

$d_{im} \leq z \leq d$, we obtain

$$R_m \frac{\partial C_m(\mathbf{x},t)}{\partial t} - K_m \nabla^2 C_m(\mathbf{x},t) = 0, \tag{4.10}$$

where we defined $c_m(\mathbf{x},t) = c(\mathbf{x},t)$ for $d_{im} \leq z \leq d$. In the immobile region $0 \leq z \leq d_{im}$, diffusion is described by

$$R_{im}(x) \frac{\partial C_{im}(\mathbf{x},t)}{\partial t} - K_{im}(x) \nabla^2 C_{im}(\mathbf{x},t) = 0. \tag{4.11}$$

The immobile $C_{im}(\mathbf{x},t)$ is defined analogously by $C_{im}(\mathbf{x},t) = C(\mathbf{x},t)$ for $0 \leq z \leq d_{im}$. Continuity of $C(\mathbf{x},t)$ and flux $-K(\mathbf{x})\nabla C(\mathbf{x},t)$ are imposed at the interface between the mobile and immobile layers, at $z = d_{im}$ [*Carslaw and Jaeger*, 1947], so that at $z = d_{im}$

$$C_m(\mathbf{x},t) = C_{im}(\mathbf{x},t), \qquad K_m \frac{\partial C_m(\mathbf{x},t)}{\partial z} = K_{im}(x) \frac{\partial C_{im}(\mathbf{x},t)}{\partial z}. \tag{4.12}$$

In the following, we assume no flux conditions at the horizontal boundaries,

$$K_m \frac{\partial C_m(\mathbf{x},t)}{\partial z}\bigg|_{z=d} = 0, \qquad K_{im}(x) \frac{\partial C_{im}(\mathbf{x},t)}{\partial z}\bigg|_{z=0}. \tag{4.13}$$

Diffusion occurrs in multiple connected continua. Dual continuum models can be divided into 'double permeability' and 'double porosity' models [*Zhang and Sun*, 2000]. In some 'dual porosity' models the immobile regions are constrained to communicate only with the mobile region and mass transfer between the immobile regions is neglected by default. Multi-continuum model that prevent mass transfer between immobile regions are also termed in literature 'comb models' [*Havlin and Ben-Avraham*, 2002a; *Bouchaud and Georges*, 1990; *Dvoretskaya and Kondratenko*, 2009].

Here, we assume that the conductivity K_m in the mobile layer is much larger than the maximum conductivity in the immobile layers, $K_m \gg \max_{x\in\mathbb{R}}\{K_{im}(x)\}$. This condition allows to overcome the distinction between 'double permeability' and 'double porosity' models, because the difference in the conductivity between the mobile and the immobile zone makes, by itself, horizontal diffusion in the immobile layer negligible. Referring to Figure 4.1, double (or multi) porosity models neglect horizontal diffusion in the immobile layer and immobile zones act as source terms for the mobile zone.

The simplest multi-continuum model is constituted by the coupling of two homogeneous

regions. The pioneering double permeability model of Barenblatt et al. [*Barenblatt et al.*, 1960] models flow through fractured media. In such media, flow takes place essentially only in the fractures. However, fluid may be transferred into the immobile matrix and then after a certain time back into the fractures.

In the multi continuum model, heterogeneity of the immobile layer is characterized by spatially variable bulk immobile conductivity defined by $\kappa(x) = \chi_{im} K_{im}(x)$ and spatially variable bulk retardation factor defined by $\rho(x) = \chi_{im} R_{im}(x)$. We handle spatial heterogeneity in a stochastic framework. In a stochastic framework a medium is considered as a particular realization of an ensemble of media with the same statistical properties and spatially varying conductivity and retardation factor are modeled as spatial random fields. We consider a stationary and ergodic medium, with a finite correlation. Considering an observation scale far larger than the correlation scale, we can approximate the medium organization in bins, where diffusion properties in each bins are independent. Thus, such medium can be completely defined by a single point distribution of the diffusion parameters. A schema of the model is given in Figure 4.1. Referring to the figure heterogeneity of the immobile layer is organized in bins. At each bin is assigned independently a random bulk cinductivity taken from a distribution $p_\kappa(\kappa)$ and a random bulk retardation taken from a distribution $p_\rho(\rho)$.

4.3.2 Vertical Average

In the following, we derive the governing equations for the average mobile particle distribution $c_m(x,t)$, which is defined as

$$c_m(x,t) = \frac{1}{d_m} \int_{d_{im}}^{d} dz\, C_m(\mathbf{x},t). \tag{4.14}$$

Averaging of (4.10) over the vertical gives for $c_m(x,t)$

$$R_m \frac{\partial c_m(x,t)}{\partial t} - K_m \frac{\partial^2 c_m(x,t)}{\partial x^2} = -\frac{K_{im}(x)}{d_m} \left. \frac{\partial C_{im}(\mathbf{x},t)}{\partial z} \right|_{z=d_{im}}, \tag{4.15}$$

where we used the flux continuity condition (4.12) and the boundary conditions (4.13). Continuity in $c(\mathbf{x},t)$ at the interface defines the boundary condition for the diffusion problem (4.11) in the immobile region. The system of equations (4.11) and (4.15) can be closed as follows. In the model medium under consideration, the conductivity K_m in the mobile layer is much larger than the maximum conductivity in the immobile layers, $K_m \gg \max_{x\in\mathbb{R}}[K_{im}(x)]$. This

assumption has two effects on the dynamic of the model: (i) the concentration in the mobile zone equilibrates much faster that the one in the immobile zone, (ii) mass transfer in the immobile zone is sub-leading compared to the mass transfer in the mobile layer.

These processes are controlled by the characteristic time scales for vertical diffusion in the mobile and immobile layers, defined by

$$\tau_m = \frac{d_m^2 R_m}{K_m}, \qquad \tau_{im}(x) = \frac{d_{im}^2 R_{im}(x)}{K_{im}(x)}. \tag{4.16}$$

Considering $\tau_m \ll \min_{x\in\mathbb{R}}[\tau_{im}(x)]$ the distribution $C_m(\mathbf{x}, t)$ in the mobile layer will equilibrate much faster than $C_{im}(\mathbf{x}, t)$ in the immobile layers. Consequently, at observation times much larger than τ_m, we can approximate

$$C_m(\mathbf{x}, t) \approx c_m(x, t). \tag{4.17}$$

Considering mass transfer in the immobile layer, the condition $K_m \gg \max_{x\in\mathbb{R}}[K_{im}(x)]$ makes horizontal diffusion in the immobile layer negligible for two inter-related reasons. Firstly because transition time in the immobile layer is far larger than in the mobile layer and horizontal diffusion in the immobile layer is slower respect horizontal diffusion in the mobile layer. Secondly because, in a particle tracking framework, the probability for a particle in the immobile layer to move in the mobile zone is far higher respect the probability to move horizontally in the immobile layer.

Thus, we disregard horizontal diffusion in the immobile layers. Based on these assumptions, we can approximate the diffusion problem (4.11) in the immobile layer by

$$R_{im}(x)\frac{\partial C_{im}(\mathbf{x}, t)}{\partial t} - K_{im}(x)\frac{\partial^2 C_{im}(\mathbf{x}, t)}{\partial z^2} = 0, \tag{4.18}$$

with the boundary conditions

$$C_{im}(\mathbf{x}, t)|_{z=d_m} = c_m(x, t), \qquad K_{im}(x)\left.\frac{\partial C_{im}(\mathbf{x}, t)}{\partial z}\right|_{z=0} = 0. \tag{4.19}$$

These assumptions are validated using particle tracking simulations.

From (4.18), we obtain by vertical integration for the boundary flux term on the right side

of (4.15)

$$-\frac{K_{im}(x)}{d_m}\left.\frac{\partial C_{im}(\mathbf{x},t)}{\partial z}\right|_{z=d_{im}} = R_{im}(x)\frac{d_{im}}{d_m}\frac{\partial c_{im}(x,t)}{\partial t}, \tag{4.20}$$

where we defined the average immobile concentration

$$c_{im}(x,t) = \frac{1}{d_{im}}\int_0^{d_{im}} dz\, C_{im}(\mathbf{x},t). \tag{4.21}$$

The diffusion problem (4.18)–(4.19) can be solved explicitly in Laplace space, see Appendix C.2. The Laplace transform is defined in *Abramowitz and Stegun* [1965]. Laplace transformed quantities are denoted here by a tilde, λ is the Laplace variable. In Appendix C.2, we derive for the average immobile concentration

$$c_{im}(x,t) = \int_0^t dt' g[t-t'|\tau_{im}(x)]c_m(x,t) - c_{im}(x,0)\int_0^t dt' g[t-t'|\tau_{im}(x)] + c_{im}(x,0). \tag{4.22}$$

The memory function $g[t|\tau_{im}(x)]$ is defined in terms of its Laplace transform as

$$g^*[\lambda|\tau_{im}(x)] = \frac{1}{\sqrt{\lambda\tau_{im}(x)}}\tanh\left[\sqrt{\lambda\tau_{im}(x)}\right]. \tag{4.23}$$

The memory function depends on the properties of the immobile region only and it is an intrinsic characteristic of the medium. Figure 4.2 shows the inverse Laplace transform (5.32) for a given position x. In this work Laplace inversion is computed numerically using a Matlab function for numerical inversion by the Hoog algorithm [*Hollenbeck*, 1998].

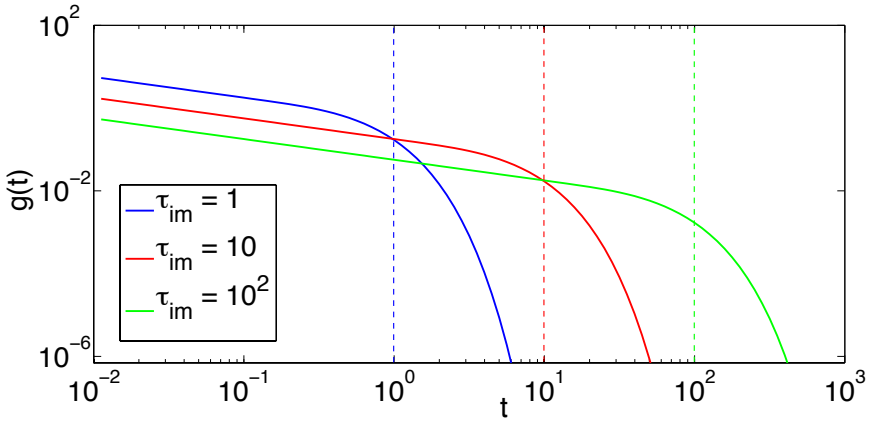

Figure 4.2: *Memory function $g[t|\tau_{im}]$ for an homogeneous immobile zone plotted in function of time for different values of K_{im} in double logarithmic scale. Parameters: $R_m = 1$, $R_{im} = 1$, $d_m = 1$, $d_{im} = 1$, $K_m = 100$, $K_{im} = 1, 10^{-1}$ and 10^{-2}. Vertical dashed lines indicate the characteristic timescales given by the characteritic times of the immobile zones for the different curves: $\tau_{im} = 1, 10$ and 10^2.*

The function $g[t|\tau_{im}]$ decrease as $t^{-1/2}$ for time smaller than the characteristic time of the immobile layer τ_{im} and then, once the immobile region is in equilibrium, it decreases to zero exponentially.

Combining (4.22) with (4.20) and using the resulting expression in (4.15), we obtain for the vertically averaged mobile density $\bar{c}_m(x,t)$ the closed equation

$$\rho_m \frac{\partial c_m(x,t)}{\partial t} + \frac{\partial}{\partial t}\int_0^t dt' \varphi(t-t'|x) c_m(x,t) = \kappa_m \frac{\partial^2 c_m(x,t)}{\partial x^2} + c_{im}(x,0)\varphi(t|x). \tag{4.24}$$

We define the mobile and immobile volume fractions by $\chi_m = d_m/d$ and $\chi_{im} = d_{im}/d$ and the bulk retardation $\rho_m = \chi_m R_m$ and the bulk diffusion $\kappa_m = \chi_m K_m$ coefficient. The memory function $\varphi(t|x)$ is defined by

$$\varphi(t|x) = \rho_{im}(x) g[t|\tau_{im}(x)], \tag{4.25}$$

with the bulk immobile retardation coefficient $\rho_{im}(x) = \chi_{im} R_{im}(x)$. We also define the bulk immobile diffusion $\kappa_{im} = \chi_{im} K_{im}(x)$, thus the characteristic immobile diffusion time is $\tau_{im}(x) = d_{im}^2 \rho_{im}(x)/\kappa_{im}(x)$. The total upscaled concentration $c(x,t)$ comprehensive of the contribution of the mobile and the immobile region, is given by:

$$c(x,t) = \frac{1}{d}\int_0^d C(\mathbf{x},t)\, dz = \chi_m c_m(x,t) + \chi_{im} c_{im}(x,t). \tag{4.26}$$

Same initial conditions in the mobile and immobile zone

Considering the same initial condition in the mobile and in the immobile layer $c_{im}(x,0) = c_m(x,0)$ we can re-write (4.24) in Laplace space as:

$$\lambda\left[\rho_m + \varphi^*(\lambda|x)\right] c_m^*(x,\lambda) - \kappa_m \frac{\partial^2 c_m^*(x,\lambda)}{\partial x^2} = [\rho_m + \varphi^*(\lambda|x)] c_m(x,0). \tag{4.27}$$

Equivalently, in time domain, equation (4.27) gives the following non-local equation for the mobile zone, which represents a delayed diffusive model [*Dentz and Tartakovsky*, 2006]:

$$\frac{\partial c_m(x,t)}{\partial t} - \int_0^t \mathcal{D}(t-t'|x)\, \frac{\partial^2 c_m(x,t')}{\partial x^2}\, dt' = 0 \tag{4.28}$$

where the function $\mathcal{D}(t|x)$ is the inverse Laplace transform of $\mathcal{D}^*(\lambda|x) = \kappa_m/[\rho_m + \varphi^*(\lambda|x)]$.

Zero initial condition in the immobile zone

Considering a zero initial condition for the immobile zone: $c_{im}(x,0) = 0$, the concentration of the immobile zone in Laplace space, from (4.22), reads:

$$c_{im}^*(x,\lambda) = g^*[\lambda|\tau_{im}(x)]\; c_m^*(x,\lambda) \tag{4.29}$$

and the effective equation for the mobile zone reads:

$$\lambda\left[\rho_m + \varphi^*(\lambda|x)\right] c_m^*(x,\lambda) - \kappa_m \frac{\partial^2 c_m^*(x,\lambda)}{\partial x^2} = \rho_m c_m(x,0). \tag{4.30}$$

Thus, in time domain we obtain:

$$\rho_m \frac{\partial c_m(x,t)}{\partial t} + \int_0^t dt'\, \varphi(t-t'|x)\, c_m(x,t') - \kappa_m \frac{\partial^2 c_m(x,t)}{\partial x^2} = 0. \tag{4.31}$$

Comparison of (4.31) and (4.28) evidences that different initial condition in the immobile zone implies different effective models. Considering the same initial condition in the mobile and in the immobile zone, that means an equilibrium condition, we obtain the governing eq. (4.28) which is mass conservative. Differently, starting with a non-equilibrium condition, we obtain (4.31), which is not mass conservative.

The total concentration in function of the concentration in the mobile zone is:

$$c^*(x,\lambda) = \{\chi_m + \chi_{im} g^*[\lambda|\tau_{im}(x)]\}\, c_m^*(x,\lambda). \tag{4.32}$$

In the following, we distinguish between the dual continuum model, consisting of a high and low conductivity layer and the multi continuum model characterized by spatially varying diffusion proprieties in the immobile layer. In order to investigate the diffusion behavior in the multi-continuum medium, we will further average Equation (4.24) over the distribution of the diffusion properties in the heterogeneous low conductivity layer.

4.3.3 Ensemble Average

In order to obtain an upscaled effective formulation, we average the effective governing equations (4.24) and (4.22) horizontally over the immobile zone. Ensemble average over the heterogeneity of the immobile zone of equations (4.24) gives:

$$\rho_m \frac{\partial \bar{c}_m(x,t)}{\partial t} + \frac{\partial}{\partial t}\int_0^t dt' \overline{\varphi(t-t'|x)\, c_m(x,t')} = \kappa_m \frac{\partial^2 \bar{c}_m(x,t)}{\partial x^2} + \overline{c_{im}(x,0)\varphi(t|x)}. \tag{4.33}$$

where the overbar indicates ensemble average. In the last term of eq. (4.33), the initial condition $c_{im}(x,0)$ is deterministic and therefore we can break ensemble average:

$$\overline{c_{im}(x,0)\varphi(t|x)} = c_{im}(x,0)\overline{\varphi(t|x)}. \tag{4.34}$$

We define a global memory function $\varphi(t)$ given by the ensemble average of the local memory functions $\varphi(t|x)$ given in (4.25) associated at each immobile zone:

$$\varphi(t) = \overline{\varphi(t|x)}. \tag{4.35}$$

The average can be executed explicitly and we obtain:

$$\varphi(t) = \overline{\rho(x) g[t|\tau(x)]} = \int d\rho \int d\tau\; p_{\rho,\tau}(\rho,\tau)\, \rho\, g(t|\tau), \tag{4.36}$$

where $p_{\rho,\tau}(\rho,\tau)$ is the joint distribution of the variable ρ and τ. In order to further develop equation (4.36), we consider the expression for $g^*(\lambda|\tau)$ given in (5.32) and we notice that $g^*(\lambda|\tau)$ is precisely function of the product $\lambda\tau$. This implies that $g(t|\tau)$ can be expressed in

function of the single variable function $g'(t/\tau)$ as:

$$g(t|\tau) = \frac{1}{\tau}\, g'\left(\frac{t}{\tau}\right) \tag{4.37}$$

where $g'(t) \equiv g'(t|1)$ is the inverse Laplace transform of $g^*(\lambda) \equiv g^*(\lambda|1)$. Thus, Eq. (4.36) can be re-written as:

$$\varphi(t) = \overline{\rho(x) g[t|\tau(x)]} = \int d\rho \int d\tau\; p_{\rho,\tau}(\rho,\tau)\, \frac{\rho}{\tau}\, g'\left(\frac{t}{\tau}\right). \tag{4.38}$$

The joint distribution $p_{\rho,\tau}(\rho,\tau)$ of Eq. (4.38) can be expressed by using of Bayes' theorem as:

$$p_{\rho,\tau}(\rho,\tau) = p_\rho(\rho)\, p_\tau(\tau|\rho), \tag{4.39}$$

and the conditional distribution $p_\tau(\tau|\rho)$ is defined in terms of the distribution of conductivity $p_\kappa(\kappa)$ as:

$$p_\tau(\tau|\rho) = \frac{d_{im}^2 \rho}{\tau^2}\, p_\kappa\left(\frac{d_{im}^2 \rho}{\tau}\right). \tag{4.40}$$

Back to the ensemble average over the governing equation of the mobile zone, considering the second term of eq. (4.33) we have a problem of closure. We close the equation by a mean field approximation:

$$\overline{\varphi(t-t'|x)\, c_m(x,t)} \approx \overline{\varphi(t|x)}\; \bar{c}_m(x,t). \tag{4.41}$$

Thus we obtain the following upscaled equation for the average mobile concentration:

$$\rho_m \frac{\partial \bar{c}_m(x,t)}{\partial t} + \frac{\partial}{\partial t} \int_0^t dt' \varphi(t-t')\, \bar{c}_m(x,t') = \kappa_m \frac{\partial^2 \bar{c}_m(x,t)}{\partial x^2} + c_{im}(x,0)\varphi(t). \tag{4.42}$$

In order to obtain an upscaled expression for $c_{im}(x,t)$ we average eq. (4.22) and we have:

$$\bar{c}_{im}(x,t) = \int_0^t dt'\, \overline{g[t-t'|\tau(x)]\, c_m(x,t')} - \int_0^t dt' \overline{c_{im}(x,0) g[t-t'|\tau(x)]} + \bar{c}_{im}(x,0). \tag{4.43}$$

The initial value $c_{im}(x,0)$ is deterministic so that the last average in the previous equation does not represent a closure problem. The closure problem given by $\overline{g[t-t'|\tau(x)]\, c_m(x,t')}$ is

closed, as for (4.33), using mean field approximation. Thus we obtain:

$$\bar{c}_{im}(x,t) = \int_0^t dt'\, g(t-t')\, \bar{c}_m(x,t') - c_{im}(x,0) \int_0^t dt' g(t-t') + c_{im}(x,0) \tag{4.44}$$

where we defined:

$$g(t) = \overline{g[t|\tau(x)]} = \int_0^\infty p_\tau(\tau)\, g(t|\tau)\, d\tau. \tag{4.45}$$

The total concentration $\bar{c}(x,t)$ is obtain from averaging of (4.26) and we easily obtain:

$$\bar{c}(x,t) = \chi_m \bar{c}_m(x,t) + \chi_{im} \bar{c}_{im}(x,t). \tag{4.46}$$

Although the characterised time $\tau(x)$ depends on the ratio between the bulk retardation $\rho_{im}(x)$ and the bulk conductivity $\kappa_{im}(x)$, the dynamic of system characterized by spatially variable conductivity or spatially variable retardation factor is very different. Indeed a variable conductivity model corresponds to a barrier model, while a model with a space dependent retardation factor can be mapped into a trap model [*Havlin and Ben-Avraham*, 2002a]. For this reason in the following we consider the two cases separately and indeed we obtain different results. We consider the two cases: (i) constant $\rho_{im} = \rho_0$, variable κ_{im} and (ii) constant $\kappa_{im} = \kappa_0$, variable ρ_{im}.

4.3.3.1 Constant retardation factor

In the case of constant $\rho_{im} = \rho_0$ and variable $\kappa_{im}(x)$, the distribution of the retardation factor can be written as $p_\rho(\rho) = \delta(\rho - \rho_0)$, so that the joint distribution in (4.38) is given by:

$$p_{\rho,\tau}(\rho,\tau) = \delta(\rho - \rho_0)\; p_\tau(\tau|\rho) \tag{4.47}$$

and the marginal distribution of the characteristic times of the immobile zone τ in function of the distribution of the conductivity $p_\kappa(\kappa)$ reads:

$$p_\tau(\tau) = \frac{d_{im}^2 \rho_0}{\tau^2}\; p_\kappa\left(\frac{d_{im}^2 \rho_0}{\tau}\right). \tag{4.48}$$

Substituting (4.47) in the expression for the global memory function given in (4.38), we have:

$$\varphi_\kappa(\tau) = \rho_0 \int d\tau\; p_\tau(\tau) \frac{1}{\tau}\, g'\left(\frac{t}{\tau}\right), \tag{4.49}$$

where the subscript κ of the memory function indicates that it refers to a distribution of bulk conductivity. Considering the change of variable $y = t/\tau$ in the previous equation, we obtain:

$$\varphi_\kappa(t) = \rho_0 \int dy \, \frac{1}{y} \, p_\tau \left(\frac{t}{y} \right) \, g'(y) \, . \tag{4.50}$$

The previous equation indicates that the temporal behaviour of the memory function $\varphi_\kappa(t)$ is determined by the distribution of the characteristic time of the immobile zone $p_\tau(\tau)$. Comparing the definition of $\varphi_\kappa(t)$ given in (4.49) and the definition of $g(t)$, given in (4.45), and considering the relation between $g(t)$ and $g'(t/\tau)$ given in (4.37), we see that for a constant retardation factor ρ_0 we have:

$$g(t) = \frac{\varphi_\kappa(t)}{\rho_0}. \tag{4.51}$$

4.3.3.2 Constant conductivity

In the case of constant bulk conductivity $\kappa_{im} = \kappa_0$ in the immobile zone and spatially variable retardation factor $\rho_{im}(x)$, the joint distribution in (4.38) is:

$$p_{\rho,\tau}(\rho, \tau) = p_\rho(\rho) \, \delta \left(\tau - \frac{d_{im}^2 \rho}{\kappa_0} \right) . \tag{4.52}$$

Consequently, the marginal distribution of the characteristic times results:

$$p_\tau(\tau) = \int d\rho \; p_\rho(\rho) \, \delta \left(\tau - \frac{d_{im}^2 \rho}{\kappa_0} \right) = \frac{\kappa_0}{d_{im}^2} \; p_\rho \left(\frac{\tau \kappa_0}{d_{im}^2} \right) \tag{4.53}$$

and the memory function for the multi continuum model with variable retardation factor is:

$$\varphi_\rho(t) = \frac{\kappa_0}{d_{im}^2} \int d\tau \; p_\tau(\tau) \; g' \left(\frac{t}{\tau} \right) . \tag{4.54}$$

where the subscript ρ indicates that the memory function refers to a distribution of bulk retardation factor. Considering the same change of variable $y = t/\tau$ as in (4.49), we obtain:

$$\varphi_\rho(t) = \frac{\kappa_0}{d_{im}^2} \int dy \, \frac{t}{y^2} \, p_\tau \left(\frac{t}{\tau} \right) \, g'(y) \, . \tag{4.55}$$

Comparing the memory functions for the case of variable conductivity, given in (4.50), and variable retardation factor, given in (4.55), we notice that in both cases the temporal behaviour of the memory function depends on the distribution of the characteristic time of the immobile

zone $p_\tau(\tau)$, but the same distribution of characteristic times determines different scaling of the memory function, because the integrands are different.

4.3.4 Dual Continuum Model

In the following we consider a dual continuum model characterized by a homogeneous immobile zone. The model is similar to the well known comb models for diffusion in disordered media [*Havlin and Ben-Avraham*, 2002a]. Anomalous behaviour in comb model has been already studied. *Metzler and Klafter* [2000] studied sub-diffusion in comb model by particle tracking methods and *Arkhincheev* [2000] deduced an exact solution for a generalized diffusion equation taking into account a random disappearance and birth of the diffusion particles. More recently *Dvoretskaya and Kondratenko* [2009] studied anomalous subdiffusion in comb models considering an infinite immobile zone and *Iomin* [2011] derived subdiffusion in fractal comb.

We present the dual continuum model as a particular case of the multi continuum model. The simpler dual continuum model enables us to discuss some basic feature of the proposed model. Considering an homogeneous immobile layer characterized by a bulk conductivity κ_{im} and a bulk retardation factor ρ_{im}, the joint distribution in the equation of the global memory function (4.36) is:

$$\rho_{\rho,\tau}(\rho,\tau) = \delta(\rho - \rho_{im})\,\delta(\tau - \tau_{im}) \tag{4.56}$$

with $\tau_{im} = d_{im}^2 \rho_{im}/\kappa_{im}$. Thus the memory function $g(t)$ defined in (4.45) and the global memory function $\varphi(t)$ defined in (4.36) depend on time only. In Laplace space, the memory function for the dual continuum model, substituting (4.56) in (4.36) and considering (5.32) with $\tau_{im}(x) \equiv \tau_{im}$, reduces to:

$$\varphi^*(\lambda) = \rho_{im} \frac{1}{\sqrt{\lambda \tau_{im}}} \tanh \sqrt{\lambda \tau_{im}}. \tag{4.57}$$

Clearly, Eq.(4.57) can be also obtained directly from (4.25) and (5.32) considering a constant retardation factor $\rho_{im}(x) = \rho_{im}$ and characteristic time $\tau_{im}(x) = \tau_{im}$.

In the derivation of the multi continuum model we assumed mean ergodicity. In Appendix C.3 is briefly discussed the error we commit considering ensemble average instead of spatial average. In the special case of the dual continuum model the fact that we do not need ensemble average over the immobile zone (because it is homogeneous) implies less assumptions in the derivation proposed.

4.4 Diffusion Behaviour

We discuss the diffusion behaviour of the multi continuum model derived in the previous section using explicit Laplace solutions and numerical simulations. We take into consideration the mobile concentration of the mobile zone $\overline{c}_m(x,t)$, its mean squared displacement (MSD) and its first passage time distribution (FPTD). Explicit analytical solutions are given in Laplace space and temporal behaviour shown in the figures are obtained by numerical inversion of the solution in Laplace space by using the Hoog algorithm [*Hollenbeck*, 1998]. Numerical simulation are performed using the TDRW scheme presented in Section 4.2.2. For brevity we do not give the solutions for $\overline{c}_{im}(x,t)$ and $\overline{c}(x,t)$ that can be easily derived from $\overline{c}_m(x,t)$ by considering (4.44) and (4.46).

4.4.1 Solutions

Here we give analytical solutions in Laplace space for $\overline{c}_m(x,t)$, its MSD and its FPTD for the dual and the multi composite models.

4.4.1.1 Mobile concentration $\overline{c}_m(x,t)$

As initial condition for the mobile zone, we consider a pulse injection in the origin. We model it as an instantaneous imposed value c_0 over an infinitesimal distance d_0, centered in $x = 0$

$$\overline{c}_m(x,0) = c_0 d_0 \delta(x), \tag{4.58}$$

where $\delta(x)$ is the delta function and in case of a finite volume representation d_0 can be given by the discretization of the system. Note that the product $c_0 d_0$ represents the total mass injected in the system. Considering in the immobile zone the same initial condition $\overline{c}_{im}(x,0) = \overline{c}_m(x,0)$, the solution of (4.42) is:

$$\overline{c}^*_m(x,\lambda) = \sqrt{\frac{\rho_m + \varphi^*(\lambda)}{4\,\kappa_m\,\lambda}}\, e^{-\sqrt{\frac{\lambda\,[\rho_m+\varphi^*(\lambda)]}{\kappa_m}}\,|x|}, \tag{4.59}$$

where, for the dual continuum model the memory function $\varphi(t)$ is given in (4.57) and for the multi continuum model with spatially variable conductivity $\varphi(t) \equiv \varphi_\kappa(t)$ given by (4.49) and for spatially variable retardation factor $\varphi(t) \equiv \varphi_\rho(t)$ given in (4.54).

4.4.1.2 Mean square displacement

In the following we consider the MSD defined in (4.8) for the mobile concentration. In Laplace space the definition of the MSD given in (4.8) is:

$$m_2^*(\lambda) = \int_{-\infty}^{\infty} x^2\, \overline{c}_m^*(x,\lambda)\, dx. \tag{4.60}$$

Substituting in the previous equation the expression for $\overline{c}_m(x,\lambda)$ given in (5.29) we obtain:

$$m_2^*(\lambda) = \frac{2\,\kappa_m}{\lambda^2\,[\rho_m + \varphi^*(\lambda)]} \tag{4.61}$$

where, as before the memory function $\varphi(t)$ for the dual continuum model is given in (4.57) and for the multi continuum model in (4.49) for variable conductivity and in (4.54) for variable retardation factor.

4.4.1.3 First passage time distribution

According to the definition of *Risken* [1989], the FPTD $f(t)$ for the mobile concentration $\overline{c}_m(x,t)$ is defined as:

$$f(t) = -\int_{-\infty}^{x_c} \frac{\partial \overline{c}_m(x,t)}{\partial t}\, dx. \tag{4.62}$$

where x_c is the control point where the FPTD is computed. Considering the effective expression for $\overline{c}_m(x,t)$ given in (4.28) for the same initial conditions in the mobile and in the immobile zone, the FPTD reads:

$$f(t) = -\int_{-\infty}^{x_c}\int_0^{\infty} \mathcal{D}(t-t')\frac{\partial^2 \overline{c}_m(x,t')}{\partial x^2}\, dt' dx. \tag{4.63}$$

where $\mathcal{D}(t) = \overline{\mathcal{D}(t|x)}$. Equivalently in Laplace space we have $\mathcal{D}^*(\lambda) = \kappa_m/[\rho_m + \varphi^*(\lambda)]$ and executing the integral respect to the space variable, Eq. (4.63) reads:

$$f^*(\lambda) = \frac{\kappa_m}{\rho_m + \varphi^*(\lambda)} \frac{\partial \overline{c}_m^*(x,\lambda)}{\partial x}\bigg|_{x=x_c}. \tag{4.64}$$

Substituting in the previous equation the solution of $\overline{c}_m^*(x,\lambda)$ given in (5.29), the FPTD in Laplace space results:

$$f^*(\lambda) = \frac{1}{2}\, e^{-\sqrt{\frac{\lambda\,[\rho_m + \varphi^*(\lambda)]}{\kappa_m}}\,|x_c|} \tag{4.65}$$

and as before the memory function $\varphi(t)$ is given in (4.57) for the dual continuum model and in (4.49) and (4.54) for the multi continuum models.

4.4.2 Dual Continuum Model

In the following we consider the temporal behavior of $\overline{c}_m(x,t)$ for the dual continuum model given in (5.29), its MSD, and its FPTD. We show that the dual composite model derived can explain anomalous pre-asymptotic behaviours in diffusion problems. The dual continuum model derived differ from the classical diffusion equation because of the memory term. Consequently, whenever anomalous behaviour occurs, it must be due to the memory function $\varphi(t)$.

4.4.2.1 Characteristic times

Here we discuss the characteristic times that control non Fickian behaviour of the dual continuum model observed in Figure 4.3 and we study if we can obtain anomalous scaling. Considering that the dual continuum model differs from a normal diffusion model because of the memory function given in (4.57), we study when the memory function is the leading term in the expression of $\overline{c}_m(x,t)$ given in (5.29) and if it can scale anomalously.

For time smaller than the characteristic time of the immobile zone $t \ll \tau_{im}$, expanding (4.57) for small λ for $\lambda\tau_{im} \gg 1$, the Laplace transform of memory function scales as:

$$\varphi^*(\lambda) \simeq \rho_{im}(\lambda\tau_{im})^{-1/2}, \tag{4.66}$$

or equivalently in time domain like $\varphi(t) \simeq \rho_{im}\sqrt{\pi/(\tau_{im}t)}$. This scaling is leading in the dynamic of $\overline{c}^*_m(x,\lambda)$ given in eq. (5.29) and implies anomalous behaviour if $\rho_{im}\,(\lambda\tau_{im})^{-1/2} \gg \rho_m$. If this condition is not verified, the memory function is sub-leading and $\overline{c}^*_m(x,\lambda)$ does not scale anomalously. Conditions $\lambda\tau_{im} \gg 1$ and $\rho_{im}\,(\lambda\tau_{im})^{-1/2} \gg \rho_m$ imply in time domain that anomalous behaviour arises in the following pre-asymptotic regime:

$$\left(\frac{\rho_{im}}{\rho_m}\right)^{-2}\tau_{im} \equiv \tau_S \ll t \ll \tau_{im}. \tag{4.67}$$

Time scale separation in (4.67) implies: $\rho_{im} \gg \rho_m$ as prerequisite to observe anomalous behaviour. Anomalous behaviour persists until $t \ll \tau_{im}$ with $\tau_{im} = d^2_{im}\rho_{im}/\kappa_{im}$ the characteristic time of the immobile zone, which is the mean time for the immobile zone to reach equilib-

rium by diffusion along the vertical direction. For $\lambda\tau_{im} \ll 1$ the Laplace transform of memory function given in (4.57) tends to the constant value:

$$\lim_{\lambda\tau\ll 1} \varphi^*(\lambda) \simeq \rho_{im}. \tag{4.68}$$

Thus, asymptotically, for $t \gg \tau_{im}$ the double continuum system acts as an equivalent homogeneous one with $\varphi^*(\lambda) \simeq \rho_{im}$.

Anomalous behaviour starts, as indicated in (4.67), for time larger than a characteristic time that we called τ_S. In order to give a physical meaning to the characteristic time τ_S, we call d_z the penetration length of mass solute into the immobile layer by diffusion after time $t = \tau_S$, so that $\tau_S = d_z^2 R_{im}/K_{im}$. Therefore condition in (4.67), $t \gg \tau_S$, can be re-written as: $d_z R_{im} \gg d_m R_m$. The previous condition indicates that the amount of mass that has entered into the immobile zone after time τ_S is bigger than the amount of mass into the mobile one. For time smaller than τ_S, diffusion takes place basically only into the mobile layer and the contribution of the immobile one is negligible. After the time τ_S enough solute mass entered the immobile zone, its contribution is relevant in the dynamic of the system and the scaling term of the memory function induces anomalous scaling in $\bar{c}_m(x,t)$.

In the following we derive and discuss the anomalous scaling for $\bar{c}_m(x,t)$, its MSD and its FPTD observable in the pre-asymptotic regime given (4.67) considering the condition $\rho_{im} \gg \rho_m$.

4.4.2.2 Mobile concentration $\bar{c}_m(x,t)$

We consider temporal evolution of $\bar{c}_m(x,t)$ given by inverse Laplace transform of (5.29). Figure 4.3 shows the temporal evolutions of $\bar{c}_m(x,t)$ for the dual continuum medium obtained analytically from eq. (5.29) and numerically using the TDRW particle tracking. We notice that curves associated at different characteristic times of the immobile zone τ_{im} behave differently for time $t < \tau_{im}$. For time $t > \tau_{im}$ the system behaves as an equivalent homogeneous one and all the curves scale as $\bar{c}_m(x,t) \sim t^{-1/2}$, as in a normal diffusion.

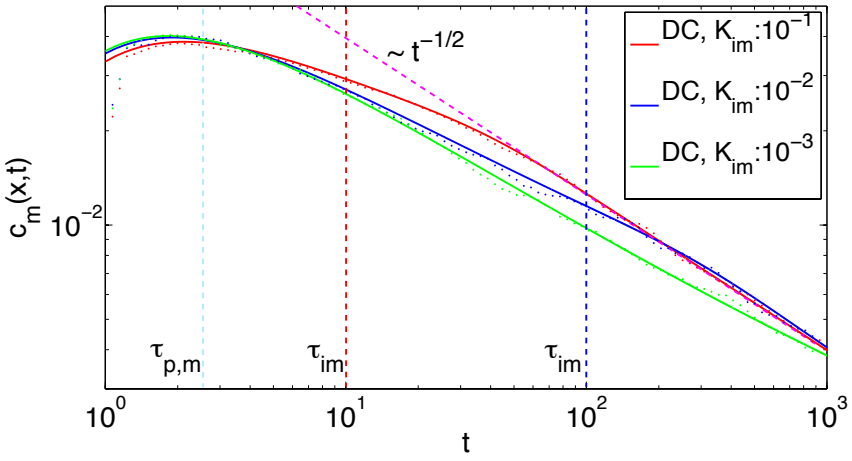

Figure 4.3: *Temporal evolution of $c_m(x,t)$ for the dual continuum model using the analytical solution given in* (5.29) *and numerical simulaitons for different values of the conductivity of the immobile layer $K_{im} = 10^{-1}, 10^{-2}, 10^{-3}$. Parameters: observation point $x = 5$, $R_m = 1$, $R_{im} = 1$, $d_m = 2$, $d_{im} = 2$, $K_m = 10$. Vertical dashed lines indicate the peak mean arrival time $\tau_{p,m} = x^2 R_m / K_m$ due to diffusion in the mobile layer, common for all the curves, and $\tau_{im} = d_{im}^2 R_{im} / K_{im}$ are the characteristic times of the immobile zone related to the different curves. Parameters numerical simulation: horizontal and vertical discretization: $\Delta_x = \Delta_z = 0.5$, number of particles: $np = 5 * 10^6$.*

Anomalous scaling of the mobile concentration is obtained subtituting the temporal scaling of the memory function given in (4.66) in the solution for $\bar{c}_m(x,t)$ given in (5.29) and expanding the obtained equation for $\lambda \tau_{im} \ll 1$, we obtain

$$\bar{c}_m^*(x,\lambda) \simeq \sqrt{\frac{\rho_{im} \tau_{im}^{-1/2}}{4\kappa_m}} \lambda^{-3/4}. \tag{4.69}$$

Equivalently, considering the inverse Laplace transform of the previous equation, we derive that the dual continuum model in time domain gives the following sub-diffusive anomalous scaling:

$$\bar{c}_m(x,t) \simeq \frac{1}{2\Gamma(3/4)} \left(\frac{\rho_{im} \kappa_{im}}{d_{im}^2 \kappa_m^2} \right)^{1/4} t^{-1/4}, \tag{4.70}$$

where $\Gamma(\cdot)$ is the gamma function. Figure (4.4) displays inverse Laplace transform of $\bar{c}_m^*(x,\lambda)$ given in (5.29) focusing on the anomalous behaviour. Analytical solution istested using numerical simulation. Temporal evolution of $\bar{c}_m(x,t)$ scales anomalously as $t^{-1/4}$, as derived in (4.70), for time smaller than τ_{im}, and then scales as in a homogeneous medium as $t^{-1/2}$. The time that corresponds to the peak in the temporal evolution of the concentration, $\tau_{p,m}$, is given by the diffusion parameters of the mobile zone $\tau_p = x^2 \rho_m / \kappa_m$ with x the distance of the observation point. The first characteristic time τ_S given in (4.67), which indicates when anomalous

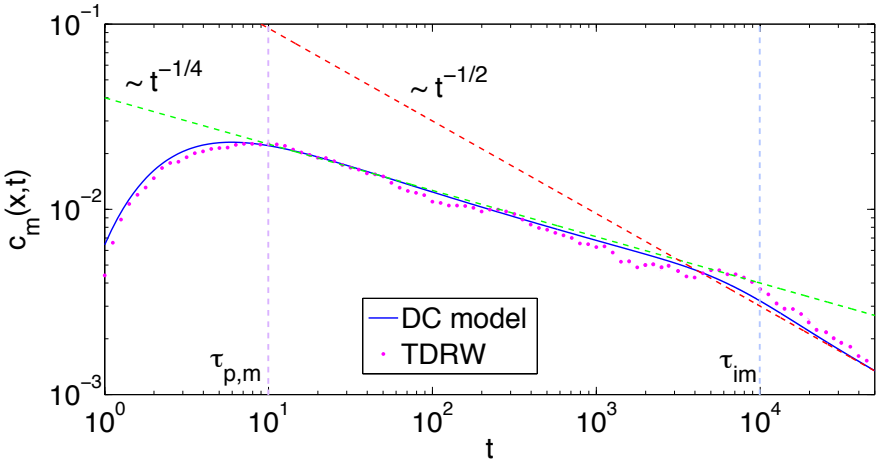

Figure 4.4: *Temporal evolution of $\bar{c}_m(x,t)$ using the analytical solution given in* (5.29) *and TDRW simulaiton. Parameters: $K_m = 10$, $K_{im} = 10^{-2}$, $d_m = 0.1$, $d_{im} = 10$, $R_m = 1$, $R_{im} = 1$, $x = 10$. Dash lines: normal behaviour $\bar{c}_m(t) \sim t^{-1/2}$, anomalous subdiffusive behaviour $\bar{c}_m(t) \sim t^{-1/4}$, mean peak arrival time due to the diffusion parameter of the mobile zone $\tau_{p,m} = x^2 R_m / K_m$, characteritis time of the immobile zone to reach equilibrium $\tau_{im} = d_{im}^2 R_{im} / K_{im}$. Parameters numerical simulation: horizontal discretization: $\Delta_x = 1$, vertical discretization: $\Delta_z = 0.5$, number of particles: $np = 10^6$.*

behavior starts, is smaller than $\tau_{p,m}$ and therefore we observe anomalous behaviour straight after $\tau_{p,m}$.

4.4.2.3 Mean square displacement

Substituting the anomalous scaling of the memory function given in (4.66) in the solution for the MSD given in (4.61) we have:

$$m_2^*(\lambda) \simeq \frac{2\kappa_m}{\rho_{im}\tau_{im}^{-1/2}} \lambda^{-3/2}, \tag{4.71}$$

which in time domain results:

$$m_2(t) \simeq 4\kappa_m \sqrt{\frac{\tau_{im}}{\pi \rho_{im}^2}}\, t^{1/2}. \tag{4.72}$$

The MSD increases with the square root of time, which indicates a sub-diffusive behaviour. Asymptotically the memory function $\varphi^*(\lambda) \simeq \rho_{im}$ (see (4.68)) and therefore, considering the inverse Laplace transform of (4.61), with $\varphi^*(\lambda)$ constant, the MSD grows linearly with time as in a classical diffusion problem: $m_2(t) \sim t$.

Figure 4.5 shows the MSD given in (4.61) and TDRW numerical simulations, focusing on anomalous behaviour. We observe that for time smaller than τ_{im} the MSD increases with time

as $t^{1/2}$ and for time larger than τ_{im} it increases linearly with time.

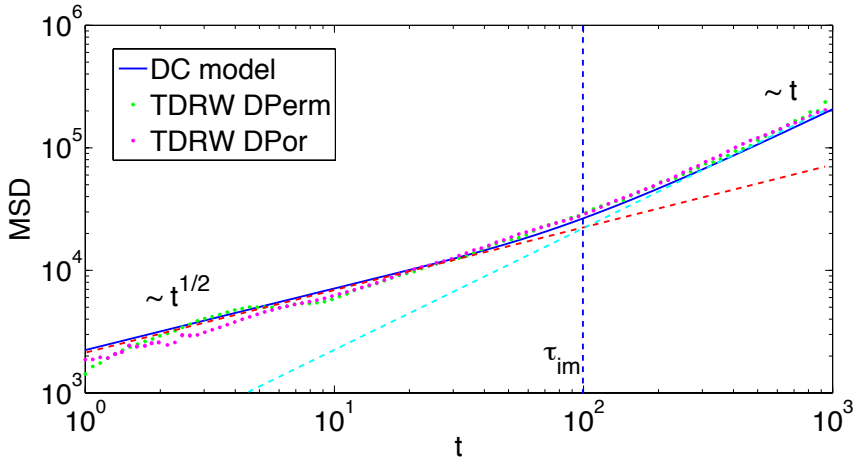

Figure 4.5: *Mean square displacement for the dual continuum model. Numerical simulation are preformed blocking by default horizontal diffusion in the immobile layer (as in 'double porosity' models) and without blocking by default horizontal diffusion in the immobile layer (as in 'double permeability' models). Parameters:* $\kappa_m = 10$, $\kappa_{im} = 10^{-2}$, $d_m = 1$, $d_{im} = 1$, $\rho_m = 10^{-3}$, $\rho_{im} = 1$.

4.4.2.4 First passage time distribution

Considering the anomalous scaling of the memory function given in (4.66) in the expression for the FPTD given in (4.65) we obtain:

$$f^*(\lambda) = \frac{1}{2} e^{-\sqrt{\frac{\tau_{im}^{-1/2}}{\kappa_m}} \lambda^{1/4} |x_c|}, \tag{4.73}$$

which corresponds to a Levy stable distribution. Expanding the previous equation for small λ and using the Tauberian theorem, we obtain that FPTD in time domain scales as $f(t) \sim t^{-5/4}$. Asymptotically, as stated before, $\varphi^*(\lambda) = \rho_{im}$ and the FPTD in time domain results:

$$f(t) \simeq \frac{1}{2} \sqrt{\frac{\rho_m + \rho_{im}}{4\,\kappa_m \pi}}\, |x_c|\, \frac{e^{-\frac{\rho_m + \rho_{im}}{4\kappa_m t} x_c^2}}{t^{3/2}}. \tag{4.74}$$

Expanding the previous equation for large times FPTD scales as $f(t) \sim t^{-3/2}$, which corresponds to the normal scaling of the FPTD for normal diffusion in $d = 1$ spatial dimensional medium. Figure 4.6 illustrates the anomalous scaling of the FPTD for the double continuum model. In the figure is highlighted the pre-asymptotic anomalous scaling as $f(t) \sim t^{-5/4}$ till τ_{im} and the normal scaling as $f(t) \sim t^{-3/2}$ for larger time.

Scaling of temporal evolution, mean square displacement and first passage time distribu-

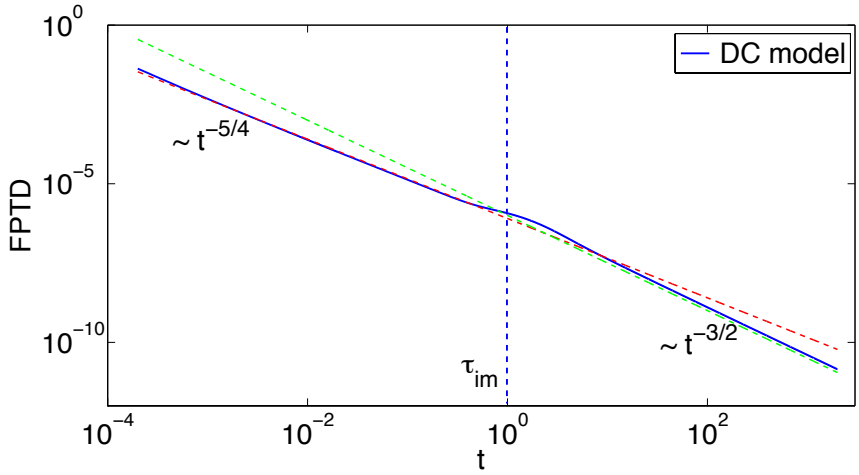

Figure 4.6: *First passage time distribution for the double continuum model. Parameters:* $x_c = 10$, $R_m = 0.01$, $R_{im} = 1$, $d_m = 10$, $d_{im} = 10$, $K_m = 10$, $K_{im} = 0.01$

tion for $\bar{c}_m(x,t)$ are summed in Table 4.1.

Scaling for $\bar{c}_m(x,t)$							
Model		**Temporal evolution**		**MSD**		**FPTD**	
		asymp.	pre-asymp.	asymp.	pre-asym..	asymp.	pre-asym
DC		$t^{-1/2}$	$t^{-1/4}$	t	$t^{1/2}$	$t^{-3/2}$	$t^{-5/4}$
MC	$\kappa_{im}(x)$	$t^{-1/2}$	$t^{-\beta/2}$	t	t^{β}	$t^{-3/2}$	$t^{-1-\beta/2}$
	$\rho_{im}(x)$	$t^{-\beta/2}$		t^{β}		$t^{-1-\beta/2}$	

Table 4.1: *Anomalous scaling of temporal evolution of* $\bar{c}_m(x,t)$*, mean square displacement (MSD) and first passage time distribution (FPTD) for* $\bar{c}_m(x,t)$*. Initial condition:* $\bar{c}_m(x,0) = \bar{c}_{im}(x,0) = c_0 d_0 \delta(x)$ *with* $c_0 d_0 = 1$*. In the table is given asymptotic and pre-asymptotic scaling for the dual continuum (DC) and the multi continuum (MC) model. For the MC model we consider spatially variable* $\kappa_{im}(x)$ *distributed according to a truncated power law distribution and spatially variable* $\rho_{im}(x)$ *distributed according to a power law distribution.* β *is the exponent of the truncated and pure power law distributions and* $0.5 < \beta < 1$*.*

4.4.3 Multi Continuum Model with Constant Conductivity

In this section we consider a multi continuum model where heterogeneity of the immobile zone is given by a spatially variable retardation coefficient $\rho_{im}(x)$. Heterogeneity in the immobile zone induces a distribution of characteristic time in the immobile zone given by $\tau(x) = d_{im}^2 \rho_{im}(x)/\kappa_{im}$. The general expression for the distribution of characteristic times of the immobile zone p_τ in function of the distribution of bulk retardation coefficient p_ρ has been derived in (4.54). As we noticed for the dual continuum model, scaling of the memory function can induce anomalous scaling in the temporal evolution of $\bar{c}_m(x,t)$, its MSD and its

FPTD. In order to obtain an anomalous, or rather fractal, behavior of the memory function $\varphi_\rho(t)$ we consider a fractal distribution of characteristic times. We take the following power law distribution:

$$p_\tau(\tau) = \frac{\alpha}{\tau_1}\left(\frac{\tau_1}{\tau}\right)^{\alpha+1}\Theta(\tau-\tau_1) \tag{4.75}$$

where the Heaviside function $\Theta(\cdot)$ implies a sharp cut off for values τ smaller than the cut off time τ_1 and $\alpha < 1$. Thus we substitute the power law distribution given in (4.75) into the global memory function for a spatially varying bulk retardation coefficient given in (4.54) and re-arranging the terms we obtain:

$$\varphi_\rho(t) = \frac{\kappa_{im}}{d_{im}^2}\,\alpha\,\tau_1^\alpha\,t^{-\alpha}\int_0^{t/\tau} dy\; y^{\alpha-1}g'(y) \tag{4.76}$$

and considering that $g'(y)$ decreases as $y^{-1/2}$ for $y \ll 1$ and then goes exponentially to zero, the integral in (4.76) can be easily solved. For $\alpha < 1$ the memory function reads:

$$\varphi_\rho(t) \simeq \frac{\kappa_{im}}{d_{im}^2}\,\frac{\alpha\,\tau_1^\alpha}{\alpha-1/2}\,t^{-\alpha}. \tag{4.77}$$

The Laplace transform of the memory function given in (4.77) with $\alpha > 1/2$ reads:

$$\varphi_\rho^*(\lambda) \simeq \frac{\kappa_{im}}{d_{im}^2}\frac{\alpha\,\tau_1^\alpha}{\alpha-1/2}\,\frac{\lambda^{\alpha-1}}{\Gamma(1-\alpha)}. \tag{4.78}$$

Details on the Lapalce transform performed here and in the following are given in Appendix C.4.

4.4.3.1 Characteristic times

As discussed above for the dual continuum model, anomalous behaviour arises for $\varphi^*(\lambda) \gg \rho_m$. Here, considering the expression for $\varphi_\rho^*(\lambda)$ derived in (4.78), for $\alpha < 1$, this condition is always fulfilled for small λ. In time domain, it implies that for large time the memory function remains the leading term in the expression of the mobile concentration, (5.29), its MSD, (4.61) and its FPTD, (4.65). Therefore anomalous scaling of the memory function implies asymptotic anomalous scaling of $\bar{c}_m(x,t)$ and also of its MSD and its FPTD.

Considering the distribution of characteristi times of the immobile zone $p_\tau(\tau)$ given in

(4.75), we can compute the mean characteritic time of the immobile zone, that is:

$$\overline{\tau} = \int \tau \, p_\tau(\tau) \, d\tau = \frac{\alpha}{1-\alpha} \tau_1 \tag{4.79}$$

with $0.5 < \alpha < 1$.

4.4.3.2 Mobile concentration $\overline{c}_m(x,t)$

Substituting the anomalous scaling of the memory function $\varphi_\rho(\tau)$ derived in (4.78) in the expression for the temporal evolution of $\overline{c}_m(x,t)$ given in (5.29), and expanding it for small λ, we obtain:

$$\overline{c}^*_m(x,\lambda) \simeq \sqrt{\frac{\kappa_{im}}{d^2_{im}} \frac{\alpha \, \tau_1^\alpha}{\alpha - 1/2} \frac{1}{\Gamma(1-\alpha)} \frac{1}{4\kappa_m}} \, \lambda^{\frac{\alpha}{2}-1}. \tag{4.80}$$

Equivalently, in time domain, inverse Laplace transform of (4.80) gives $\overline{c}_m(x,t) \sim t^{-\alpha/2}$. Figure 4.7 shows temporal evolution of $\overline{c}_m(x,t)$ given by inverse Laplace transform of (5.29) with the power law distribution of characteristic time in the immobile layer given in (4.75). Temporal evolution of $\overline{c}_m(x,t)$ scales anomalously according to (4.80). Numerical simulations confirm analytical solutions.

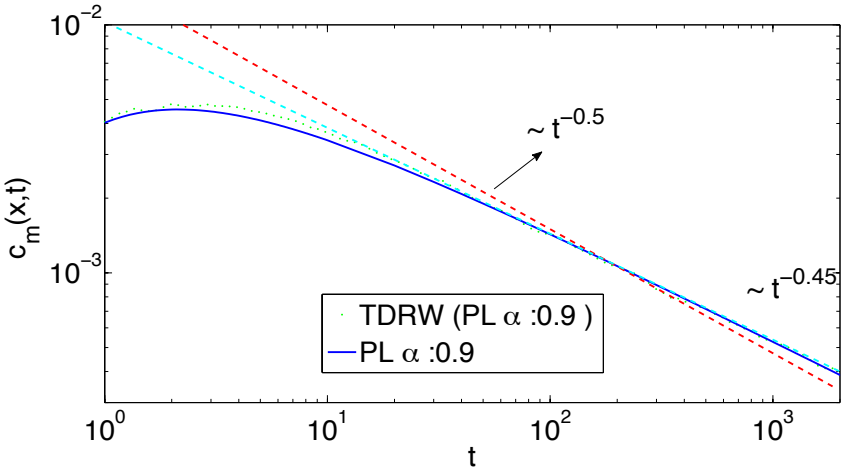

Figure 4.7: *Temporal evolution of $\overline{c}_m(x,t)$ for the multi continuum model with a spatially variable bulk retardation factor $\rho_{im}(x)$. Continuous line: temporal evolution for $\overline{c}_m(x,t)$ given in* (5.29)*, dots: TRDW simulation, dash lines: normal scaling ($t^{-1/2}$) and anomalous scaling $t^{-0.45}$ Considered parameters: $K_m = 150$, $K_{im} = 1$, $d_m = 0.05$, $d_{im} = 1$, $R_m = 10^{-5}$, $x_c = 50$ and τ_{im} distributed according to the power law distribution given in* (4.75) *with $\tau_1 = 1$, $\alpha = 0.9$. Parameters numerical simulations: 10^3 realization with 10^5 particles each. Horizontal discretization: $\Delta_x = 1$, vertical discretization: $\Delta_z = 0.25$.*

4.4.3.3 Mean squared displacement

Anomalous behaviour for the MSD is obtained substituting the anomalous scaling of the memory function φ_ρ given in (4.78) into the expression for the MSD given in (4.61). Considering the limit $\varphi_\rho^*(\lambda) \gg \rho_m$ we obtain:

$$m_2^*(\lambda) \simeq 2\,\kappa_m \frac{d_{im}^2}{\kappa_0} \frac{\alpha - 1/2}{\alpha\,\tau_1^\alpha} \frac{\Gamma(1-\alpha)}{\lambda^{\alpha-1}}, \tag{4.81}$$

and doing the inverse Laplace transform we have the following anomalous scaling: $m_2(t) \simeq t^\alpha$. Figure 4.8 shows the inverse Laplace transform of the MSD given in eq. (4.61) considering power law distribution of characteristic times compared with numerical simulation. We take the power law distribution given in (4.75) with $\alpha = 0.7$. MSD scales anomalously as derived in (4.81), instead of increasing linearly with time as in a normal diffusion.

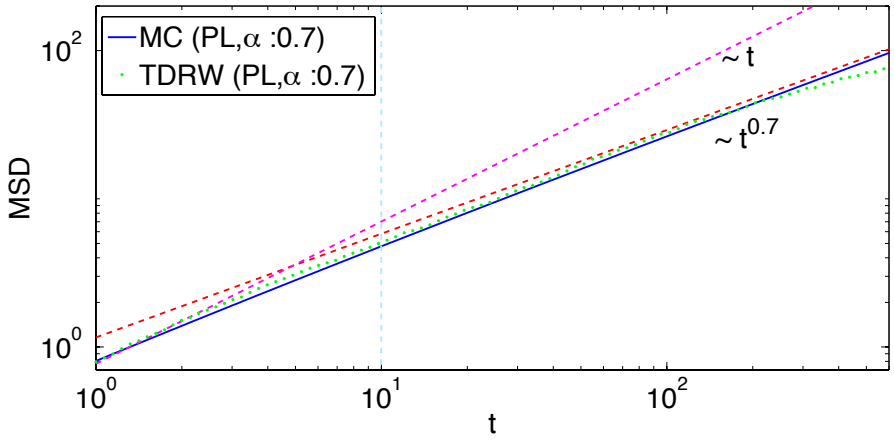

Figure 4.8: *Mean square displacement for the multi continuum model with a spatially variable bulk retardation factor $\rho_{im}(x)$. Continuous line: analytical solution given in* (4.61)*, dots: TDRW simulation, dash lines: normal behaviour ($m_2(t) \sim t$) and asymptotic scaling ($m_2(t) \sim t^{0.7}$). Parameters: $K_m = 10$, $K_{im} = 0.1$, $d_m = 1$, $d_{im} = 10$, $R_m = 0.005$, τ_{im} distributed according to the power law distribution given in* (4.75) *with $\tau_1 = 1$, $\alpha = 0.7$. Vertical line indicates the characteristic time τ_S. Parameters numerical simulation: 10^3 realization with 10^5 particles each. Horizontal discretization: $\Delta_x = 1$, vertical discretization: $\Delta_z = 0.25$.*

4.4.3.4 First passage time distribution

Anomalous scaling of the FPTD is computed by inserting anomalous scaling of the memory function φ_ρ given in (4.78) into the expression for the FPTD derived in (4.65):

$$f^*(\lambda) \simeq \frac{1}{2} e^{-\sqrt{\frac{1}{\kappa_m}\frac{\kappa_0}{d_{im}^2}\frac{\alpha\,\tau_1^\alpha}{\alpha-1/2}\frac{\lambda^\alpha}{\Gamma(1-\alpha)}}|x_c|}. \tag{4.82}$$

Expanding the previous equation for small λ and considering its inverse Laplace transform, we obtain that the FPTD scales asymptotically as $f(t) \sim t^{-1-\frac{\alpha}{2}}$. Anomalous scaling derived in (4.82) is tested by numerical simulations. In Figure 4.9 is compared TDRW simulation with analytical solution for FPTD given in (4.65) for a power law distribution of characteristic time in the immobile layer with $\alpha = 0.7$. Numerical simulation and analytical solution coincide and we observe that FPTD scales anomalously as $f(t) \sim t^{-1.35}$ as predicted from (4.82).

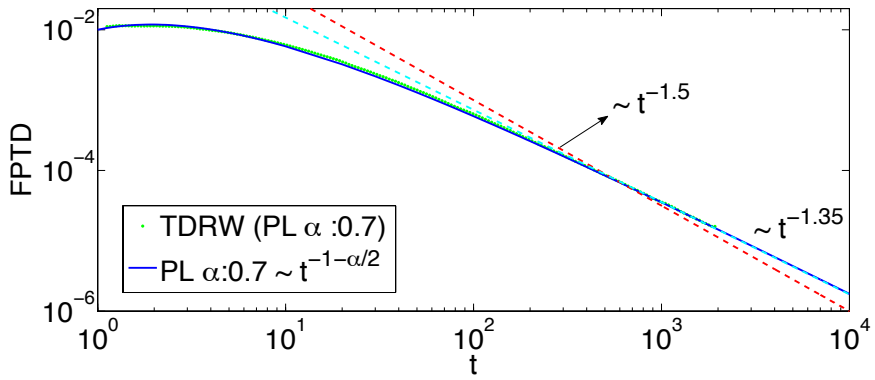

Figure 4.9: *FPTD for the multi continuum model with a spatially variable bulk retardation factor* $\rho_{im}(x)$. *Parameters:* $\kappa_m = 150$, $\kappa_{im} = 1$, $\chi_m = 0.05$, $\chi_{im} = 1$, $\rho_m = 10^{-5}$, $x_c = 50$ *and* τ_{im} *distributed according to the power law distribution given in* (4.75) *with* $\tau_1 = 1$, $\alpha = 0.7$. *Parameters numerical simulations:* 10^3 *realizations with* 10^5 *particles each, horizontal discretization:* $\Delta_x = 1$, *vertical discretization:* $\Delta_z = 0.25$.

In Figure (4.10) we test with numerical simulations the anomalous scaling derived analytically in (4.82) for $\alpha = 0.6$ and $\alpha = 0.9$.

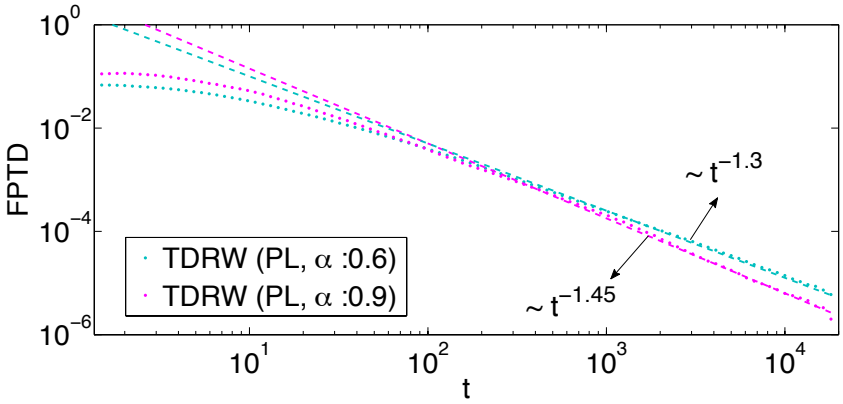

Figure 4.10: *FPTD of $\bar{c}_m(x,t)$ for a multi continuum model with a power law distributions of $\rho_{im}(x)$. Parameters: $\kappa_m = 10$, $\kappa_{im} = 1$, $\chi_m = 1$, $\chi_{im} = 1$, $\rho_m = 0.5$, $x_c = 10$, τ_{im} power law distributed according to (4.75) with $b = 1$ and α indicated in the figure. Parameters numerical simulations: 10^3 realization with 10^4 particles each. Horizontal discretization: $\Delta_x = 1$, vertical discretization: $\Delta_z = 0.25$.*

4.4.4 Multi Continuum Model with Constant Retardation Factor

In this section we consider an heterogeneous immobile zone due to spatially variable bulk conductivity $\kappa(x)$. Heterogeneity is characterized by a truncated power law distribution of characteristic times $p_\tau(\tau)$ in the immobile zone.

We choose a truncated power law distribution with a strong power law, instead of a power law distribution as in the previous section because here, choosing a pure power law gives normal behaviour. This is due to the different structures of the memory functions for the two cases, compare (4.54) and (4.49). This is discussed in detail in Appendix C.4.

In order to keep the derivation simple we consider a truncated power law distribution sharply truncated at two characteristic times τ_1 and τ_2:

$$p_\tau(\tau) = \frac{1-\beta}{\tau_2^{1-\beta} - \tau_1^{1-\beta}}\, \tau^{-\beta}\, \Theta(\tau_2 - \tau)\, \Theta(\tau - \tau_1) \tag{4.83}$$

where $\Theta(\cdot)$ is the Heaviside function, that is equal to one if its argument is larger than zero and zero otherwise and therefore it implies sharp truncation of the power law distribution for $\tau < \tau_1$ and $\tau > \tau_2$. Considering that conductivity of the mobile zone must be far larger than the one of the immobile one: $K_m \gg \max_{x\in\mathbb{R}}\{K_{im}(x)\}$, we have to consider:

$$\tau_1 = \min_{x\in\mathbb{R}}\{\tau(x)\} = \frac{d_{im}^2 R_{im}}{\max_{x\in\mathbb{R}}\{K_{im}(x)\}} \gg \frac{d_{im}^2\, R_{im}}{K_m}. \tag{4.84}$$

Truncation in the distribution of characteristic times implies that anomalous behavior can not be observed asymptotically. In the following we discuss the characteristic times which control anomalous behaviour and the anomalous scaling of the temporal behaviour of $\bar{c}_m(x,t)$, its related MSD and FPTD.

4.4.4.1 Characteristic times

The memory function for a truncated power law distribution of characteristic times due to a spatially variable conductivity field is obtain by substituting the truncated power law given in (5.51) into the expresion for the memory function given in (4.49):

$$\varphi_\kappa(t) = \frac{\rho_0\ (1-\beta)}{\tau_2^{1-\beta} - \tau_1^{1-\beta}} t^{-\beta} \int_{t/\tau_2}^{t/\tau_1} y^{\beta-1}\ g'\,(y)\ dy. \tag{4.85}$$

From the behaviour of $g(t|\tau)$ shown in Figure 4.2, we considering that the function $g'(y)$ decreases as $g'(y) \sim y^{-1/2}$ for y smaller than 1 and then goes exponentially to zero. Because of the truncation in the power law distribution given in (5.51) the improper integral in (4.85) can converge and for $1/2 < \beta < 1$ we have:

$$\varphi_\kappa(t) \simeq \rho_0 \frac{1-\beta}{\tau_2^{1-\beta} - \tau_1^{1-\beta}} \frac{t^{-\beta}}{\beta - \frac{1}{2}} \left[1 - \left(\frac{t}{\tau_2}\right)^{\beta-1/2}\right]. \tag{4.86}$$

Considering that $t \ll \tau_2$ the second term in the squared bracket is sub-leading and so the global memory function behave as a truncated power law by itself:

$$\varphi_\kappa(t) \simeq \frac{\rho_0}{\tau_2^{1-\beta} - \tau_1^{1-\beta}} \frac{1-\beta}{\beta - \frac{1}{2}}\ t^{-\beta}. \tag{4.87}$$

The Laplace transform of the global memory function $\varphi_\kappa(t)$ given in (4.86) is

$$\varphi_\kappa^*(\lambda) \simeq \frac{\rho_0}{\tau_2^{1-\beta} - \tau_1^{1-\beta}} \frac{1-\beta}{\beta - \frac{1}{2}} \left[\lambda^{\beta-1}\Gamma(1-\beta) - \frac{\lambda^{-1/2}\Gamma(0.5)}{\tau_2^{\beta-1/2}}\right] \tag{4.88}$$

and considering the second term in the square brackets sub-leading, we obtain:

$$\varphi_\kappa^*(\lambda) \simeq \frac{\rho_0}{\tau_2^{1-\beta} - \tau_1^{1-\beta}} \frac{1-\beta}{\beta - \frac{1}{2}}\ \lambda^{\beta-1}\Gamma(1-\beta). \tag{4.89}$$

Figure 4.11 illustrates the time behaviour of the global memory function given in (4.86) for different cut-off τ_2 and different exponent β. As illustrated in the figure the global memory

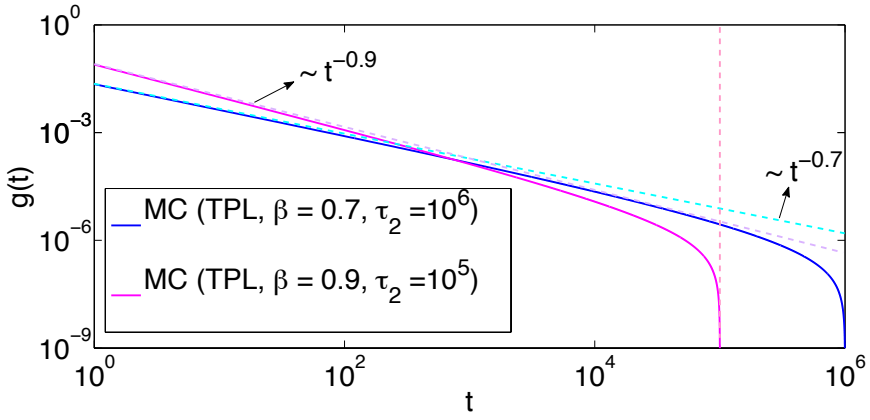

Figure 4.11: *Global memory function for a truncated power law distribution of conductivities. Analytical expression is given in* (4.86)*. Parameters:* $\chi_{im} = 1$ *and* $R_{im} = 1$*,* β *and* τ_2 *are indicated in the figure legend.*

functions decrease as $t^{-\beta}$ till the respectively cut off times τ_2 and then go exponentially to zero.

As discussed previously for the double continuum model, anomalous behaviour of $\overline{c}_m(x,t)$ is observed in a pre-asymptotic regime, for $\varphi^*(\lambda) \gg \rho_m$ and $t \ll \tau_2$. The combination of these two conditions, implies that the time t to observe anomalous behaviour must be:

$$t \ll \left[\frac{\rho_m}{\rho_0}\frac{\beta - 1/2}{1-\beta}\left(\tau_2^{1-\beta} - \tau_1^{1-\beta}\right)\right]^{-\frac{1}{\beta}} = \tau_a. \tag{4.90}$$

In turn, as for the dual continuum model, it implies that anomalous behaviour is observed for $\tau_1 \ll t \ll \tau_a$ and time scale separation requires that the bulk retardation of the immobile zone must be far larger than the bulk retardation of the mobile zone:

$$\rho_{im} \lll \rho_m. \tag{4.91}$$

This condition joint to the model geometry cause that the method of choice for the numerical simulations, a TDRW, is not very efficient. Because of (4.91), and the definition of transition time given in (4.5), transition times for the mobile zone are far smaller than transition time in the immobile zone. And because of the model geometry given in Figure 4.1 and the fact that $\kappa_m \gg \max_{x\in\mathbb{R}}\{\kappa_{im}(x)\}$, computational time is spent doing many steps in the mobile zone where the transition times are extremely far smaller than time increments in the immobile zone.

Notice that considering a spatially variable bulk conductivity $\kappa_{im}(x)$ or a spatially variable

bulk retardation coefficient $\rho_{im}(x)$, we obtain the same scaling of the memory function.

$$\varphi_\rho(t) \sim \varphi_\kappa(t) \sim t^{-\beta} \qquad 1/2 < \beta < 1 \tag{4.92}$$

for time $t_1 \ll t \ll \tau_a$ with τ_a defined in (4.90).

The same scaling in the global memory function $\varphi(t)$ implies the same anomalous scaling of temporal evolution of concentration $\bar{c}_m(x,t) \sim t^{-\beta/2}$ (from eq. (4.80)), of MSD $m_2(t) \sim t^\beta$ and of FPTD $f(t) \sim t^{-\frac{\beta}{2}-1}$.

The difference relies in the different distribution we have to consider in order to obtain anomalous scaling. Considering a spatially varying distribution of conductivity, in order to have an anomalous behavior we need a cut-off in the distribution, otherwise the memory function $\varphi_\kappa(\tau)$ is not integrable for $\beta > 1/2$ and with $\beta < 1/2$ we do not have anomalous behaviour because the scaling term is sub-leading. Thus with a spatially variable conductivity we can have or a fractal distribution of τ_{im} and normal behaviour or a truncated fractal distribution of conductivity and anomalous scaling. Differently with a distribution of retardation coefficient we do not need a cut off in the distribution of characteristic time in order to be able to integrate $\varphi_\rho(\tau)$ and we can have a fractal distribution of τ_{im} and anomalous scaling. Moreover notice the same scaling of the memory function are obtained considering different scaling in the distributions of characteristic times. Considering a distribution of conductivities $\kappa(x)$ the memory function scales as $\varphi_\kappa(t) \sim t^{-\beta}$ considering a distribution of characteristic time which scales as $p_\tau(\tau) \sim \tau^{-\beta}$ (see (4.83)); differently considering a spatially variable retardation factor $\rho(x)$the same scaling of the memory function $\varphi_\rho(t) \sim t^{-\beta}$ is obtained with a distribution that scales as $p_\tau(\tau) \sim \tau^{-1-\beta}$ (see (4.75)). For completeness in the following we give the solutions for the temporal evolution of the mobile concentration, its MSD and its FPTD.

4.4.4.2 Mobile concentration $\bar{c}_m(x,t)$

Temporal evolution of $\bar{c}_m(x,t)$ for the multi continuum model is shown in Figure (4.13). Temporal behaviour is obtained by inverse Laplace transform of (5.29) and $\varphi(t)$ is given in eq.(4.49). Heterogeneity in the immobile zone is given by a truncated power law distribution of conductivities in the immobile zone. Analytical solution is verified by numerical simulation. Referring to Figure 4.13 we notice that the peak arrival time t_p is given by the parameters of the mobile zone $t_p = x_c^2 R_m / K_m$. For time larger that $\bar{c}_m(x,t)$ scales as $\bar{c}_m(x,t) \sim t^{-1/2}$ as in

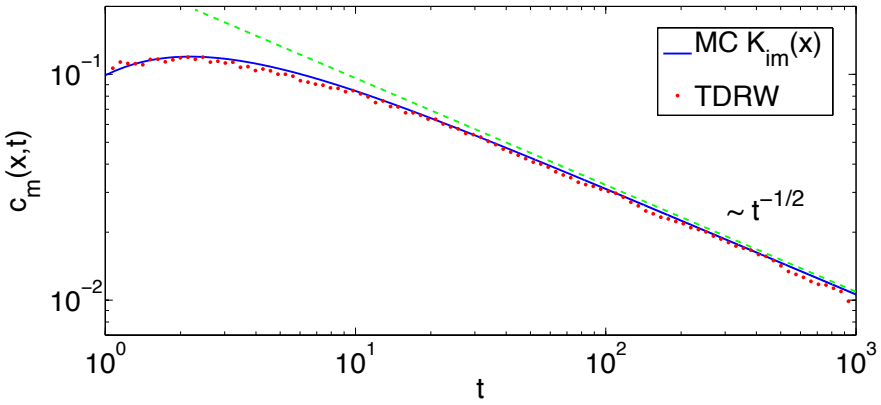

Figure 4.12: *Temporal evolution of $\bar{c}_m(x,t)$ for multi continuum model with truncated power law distributions (TPL) of conductivity in the immobile layer: normal behaviour. Simulation parameters: $K_m = 1$, $d_m = 1$, $d_{im} = 1$ $R_m = 1$, $R_{im} = 1$, $\tau_{im}(x) = d_{im}^2 S_{im}/K_{im}(x)$: distributed according to eq. (5.51) with $\tau_1 = 10$, $\tau_2 = 10^8$ and $\beta = 0.8$. Temporal evolution computed at distance: $x_c = 2$ from the injection point. Parameters numerical simulation:10^3 realizations with 10^5 particles each. Horizontal discretization: $\Delta x = 1$, vertical discretization: $\Delta z = 0.25$.*

a normal $d = 1$ dimensional diffusion process.

Considering the anomalous scaling of the memory function derived in (4.89) and substituting it in the solution for the $\bar{c}_m^*(x,\lambda)$ given in eq. (5.29) for small λ we obtain:

$$\bar{c}_m^*(\lambda) \simeq \sqrt{\frac{\rho_{im}}{\tau_2^{1-\beta} - \tau_1^{1-\beta}} \frac{1-\beta}{\beta - \frac{1}{2}} \frac{\Gamma(1-\beta)}{4\kappa_m}}\, \lambda^{\frac{\beta}{2}-1}. \tag{4.93}$$

Equivalently in time domain we have the following anomalous behaviour $\bar{c}_m(t) \sim t^{-\frac{\beta}{2}}$ with $1/2 < \beta < 1$. In Figure 4.13 are plotted the inverse Laplace transforms of (5.29) computed numerically [*Hollenbeck*, 1998], focusing on anomalous scaling.

In Figure 4.13 we observe the different scaling we can obtain for the temporal evolution of $\bar{c}_m(x,t)$ in function of the distribution of $\kappa_{im}(x)$ derived in (4.93). In the pre-asymptotic regime discussed previously the concentration of the mobile zone scales as: $\bar{c}_m(x,t) \sim t^{-\frac{\beta}{2}}$ with $1/2 < \beta < 1$.

4.4.4.3 Mean square displacement

Substituting the scaling behaviour of the global memory function given in (4.89) in the expression for the MSD derived in (4.61) we have:

$$m_2^*(\lambda) =\simeq \frac{2\kappa_m}{\rho_{im}} \frac{\tau_2^{1-\beta} - \tau_1^{1-\beta}}{\Gamma(1-\beta)} \frac{\beta - \frac{1}{2}}{1-\beta} \lambda^{-\beta-1} \tag{4.94}$$

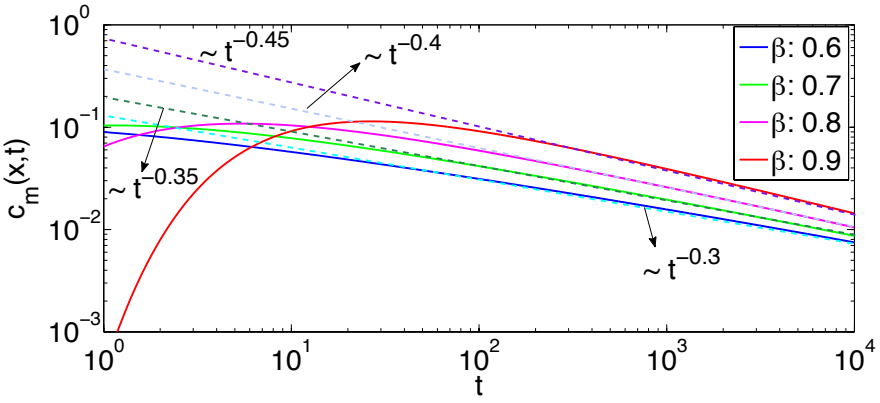

Figure 4.13: *Temporal evolution of* $\bar{c}_m(x,t)$ *given in* (5.29) *for the multi continuum model considering a truncated power law distribution of conductivity in the immobile layer. Anomalous scaling:* $\bar{c}_m(x,t) \sim t^{-\frac{\beta}{2}}$ *with* $1/2 < \beta < 1$. *Parameters:* $\rho_m = 10^{-4}$, $\rho_{im} = 1$, $\chi_m = 0.02$, $\chi_{im} = 10$, $\kappa_m = 40$, $\tau_{im}(x) = \chi_{im}^2 \rho_{im}/\kappa_{im}(x)$*: distributed according to the truncated power law distribution given in* (5.51) *with* $\tau_2 = 250$, $\tau_2 = 10^7$ *and* β *indicated in the figure from 0.6 to 0.9, distance observation point from the injection point* $x = 2$.

and considering its inverse Laplace transform we have the following scaling in time domain: $m_2(t) \simeq t^{\beta}$. In Figure 4.14 we plot the MSD for the multi continuum model given in (4.61) for different truncated distributions of $\kappa_{im}(x)$. Figure 4.14 shows the sub-diffusive anomalous scaling derived analytically.

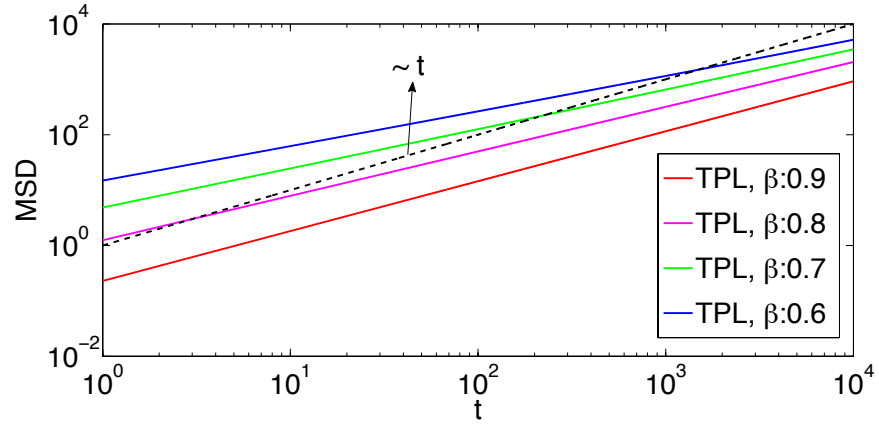

Figure 4.14: *Mean squared displacement given in* (4.61) *for the multi continuum model, considering a truncated power law distribution of conductivity in the immobile layer. Parameters:* $\rho_m = 0.0001$, $\rho_{im} = 1$, $\chi_m = 0.02$, $\chi_{im} = 10$, $\kappa_m = 40$, τ_{im}*: distributed according to the truncated power law given in* (5.51) *with* $\tau_1 = 250$, $\tau_2 = 10^7$ *and* β *indicated in the figure from 0.6 to 0.9.*

4.4.4.4 First passage time distribution

Anomalous FPTD is obtained substituting (4.89) into the definition of the FPTD derived in (4.65):

$$f^*(\lambda) \simeq \frac{1}{2} e^{-\sqrt{\frac{\rho_{im}}{\kappa_m} \frac{\Gamma(1-\beta)}{\tau_2^{1-\beta}-\tau_1^{1-\beta}} \frac{1-\beta}{\beta-\frac{1}{2}}} \lambda^{\frac{\beta}{2}} |x|}. \tag{4.95}$$

The previous equation corresponds to a Levy stable distribution. Expanding (4.95) for small λ and using the Tauberian theorem to compute the inverse Laplace transform, we obtain the follow anomalous scaling for the FPTD: $f(t) \sim t^{-\frac{\beta}{2}-1}$, with $1/2 < \beta < 1$ (see Appendix C.4). As seen previously, asymptotically, the Laplace transform of memory function tends to a constant value. Considering the inverse Laplace transform of (4.65) with $\varphi^*(\lambda) \simeq \rho_{im}$ we obtain that asymptotically the FPTD scales as $f(t) \sim t^{-3/2}$, as in an equivalent homogeneous medium. In Figure 4.15 we plot the FPTD for the multi continuum model given in (4.65) for different exponents of the truncated power law distribution of bulk conductivity. We observe the anomalous scaling of the FPTD derived analytically.

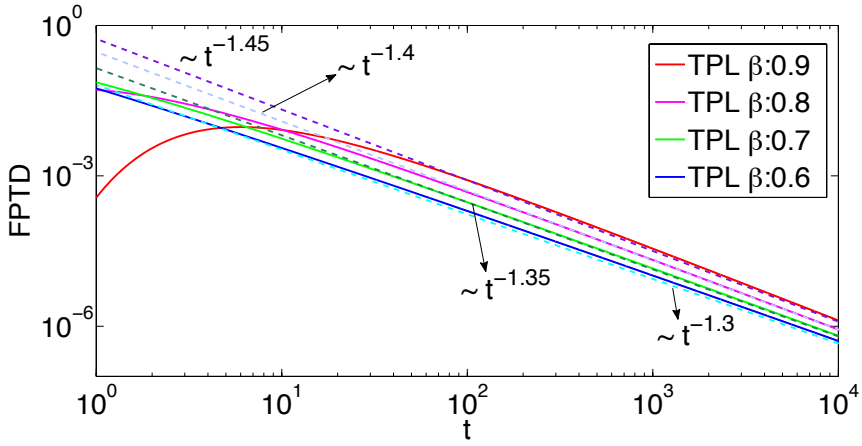

Figure 4.15: *FPTD for the multi continuum model given in* (4.65) *considering a truncated power law distribution of bulk conductivity. Parameters:* $\rho_m = 10^{-4}$, $\rho_{im} = 1$, $\chi_m = 0.02$, $\chi_{im} = 10$, $\kappa_m = 40$, $x = 2$, τ_{im}*: distributed according to the truncated power law given in* (5.51) *with* $\tau_1 = 250$, $\tau_2 = 10^7$ *and* β *indicated in the figure from 0.6 to 0.9.*

Anomalous scaling for the temporal evolution, MSD and FPTD of $\bar{c}_m(x,t)$ are summed concisely in Table 4.1.

4.5 Conclusions

Anomalous diffusion has been observed largely observed in heterogeneous media and media heterogeneity gives rise to a distribution of time scales. On this basis, we derived a multi continuum model characterized by distribution of characteristic times.

The multi continuum models derived lead to anomalous behaviour in diffusion problems of a scalar quantity $\bar{c}_m(x,t)$. The models link anomalous scaling to a statistical description of media heterogeneity. The dual continuum model derived shows pre-asymptotic anomalous scaling, until a characteristic time given by the mean diffusion time in the immobile zone. Unlike the earlier double porosity/permeability models [*Barenblatt et al.*, 1960; *Warren and Root*, 1963; *Dykhuizen*, 1987; *Peters and Klavetter*, 1988; *Dykhuizen*, 1990; *Bai et al.*, 1993]), which consider quasi-equilibrium in each zone and first order mass transfer between the mobile and the immobile regions, we considered non-equilibrium in the immobile zone which origins anomalous behaviour. In the pre-asymptotic regime a sub-diffusive behaviour leads the MSD of $\bar{c}_m(x,t)$ scaling as $t^{1/2}$, its FPTD as $t^{-5/4}$ and its temporal evolution as $t^{-1/4}$. Asymptotically diffusion becomes normal: MSD increases linearly in time, FPTD decreases as $t^{-3/2}$ and temporal evolution as $t^{-1/2}$. In order to have sub-diffusion the bulk retardation coefficient (or total storativity in the case of flow problem) of the mobile region must be far smaller that the one of the immobile region. This condition is typically satisfied in fractured media, where anomalous behaviour is observed. Increasing the heterogeneity of the model, a distribution of diffusion parameters in the immobile layer leads to a larger range of anomalous sub-diffusive behaviours. Considering a distribution of conductivity we obtain pre-asymptotic anomalous behaviour, where MSD of $\bar{c}_m(x,t)$ scales as t^{β}, FPTD as $t^{-\beta/2-1}$ and temporal evolution as $t^{-\beta/2}$, with $0.5 < \beta < 1$. Asymptotically diffusion became normal. Differently a distribution of retardation coefficients, or storativities considering a flow problem, can model the same anomalous scaling also asymptotically and not only pre-asymptotically. The results obtained are in accord with the theoretical work of Bouchaud on diffusion in disordered media [*Bouchaud and Georges*, 1990]. Bouchaud demonstrated that a barrier model, equivalent to a variable conductivity model can not lead to an asymptotic anomalous behaviour, while a trap model, that can be mapped into a variable storativity model, can lead to anomalous asymptotic sub-diffusive behaviour. In this work we link the anomalous behavior in diffusion process to media heterogeneity. Spatial distribution of hydraulic parameters implies in diffusion problem a distribution of timescales. We link the spatial distribution of diffusion parameters to

a distribution of timescales and we link the anomalous behaviour to particular distribution of timescales. We point out that the same time scale distribution in a medium characterized by variable conductivity and variable retardation coefficient induces different asymptotic behaviours. This indicates that the dynamic of a medium characterized by spatially variable conductivity and spatially variable retardation factor is intrinsically different.

Chapter 5

Catchment Response in Frequency Domain

[I]

Anomalous temporal scaling of catchment responses in discharge and groundwater levels observed in hydrological systems are commonly explained by fractal models, which, however, often lack a relation to the medium characteristics and are rather descriptive. Here we employ a multi-continuum approach to model such anomalous behavior. This approach is based on a stochastic model description of the medium heterogeneity, and thus, in principle, allows to relate the catchment response to the distribution of hydraulic parameters. The temporal scaling of groundwater levels and discharge is quantified in frequency domain by the transfer function $\Theta(\omega)$, which is defined as the ratio between the spectra of catchment response and recharge. The transfer function may scale with frequency ω as $\Theta(\omega) \sim \omega^{-\beta}$. While the classical linear and Dupuit models predict exponents of $\beta = 2$ and $\beta = 1$, respectively, the proposed multi-continuum models can explain exponents $1/2 < \beta < 2$. Moreover we revise and integrate the classical linear first-order and Dupuit models in the light of the aquifer dynamics, showing that the scaling exponent of the related transfer functions depends on the boundary condition chosen at the discharge boundary. We systematically analyze the catchment response in the proposed multicontinuum models, and identify and quantify the time scales which characterize the dynamics of the catchment response to recharge.

[I]This chapter is part of a paper *Temporal Scaling of Groundwater Levels and Discharge in Dual and Multi-Continuum Catchment Models*, Russian A., M. Dentz, T. Le Borgne, J. Carrera and J. Jimenez-Martinez; to be submitted to Water Resources Research. Part of the work in this chapter have contributed to the paper: *A frequency domain analysis to characterize heterogeneity and recharge mechanisms in a fractured crystalline-rock aquifer* Jiménez-Martínez J., L. Longuevergne, T. Le Borgne, P. Davy, A. Russian, O. Bour; under review in Water Resources Research.

5.1 Introduction

The understanding of the relation between aquifer discharge and recharge is a fundamental problem in hydrology. Often, aquifer discharge into a river or any outfall is the only information available when studying the groundwater system of a basin. This information may be enough to model regional flow, disregarding the details at local scales [*Duffy and Lee*, 1992]. The discharge of a catchment is a measure for the recharge at basin-scale, and variations in the discharge represent the dynamic response of an aquifer to changes in recharge. A clear understanding of the ground water system dynamics and the recharge processes is fundamental to improve our ability to manage groundwater resources.

Modeling aquifer recharge is a challenging problem due to the variety of physical processes involved and the limited information available on hydraulic parameters, aquifer properties and geometry [*Scanlon et al.*, 2002]. Because of the scarcity of information and the intrinsic complexity in the recharge process, it is useful to keep the models of aquifer recharge simple and linked to a stochastic medium description.

One of the main characteristics in aquifer recharge is the temporal variability in the recharge process. Rainfall enters the aquifer system in an irregular way, but the hydrograph related to the discharge, $q(t)$, or to the groundwater lever $h(x,t)$, are characterized by a certain periodicity [e.g., *Gelhar and Wilson*, 1974; *Besbes and De Marsily*, 1984; *Duffy and Cusumano*, 1998; *Manga*, 1999]. The simplest way to describe this behavior is to consider the catchment as a linear input-output system, where the input (rainfall) and the output (groundwater head variation or the consequent discharge) are related linearly through a transfer function. The transfer function quantifies the action of the aquifer on the discharge dynamics. In this context, the aquifer is considered a linear filter whose properties depend on the medium characteristics and flow processes in the medium [e.g., *Gelhar*, 1974; *Freeze*, 1975; *Duffy and Gelhar*, 1985; *Juki and Denijuki*, 2004; *Zhang*, 2004]. Spectral analysis provides a useful tool to characterize the input and output signals and analyze the filter properties of the aquifer [e.g., *Gelhar*, 1974]. In this framework, the aquifer dynamics are quantified by the power spectrum of the transfer function, which in the following is termed the frequency transfer function $\Theta(\omega)$.

Classical aquifer models to determine the transfer function are the linear reservoir (LR) model and the linear Dupuit (LD) aquifer model [e.g., *Gelhar*, 1974]. The LR model is 0–dimensional and thus disregards spatial variations of hydraulic head. The LD model is 1–dimensional and describes flow in the aquifer based on the linearized Dupuit-Forchheimer

hypothesis [e.g., *Bear*, 1972]. These models are illustrated schematically in Figure 5.1. They predict that for high frequencies ω, the transfer function related to the discharge flux scales as $\Theta(\omega) \sim \omega^{-\beta}$. The LR model predicts a scaling exponent of $\beta = 2$ [*Gelhar*, 1974], the LD model a scaling exponent of $\beta = 1$ [*Gelhar*, 1974; *Molenat et al.*, 1999]. The difference in the scaling exponents implies a difference in the aquifer response dynamics.

Scaling behaviors with exponents $\beta \neq 1, 2$ are called 'anomalous'. A series of studies have shown that groundwater levels and discharge signals [e.g., *Zhang and Yang*, 2010; *Labat et al.*, 2002; *Zhang*, 2004; *Molenat et al.*, 1999, 2000; *Jiménez-Martínez et al.*, 2012] as well as river runoff [e.g., *Tessier et al.*, 1996; *Kantelhardt et al.*, 2003; *Zhang*, 2005; *Kantelhardt et al.*, 2006; *Koscielny-Bunde et al.*, 2006; *Livina et al.*, 2007; *Little and Bloomfield*, 2010] may scale anomalously. Such behavior cannot be explained by classical recharge models, which are based on the representation of the aquifer as a homogeneous porous medium. Geological media are in general heterogeneous and thus the flow dynamics are more complex than in homogeneous media. Specifically, spatial heterogeneity induces a spectrum of transfer time scales, which the classical models are not able to describe. For example, after a recharge event, a portion of water may flow quickly to the discharge point according to the piezometric head gradient, whereas another portion may infiltrate in low permeability regions and get stored there to be released slowly at a later time. As indicated by *Hurst* [1951], long-range correlations in river responses indicate that water storage and discharge processes occur over a wide range of temporal scales [*Tessier et al.*, 1996; *Fiori et al.*, 2009; *Duffy*, 2010].

Anomalous scaling of the frequency transfer function is typically modeled using multi-fractal approaches [e.g., *Turcotte and Greene*, 1993; *Tessier et al.*, 1996; *Kantelhardt et al.*, 2003; *Labat et al.*, 2011]. A limitation of these models is that the fractal dimension is not directly linked to the spatial organization of the aquifer, and it can vary depending on the experimental conditions used to determine it [e.g., *Little and Bloomfield*, 2010]. For these reasons, the interpretation of multi-fractal models is rather difficult [*Tessier et al.*, 1996], which limits their usefulness for prediction [*Labat et al.*, 2002]. *Zhang* [2004] pointed out that anomalous scaling in the aquifer response may be due to medium heterogeneity, or fractality of the recharge process, or a combination of both.

In this paper we focus on the role of medium heterogeneity for the anomalous scaling of the aquifer response to recharge. The objective is to establish a physical model that renders a wide range of water storage scales, that is able to explain anomalous behavior and that allows to link the anomalous dynamics of the discharge process to the distribution of storage scales

as reflected in the physical aquifer characteristics. To this end, we consider dual and a multi-continuum aquifer models that can explain pre-asymptotic anomalous scaling of the transfer function due to the medium heterogeneity. Early double porosity and double permeability models assume that the mobile and the immobile zones are each in quasi-equilibrium and therefore mass transfer is approximated as a first order process [e.g. *Barenblatt et al.*, 1960; *Warren and Root*, 1963; *Dykhuizen*, 1987, 1990]. Our approach takes into account non-equilibrium effects in the immobile zone, which gives rise to anomalous behaviour. In the following, we revisit and extend the classical recharge models and discuss their physical meanings in the light of the resulting aquifer dynamics. On the basis of these classical model, we dervie dual and multi-continuum recharge models which are able to explain anomalous scaling of the frequency transfer function and link this behavior to a statistical description of the medium heterogeneity.

In the following we consider two classical models: the linear reservoir (LR) model and the linear Dupuit (LD) model with different boundary conditions at the discharge point. In modeling recharge dynamics as an input-output problem, linearity implies that the output signal (the groundwater level or the consequent discharge) represents a unique response to a given input (recharge). It is assumed that the recharge $r(t)$ is spatially uniform. Considering ground water discharge $q(t)$ as output, it can be written as a linear functional of the input signal $r(t)$,

$$q(t) = \int_{-\infty}^{\infty} f_q(\tau)\, r(t-\tau) d\tau, \tag{5.1}$$

where $f_q(\tau)$ is the discharge impulse response function, or filter, of the system [*Wiener*, 1949]. This convolution on the right side transforms to a product in frequency domain. The Fourier transform here is defined by

$$F(\omega) = \int_{-\infty}^{\infty} f(t) \exp(-i\omega t) dt, \qquad f(t) = \int_{-\infty}^{\infty} F(\omega) \exp(i\omega t) \frac{d\omega}{2\pi} \tag{5.2}$$

with i the imaginary unit. Taking the Fourier transform of (5.1) and solving for the Fourier transform of $f_q(t)$, we obtain the complex frequency discharge response function $F_q(\omega)$ as the

ratio of the Fourier transform of the discharge $Q(\omega)$ and the recharge $R(\omega)$,

$$F_q(\omega) = \frac{Q(\omega)}{R(\omega)}. \tag{5.3}$$

Its square is the frequency transfer function (FTF) [*Box and Jenkins*, 1970]:

$$\Theta_q(\omega) = |F_q(\omega)|^2. \tag{5.4}$$

The discharge FTF $\Theta_q(\omega)$ characterizes the dynamics of the catchment at basin scale and allows to model recharge dynamics to predict the aquifer response to various hydrological scenarios.

5.1.1 Linear Reservoir Model

In the LR model an aquifer is considered as a lumped linear reservoir system. It is a 0-dimensional model, where spatial variation of water levels are neglected and the average thickness of the saturated zone $h(t)$ is a function of time only [*Gelhar*, 1974; *Bear*, 1972]. A schematic illustration of the model is given in Figure 5.1. The governing equation of the LR model is

$$S\frac{dh(t)}{dt} = -q(t) + r(t), \qquad q(t) = a[h(t) - h_0], \tag{5.5}$$

where S is the storage coefficient $[-]$, $q(t)$ is the outgoing flux per unit area of aquifer surface $[LT^{-1}]$, a is an outflow constant $[T^{-1}]$, h_0 is the reference level of the adjacent outfall body of water, and $r(t)$ is recharge $[LT^{-1}]$ per unit area of the aquifer. For simplicity in the following we set the reference level h_0 to zero without loss of generality. The discharge FTF for the LR model is:

$$\Theta_q(\omega) = \frac{1}{1 + (t_\ell \omega)^2}, \tag{5.6}$$

where t_ℓ is a characteristic response time given by $t_\ell = S/a$ [*Gelhar and Wilson*, 1974]. Frequencies lower than t_ℓ^{-1} are not damped by the system, while for higher frequencies the transfer function scales as $\Theta_q(\omega) \sim \omega^{-2}$.

In addition to the groundwater discharge $q(t)$, we consider also the groundwater level $h(t)$

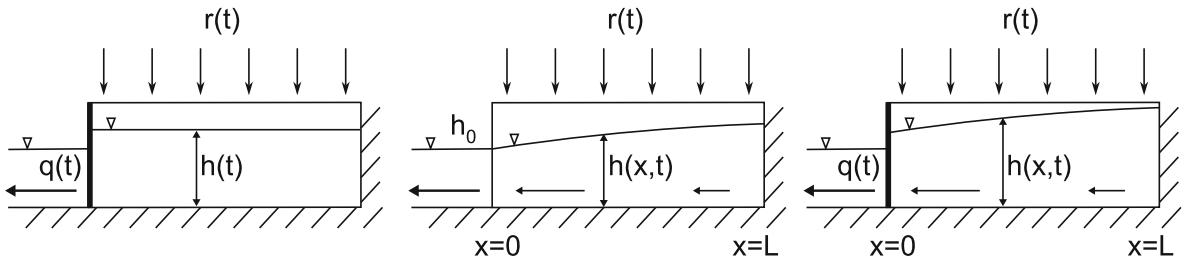

Figure 5.1: *Conceptual illustration of the classical recharge models. From left: LR model, LD model with Dirichlet BC, Dupuit model with Cauchy BC. In the figures: $q(t)$ stream discharge, $r(t)$ aquifer recharge, considered uniform, $h(x,t)$ or $h(t)$ hydraulic head, L length of the catchment, h_0 head level of the outfall basin. h_0 indicates the imposed fixed head at the BC of the LD model with Dirichlet BC. In the LR model and in the LD model with Cauchy BC $q(t)$ indicates the imposed flux BC. In the Dupuit models at $x = L$ no-flux BC at the watershed is imposed.*

as output signal in the input-output catchment model. The head FTF, $\Theta_h(\omega)$, is given by:

$$\Theta_h(\omega) = \left| \frac{H(\omega)}{R(\omega)} \right|^2. \tag{5.7}$$

In the LR model the groundwater head and discharge flux are related by the outflow constant a as given in (5.5). Setting the reference level h_0 to 0, the head FTF $\Theta_h(\omega)$ is related to the discharge FTF as: $\Theta_q(\omega) = a^2\Theta_h(\omega)$. Consequently, the head FTF for the LR model reads:

$$\Theta_h(\omega) = \frac{1}{a + (\omega S)^2}. \tag{5.8}$$

Notice that the scaling for large frequencies for both the groundwater discharge and the ground water level is the same $\Theta_h(\omega) \sim \Theta_q(\omega) \sim \omega^{-2}$.

5.1.2 Linear Dupuit Model

The LD model is based on the linearized form of the Dupuit approximation [*Bear*, 1972], which is given by [*Gelhar*, 1974]

$$S\frac{\partial h(x,t)}{\partial t} - T\frac{\partial^2 h(x,t)}{\partial x^2} = r(t), \tag{5.9}$$

where S is storativity, $h(x,t)$ hydraulic head, T transmissivity and $r(t)$ recharge per unit area of the aquifer. The head frequency transfer function is defined as above as

$$\Theta_h(x,\omega) = \left|\frac{H(x,\omega)}{R(\omega)}\right|^2. \tag{5.10}$$

It is obtained from the solution of the temporal Fourier transform of (5.9),

$$i\omega S H(x,\omega) - T\frac{\partial^2 H(x,\omega)}{\partial x^2} = R(\omega) + S\,h(x,0). \tag{5.11}$$

In order to compare the discharge flux with the recharge, it is convenient to consider the discharge per unit area of the surface of the aquifer. Per Darcy's law, the discharge per unit area in Fourier space, $Q(\omega)$, is given by,

$$Q(\omega) = \frac{T}{L}\left.\frac{\partial H(x,\omega)}{\partial x}\right|_{x=0}. \tag{5.12}$$

As illustrated in Figure 5.1, the Dupuit model represents an homogeneous catchment with a no flow boundary condition (BC) at the watershed (Neumann BC) $[\partial h(x,t)/\partial x]_{x=L} = 0$. At the discharge boundary typically prescribed head (Dirichlet BC) is assumed [e.g. *Gelhar*, 1974; *Molenat et al.*, 1999]. However, Dirichlet discharge boundary conditions may not always be realistic and in many situation Cauchy BCs may be more appropriate [e.g., *Bear*, 1972]. In the following we discuss the behaviour of the FTF depending on the choice of the discharge boundary conditions.

5.1.2.1 Dirichlet Boundary Condition

The Dirichlet BC prescribes the head at the discharge boundary at $x = 0$, $h(x = 0, t) = t) = h_0$. Without loss of generality we set $h_0 = 0$ in the following. Furthermore, we refer to the LD model with Dirichlet boundary conditions as LDD model in the following. With this BC, the

solution of (5.11) is given by

$$H(x,\omega) = \frac{R(\omega)}{i\omega S}\left\{1 - \frac{\cosh\left[p(\omega)\left(\frac{x}{L}-1\right)\right]}{\cosh\left[p(\omega)\right]}\right\}, \tag{5.13}$$

see also [*Gelhar*, 1974]. We defined here

$$p(\omega) = \sqrt{i\omega t_L}, \qquad t_L = L^2 S/T. \tag{5.14}$$

The characteristic response time t_L represents the mean diffusion time over the length of the aquifer. The importance of the aquifer response rate given by t_L^{-1} is discussed in *Erskine and Papaioannou* [1997]. Using (5.13) in (5.12) and the definition of the discharge response function (5.2) we obtain the following expression for the discharge FTF,

$$\Theta_q(\omega) = \frac{1}{\omega t_L}\left|\tanh[p(\omega)]\right|^2. \tag{5.15}$$

The head FTF defined by (5.10) can be directly read of expression (5.13) and is given by

$$\Theta_h(x,\omega) = \frac{1}{\omega^2 S^2}\left|1 - \frac{\cosh\left[p(\omega)\left(\frac{x}{L}-1\right)\right]}{\cosh\left[p(\omega)\right]}\right|^2. \tag{5.16}$$

Notice that $\Theta_h(x,\omega)$ and $\Theta_q(\omega)$ are characterized by different scalings unlike in the LR model. For high frequencies, $\Theta_q(\omega)$ scales as ω^{-1}. The scaling of $\Theta_h(x,\omega)$ depends on the observation point x. Close to the discharge point at $x = 0$, it scales as ω^{-1}, that is, like the discharge FTF. For an observation point near the watershed at $x = L$ and $\omega \gg t_L^{-1}$ it scales as ω^{-2}, which is the scaling behavior of the LR model at high frequencies. The behaviors of $\Theta_q(\omega)$ and $\Theta_h(x,\omega)$ are illustrated in Figures 5.2 and 5.3, respectively.

5.1.2.2 Cauchy Boundary Condition

The Cauchy boundary condition relates the discharge flux with the difference of the boundary head and a reference head h_0 in the outfall as

$$\frac{T}{L}\frac{\partial h(x,t)}{\partial x}\bigg|_{x=0} = a\left[h(0,t) - h_0\right], \tag{5.17}$$

where a is an outflow constant. Without loss of generality the reference level is set to zero $h_0 = 0$. Furthermore, we refer to the LD model with Cauchy Boundary conditions as LDC in

the following. With this BC the solution of (5.11) is given by

$$H(x,\omega) = \frac{R(\omega)}{i\omega S}\left\{1 - \frac{\cosh\left[p(\omega)\left(\frac{x}{L}-1\right)\right]}{\frac{p(\omega)T}{aL^2}\sinh[p(\omega)] + \cosh[p(\omega)]}\right\}, \tag{5.18}$$

with $p(\omega)$ given by (5.14). Notice that for $p(\omega)T/L^2 \ll a$, (5.18) reduces to (5.13). This implies that in the time regime $t \gg (ST)/(aL)^2$ the dynamics of the LDD and LDC models are the same. Using (5.18) in (5.12), the discharge frequency transfer function $\Theta_q(\omega)$ is

$$\Theta_q(\omega) = \frac{a^2}{\omega^2 S^2}\left|\frac{\tanh[p(\omega)]}{\tanh[p(\omega)] + \frac{aL^2}{p(\omega)T}}\right|^2. \tag{5.19}$$

That head FTF again can be directly read of from (5.18) according to (5.10) and is given by

$$\Theta_h(\omega) = \frac{1}{\omega^2 S^2}\left|1 - \frac{\cosh\left[p(\omega)\left(\frac{x}{L}-1\right)\right]}{\frac{p(\omega)T}{aL^2}\sinh[p(\omega)] + \cosh[p(\omega)]}\right|^2, \tag{5.20}$$

Notice that for large ω, the head FTF $\Theta_h(x,\omega) \sim a^{-1}\Theta_q(\omega) \propto \omega^{-2}$. Both transfer functions scale as ω^{-2}. The behavior of the head FTF is at large frequencies independent from the observation point x, as in the LR model. In fact, in the Appendix D.1 we show that the LR model can be obtained from the horizontal average of the LDC model.

5.1.3 Discussion

Here we briefly discuss the dynamics of the models presented above focusing on the scaling of the corresponding transfer functions illustrated in Figures 5.2 and 5.3). The discharge FTF $\Theta_q(\omega)$ for the models considered above are shown in Figure 5.2. The dynamics of $\Theta_q(\omega)$ is controlled by a single characteristic frequency ω_L, the aquifer response rate [*Erskine and Papaioannou*, 1997]. The aquifer response rate is given by $\omega_L = t_L^{-1} = T/(L^2S)$ for the LD models and by $\omega_L = t_\ell^{-1} = a/S$ for the LR model. For frequencies lower than ω_L, $\Theta_q(\omega)$ is equal to one for all the models considered, while for larger frequencies it decreases and scales according to the related recharge model. For the LDD model, the FTF scales as $\Theta_q \sim \omega^{-1}$, and for the LR and LDC models as $\Theta_q \sim \omega^{-2}$. This means that long time components in the recharge spectrum, with frequencies lower than the aquifer response rate are not smoothed by the system and their variations reflect unaltered on the output. Higher frequency components of the recharge spectra are smoothed according to the model considered. Moreover, Figure 5.2

shows that the LDC model slightly differs from the LR model only in an intermediate frequency regime, while for $\omega \ll t_L^{-1}$ and $\omega \gg t_L^{-1}$ the two models coincide. For this reason, in the following, we disregard the first order linear model, and focus on the two LD models.

It is also interesting to note, that *Gelhar* [1974] derived the outflow constant a, which is characteristic of the LR model, from the LDD model and obtained $a = L^2/(3T)$. In Appendix D.1 we show that the LR model in fact corresponds to the LDC model. As outlined above, the behaviors of the LDC and LDD models are different. Thus, we conclude that the derivation of the outflow constant a from the LDD is rather inconsistent. Alternatively, we propose to determine a by comparing the response time of the LR model, which is $t_\ell = S/a$, and the response time of the LD models $t_L = L^2 S/T$. This leads to $a = L^2/T$.

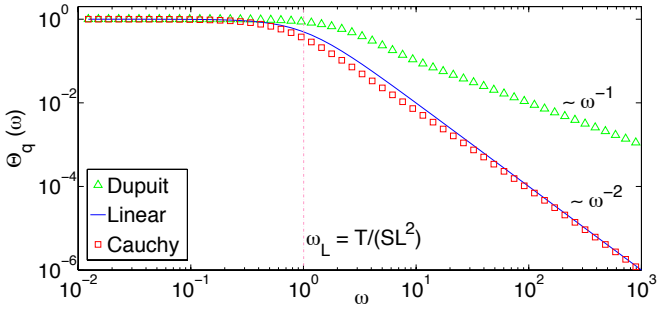

Figure 5.2: *FTF for discharge $\Theta_q(\omega)$. Shown are the (triangles) LDD model, (squares) LDC model (solid line) LR model. The vertical dotted line indicates the aquifer response rate ω_L which is $\omega_L = t_L^{-1} = T/(L^2 S)$ for the LD model and $\omega_L = t_\ell^{-1} = a/S$ for the LR model. The parameters used are $S = 1$, $T = 1$, $L = 1$.*

Figure 5.3 displays $\Theta_h(x, \omega)$ for the LDD and LDC models for different observation points: $x = L$, $x = L/20$ and $x = L/100$. All the $\Theta_h(x, \omega)$ are constant until the aquifer response rate ω_L discussed above, and then decrease according to respective model behavior. Considering the LDC model, the scaling of $\Theta_h(x, \omega)$ does not depend on the observation point in the aquifer and it scales as $\Theta_h(x, \omega) \sim \omega^{-2}$ analogously to $\Theta_q(x, \omega)$ displayed in Figure 5.2.

For the LDD model, in contrast, the scaling of $\Theta_h(x, \omega)$ depends on x. The spatial dependency of $\Theta_h(x, \omega)$ in the LDD model introduces a second characteristic time $t_x = Sx^2/T$, which is given by the mean diffusion time from the observation point to the discharge point. Depending on the observation point x, the head FTF $\Theta_h(x, \omega)$ scales as ω^{-1} until $\omega_x = t_x^{-1}$ and for $\omega \gg \omega_x$, it scales as ω^{-2} as in the LDC and LR models. The scaling ω^{-1} is observed if we have scale separation between the aquifer response time $t_L = L^2 S/T$ and t_x. Close to the discharge point, the transfer function for the ground water level $\Theta_h(x, \omega)$ scales similarly to $\Theta_q(\omega)$. Indeed, the discharge flux is given by Darcy's law and near the discharge point, for

$x \to 0$, we can approximate

$$\left.\frac{\partial h(x,t)}{\partial x}\right|_{x=0} \simeq \frac{h(x,t)}{x}. \tag{5.21}$$

Note that we set $h(x=0,t)=0$. Thus, $\Theta_q(\omega)$ and $\Theta_h(x,\omega)$ scale the same way close to the discharge point. Close to the watershed $\Theta_h(L,\omega) \sim \omega^{-2}$ behaves as for the LR because the system resembles a linear reservoir.

Furthermore, we observe that the value of the head FTF at $\omega = 0$ depends on the respective LD model. Taking the limit $\omega \to 0$ in $\Theta_h(x,\omega)$, (5.13), for the LDD model gives

$$\lim_{\omega\to 0} \Theta_h(x,\omega) = \left| -\frac{x^2}{2T} + \frac{Lx}{T} \right|^2 \tag{5.22}$$

For the LDC model we obtain from taking $\omega \to 0$ in (5.18),

$$\lim_{\omega\to 0} \Theta_h(x,\omega) = \left| -\frac{x^2}{2T} + \frac{Lx}{T} + \frac{1}{a} \right|^2. \tag{5.23}$$

For large values of a, the FTFs of the LDD and LDC models coincide. In general they are different, however. The values of both FTF decrease at $\omega = 0$ as the observation point gets closer to the discharge boundary.

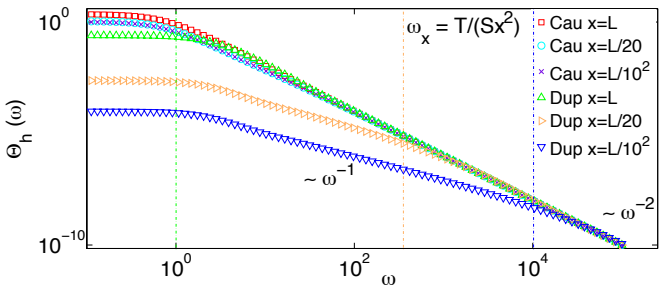

Figure 5.3: *Head FTF $\Theta_h(\omega)$ for different observation points for the LDD and LDC models. The vertical dotted lines indicate the characteristic frequencies $\omega_x = t_x^{-1} = T/(x^2S)$ for the different observation points at $x = L$, $L/20$ and $L/10^2$. The parameters used are $S = 1$, $T = 1$, $L = 1$.*

5.2 Multi-Continuum Recharge Models

In this section we present multi-continuum recharge models which account for the impact of regions of different hydraulic properties in the aquifer. The models derived assume that the water entering the aquifer infiltrates into a conductive region through which it may flow to

the discharge point according to the hydraulic gradient, and from which it may infiltrate into less conductive zones, where it can get trapped and again slowly released. For simplicity, the conductive zone is called mobile region, while the less conductive one is called immobile region. The wide range of temporal scales which characterize natural problems [*Tessier et al.*, 1996; *Fiori et al.*, 2009; *Duffy*, 2010], can arise here from an heterogeneous immobile layer, which statistically described by a distribution of hydraulic parameters. For completeness we take into account also the case of an homogeneous immobile layer, which reduces the multi-continuum recharge model to a dual-continuum recharge model. The underlying conceptual models are illustrated schematically in Figure 5.4.

5.2.1 Model Derivation

The governing equation of the multi-continuum recharge model is given by the flow equation

$$s(\mathbf{x})\frac{\partial h(\mathbf{x},t)}{\partial t} - \nabla \cdot [K(\mathbf{x})\nabla h(\mathbf{x},t)] = 0, \tag{5.24}$$

where $\mathbf{x} = (x,z)^T$. In the immobile region, $0 < z < d_{im}$, specific storativity and hydraulic conductivity are variable in x–direction, $s(\mathbf{x}) = s_{im}(x)$ and $K(\mathbf{x}) = K_{im}(x)$, while in the mobile region, $d_{im} < z < d$, both specific storativity and hydraulic conductivity are constant, $s(\mathbf{x}) = s_m$ and $K(\mathbf{x}) = K_m$. The system is driven by the recharge $r'(t)$ at the upper horizontal boundary of the mobile layer, which yields the boundary condition

$$K_m\frac{\partial h(\mathbf{x},t)}{\partial z} = r'(t), \qquad z = d. \tag{5.25}$$

At the lower boundary a no flux boundary condition is specified

$$K_{im}(x)\frac{\partial h(\mathbf{x},t)}{\partial z} = 0, \qquad z = 0. \tag{5.26}$$

As initial condition we set $h(\mathbf{x},0) = 0$. The hydraulic heads in the mobile and immobile regions are denoted by $h_{im}(\mathbf{x},t) = h(\mathbf{x},t)$ for $0 < z < d_{im}$, and $h_m(\mathbf{x},t) = h(\mathbf{x},t)$ for $d_{im} < z < d$. Both head and flux are continuous at the interface between the two mobile and immobile regions

$$h_m(\mathbf{x},t) = h_{im}(\mathbf{x},t), \qquad K_m\frac{\partial h_m(\mathbf{x},t)}{\partial z} = K_{im}(x)\frac{\partial h_{im}(\mathbf{x},t)}{\partial z}, \qquad z = d_{im}. \tag{5.27}$$

5.2.1.1 Vertical Average

In order to arrive at an effective description, we average the flow equation (5.24) vertically. The average hydraulic heads in the mobile and immobile regions are defined as

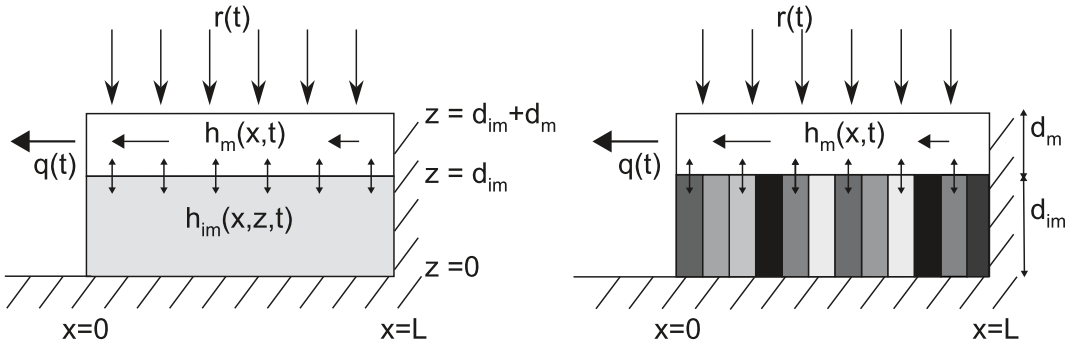

Figure 5.4: *On the left: dual-continuum model, on the right: multi-continuum model. The catchment of longitude L and thickness $d = d_m + d_{im}$ is split into a superficial layer of thickness d_m, which represents the mobile layer and a lower less permeable layer, of thickness d_{im}, which is the immobile layer; $q(t)$ is the stream discharge, $r'(t)$ the aquifer recharge and $h_m(x,t)$ and $h_{im}(\mathbf{x},t)$ the hydraulic heads in the mobile and in the immobile zones, respectively.*

$$\overline{h}_{im}(x,t) = \frac{1}{d_{im}} \int_0^{d_{im}} dz\, h_{im}(\mathbf{x},t), \qquad \overline{h}_m(x,t) = \frac{1}{d_m} \int_{d_{im}}^{d} dz\, h_m(\mathbf{x},t) \tag{5.28}$$

By averaging of (5.24) over the mobile region, we obtain for $\overline{h}_m(x,t)$ the governing equation

$$S_m \frac{\partial \overline{h}_m(x,t)}{\partial t} - T_m \frac{\partial^2 \overline{h}_m(x,t)}{\partial x^2} = r(t) - K_{im}(x) \left. \frac{\partial h_{im}(\mathbf{x},t)}{\partial z} \right|_{z=d_{im}}, \tag{5.29}$$

where we used the continuity condition (5.27) and defined the storage capacity $S_m = s_m d_m$ and transmissivity $T_m = K_m d_m$ of the mobile region, as well as recharge $r(t) = d_m r'(t)$. The last term in (5.29) represents the flux at the interface between mobile and immobile regions and it is obtained from the solution of the flow equation in the immobile domain, which is given by

$$s_{im}(x) \frac{\partial h_{im}(\mathbf{x},t)}{\partial t} - K_{im}(x) \frac{\partial^2 h_{im}(\mathbf{x},t)}{\partial z^2} = 0, \tag{5.30}$$

Notice that we have disregarded flow in horizontal direction in the immobile layer because it is small compared to the one in the more conductive region. Furthermore, we assume that vertical equilibrium in the mobile layer is reached fast so that we can set $h_m(\mathbf{x},t) \approx \overline{h}_m(x,t)$.

Thus, the boundary condition for $h_{im}(\mathbf{x},t)$ at $z = d_{im}$, which follows from the continuity condition (5.27), can be written as $h_{im}(\mathbf{x},t) = \overline{h}_m(x,t)$. At $z = 0$, the no-flux condition reads as$\partial h_{im}(\mathbf{x},t)/\partial z = 0$. The averaged immobile head can be expressed in term of the convolution product [*Russian et al.*, 2012]

$$\overline{h}_{im}(x,t) = \int_0^t d\tau\, g[t,\tau_{im}(x)]\, \overline{h}_m(x,t-\tau), \tag{5.31}$$

with $\tau_{im}(x) = d_{im}^2 s_{im}(x)/K_{im}(x)$. The kernel function $g[t,\tau_{im}(x)]$ is obtained from the solution of (5.30) for the boundary condition $h_{im}(\mathbf{x},t) = \delta(t)$ at $z = d_{im}$. In Fourier space, it is given by

$$g^*[\lambda,\tau_{im}(x)] = \frac{1}{\sqrt{i\omega\tau_{im}(x)}} \tanh\left[\sqrt{i\omega\tau_{im}(x)}\right]. \tag{5.32}$$

The temporal behavior of $g[t,\tau_{im}(x)]$, see Figure 5.5 is well known from multirate mass transfer models for solute transport in multi-continuum media [*Haggerty and Gorelick*, 1995; *Carrera et al.*, 1998]. For $t \ll \tau_{im}$, we observe the characteristic $t^{-1/2}$ behavior, and an exponential cut-off for $t \gg \tau_{im}$.

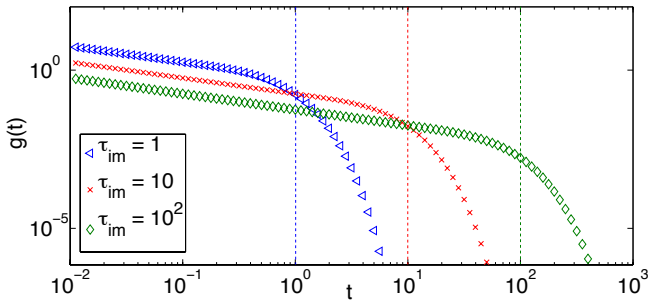

Figure 5.5: *Temporal evolution of $g(,\tau_{im})x$ for (triangles) $\tau_{im} = 1$, (crosses) 10, and (rhombi) 10^2. The parameters used are $S_{im} = 1$, $d_{im} = 1$, $T_{im} = 1$.*

By vertical integration of (5.30), we find that the flux term on the right side of (5.29) is equal to the time derivative of (5.31). Using this in (5.29), we obtain the non-local flow equation

$$S_m \frac{\partial \overline{h}_m(x,t)}{\partial t} + \frac{\partial}{\partial t}\int_0^t dt'\varphi(x,t-t')\overline{h}_m(x,t') - T_m \frac{\partial^2 \overline{h}_m(x,t)}{\partial^2 x} = r(t), \tag{5.33}$$

where we define the memory function $\varphi(x,t)$ by:

$$\varphi(x,t) = S_{im}(x) g[t,\tau_{im}(x)]. \tag{5.34}$$

with $S_{im}(x) = d_{im}s_{im}(x)$. Notice that Eq. (5.38) is analogous to the LD model given in (5.9), but reflects the presence of different storage time scales in the medium, which gives rise to the non-local term. The memory function represents the dynamics of the recharge and storage process in the immobile layer. In this sense, (5.38) can be seen as a time non-local LD model.

5.2.1.2 Ensemble Average

We handle spatial heterogeneity of the immobile zone in a stochastic framework and spatially varying hydraulic conductivity is modeled as spatial random fields. We consider a stationary and ergodic medium, with a finite correlation. For an observation scale far larger than the correlation scale of the random medium, we can approximate the medium organization in bins, where conductivities in each bins are independent. Thus, such medium can be completely defined by a single point distribution. Referring to Figure (5.4) heterogeneity of the immobile layer is organized in bins and at each bin is assigned independently a random conductivity from a distribution.

In order to obtain an upscaled effective formulation, we average the effective governing equations (5.38) horizontally over the immobile zone. Ensemble average over the heterogeneity of the immobile zone of equations (4.24) gives:

$$S_m \frac{\partial \langle \overline{h}_m(x,t) \rangle}{\partial t} + \frac{\partial}{\partial t} \int_0^t dt' \langle \varphi(t-t'|x)\, h_m(x,t') \rangle = T_m \frac{\partial^2 \langle \overline{h}_m(x,t) \rangle}{\partial x^2} + \langle r(t) \rangle \tag{5.35}$$

where the square brackets indicate ensemble average. Ensemble average in the second term of eq. (5.35) can not be executed explicitly. Thus, we use field approximation and we break the ensemble average:

$$\langle \varphi(t-t'|x)\, \overline{h}_m(x,t) \rangle \approx \langle \varphi(t|x) \rangle\ \langle \overline{h}_m(x,t) \rangle. \tag{5.36}$$

We define a global memory function $\varphi(t)$ given by the ensemble average of the local memory functions $\varphi(t|x)$ associated at each immobile zone:

$$\varphi(t) = \langle \varphi(t|x) \rangle. \tag{5.37}$$

Thus, we obtain the following upscaled equation:

$$S_m \frac{\partial \overline{h}_m(x,t)}{\partial t} + \frac{\partial}{\partial t}\int_0^t dt' \varphi(t-t')\overline{h}_m(x,t') - T_m \frac{\partial^2 \overline{h}_m(x,t)}{\partial^2 x} = r(t), \tag{5.38}$$

where, for brevity of notation, we omit the square brackets. In the following we also omit the square brackets for brevity of notation.

5.2.1.3 Solutions

Notice that when the mobile and the immobile zone are vertically in equilibrium, as we discuss in the following, (5.38) reduces asymptotically to a local flow equation for an equivalent homogeneous media

$$S_a \frac{\partial \overline{h}_m(x,t)}{\partial t} - T_m \frac{\partial^2 \overline{h}_m(x,t)}{\partial^2 x} = r(t), \tag{5.39}$$

with a total storativity given by: $S_a = S_m + \langle S_{im} \rangle$ where $\langle S_{im} \rangle$ indicate the ensemble average of $S_{im}(x)$ in the multi-continuum case and is equal to S_{im} in the dual-continuum case. Equation (5.38) can be conveniently written in frequency domain as

$$i\omega S_e(\omega) H_m(x,\omega) - T_m \frac{\partial^2 H_m(x,\omega)}{\partial^2 x} = R(\omega), \tag{5.40}$$

where we defined an effective function $S_e(\omega)$:

$$S_e(\omega) = S_m + \varphi(\omega). \tag{5.41}$$

In frequency domain, the governing equation of the multi-continuum recharge model (5.40) is equal in form to the Fourier transform of the LD model given in (5.11), with $S_e(\omega)$ instead of S. Consequently, the expression for the frequency transfer functions for the recharge multi-continuum models, can be obtain by substituting S by $S_e(\Omega)$ in the respective expressions for the LD models.

Dirichlet Boundary Condition Thus, solution of (5.40) results: The transfer function for the multi-continuum model with Dirichlet BC related to the ground water level reads:

$$H(x,\omega) = \frac{R(\omega)}{i\omega S_e(\omega)} \left\{ 1 - \frac{\cosh\left[p_e(\omega)(1-x')\right]}{\cosh[p_e(\omega)]} \right\}, \tag{5.42}$$

with $p_e(\omega) = \sqrt{i\omega\tau_e(\omega)}$ and $\tau_e(\omega) = L^2 S_e(\omega)/T_m$ and the discharge FTF:

$$\Theta_q(\omega) = \left| \frac{1}{i\omega\tau_e(\omega)} \tanh[p_e(\omega)] \right|^2. \tag{5.43}$$

Cauchy Boundary Condition Considering Cauchy BC at the discharge, solution of (5.40) is:

$$H(x,\omega) = \frac{R(\omega)}{i\omega S_e(\omega)} \left\{ 1 - \frac{\cosh\left[p_e(\omega)(1-x')\right]}{\frac{p_e(\omega)T}{aL^2}\sinh[p_e(\omega)] + \cosh[p_e(\omega)]} \right\} \tag{5.44}$$

and discharge FTF is given by:

$$\Theta_q(\omega) = \left| \frac{aL}{i\omega S_e(\omega)} \left\{ \frac{\tanh[p_e(\omega)]}{\tanh[p_e(\omega)] + \frac{aL^2}{p_e(\omega)T}} \right\} \right|^2. \tag{5.45}$$

5.2.2 Dual-Continuum Recharge Model

Considering an homogeneous immobile zone, the multi-continuum model reduces to a dual-continuum one. The governing equation is given by (5.38) with s_{im} and K_{im} instead of $s_{im}(x)$ and $K_{im}(x)$. Considering equation (5.32), where $\tau_{im}(x) = \tau_{im}$, the characteristic time τ_{im} indicates the mean time for the immobile zone to reach equilibrium by diffusion along the vertical direction. For times larger than τ_{im}, considering $\omega \gg \tau_{im}^{-1}$, the memory function (5.32) scales as $g(\omega) \sim (\omega\tau_{im})^{-1/2}$ and therefore also $S_e(\omega)$ given in (5.41) can scales as $S_e(\omega) \sim \omega^{-1/2}$ if

$$S_{im}(\omega\tau_{im})^{-1/2} \gg S_m. \tag{5.46}$$

The previous condition is satisfied for $\omega \ll (S_{im}/S_m)^2/\tau_{im}$, which identifies a characteristic threshold frequency ω_S or equivalently a characteristic time $\tau_S = \omega_S^{-1}$ given by:

$$\tau_S = \left(\frac{S_m}{S_{im}}\right)^2 \tau_{im} = \frac{d_{im}^2 S_m^2}{T_{im} S_{im}} \tag{5.47}$$

and anomalous scaling of $S_e(\omega)$ is defined in the interval:

$$\tau_{im}^{-1} \ll \omega \ll \tau_S^{-1}. \tag{5.48}$$

In order to interpret the characteristic time τ_S, when anomalous behaviour starts, we call Δz the characteristic penetration of water by diffusion into the immobile layer after the time τ_S: $\Delta z = \sqrt{T_{im}\tau_S/S_{im}}$ and (5.46) can be re-written as: $\Delta z\, S_{im} \gg d_m S_m$ which indicates that the

amount of water into the immobile layer must be larger than the amount of water into the mobile one. For time smaller than τ_S, flow takes place basically only into the mobile layer and the contribution of the immobile one is negligible. After the time τ_S enough water infiltrated into the immobile zone and its contribution is relevant.

In the following we focus on the anomalous scaling of the transfer functions for the dual-continuum model considering the anomalous scaling of $S_e(\omega)$ in the pre-asymptotic regime defined in (5.48).

5.2.2.1 Dirichlet Boundary Condition

Considering the double continuum model with Dirichlet BC, the transfer function given in (5.43) scales anomalously as:

$$\Theta_q(\omega) \simeq \frac{T_m}{S_{im}L^2}\left(\frac{\omega}{\tau_{im}}\right)^{-1/2} \tag{5.49}$$

instead of the $\Theta_q(\omega) \sim \omega^{-1}$ as in the classical local LD model with Dirichlet BC. For ω larger than τ_S^{-1}, $\Theta_q(\omega)$ tends to the classical scaling $\Theta_q(\omega) \sim \omega^{-1}$. The behaviour of the $\Theta_q(\omega)$ is shown in Figure 5.6. For large ω, which corresponds to short times the flow takes place essentially only in the more conductive zone and $\Theta_q(\omega)$ behaves as in a homogeneous media characterized by the parameters of the mobile zone. After a time τ_S enough water has entered the immobile zone, its contribution is relevant and we can observe anomalous scaling until time τ_{im}, when also the immobile zone is in equilibrium along the vertical direction and the system behaves as an equivalent homogeneous media and follows the classical behaviour of the LD model.

The scaling of the head FTF $\Theta_h(\omega)$, as discussed previously in Section 5.1.2.1, depends on the observation point x in the aquifer. Near the watershed, for x to L, instead of the classical scaling ω^{-2}, in the pre-asymptotic regime given in (5.48), we obtain $\Theta_h(\omega) \sim \omega^{-1}$. At the discharge point, for x to 0, instead of ω^{-1} we have $\Theta_h(\omega) \sim \omega^{-1/2}$. For this reason in the following we point out only the scaling of $\Theta_q(\omega)$ which is characteristic of the model and does not depend on the observation point.

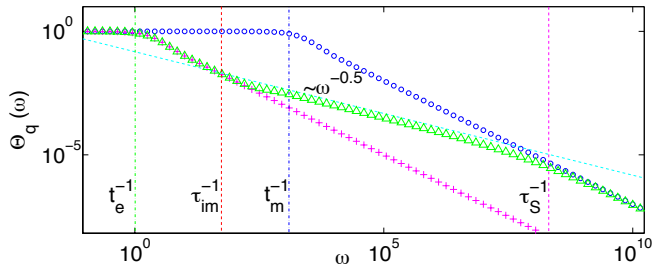

Figure 5.6: *Frequency transfer function for ground water discharge for the dual-continuum model with Dirichlet BC (triangles). Dots: $\Theta_q(\omega)$ considering only the mobile layer; crosses: $\Theta_q(\omega)$ for homogeneous equivalent model with effective storativity given by* (5.2.1.3)*. Anomalous scaling $\omega^{-0.5}$ is indicated with the continuous line. Vertical dashed lines mark the characteristic times (given on the left side) that control the dynamic of the system: $t_m = L^2 S_m / T_m = 10^{-3}$, $t_e = L^2 S_a / T_m = 1.001$, $\tau_{im} = d_{im}^2 S_{im} / T_{im} = 10^{-2}$, $\tau_S = 10^{-8}$ given in* (5.47)*. The parameters used are: $S_m = 0.1$, $S_{im} = 100$, $d_m = 0.01$, $d_{im} = 0.01$, $T_m = 1$, $T_{im} = 0.01$, $L = 1$.*

5.2.2.2 Cauchy Boundary Condition

Considering the dual-continuum model with Cauchy BC, the discharge FTF defined in (5.45) in the pre-asymptotic regime given in eq. (5.48) and discussed previously, scales as:

$$\Theta_q(\omega) \sim \frac{a^2 \tau_{im}}{S_{im}^2} \omega^{-1}. \tag{5.50}$$

Figure 5.7 shows $\Theta_q(\omega)$ as a function of frequency, displaying the anomalous pre-asymptotic regime between $\tau_{im}^{-1} = S_{im} T_{im} / d_{im}^2$ and τ_S discussed in equation (5.47) where the $\Theta_q \sim \omega^{-1}$ instead of ω^{-1}.

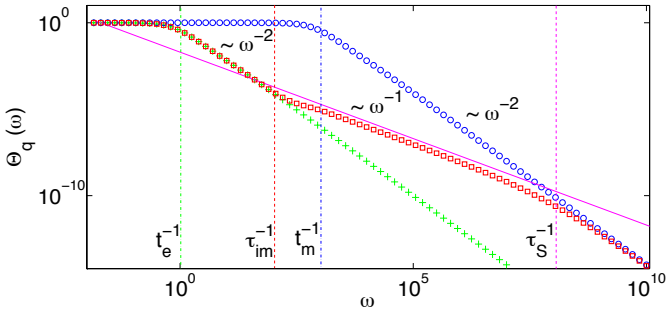

Figure 5.7: *Frequency transfer function for ground water discharge in dual-continuum model with Cauchy BC (squares). Dots: $\Theta_q(\omega)$ considering only the mobile layer; crosses $\Theta_q(\omega)$ for homogeneous equivalent model with effective storativity given by* (5.2.1.3)*. Anomalous scaling ω^{-1} is indicated with the continuous line. Vertical dashed lines mark the characteristic times (given on the left side) that control the dynamics of the system: $t_m = L^2 S_m / T_m = 10^{-3}$, $t_e = L^2 S_a / T_m = 1.001$, $\tau_{im} = d_{im}^2 S_{im} / T_{im} = 10^{-2}$, $\tau_S = 10^{-8}$ given in* (5.47)*. The parameters used are: $S_m = 0.1$, $S_{im} = 100$, $d_m = 0.01$, $d_{im} = 0.01$, $K_m = 1$, $K_{im} = 0.01$, $L = 1$.*

The transfer function related to the ground water level, as previously pointed out for the Dupuit model with Cauchy BC, for large ω is given by: $\Theta_h(x,\omega) \simeq \Theta_q(\omega)/a^2$ independently from the observation point and therefore the same anomalous scaling arises.

5.2.3 Multi-Continuum Recharge Model

Instead of the simple two layers geometry, we consider an heterogeneous immobile zone that we characterize statistically by a distribution of of characteristic times $\tau_{im}(x)$. In the following, considering that the intrinsic storativity is usually less variable respect to the hydraulic conductivity, we consider an immobile layer of thickness d_{im}, with an intrinsic storativity s_{im} and a space dependent conductivity $K_{im} = K_{im}(x)$, so that the distribution of $\tau_{im}(x) = d_{im}^2 s_{im}/K_{im}(x)$, is linked to the distribution of $K_{im}(x)$. In order to reflect a broad distribution of mass transfer scales, accounting for the existence of a largest scale (see discussion in *Dentz et al.* [2004]), we consider a truncated power law distribution of the characteristic times in the immobile zone that for brevity we call τ:

$$P(\tau) = \frac{1-\beta}{\tau_c}\left(\frac{\tau}{\tau_c}\right)^{-\beta} H(\tau_c - \tau) \tag{5.51}$$

where τ_c is the cut off of the distribution and $H(\cdot)$ is the Heaviside function, which is equal to one if its argument is larger than zero and zero otherwise. According to *Russian et al.* [2012], we consider an exponent β between 0.5 and 1 and we define a global memory function $\psi(t)$ given by superposition of the local memory function $\varphi[\tau(x),t]$ related to each immobile region:

$$\psi(t) = \langle \varphi(\tau(x),t)\rangle = \int_0^\infty P(\tau)\, g(\tau,t)\ d\tau \tag{5.52}$$

where the square brackets indicate ensemble average over a coarse grain resolution scale.

Considering an exponent of the truncated power law distribution given in (5.51): $1/2 < \beta < 1$ the global memory function defined in (5.52) results:

$$\psi(t) = S_{im}\frac{1-\beta}{\beta-\frac{1}{2}}\frac{t^{-\beta}}{\tau_c^{1-\beta}}\left[1-\left(\frac{t}{\tau_c}\right)^{\beta-\frac{1}{2}}\right] \tag{5.53}$$

Notice that the second term in the squared brackets in (5.53) is sub-leading because of $t \ll \tau_c$ and the global memory function behaves as a power law by itself: $\psi(t) \sim t^{-\beta}$. Analogously

that for the double continuum model we can identify a pre-asymptotic regime:

$$\tau_c^{-1} \ll \omega \ll \tau_S^{-1}, \tag{5.54}$$

with τ_c the cut off time of the truncated power law distribution (5.51) and τ_S, analogously to (5.47), is equal to

$$\tau_S = \left(\frac{S_{im}}{S_m}\right)^{\frac{1}{\beta-1}} \tau_c. \tag{5.55}$$

where $S_e(\omega) \simeq \psi(\omega) \sim \omega^{\beta-1}$. The characteristic time τ_S as discussed for the double continuum model represents the time needed so that enough water enters the less permeable layer and its contribution is relevant in the dynamic of the whole system.

In the following we consider the multi continuum recharge model with Dirichlet and Cauchy BC and we focus on the anomalous behaviour of the transfer function we can observe in the pre-asymptotic regime identified in (5.54).

5.2.3.1 Dirichlet Boundary Condition

Considering the multi-continuum recharge model with Dirichlet BC, in the pre-asymptotic regime given in (5.54) the transfer function related to the ground water discharge (see eq. (5.43)) can have the following anomalous scaling:

$$\Theta_q(\omega) \simeq \left|\frac{T_m}{L^2\omega S_e(\omega)}\right| \simeq \frac{T_m}{L^2 S_{im}} \frac{\beta - \frac{1}{2}}{1-\beta} \frac{\tau_c^{1-\beta}}{\Gamma(1-\beta)}\, \omega^{-\beta} \tag{5.56}$$

with $0.5 < \beta < 1$. The transfer function related to the ground water level, as discussed above, depends on the observation point, near the watershed it reads:

$$\Theta_h(L,\omega) = \left[\frac{1}{S_{im}} \frac{\beta - \frac{1}{2}}{1-\beta} \frac{\tau_c^{1-\beta}}{\Gamma(1-\beta)}\right]^2 \omega^{-2\beta}. \tag{5.57}$$

which corresponds to the anomalous scaling of the Cauchy model as derived in the following, while near the discharge point it can scale as $\Theta_h(x \ll 1, \omega) \sim \Theta_q(\omega) \sim \omega^{-\beta}$. Figure 5.8 shows the scaling of the head FTF for different exponents β of the hydraulic conductivity distribution.

As pointed out in Figure 5.9 the dynamic of the multi-continuum model, analogously that for the double continuum model, is controlled by 3 characteristic times: τ_S given in (5.55), τ_c the cutoff of the truncated power law distribution of characteristic times and the aquifer

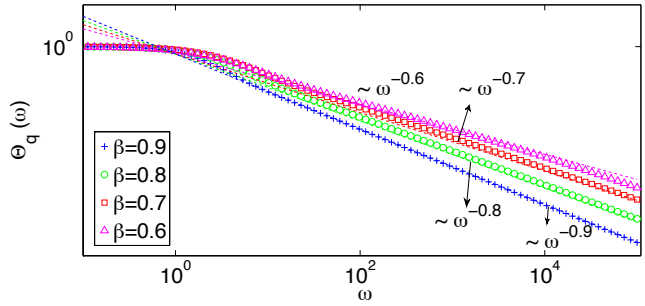

Figure 5.8: *Anomalous scaling of the frequency transfer function for the discharge in multi continuum recharge model with Dirichlet BC. Continuous lines: $\Theta_q(\omega)$ for different values of the exponent β of the truncated power law distribution of τ given in* (5.51)*. Anomalous scaling is highlighted with dash lines corresponding to $\omega^{-\beta}$.*

response rate for an equivalent homogeneous media $t_e = \frac{L^2 S_a}{T_m}$. For times shorter than τ_S or $\omega \ll \tau_S^{-1}$, flow takes place, essentially, only in the mobile layer, the multi-continuum model behaves as an homogeneous model characterized by the parameters of the mobile zone and Θ_q scales as in the classical Dupuit model $\Theta_q \sim \omega^{-1}$. Between τ_S and the cutoff of the truncated power law distribution τ_C, the recharge model is affected by the heterogeneity of the immobile zone and we can have the anomalous scaling given in (5.56). The cut off time τ_c represents the largest characteristic time of the immobile layer, for times larger than τ_c, the mobile and immobile layer are vertically in equilibrium and the model behaves as an equivalent homogeneous system, characterized by the asymptotic value of $S_e(\omega)$ given in (5.2.1.3). The correspondent equivalent aquifer response time, which determines equilibrium along the length L of the aquifer, reads: $t_e = \frac{L^2 S_a}{T_m}$. with $S_a = S_m + S_{im}$.

5.2.3.2 Cauchy Boundary Condition

Considering the multi-continuum recharge model with Cauchy BC in the pre-asymptotic regime discussed previously, we obtain the following pre-asymptotic anomalous scaling for $\Theta_q(\omega)$defined in (5.45):

$$\Theta_q(\omega) \simeq \left[\frac{a}{S_{im}} \frac{\beta - \frac{1}{2}}{1-\beta} \frac{\tau_c^{1-\beta}}{\Gamma(1-\beta)} \right]^2 \omega^{-2\beta} \tag{5.58}$$

and $\Theta_h(\omega) \simeq \Theta_q(\omega)/a^2$ which corresponds to the limit of Θ_h for the multi-continuum model with Dirichlet BC for $x \to L$ given in (5.57). Figure 5.10 shows the anomalous scaling for $\Theta_q(\omega)$ of a multi-continuum model with Cauchy BC for different β. Notice that the pre-

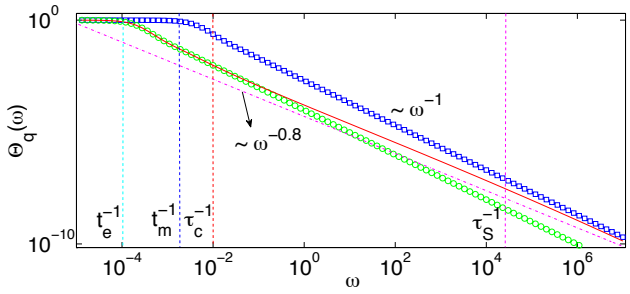

Figure 5.9: *Frequency transfer function for ground water discharge in the multi continuum model with Dirichlet BC (squares, blue) $\Theta_q(\omega)$ considering only the mobile layer, (continuous line, red) multi permeability model, (circles, green) homogeneous equivalent model with effective storativity given by* (5.2.1.3)*, (dotted line, magenta) power law $\omega^{-0.8}$ in order to evidence the anomalous pre-asintotic scaling. The vertical dashed lines indicate the characteristic times of the system: $t_m = L^2 S_m / T_m$, $t_e = L^2 S_a / T_m$, τ_c is the cut off of the truncated power law distribution given in* (5.51) *and τ_S is given by* (5.55)*. The parameters used are: $s_m = 0.05$, $s_{im} = 1$, $d_m = 1$, $d_{im} = 1$, $T_m = 100$, cut off of the power law distribution: $\tau_c = 100$, exponent $\beta = 0.8$.*

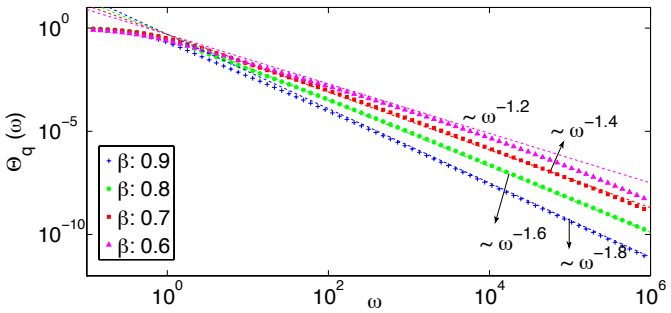

Figure 5.10: *Anomalous scaling of the frequency transfer function for the discharge $\Theta_q(\omega)$ in a multi continuum model with Cauchy BC. In the figure: $\Theta_q(\omega)$ for different values of the exponent of the power law distribution of characteristic times of the immobile layer given in* (5.51)*: crosses: $\beta = 0.9$, dots: $\beta = 0.8$, squares: $\beta = 0.7$, triangles: $\beta = 0.6$. Dash lines highlight the anomalous scaling $\omega^{-2\beta}$. Parameters used: $S_m = 1$, $S_{im} = 100$, $d_m = 0.01$, $d_{im} = 0.01$, $T_m = 1$, $T_{im} = 0.05$, $L = 1$, $\tau_c = 100$.*

asymptotic regimes, where anomalous scaling arise, vary with the exponent β according to (5.54) and (5.55).

5.3 Conclusions

This work deals with the aquifer recharge/discharge dynamic in frequency domain. In the first part of this paper we revise and extend the classical first order and Dupuit linear models. We point out that in the Dupuit model the scaling of the transfer function depends on the boundary condition at the discharge point. Considering Dirichlet boundary condition the discharge FTF scales as $\Theta_q \sim \omega^{-1}$, while the head FTF Θ_h depends on the observation point

into the basin: near the discharge it scales as Θ_q while near the watershed as $\Theta_h \sim \omega^{-2}$ analogously to the first order linear model. Considering Cauchy BC we derive that the transfer functions for both the discharge flux and the ground water head for large frequency scale as ω^{-2}, independently from the observation point, as in the first order linear model. Indeed we show that the first order linear model can be derived by the Dupuit model with Cauchy BC. In the second part of this paper we derive a multi-continuum recharge model based on a broad distribution of storage time scales in different regions of a spatially heterogeneous medium. The model derived can explain anomalous behaviour in a pre-asymptotic regime and link it to a distribution of hydraulic propriety of the medium. The multi continuum model considers that water entering the aquifer part flows directly to the discharge point according to the hydraulic gradient trough a more permeable layer, part gets stored in less permeable regions to be released slowly. Anomalous dynamic is controlled by two characteristic times related to the distribution of the hydraulic parameters of the immobile zone. At the beginning flow takes place, essentially, only in the more permeable zone and the first characteristic time indicates when the contribution of the immobile zones get relevant and anomalous behaviour arises. The second characteristic time indicates when anomalous dynamic ends because the system is in equilibrium and the heterogeneous catchment behave as an equivalent homogeneous one. The multi continuum model can explain the following pre-asymptotic scaling of the transfer function: $\Theta_q \sim \omega^{-\beta}$ for Dirichlet BC, eq. (5.15), and $\Theta_q \sim \omega^{-2\beta}$ for Cauchy BC, eq. (5.17), with β between 0.5 and 1. The physical model proposed can explain anomalous scaling evidenced in literature and link them to the hydraulic parameters distribution as reflected in the physical aquifer characteristics. For this reason we claim that the models proposed can be used in modeling aquifer response and their utility in predictability is higher respect the fractal models.

Chapter 6

Summary and Conclusions

This thesis focuses on the qualitatively and quantitative assessment of heterogeneity in diffusion phenomena. We take into account the flow problem at Darcy's scale and the diffusion of solute driven by Fick's law. These two problems are mathematically equivalent describing diffusion of a scalar quantity (the hydraulic head for the flow problem or the solute concentration for the diffusion of a solute) due to a potential loss (the head gradient for the flow or the gradient of the concentration for the diffusion of a solute).

Natural media are heterogeneous at different scales and heterogeneity brings complexity in the diffusion problem. Spatial variability of diffusion parameters makes a precise description of the media difficult, if not impossible, to obtain. Even if it would be possible to have a detailed description of the media, the amount of information would be practically impossible to handle and the large scale behaviour difficult to interpret. Because of these reasons we choose a stochastic approach. Stochastic approach provides a systematic way to quantify the effect of heterogeneity into large scale models. This work is centered on the integration of the effects of heterogeneity on Darcy flow and solute diffusion into large scale models which are linked with a description of natural media.

Historically, large scale descriptions of flow in heterogeneous media and diffusion phenomena have been given in terms of effective parameters, as effective conductivity for flow and effective diffusivity for diffusion. Specifically, in Darcy flow, a lot of work has been done for the estimation of an effective hydraulic conductivity since the studies of Matheron in the 60's [*Matheron*, 1967]. Exhaustive reviews for effective conductivity are given in *Renard and de Marsily* [1997] and *Sanchez-Villa et al.* [2006], and for effective diffusivity in *Dean et al.* [2007].

Nevertheless, as is known, a large scale description in terms of effective parameters in not

enough to model many phenomena (e.g. tailing in drawdown curves [*Le Borgne*, 2004] or in solute residence times in low permeability regions [*Le Borgne and Gouze*, 2008; *Gouze et al.*, 2008b] and scale dependency of effective parameters [*Sanchez-Villa et al.*, 2006; *Schulze-Makuch, D., Douglas, A. Carlson, Douglas, S. Cherkauer, Malik*, 1999]) and a large scale description in terms of an equation different from its local counterpart is needed. Whenever the behaviour of a diffusion process cannot be described by Fick's law, it is called non-Fickian or anomalous. The term 'anomalous' indicates that the mean square displacement does not increase linearly with time, as in a normal diffusion process, but rather as t^β with $\beta \neq 1$.

In this thesis we give effective descriptions of large scale behaviours in terms of both effective coefficients (as effective conductivity or diffusivity) and effective equations different from their local counterparts. We find large scale description of diffusion in heterogeneous media that can explain anomalous behaviours and link it with a description of media heterogeneity. Depending on the kind of heterogeneity we use different methods to upscale the local problems and obtain large scale descriptions. We use perturbation theory, particle tracking methods, spatial and ensemble average.

In the second chapter we upscale flow in heterogeneous media in stochastic framework using perturbations theory. We consider hydraulic conductivity spatially variable. Starting from a local scale flow equation given by the Fick's second law we obtain, after stochastic average, an effective non-local expression. Similarly to *Tartakovsky and Neuman* [1998b], we obtain a non local equation both in time and in space. Non-locality is expressed by a kernel, which depends on the correlation function that characterize the medium heterogeneity. We derive a compact formulation for $d = 1, 2$ and 3 spatial dimension.

Afterwards, we localize the effective formulation in space and we obtain a governing equation non local only in time. We give analytical solutions in Laplace space for the non-local in time formulation and we discuss the head response for a pulse injection for $d = 1, 2$ and 3 spatial dimension. Further, we localize the non-local effective description also in time and we reduce the non-local formulation into a local flow equation with a time dependent effective conductivity. We show that the time dependent conductivity obtained by localization can be equivalently derived in a more systematic way by using perturbation theory in terms of the second center moment of the hydraulic head. We show that the time dependent effective conductivity, in the limit for time to infinity, tends to the well known values of effective conductivity in heterogeneous media. For $d = 1$ it tends to the first order approximation of the harmonic mean of the local values of conductivity, for $d = 2$ to the geometric mean and for

$d = 3$ to the first order approximation of the Matheron's conjecture for a $d = 3$ dimensional media [*Matheron*, 1967]. The time dependent conductivity tends to its corresponding effective value depending on the dimensionality of the problem as $t^{-d/2}$, that means that in a $d = 3$ dimensional problem the time dependent conductivity tends to its effective value faster than in $d = 1$. It implies that an equivalent homogeneous description can be used earlier in a $d = 3$ dimensional problem respect that in $d = 1$.

This aspect is highlighted also comparing the head evolution for a pulse injection computed with the non-local in time formulation derived and the classical local one with the well known values of effective conductivity [*Matheron*, 1967]. Asymptotically, the non-local formulation can be localized and the non local formulation is equivalent to the local one, but local formulation underestimate early arrival times in the drawdown curves: drawdown curves computed with the non-local formulation starts before than the ones computed with the local formulation. Note that a correct estimation of early arrival times is highly important for risk assessment studies and well protection.

The difference in the early arrival time using the local and the non-local formulation increases as the variance and the correlation length of the conductivity field increase. This behaviour can be explained by the fact that the evolution of head in the non-local case is influenced by the values of the hydraulic conductivity at small times. In average, conductivity at small time is given by the arithmetic mean K_A, which is larger than the value of the asymptotic effective conductivity: $K_A < K_{eff}$ for any d dimension. Effective conductivity is classically defined for steady state condition, when all the heterogeneity is sampled and at this time that the non-local formulation can be localized. The characteristic time scale for the sampling of the heterogeneity τ_K is given by the correlation length of the medium heterogeneity: $\tau_K = \ell^2/K_G$ with ℓ the correlation length and K_G the geometric mean of the local hydraulic conductivities values. For time larger than τ_K the medium heterogeneity has been sampled, the non-local formulation can be localized and the effects of the heterogeneity can be described by an equivalent homogeneous model. For $t < \tau_K$ the non-local formulation must be considered.

The difference between local and non-local formulation is less pronounced for increasing spatial dimension. For $d = 1$ the error committed by using localized formulation is higher than in $d = 3$. This is because sampling efficiency increases with the dimensionality of the problem and the non-local formulation can be localized when all the heterogeneity have been sampled.

The results obtained in this chapter are only valid for a moderately heterogeneous media. In case of highly heterogeneous media different upscaling methods must be used. In Chapter 3 we address the problem of diffusion heterogeneous media numerically in a random walk perspective. Highly heterogeneous media can represent a problem also for particle tracking methods. Whenever the media are highly heterogeneous or characterized by abrupt interfaces, classical random walk can be costly because the heterogeneous diffusion properties may require a fine time-discretization in order to ensure that a particle actually 'sees' the spatial variability [*James and Chrysikolpoulos*, 2001]. In regions of low conductivity a particle may have to wait at the same site for a large number of simulation steps, which is inefficient [*McCarthy*, 1993]. Moreover, the presence of discontinuity in the conductivity field makes the use of a classical random walk complicated because it relies on the calculation of the gradient of the conductivity [*Delay et al.*, 2005]. Efficiency of classical random walk for these kind of media can be improved by the time domain random walk (TDRW) method and the continuous time random walk (CTRW) method.

In Chapter 3 we use TDRW to solve diffusion in heterogeneous media numerically and to upscale analytically diffusion problems in heterogeneous media. In the first part we show that flow and diffusion in heterogeneous media can be efficiently solved in a particle tracking framework by time domain random walk (TDRW) method [*McCarthy*, 1993; *Delay et al.*, 2002] and we extend the classical TDRW for multiple trapping process. Classical TDRW method has been largely used in literature for diffusion and transport problems in heterogeneous media (e.g. [*Banton et al.*, 1997; *Delay and Bodin*, 2001; *Delay et al.*, 2005]), but the formal equivalence between the diffusion equation an the TDRW was missed. We demonstrate the formal equivalence between the diffusion equation and the TDRW and we extend the classical TDRW to solve diffusion problem in a heterogeneous medium with multi-rate mass transfer properties in a stochastic framework. In a stochastic framework an heterogeneous medium is seen as realization of an ensemble of all possible realizations with the same statistical properties. TDRW gives the solution of a diffusion problem in one realization. Solving a diffusion problem in one realization corresponds to solve diffusion in a 'quenched' disorder. In a quenched disorder the spatially variable property of the medium are constant in time. Whenever the spatially variable diffusion properties varies randomly in time the disorder is defined 'annealed'. CTRW is an annealed model in that at each time step a random time increment is chosen independently. For a random walk in a disordered medium there is a certain probability to jump to a site recently visited and a certain site can be visited a large number of times. If the proper-

ties assigned at each site are constant in time, as in a quenched disorder, this induces certain correlation in successive random steps. If the disorder configuration varies at each time step the fact that the same site can be visited many times does not induce correlation in successive random steps [*Bouchaud and Georges*, 1990] and the effective dynamics of such a system obey a CTRW.

CTRW has been extensively used phenomenologically as large scale model to explain observed large scale anomalous behaviours in diffusion and transport problems (e.g.[*Berkowitz et al.*, 2006; *Cortis and Knudby*, 2006]). Large scale models are obtained by ensemble average over an ensemble of realizations. We point out that if we average the local scale diffusion equationone does not necessarily obtain a CTRW. Only few diffusion problems can be rigorously upscaled to a CTRW. As mentioned above, this is due to the fact that in quenched disorder successive random steps can be correlated, which represents a problem at the moment we perform ensemble average to obtain a large scale model. For this reason, upscaling flow in a spatially variable conductivity medium may not lead to an effective description as a CTRW, as proposed in *Cortis and Knudby* [2006].

In the second part of Chapter 3, starting from a TDRW, we upscale analytically a diffusion problem in a $d = 3$ dimensional medium with a random retardation coefficient and constant conductivity deriving a CTRW. A diffusion $d = 3$ dimensional media with a random retardation coefficient can be mapped into a CTRW because a random retardation coefficient implies that transition time and transition probability are independent and $d > 2$ implies that the number of new sites visited by a random walker increases linearly with the number of steps, which, in turns, makes the successive time increments uncorrelated. This upscaling procedure allows to obtain rigorously a CTRW which can model anomalous behaviour in diffusion problem and is fully parametrized by a distribution of retardation coefficients.

As we previously pointed out, the perturbation method used in the second chapter is a good choice for a moderately heterogeneous medium. In nature there are many examples of highly heterogeneous media, as fracture media, ans the results obtained in the second chapter are not reasonable correct for these type of media. In Chapter 4 we upscale diffusion in highly heterogeneous media using spatial and ensemble average in a multicontinuum approach.

Diffusion in highly heterogeneous media has been frequently handled using double porosity or permeability models. The pioneering double porosity model of *Barenblatt et al.* [1960] has been originally derived for a fracture medium, which is a perfect example of natural medium characterized by high heterogeneity. Fractures are characterized by very high conductivity

values and between the fractures there are blocks characterized by very low conductivities values.

Double porosity/permeability models represent a medium as an overlapping of two regions characterized by strongly different diffusion parameters, called 'mobile' and 'immobile' region, which exchange solute mass. The classical double porosity model of *Barenblatt et al.* [1960] and successive developments (e.g. [*Warren and Root*, 1963; *Dykhuizen*, 1987; *Peters and Klavetter*, 1988; *Dykhuizen*, 1990; *Bai et al.*, 1993]) assume that both the mobile and the immobile regions are in quasi equilibrium and mass exchange is modeled as a first order process. These models upscale flow in heterogeneous media, but can not explain anomalous scaling.

In Chapter 4 we derive a dual and a multi continuum model which can explain anomalous behaviour and link it with a statistical description of the medium heterogeneity. Anomalous behaviour arises by taking into account non-equilibrium effects in the immobile zone. We characterize anomalous behaviour by the anomalous scaling of the temporal evolution of the concentration $\overline{c}_m(x,t)$, its mean square displacement $m_2(t)$ and its first passage time distribution $f(t)$. Using space and ensemble average, we derived an effective non-local equation, equivalent to a delayed diffusion model [*Dentz and Tartakovsky*, 2006].

Considering an homogeneous immobile zone we derive a dual continuum model which can model pre-asymptotic sub-diffusive behaviour. Dual continuum model can explain the following pre-asymptotic scaling: $\overline{c}_m(x,t) \sim t^{-1/4}$, $m_2(t) \sim t^{1/2}$ and $f(t) \sim t^{-5/4}$. Asymptotically, when the medium is in equilibrium, the model behaves as an equivalent homogeneous one and temporal evolution scales as $\overline{c}_m(x,t) \sim t^{-1/2}$, mean squared displacement increases linearly with time and first time distribution as $f(t) \sim t^{-3/2}$. Taking into account an heterogeneous immobile zone, we model pre-asymptotic and asymptotic sub-diffusive anomalous scaling. The multi continuum models derived can explain the following anomalous scaling: $\overline{c}_m(x,t) \sim t^{-\beta/2}$, $m_2(t) \sim t^{\beta}$ and $f(t) \sim t^{-1-\beta/2}$ with $1/2 < \beta < 1$.

Anomalous scaling in flow and diffusion problems can be explained alternatively also by different models e.g. CTRW models [*Metzler and Klafter*, 2000; *Cortis and Knudby*, 2006]), multi rate mass transfer models [*Haggerty and Gorelick*, 1995; *Carrera et al.*, 1998], delayed diffusion models [*Dentz and Tartakovsky*, 2006] or fractal and multi-fractal models [*Ben-Avraham and Havlin*, 2000; *Lods and Gouze*, 2008; *de Dreuzy et al.*, 2010]. The value of the multi-continuum model derived relies on the fact that we link the scaling exponent β with a description of the medium heterogeneity. For this reason we think that the utility in prediction of the model derived is higher than for fractal model, where the fractal dimension can vary depending on

the type of field experiment performed to compute it. We link the scaling exponent β to a distribution of characteristic times of the immobile zone. A characteristic time of an immobile zone is given by $\tau = d^2 R_{im}/K_{im}$ with d thickness of the immobile zone, R_{im} retardation coefficient, K_{im} conductivity. A distribution of characteristic times can be due to a spatially variable retardation factor R_{im} or to a spatially variable conductivity K_{im}. The dynamic of diffusion in an heterogeneous medium characterized by spatially variable conductivity or spatially variable retardation coefficient is different. We derive that the same distribution of characteristic times gives rise to different scaling. A power law (or fractal) distribution of characteristic times due to a spatially variable retardation factor gives rise to asymptotic anomalous scaling: considering a power law distribution which scales as $p_\tau(\tau) \sim \tau^{-1-\beta}$ we have the following asymptotic scaling for the mean square displacement $m_2(t) \sim t^\beta$ with $1/2 < \beta < 1$. The same power law distribution of characteristic times due to spatially variable conductivity, leads to a normal behaviour. Considering a spatially variable conductivity field, the mean square displacement can scale in a pre-asymptotic regime as in the previous case considering a truncated power law distribution of characteristic times which scales as $p_\tau(\tau) \sim \tau^{-\beta}$. Asymptotically the behaviour became normal.

The different behaviours depending on the variability in the conductivity field or in the retardation coefficient are in accord with the literature of diffusion in disordered media. Indeed, considering the literature of diffusion in disordered media, we show that a spatially variable conductivity field corresponds to a 'symmetric barrier model', while a spatially variable retardation factor can be mapped into a 'trap model' and *Bouchaud and Georges* [1990] demonstrated that a trap model can lead to asymptotic anomalous behaviour, while a barrier model cannot.

In the last chapter we look at the problem of anomalous behaviour in the context of catchment modeling. In hydrology the catchment dynamics at basin scale are conveniently characterized by the frequency transfer function (FTF) [*Gelhar*, 1974]. Under linearity assumption, the FTF characterizes the dynamic response of an aquifer to any given input. Once a catchment is characterized by a given transfer function, it allows to predict aquifer response to various hydrological scenarios.

The classical catchment models are the zero dimensional 'linear reservoir model and the one dimensional linear Dupuit model [*Bear*, 1972; *Gelhar*, 1974]. Classical models predict that at high frequency the FTF scales as $\omega^{-\alpha}$: in the first order linear model $\alpha = 2$ and in the Dupuit model, usually considered with Dirichlet boundary condition at the discharge, $\alpha = 1$

[*Gelhar*, 1974]. In the first part of Chapter 6 we analyse the classical models in the light of recharge dynamic. We show that the scaling of the FTF depends on the discharge boundary condition and we derive that the Dupuit model with Cauchy boundary condition gives the same scaling of the first order linear model. We show that the first order linear model can be derived by horizontal average of the Dupuit model with Cauchy boundary condition at the discharge.

In nature, different scaling exponents α have been observed [*Labat et al.*, 2002; *Little and Bloomfield*, 2010; *Zhang and Yang*, 2010; *Jiménez-Martínez et al.*, 2012]. This scaling is commonly explained by fractal of multi fractal models [*Turcotte and Greene*, 1993; *Zhang*, 2005; *Labat et al.*, 2011], which, as we said, often lack a relation to the medium characteristics and are rather descriptive. A possible reason of anomalous behaviour is the aquifer heterogeneity. In the second part of Chapter 5 we model the catchment as a multicontinuum medium and we use the theory developed in the previous chapter to derive a new multicontinuum catchment model. We derive a physical model that renders a wide range of water storage scales and is capable to explain anomalous behaviour. The multi continuum model derived can explain the following anomalous scaling of the FTF: $\omega^{-\alpha}$ with $1/2 < \alpha < 1$ for Dirichlet boundary condition at the discharge and with $1 < \alpha < 2$ for Cauchy boundary condition. The model derived allows to link the anomalous dynamics of the discharge process observed in nature to a distribution of storage scales as reflected in the physical aquifer characteristics.

Appendix A

Appendix Average Flow Equation

A.1 Effective Conductivity Using Perturbation Theory

In the following we derive effective conductivity in term of spatial moment of the hydraulic head using perturbation theory. We consider the stochastic framework discussed in Chapter 2, where the conductivity field is written as: $K(\mathbf{x}) = \overline{K} + K'(\mathbf{x})$ with $\overline{K}$ ensemble mean that for stationary we take constant and $K'(\mathbf{x})$ a random fluctuation. Considering a log-normal distributed random field, $K(\mathbf{x})$ is conveniently expressed as: $K(\mathbf{x}) = e^{f(\mathbf{x})}$ with $f(\mathbf{x})$ the log-hydraulic conductivity normal distributed. For convenience in the derivation, we consider the flow equation in Fourier Laplace space. Laplace transform of the hydraulic head $h(\mathbf{x}, t)$ is indicated as $h^*(\mathbf{x}, \lambda)$ and Fourier transform as $\tilde{h}(\mathbf{k}, t)$. The Laplce transform of the flow equation in absence of sources and sink, reads:

$$\lambda h^*(\mathbf{x}, \lambda) \; - \nabla \cdot [K(\mathbf{x}) \nabla h^*(\mathbf{x}, \lambda)] = h(\mathbf{x}, 0) \tag{A.1}$$

with λ the Laplace variable. For brevity of notation the Fourier transform is indicated as:

$$\int_{\mathbf{k}'} \ldots = \int_{-\infty}^{\infty} \frac{d^d \mathbf{k}'}{(2\pi)^d} \ldots \tag{A.2}$$

where d is the dimensionality of the space and $\mathbf{k}$ the wave vector. The Fourier transform of (A.1), considering a pulse initial condition $h(\mathbf{x}, 0) = \delta(\mathbf{x})$, reads:

$$\lambda \tilde{h}^*(\mathbf{k}, \lambda) \; - 1 + \mathbf{k}^2 \overline{K} \tilde{h}^*(\mathbf{k}, \lambda) = - \int_{\mathbf{k}'} \tilde{K}'^*(\mathbf{k}') \, \mathbf{k} \cdot [\mathbf{k} - \mathbf{k}'] \; \tilde{h}^*(\mathbf{k} - \mathbf{k}', \lambda) \tag{A.3}$$

and re-arranging the terms we obtain:

$$\tilde{h}^*(\mathbf{k}, \lambda) = \frac{1}{\lambda + \mathbf{k}^2 \overline{K}} - \frac{\mathbf{k}}{\lambda + \mathbf{k}^2 \overline{1}} \int_{\mathbf{k}'} \tilde{K}'^*(\mathbf{k}') \; \mathbf{k} \cdot [\mathbf{k} - \mathbf{k}'] \; \tilde{h}^*(\mathbf{k} - \mathbf{k}', \lambda) \tag{A.4}$$

The term $1/(\lambda + \overline{K}\mathbf{k}^2)$ is the Fourier Laplace transform of the flow equation for a pulse initial condition in a homogeneous medium $h_0(\mathbf{x}, t)$, or rather the zero order perturbation:

$$h_0(\mathbf{x}, t) = \frac{e^{-\frac{\mathbf{x}^2}{4\overline{K}t}}}{(4\pi \overline{K} t)^{d/2}} \tag{A.5}$$

Therefore we can re-write equation (A.4) as:

$$\tilde{h}^*(\mathbf{k}, \lambda) = \tilde{h}_0^*(\mathbf{k}, \lambda) - \tilde{h}_0^*(\mathbf{k}, \lambda) \int_{\mathbf{k}'} \tilde{K}'^*(\mathbf{k}') \; \mathbf{k} \cdot [\mathbf{k} - \mathbf{k}'] \; \tilde{h}^*(\mathbf{k} - \mathbf{k}', \lambda) \tag{A.6}$$

and considering its inverse Laplace transform we obtain the following integral equation:

$$\tilde{h}(\mathbf{k},t) = \tilde{h}_0(\mathbf{k},t) - \int_0^t dt'\, \tilde{h}_0(\mathbf{k},t-t') \int_{\mathbf{k}'} \tilde{K}'(\mathbf{k}')\, \mathbf{k}\cdot[\mathbf{k}-\mathbf{k}']\, \tilde{h}(\mathbf{k}-\mathbf{k}',t') \tag{A.7}$$

In order to solve the integral equation (A.7) we use perturbation theory and $h(\mathbf{k},t)$ is expressed in terms of the series:

$$\tilde{h}(\mathbf{k},t) = \sum_{i=0}^{\infty} \epsilon^i\, \tilde{h}_i(\mathbf{k},t). \tag{A.8}$$

In the following we truncate the perturbation series after second order, thus that $\tilde{h}(\mathbf{k},t)$ reads as:

$$\tilde{h}(\mathbf{k},t) = \tilde{h}_0(\mathbf{k},t) + \epsilon\, \tilde{h}_1(\mathbf{k},t) + \epsilon^2 \tilde{h}_2(\mathbf{k},t). \tag{A.9}$$

Inserting eq.(A.9) in the integral equation (A.7) we obtain:

$$\begin{aligned}
\tilde{h}(\mathbf{k},t) =& \tilde{h}_0(\mathbf{k},t) + \\
&- \int_0^t dt'\, \tilde{h}_0(\mathbf{k},t-t') \int_{\mathbf{k}'} \epsilon\, \tilde{K}'(\mathbf{k}')\, \mathbf{k}\cdot[\mathbf{k}-\mathbf{k}']\, \tilde{h}_0(\mathbf{k}-\mathbf{k}',t') + \\
&- \int_0^t dt'\, \tilde{h}_0(\mathbf{k},t-t') \int_{\mathbf{k}'} \epsilon\, \tilde{K}'(\mathbf{k}')\, \mathbf{k}\cdot[\mathbf{k}-\mathbf{k}']\, \epsilon\, \tilde{h}_1(\mathbf{k}-\mathbf{k}',t') + \\
&- \int_0^t dt'\, \tilde{h}_0(\mathbf{k},t-t') \int_{\mathbf{k}'} \epsilon\, \tilde{K}'(\mathbf{k}')\, \mathbf{k}\cdot[\mathbf{k}-\mathbf{k}']\, \epsilon^2\, \tilde{h}_2(\mathbf{k}-\mathbf{k}',t').
\end{aligned} \tag{A.10}$$

The zeroth order term is $\tilde{h}_0(\mathbf{k},t)$, the first order one is:

$$\tilde{h}_1(\mathbf{k},t) = -\int_0^t dt'\, \tilde{h}_0(\mathbf{k},t-t') \int_{\mathbf{k}'} \tilde{K}'(\mathbf{k}')\, \mathbf{k}\cdot[\mathbf{k}-\mathbf{k}']\, \tilde{h}_0(\mathbf{k}-\mathbf{k}',t') \tag{A.11}$$

and the second one:

$$\begin{aligned}
\tilde{h}_2(\mathbf{k},t) = \int_0^t dt'\, \tilde{h}(\mathbf{k},t-t') \int_{\mathbf{k}'} \tilde{K}'(\mathbf{k}')\, \mathbf{k}\cdot[\mathbf{k}-\mathbf{k}'] \int_0^{t'} dt''\, \tilde{h}_0(\mathbf{k}-\mathbf{k}',t'-t'')\, [\mathbf{k}-\mathbf{k}']\cdot \\
\int_{\mathbf{k}''} \tilde{K}'(\mathbf{k}'')\, [\mathbf{k}-\mathbf{k}'-\mathbf{k}'']\, \tilde{h}_0(\mathbf{k}-\mathbf{k}'-\mathbf{k}'',t'').
\end{aligned} \tag{A.12}$$

Summing and rearranging all the terms till the second order we obtain:

$$\begin{aligned}
\tilde{h}(\mathbf{k},t) =& \tilde{h}_0(\mathbf{k},t) + \int_0^t dt' \int_0^{t'} dt'' \int_{\mathbf{k}'} \int_{\mathbf{k}''} \tilde{h}_0(\mathbf{k},t-t')\, \tilde{h}_0(\mathbf{k}-\mathbf{k}',t'-t'')\, \tilde{h}_0(\mathbf{k}-\mathbf{k}'-\mathbf{k}'',t'') \\
&\mathbf{k}\cdot[\mathbf{k}-\mathbf{k}']\tilde{K}'(\mathbf{k}')\tilde{K}'(\mathbf{k}'')\, [\mathbf{k}-\mathbf{k}']\cdot[\mathbf{k}-\mathbf{k}'-\mathbf{k}''].
\end{aligned} \tag{A.13}$$

In order to obtain an effective description we consider stochastic average and from the previous equation we have

$$\begin{aligned}\overline{\tilde{h}}(\mathbf{k},t) = &\tilde{h}_0(\mathbf{k},t) + \int_0^t dt' \int_0^{t'} dt'' \int_{\mathbf{k}'}\int_{\mathbf{k}''} \tilde{h}_0(\mathbf{k},t-t')\,\tilde{h}_0(\mathbf{k}-\mathbf{k}',t-t')\,\tilde{h}_0(\mathbf{k}-\mathbf{k}'-\mathbf{k}'',t'') \\ &\mathbf{k}\cdot[\mathbf{k}-\mathbf{k}']\; K_G^2 C_{ff}(k')\,(2\pi)^d\,\delta(\mathbf{k}'+\mathbf{k}'')\,[\mathbf{k}-\mathbf{k}']\cdot[\mathbf{k}-\mathbf{k}'-\mathbf{k}''],\end{aligned} \tag{A.14}$$

where the overline indicates the ensemble average. The terms $K_G^2 C_{ff}(\mathbf{k}')\,(2\pi)^d\delta(\mathbf{k}'+\mathbf{k}'')$ are the Fourier transform of covariance function of the random fluctuation $\overline{K'(\mathbf{x}')K'(\mathbf{x}'')}$ expressed in term of the Fourier transform of covariance function of $f'(\mathbf{x})$:

$$\overline{f(\mathbf{k}')f(\mathbf{k}'')} = \overline{\int_{\mathbf{x}} e^{i\,\mathbf{k}'\mathbf{x}} f(\mathbf{x}) \int_{\mathbf{x}} e^{i\,\mathbf{k}''\cdot\mathbf{x}} f(\mathbf{x})} = C_{ff}(\mathbf{k}')\,(2\pi)^d\delta(\mathbf{k}'+\mathbf{k}'') \tag{A.15}$$

considering that, as in Chapter 2, $\overline{K'(\mathbf{x})K'(\mathbf{x}')} = K_G^2 C_{ff}(\mathbf{x}-\mathbf{x}')$.

The integral in Eq. (A.14) can be simplified as:

$$\begin{aligned}\overline{\tilde{h}}(\mathbf{k},t) = &\tilde{h}_0(k,t) + \int_0^t dt' \int_0^{t'} dt'' \int_{\mathbf{k}'} \tilde{h}_0(\mathbf{k},t-t')\,\tilde{h}_0(\mathbf{k}-\mathbf{k}',t-t')\,\tilde{h}_0(\mathbf{k},t'') \\ &\mathbf{k}\cdot[\mathbf{k}-\mathbf{k}']\; C_{ff}(\mathbf{k}')\,(2\pi)^d\,[\mathbf{k}-\mathbf{k}']\cdot[\mathbf{k}]\; K_G^2.\end{aligned} \tag{A.16}$$

In the following we compute the effective conductivity in term of the second center moment of the hydraulic head:

$$K_{jl}^{eff}(t) = \frac{1}{2}\frac{dm_{jl}^{(2)}(t)}{dt} \tag{A.17}$$

where the diagonal components of the second spatial center moment in Fourier space, omitting the subscript jj for brevity, reads:

$$m^{(2)} = (-i)^2 \frac{\partial^2}{\partial k^2}\tilde{h}(\mathbf{k},t)\bigg|_{\mathbf{k}=0} \tag{A.18}$$

Therefore the second center moment of the hydraulic head as given in eq. (A.16), is:

$$m^{(2)} = 2\overline{K}t - 2\int_0^t dt' \int_0^{t'} dt'' \int_{\mathbf{k}'} \tilde{h}_0(-\mathbf{k}',t'-t'')\,k'^2\,C_{ff}(\mathbf{k}')\; K_G^2 \tag{A.19}$$

where $\tilde{h}_0(\mathbf{k},t) = e^{-\overline{K}\mathbf{k}^2 t}$ and therefore $\tilde{h}_0(0,t) = 1$ and

$$\left.\frac{\partial^2 \tilde{h}_0(\mathbf{k},t)}{\partial k^2}\right|_{\mathbf{k}=0} = -2\overline{K}t. \tag{A.20}$$

Considering the covariance $C_{ff}(\mathbf{x}-\mathbf{x}')$ Gaussian:

$$C_{ff}(\mathbf{x}-\mathbf{x}') = \sigma_{ff}^2 e^{\sum_j^d \frac{(x-x_j)^2}{2\ell_j^2}} \tag{A.21}$$

and assuming statistical isotropy: $\ell_j = \ell$ for $j = 1,..d$ with d spatial dimension, in Fourier space, we obtain:

$$C_{ff}(\mathbf{k}) = \ell\sqrt{2\pi}\, e^{-\frac{\mathbf{k}^2\ell^2}{2}} \tag{A.22}$$

Therefore, in Fourier space, the effective conductivity, computed using perturbation theory till second order perturbation, reads:

$$K_{eff} = \overline{K} - \int_0^t dt' \int_{-\infty}^{\infty} \frac{d^d\mathbf{k}'}{(2\pi)^d} k'^2 e^{-\overline{K}\mathbf{k}'^2 t'}\, \sigma_{ff}^2 (2\pi)^{d/2}\, \ell^3\, e^{-\frac{1}{2}\mathbf{k}'^2\ell^2}\, K_G^2 \tag{A.23}$$

In the following we compute the K^{eff} for $d = 1, 2$ and 3 spatial dimension.

Effective conductivity in a d=1 dimensional medium

Considering a one dimensional medium and solving the integrals (A.23) for d=1 dimension we have:

$$K_{eff} = \overline{K} - K_G^2\, \frac{\sigma^2}{\overline{K}} \left(1 - \frac{\ell}{\sqrt{2\,\overline{K}\,t + \ell^2}}\right) \tag{A.24}$$

and considering a consistent formulation till second order perturbation, expanding $\overline{K}$ till σ^2: $\overline{K} = K_G(1+\sigma^2/2)$ we obtain:

$$K_{eff} = K_G \left(1 - \frac{\sigma^2}{2} + \frac{\sigma^2\ell}{\sqrt{2\,K_G\;t + \ell^2}}\right) \tag{A.25}$$

Notice that its asymptotic value for large time: $K_{eff} \simeq K_G(1+\sigma^2/2)$ is the first order approximation for the harmonic mean K_H:

$$K_H = K_G\, e^{-\frac{\sigma_f^2}{2}} \simeq K_G \left(1 - \frac{\sigma^2}{2}\right) \tag{A.26}$$

which is the well known value for effective condutivity in a $d = 1$ dimensional medium [*Sanchez-Villa et al.*, 2006].

Effective conductivity in a d=2 dimensional medium

Solving eq.(A.23) for d=2 dimensions and considering a consistent formulation, as discussed above, we have:

$$K_{eff} = K_G \left(1 + \frac{\sigma^2}{2} - K_G \frac{\sigma^2 t}{2 K_G t + l^2}\right) \tag{A.27}$$

The asymptotic value for time to infinity is the geometric mean, which is the well known value for effective conductivity for $d = 2$ spatial dimension [*Matheron*, 1967]. Analytical expression for the time dependent conductivity has been tested numerically using classical random walk method (see Appendix A.2).

Effective conductivity in a d=3 dimensional medium

The solution of (A.23) for $d = 3$ spatial dimension, considering a consisten formulation, leads:

$$K_{eff} = K_G \left[1 + \frac{\sigma^2}{6} + \frac{\sigma^2 \ell^3}{3 (2 K_G t + \ell^2)^{3/2}}\right] \tag{A.28}$$

and the asymptotic value for this time dependent effective conductivity is:

$$K_{eff} = K_G \left(1 + \frac{\sigma^2}{6}\right) \tag{A.29}$$

The previous expressison is the first order expansion of Matheron's conjecture for effective conductivity in a $d = 3$ heterogeneous medium log-normally distributed [*Sanchez-Villa et al.*, 2006]. Analytical expression for the time dependent conductivity has been tested numerically using classical random walk method (see Appendix A.2).

A.2 Comparison of Effective Coefficients Using Perturbation Theory and RW

We compute numerically effective conductivity for a log-normal conductivity field using classical random walk particle tracking method. Effective conductivity has been computed in

terms of the second center moment of the particle distribution [*Dean et al.*, 2007]. Log-normal conductivity field have been generated using the Karhunen Loeve expansion of a stationary function (see Appendix A.4). Numerical simulations have been used to verify the analytical results for effective coefficients obtained using perturbation method (see Chapter 2 and Appendix A.1). Figure A.1 shows that numerical simulations are in accord with analytical results.

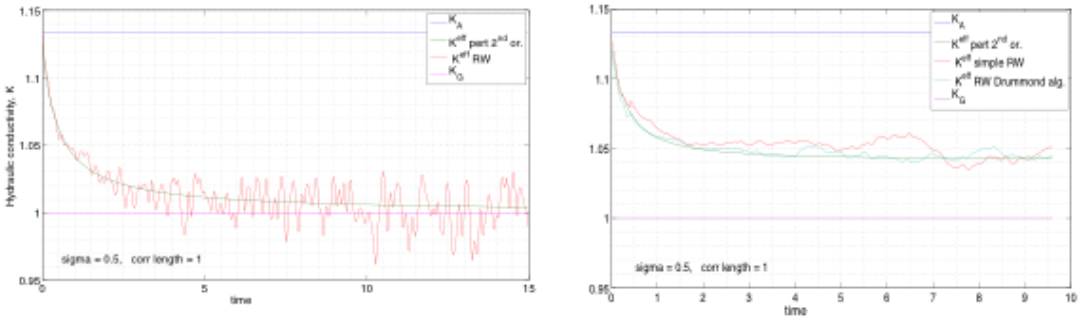

Figure A.1: *Effective conductivity for $d = 2$ and $d = 3$ spatial dimensional medium computed analytically using perturbation method (green lines) and numerically using classical RW (red lines) . For $d = 2$ spatial dimension (left) effective conductivity starts from the arithmetic mean of the local values (blue line) and decreases till the geometric mean of the local conductivities values. For $d = 3$ spatial dimension (right) effective conductivity starts from the arithmetic mean of the local values (blue line) and decreases till the effective steady state valued conjectured given by $K_{eff} = K_G e^{1+\sigma^2/6}$ [Matheron, 1967].*

A.3 Time Dependent Effective Conductivity

In the following we solve the following flow equation caracterized by a time dependent conductivity:

$$S\frac{\partial h(\mathbf{x},t)}{\partial t} - K_e(t)\nabla^2 h(\mathbf{x},t). \tag{A.30}$$

Considering the proprieties of Fourier transform, the Fourier transform of (A.30) reads:

$$S\frac{\partial \tilde{h}(\mathbf{k},t)}{\partial t} + K_e(t)\mathbf{k}^2\tilde{h}(\mathbf{k},t) \tag{A.31}$$

where $\mathbf{k}$ is the Fourier variable, and solution of (A.31) is given by:

$$\tilde{h}(\mathbf{k},t) = e^{-\mathbf{k}^2\int_0^t K_e(t')dt'} \tag{A.32}$$

that in time domain is:

$$h(\mathbf{x},t) = \frac{1}{\sqrt{4\pi\frac{1}{S}\int_0^t K_e(t')dt'}} e^{-\frac{\mathbf{x}^2 S}{4\int_0^t K_e(t')dt'}}. \tag{A.33}$$

A.4 Generation of Random Fields

In order to use particle tracking methods and compute effective parameter as stochastic averages over a large number of realizations, we generate random fields of hydraulic conductivity using the Karhunen Loève expansion of a stationary function.

In the theory of stochastic processes, the Karhunen Loève expansion is a representation of a stochastic process as an infinite linear combination of orthogonal functions, analogous to a Fourier series representation of a function on a bounded interval. The distinction is that here, the Fourier coefficients are random variables. The Karhunen Loeve expansion of a stationary random function $f(x)$ is:

$$f(x) = \lim_{N\to\infty} \frac{\sigma_{ff}\sqrt{2}}{\sqrt{N}} \sum_{l=1}^{N} \cos(\mathbf{k}^{(l)} \cdot \mathbf{x} + \phi^{(l)}) \tag{A.34}$$

where: σ_{ff} is the standard deviation of the random function $f(x)$; $\mathbf{k}^{(l)}$ are identical and independently distributed RV, distributed according to $P(k)$; $\phi^{(l)}$ are identical and independently uniformly distributed in $[0, 2\pi]$.

In order to create a random field $f(x)$, characterized by a given correlation $C_{ff}(x)$, we have to use the KL expansion with a random variable k distributed as the Fourier transform of the correlation function $C_{ff}(x)$ divided by 2π. In case of a Gaussian correlated field we have:

$$P(k) = \frac{\tilde{C}_{ff}(k)}{2\pi} = \frac{l\, e^{-\frac{k^2 l^2}{2}}}{\sqrt{2\pi}} \tag{A.35}$$

where $\tilde{C}_{ff}$ is the Fourier transform of C_{ff}. In Figure (A.2) are given 3 examples of random fields generated using the Karhunen Loeve expansion of a stationary random function.

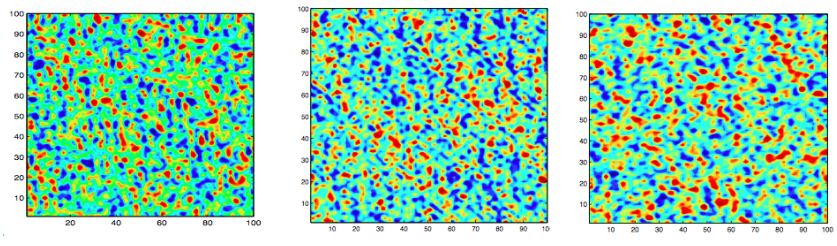

Figure A.2: *Gaussian correlated random fields generated using Karhunen Loeve expansion of a stationary random function.*

Appendix B

Appendix Diffusion in Heterogeneous Media: a Random Walk Perspective

B.1 Equivalent Homogeneous Model

We seek the equivalent homogeneous model for the heterogeneous diffusion equation (3.52). The homogeneous model is defined as

$$\phi^e \frac{\partial \overline{c}(x,t)}{\partial t} - D^e \frac{\partial^2 \overline{c}(x,t)}{\partial x^2} = 0, \tag{B.1}$$

with the effective porosity ϕ^e and effective diffusivity D^e. The aim is to determine these effective porosities. To this end, we consider the following criteria. The effective model (B.1) should reproduce the correct average steady state concentrations and solute fluxes. The steady state concentration $c_s(x) = \lim_{t\to\infty} c(x,t)$ satisfies

$$\frac{\partial}{\partial x}\phi(x) D_0 \frac{\partial}{\partial x} c_s(x) = 0. \tag{B.2}$$

For the first criterion we consider a situation with no flux boundary conditions in a bounded domain. The solution is $c_s(x) = c_0 = \text{constant}$. Thus, we obtain in equilibrium for the average bulk concentration $g(x,t) = \phi(x)c(x,t)$

$$\overline{g_s(x)} = \overline{\phi(x)c_s(x)} = \overline{\phi(x)}c_0. \tag{B.3}$$

The effective porosity ϕ^e is equal to the arithmetic average porosity $\phi^e = \phi_A$.

The second criterion refers to the average flux. We consider a scenario characterized by unit concentration at the inlet at $x = 0$ and zero concentration at the outlet at $x = L$. The solution for the concentration distribution then is given by

$$c_s(x) = -\frac{\phi_H}{L} \int_0^x \frac{dx'}{\phi(x)} \tag{B.4}$$

with ϕ_H the harmonic average porosity. Thus, the average solute flux is given by

$$\overline{\phi(x) D_0 \frac{\partial c_s(x)}{\partial x}} = \phi_H D_0 \frac{\partial \overline{c}_s(x)}{\partial x}. \tag{B.5}$$

This result is of course well known. The effective diffusivity D^e in the flux term is given by $D^e = \phi_H D_0$.

B.2 Diffusion and Multitrapping in Finite Domain

The solution for the diffusion problem (3.53) in Laplace space is given by

$$c^*(x,\lambda) = \frac{\sinh\left[(1-x)\sqrt{\frac{\lambda\phi_A}{\phi_H}}\right]}{\sinh\left(\sqrt{\frac{\lambda\phi_A}{\phi_H}}\right)}. \tag{B.6}$$

This can be checked by inspection. At times small compared to the dimensionless diffusion scale, which here is equal to 1, this means for $\lambda \gg 1$, this expression can be approximated by

$$c^*(x,\lambda) = \exp\left(-x\sqrt{\frac{\lambda\phi_A}{\phi_H}}\right). \tag{B.7}$$

The solution for $c(x,t)$ is then given by inverse Laplace transform and yields (3.60).

We now consider the equivalent case of homogeneous diffusion with multirate mass transfer. For simplicity we set here $\phi_A = \phi_H$ (note that for the parameter values used for the simulations in Section 3.2.3.2, $\phi_A \approx \phi_H$)

$$\frac{\partial c(x,t)}{\partial t} = \frac{\partial^2}{\partial x^2}\int_0^t dt' c(x,t')\mu(t-t'). \tag{B.8}$$

The memory function (3.57) is independent of space. Note that $c(x,t)$ denotes the total solute concentration, the injection, however, is with respect to the mobile solute only. Thus, by virtue of (3.30), the boundary condition for $c(x,t)$ is expressed as

$$\int_0^t dt' c(x=0,t')\mu(0,t-t') = \delta(t). \tag{B.9}$$

The solution of (B.8) in Laplace space is given by

$$c^*(x,\lambda) = \frac{\sinh\left[(1-x)\sqrt{\frac{\lambda}{\mu^*(\lambda)}}\right]}{\mu^*(\lambda)\sinh\left[\sqrt{\frac{\lambda}{\mu^*(\lambda)}}\right]}. \tag{B.10}$$

Inserting expression (3.57) for $\mu^*(\lambda)$ gives the Laplace transform of concentration in function

of $p^*(\lambda)$

$$c^*(\tilde{x},\lambda) = \frac{\lambda + \alpha[1-p^*(\lambda)]}{\lambda} \frac{\sinh\left\{(1-x)\sqrt{\lambda+\alpha[1-p^*(\lambda)]}\right\}}{\sinh\left\{\sqrt{\lambda+\alpha[1-p^*(\lambda)]}\right\}}. \tag{B.11}$$

In order to analyze the behaviors and regimes, we need to determine the behavior of $p^*(\lambda)$. For this purpose, we consider the Laplace transform of the truncated power-law (3.55), which is given by

$$\begin{aligned} p^*(\lambda) = &\frac{1}{1-(t_1/t_2)^\beta}\left[\exp(-\lambda t_1) - (t_1/t_2)^\beta \exp(-\lambda t_2)\right] \\ &+ \frac{(\lambda t_1)^\beta}{1-(t_1/t_2)^\beta}\left[\Gamma(1-\beta,\lambda t_1) - \Gamma(1-\beta,\lambda t_2)\right], \end{aligned} \tag{B.12}$$

where $\Gamma(\alpha,x)$ is the incomplete Gamma function [*Abramowitz and Stegun*, 1965]. Note that here $0<\beta<1$. For times larger than the cut-off time t_2, which corresponds to $\lambda \ll t_2^{-1}$, this expression can be approximated by

$$p^*(\lambda) \approx 1 - \bar{t}\lambda, \qquad\qquad \bar{t} = t_1 \frac{\beta}{1-\beta}\frac{(t_2/t_1)^{1-\beta}-1}{1-(t_1/t_2)^\beta}. \tag{B.13}$$

Note that $\bar{t}$ is the mean trapping time. Inserting the latter into (B.11) gives

$$c^*(\tilde{x},\lambda) = (1+\alpha\bar{t})\frac{\sinh\left[(1-x)\sqrt{\lambda(1+\alpha\bar{t})}\right]}{\sinh\left[\sqrt{\lambda(1+\alpha\bar{t})}\right]}. \tag{B.14}$$

Let us consider now the λ range for which the argument of the hyperbolic sine is small compared to 1. This is the case for $\lambda \ll (1+\alpha\bar{t})$, which gives in time, $t \gg (1+\alpha\bar{t}) = t_c$. The scale t_c is essentially given by the trapping rate α and the mean trapping time. This scale corresponds to the time at which concentration is cut-off. Specifically, if the cutoff time t_2 is much smaller than t_c, $t_2 \ll t_c$, we observe the characteristic $t^{-3/2}$ behavior in the time regime $t_2 \ll t \ll t_c$ because in this regime, concentration behaves as in the case without traps, but characterized by a renormalized diffusion coefficient.

In the time regime $t_1 \ll t \ll t_2$, (B.13) can be approximated by

$$p^*(\lambda) \approx 1 - a_\beta \lambda^\beta, \qquad\qquad a_\beta = t_1^\beta \Gamma(1-\beta) \tag{B.15}$$

Inserting the latter into (B.11), gives

$$c^*(x,\lambda) = (1+\alpha a_\beta \lambda^{\beta-1}) \frac{\sinh\left[(1-x)\sqrt{\lambda+\alpha a_\beta \lambda^\beta}\right]}{\sinh\left[\sqrt{\lambda+\alpha a_\beta \lambda^\beta}\right]}. \tag{B.16}$$

For $\lambda \ll t_1^{-1}[\alpha\Gamma(1-\beta)]^{-\frac{1}{\beta}}$, this means, if the argument of the hyperbolic sine is small, this expression can be approximated as

$$c^*(x,\lambda) \approx \alpha a_\beta \lambda^{\beta-1}, \tag{B.17}$$

which yields the power-law behavior

$$c(x,\lambda) \propto t^{-\beta} \tag{B.18}$$

for times $t \gg t_1[\alpha\Gamma(1-\beta)]^{\frac{1}{\beta}}$. Note, however, that this power-law behavior can only be observed if the cut-off scale t_2 is larger than $t_1[\alpha\Gamma(1-\beta)]^{\frac{1}{\beta}}$. In this case, one obtains the intermediate power-law time regime $t_1[\alpha\Gamma(1-\beta)]^{\frac{1}{\beta}} \ll t \ll t_2$.

Appendix C

Appendix Anomalous Diffusion in Composite Media

C.1 TDRW Numerical Implementation

Here we give details on the numerical simulation used to validate analytical solutions of the proposed model using TDRW scheme. In the numerical simulations the discretized concentration $C_i(t)$, is given in term of the particle density $n_i'(t)$, computed as the number of particles in the i-th bin divided by the total particle number N:

$$n_i'(t) = \lim_{N\to\infty} \frac{N_i(t)}{N}. \tag{C.1}$$

Considering the following initial condition:

$$C(\mathbf{x}, t=0) = \frac{1}{d_m + d_{im}}\,\delta(x), \tag{C.2}$$

so that

$$\int C(\mathbf{x}, t) d\mathbf{x} = 1, \tag{C.3}$$

initially we have in the mobile and in the immobile layer:

$$\begin{aligned} \int_{-\infty}^{\infty} dx \int_0^{d_{im}} dz\; C_{im}(\mathbf{x}, t=0) &= \frac{d_{im}}{d_m + d_{im}} \\ \int_{-\infty}^{\infty} dx \int_{d_{im}}^{d} dz\; C_m(\mathbf{x}, t=0) &= \frac{d_m}{d_m + d_{im}} \end{aligned} \tag{C.4}$$

The upscaled concentration are given by the average over the vertical direction as defined in (4.14) and therefore the initial conditions for the upscaled concentrations are:

$$c_m(x, t=0) = c_{im}(x, t=0) = \frac{1}{d_m + d_{im}}\delta(x). \tag{C.5}$$

As explain in *Dentz et al.* [2012] the particle traking is eprformed for the qunatity $n_i = R_i \Delta_V c_i$ with Δ_V the discretization of the domani, assumed constant, and R_i the retardatio factor. Consequently for the particle density n_i the initial condition results:

$$n_m(x, t=0) = \chi_m R_m \Delta_x\, \delta(x) \qquad\qquad n_{im}(x, t=0) = \chi_{im} R_{im} \Delta_x\, \delta(x) \tag{C.6}$$

with $\chi_m = d_m/(d_m + d_{im})$ and $\chi_{im} = d_{im}/(d_m + d_{im})$. From this we obtain that: $\int dx\; [n_m(x,t) + n_{im}(x,t)] = \chi_m R_{im} L + \chi_{im} R_{im} L$ which is not in general equal to one. We perform the particle tracking by the injection N_m and N_{im} particles respectively in the mobile and in the immobile

layer homogeneously distributed at $x = 0$ along the vertical direction. N_m and N_{im} are given by:

$$N_m(t=0) = \frac{d_m R_m}{d_m R_m + d_{im} R_{im}} N \qquad N_{im}(t=0) = \frac{d_{im} R_{im}}{d_m R_m + d_{im} R_{im}} N \tag{C.7}$$

Thus the initial condition for the particle density $n'_i(t) = N_i(t)/N$ is:

$$n'_m(t=0) = \frac{\chi_m R_m}{\chi_m R_m + \chi_{im} R_{im}} \qquad n'_{im}(t=0) = \frac{\chi_{im} R_{im}}{\chi_m R_m + \chi_{im} R_{im}} \tag{C.8}$$

Thus, in order to obtain the $n_i(t)$ that we actually want to determine, we have to multiply the outcome of our TDRW simulation by a factor of $(\chi_m R_{im} + \chi_{im} R_{im})$

$$n_m(t) = n'_m(t)\,(\chi_m R_{im} + \chi_{im} R_{im}) \qquad n_{im}(t) = n'_{im}(t)\,(\chi_m R_{im} + \chi_{im} R_{im}) \tag{C.9}$$

and finally the averaged total concentration $c(x,t)$ can be expressed in terms of the numerically determined densities $n'_i(t)$ as:

$$\overline{c}(x,t) = \left[\chi_m \frac{n'_m(x,t)}{d_m R_m} + \chi_{im} \frac{n'_{im}(x,t)}{d_{im} R_{im}}\right](\chi_m R_m + \chi_{im} R_{im}). \tag{C.10}$$

C.2 Solution of Diffusion in the Immobile Zone

Here we derive the expression for the memory function $g[t|\tau_{im}(x)]$ given in (5.32) and the expression for $c_{im}(x,t)$ given in terms of $c_m(x,t)$ and $g[t|\tau_{im}(x)]$ in (4.22). Derivation is given in Laplace space by solution of (4.18) with (4.19) as boundary conditions. In Laplace space equation (4.18) reads:

$$\lambda\, R_{im}(x)\, C^*_{im}(\mathbf{x},\lambda) - K_{im}(x)\, \frac{\partial^2 C^*_{im}(\mathbf{x},\lambda)}{\partial z^2} = R_{im}(x)\, C_{im}(\mathbf{x},0) \tag{C.11}$$

In order to solve the previous equation we define the auxiliary function:

$$a(\mathbf{x},t) = C_{im}(\mathbf{x},t) - C_{im}(\mathbf{x},0) \tag{C.12}$$

which solve, in Laplace space, the following equation:

$$\lambda\, R_{im}(x)\, a^*(\mathbf{x},\lambda) - K_{im}(x)\, \frac{\partial^2 a^*(\mathbf{x},\lambda)}{\partial z^2} = 0 \tag{C.13}$$

with boundaries conditions:

$$\frac{\partial a^*(\mathbf{x},0,\lambda)}{\partial z} = 0 \qquad\qquad a^*(\mathbf{x},d_{im},\lambda) = c^*_m(x,\lambda) - \frac{C_{im}(\mathbf{x},0)}{\lambda}, \tag{C.14}$$

and $a(\mathbf{x},0) = 0$ as initial condition. Therefore we consider its associated Green's function $G^*(\mathbf{x},\lambda)$ which solves equation (C.13) with boundary conditions:

$$\frac{\partial G^*(\mathbf{x},0,\lambda)}{\partial z} = 0 \qquad\qquad G^*(\mathbf{x},d_{im},\lambda) = 1. \tag{C.15}$$

Thus, $a^*(\mathbf{x},\lambda)$ can be re-written as:

$$a^*(\mathbf{x},\lambda) = G^*(\mathbf{x},\lambda)\ \left[\bar{c}^*_m(x,\lambda) - \frac{C_{im}(\mathbf{x},0)}{\lambda}\right] \tag{C.16}$$

and $C^*_{im}(\mathbf{x},\lambda)$ as:

$$C^*_{im}(\mathbf{x},\lambda) = G^*(\mathbf{x},\lambda)\left[c^*_m(x,\lambda) - \frac{C_{im}(\mathbf{x},0)}{\lambda}\right] + \frac{C_{im}(\mathbf{x},0)}{\lambda}. \tag{C.17}$$

The Green's function $G^*(\mathbf{x}, \lambda)$, solution of eq. (C.13) with (C.15) boundary conditions, is:

$$G^*(\mathbf{x}, \lambda) = \frac{\cosh\left(\sqrt{\frac{\lambda z^2 R_{im}(x)}{K_{im}(x)}}\right)}{\cosh\left(\sqrt{\frac{\lambda d_{im}^2 R_{im}(x)}{K_{im}(x)}}\right)}. \tag{C.18}$$

Averaging eq. (C.17) over the z direction we obtain:

$$c_{im}^*(x, \lambda) = g^*(x, \lambda)\left[c_m^*(x, \lambda) - \frac{c_{im}(x, 0)}{\lambda}\right] + \frac{c_{im}(x, 0)}{\lambda} \tag{C.19}$$

where we defined:

$$c^*(x, \lambda) = \frac{1}{d_{im}} \int_0^{d_{im}} C^*(\mathbf{x}, \lambda)\, dz \qquad g^*(\lambda|\tau_{im}(x)) = \frac{1}{d_{im}} \int_0^{d_{im}} G^*(\mathbf{x}, \lambda)\, dz. \tag{C.20}$$

with $\tau_{im}(x) = d_{im}^2 R_{im}(x)/K_{im}(x)$. The result $g^*[x|\tau_{im}(x)]$ of the vertical integration of (C.18) is given in eq. (5.32) in the text. Considering the inverse Laplace transform of (C.19) we obtain (4.22).

C.3 Laplace Transforms

The Laplace transform of t^α for $\alpha > -1$ is

$$\mathcal{L}\{t^\alpha\} = \int_0^\infty dt t^\alpha e^{-\lambda t} \tag{C.21}$$

$$= \lambda^{-1-\alpha} \int_0^\infty dt t^\alpha e^{-t} \tag{C.22}$$

$$= \lambda^{-1-\alpha}\Gamma(\alpha+1), \tag{C.23}$$

where $\Gamma(\cdot)$ is the gamma function [*Abramowitz and Stegun*, 1965]. Differently, considering the Laplace transform of $t^{-\alpha-1}$ with $\alpha > 1$, the previous integral is not normalizable. For $1 < \alpha < 2$ the behaviour of the Laplace transform of $h(t) = t^{-\alpha}$ can be approximate by [*Dentz and Berkowitz*, 2003]:

$$h^*(\lambda) \simeq 1 - c_\alpha \lambda^\alpha \tag{C.24}$$

with

$$c_\alpha \equiv \int_0^\infty dt\ t\ h(t). \tag{C.25}$$

C.4 Multi Continuum Model with Constant Retardation Factor: Power Law Distribution

In this appendix we consider the anomalous behaviours we can obtain considering a multi continuum model where heterogeneity of the immobile zone is given by a spatially variable conductivity. As we have seen previously, anomalous behaviour is due to anomalous scaling of the memory function $\varphi(t)$ that here we indicate with $\varphi_\kappa(t)$. The memory function for a variable conductivity field, $\varphi_\kappa(t)$, is expressed in function of a distribution of characteristic times of the immobile zone as derived in (4.49). In order to obtain an anomalous, or rather fractal, behaviour in $\varphi_\kappa(t)$ we consider a fractal distribution of characteristic times. Spatial distribution of characteristic times is due to a spatially variable conductivity field so that $\tau(x) = d_{im}^2 \rho_{im} / \kappa_{im}(x)$. We consider the following normalized power law distribution of characteristic times:

$$p_\tau(\tau) = \frac{\tau_1^{\beta-1}}{\Gamma(\beta-1)} \frac{e^{-\tau_1/\tau}}{\tau^\beta} \tag{C.26}$$

where $\beta > 1$ for normalization of the distribution $p_\tau(\tau)$. We substitute in equation for the global memory function:

$$\varphi_\kappa(t) = t^{-\beta} \frac{\tau_1^{\beta-1}}{\Gamma(\beta-1)} \int_0^\infty e^{-\frac{\tau_1}{t} x} x^{\beta-1} g'(x)\, dx \tag{C.27}$$

Considering that $g'(x)$ decreases exponentially for $x > 1$ (see equation (5.32) or figure 4.2), the previous improper integral converges for $\beta > 1/2$; although we already have β larger than 1 in order to normalize the distribution $p(\tau)$. In order to pass in Laplace space, considering that $\beta > 1$, we use the Tauberian theorem *Dentz and Berkowitz* [2003]:

$$\mathcal{L}\{t^{-\beta}\} \sim 1 - (\lambda\tau)^{\beta-1} + ... \tag{C.28}$$

Therefore when we consider the behaviour for time to infinity (or equivalently $\lambda \ll \tau^{-1}$), the global memory function tends to 1. When we substitute this result in the equation (5.29) we see that asymptotically, expanding $\overline{c}_m^*(x,\lambda)$ for small λ, we have $\overline{c}_m^*(x,\lambda) \sim \lambda^{-1/2}$, or equivalently, in time domain: $\overline{c}_m(x,t) \sim t^{-\frac{1}{2}}$, which corresponds to a normal scaling. Note that considering a variable retardation field and a power law distribution of characteristic times we obtained an anomalous scaling while here, considering a spatially variable conductivity field a distribution of characteristic times does not lead to anomalous behaviour.

Appendix D

Appendix Catchment Response in Frequency Domain

D.1 First Order Linear Model from Dupuit Model

Here we derive the zero dimensional LR model from a higher dimensional model. Horizontal average over the catchment size L of the governing equation of the LD model, given in (5.9), with Cauchy BC, gives:

$$S\frac{d\langle h(t)\rangle}{dt} = -a\left[h(x=0,t) - h_0\right] + r(t), \tag{D.1}$$

where

$$\langle h(t)\rangle = \frac{1}{L}\int_0^L h(x,t)\, dx. \tag{D.2}$$

Expression (D.1) is analogous to the governing equation of the LR model given in (5.5), except for the local term $h(x=0,t)$. The two equations are equivalent if we can approximate $h(x=0,t) \simeq \langle h(t)\rangle$, which implies that the piezometric gradient in the aquifer is small. Furthermore, without any assumption on the piezometric gradient, the two models are equivalent at very small or large times. At large times, for $t \gg t_L$ with $t_L = L^2S/T$ the system is horizontally in equilibrium, $h(x,t) = \langle h(t)\rangle$ and the two models are equivalents. At short times $t \ll t_L$ the LR model and the integrated LD model with Cauchy BC also coincide considering equilibrium initial boundary conditions: $h(x,0) = h_0$ that implies: $h(0, t \ll t_L) \simeq \langle h(t \ll t_L)\rangle$. LR model and LD model with Cauchy BC, are compared in Figure 5.2. Indeed considering horizontal integration of the head FTF for the LD model with Cauchy BC given in (5.18) we have:

$$\langle \Theta_h(\omega)\rangle = \frac{1}{L}\int_0^L \Theta_h(x,\omega)\, dx = \left|\frac{1}{i\omega S}\left\{1 - \frac{a}{i\omega S}\,\frac{\tanh[p(\omega)]}{\tanh[p(\omega)] + \frac{aL^2}{Tp(\omega)}}\right\}\right|^2. \tag{D.3}$$

In the limit of $\omega \ll T/(SL^2)$, first order Taylor expansion of (D.3), for $p(\omega) \ll 1$, leads to

$$\Theta_h(\omega) = \left|\frac{1}{a + i\omega S}\right|^2, \tag{D.4}$$

which is equivalent to the head FTF of the LR model $\Theta_h(\omega)$ given in (5.8). In fact the characteristic time t_L we take into account for the Taylor expansion is the mean diffusion time over a catchment of size L; $t \gg t_L$ implies that the catchment is horizontally in equilibrium and we can neglect spatial variation of the hydraulic head as in the LR model.

Bibliography

Abramowitz, M., and I. Stegun (1965), *Handbook of Mathematical Functions with Formulas, Graphs, and Mathematical Tables*, 1094 pp., Dover Publications, New York.

Acuna, J. a., and Y. C. Yortsos (1995), Application of Fractal Geometry to the Study of Networks of Fractures and Their Pressure Transient, *Water Resources Research*, *31*(3), 527, doi:10.1029/94WR02260.

Alonso, E. E., and R. J. Krizek (1974), Randomness of settlement rate under stochastic load, *J. of the engineering Mechanics Division-ASCE*, *100*, 1211–1226.

Arkhincheev, V. E. (2000), Anomalous diffusion and charge relaxation on comb model: exact solutions, *280*, 304–314.

Bai, M., D. Elsworth, and J.-C. Roegiers (1993), Multiporosity/Multipermeability Approach to the Simulation of Naturally Fractured Reservoirs, *Water Resources Research*, *29*(6), 1621–1633.

Banton, O., F. Delay, and G. Porel (1997), A new time domain random walk method for solute transport in 1-{D} heterogeneous media, *Ground Water*, *35*, 1008–1013.

Barenblatt, G., I. P. Zheltov, and I. Kochina (1960), Basic Concepts in the Theory of Seepage of Homogeneous Liquids in Fissured Rocks [Strata], *PMM*, *24*(5), 825–864.

Barker, J. A. (1988), A Generalized Radial Flow Model for Hydraulic Tests in Fractured Rock, *Water Resources Research*, *24*(10), 1796–1804.

Bear, J. (1972), *Dynamics of fluids in porosu media*, dover ed., American Elsevier Publishing Company, New York.

Beck, J. V., K. D. Cole, A. Haji-Sheikh, and B. Litkouhi (1992), *Heat Conduction Using Green's Functions*, 522 pp., Washington.

Ben-Avraham, D., and S. Havlin (2000), *Diffusion and Reactions in Fractals and Disordered Systems*, 316 pp., Press, Cambridge University, The Edinburgh Building, Cambridge CB2 2RU, UK, Cambridge.

Benson, D. A., and M. M. Meerschaert (2009), A simple and efficient random walk solution of multi-rate mobile/immobile mass transport equations, *Adv. Water Resour.*, *32*, 532–539.

Berkowitz, B., J. Klafter, R. Metzler, and H. Scher (2002), Physical pictures of transport in heterogeneous media: Advection-dispersion, random-walk, and fractional derivative formulations, *Water Resour. Res.*, *38*(10), 1191, doi:10.1029/2001WR001030.

Berkowitz, B., A. Cortis, M. Dentz, and H. Scher (2006), Modeling non-Fickian transport in geological formations as a continuous time random walk, *Rev. Geophys.*, *44*, RG2003.

Bertin, H., M. Panfilov, and M. Quintard (2000), Two Types of Transient Phenomena and Full Relaxation Macroscale Model for Single Phase Flow through Double Porosity Media, *Transport in Porous Media*, pp. 73–96.

Besbes, M., and G. De Marsily (1984), From infiltration to recharge: use of a parametric transfer function, *Journal of Hydrology*, *74*, 271–293.

Bodin, J., G. Porel, and F. Delay (2003), Simulation of solute transport in discrete fracture networks using the time domain random walk method, *Earth Planet. Sci. Lett.*, *208*, 297–304.

Bouchaud, J.-P., and A. Georges (1990), Anomalous diffusion in disordered media: Statistical mechanisms, models and physical applications, *Physics Reports*, *195*(4-5), 127–293, doi:10.1016/0370-1573(90)90099-N.

Box, G. E. P., and G. M. Jenkins (1970), *Time Series Analysis, Forecasting and Control*, Holden-Day, San Francisco.

Carrera, J. (1993), An overview of uncertainties in modelling groundwater solute transport, *Journal of Contaminant Hydrology*, *13*(1-4), 23–48, doi:10.1016/0169-7722(93)90049-X.

Carrera, J., X. Sánchez-Vila, I. Benet, A. Medina, G. Galarza, and J. Guimerà (1998), On matrix diffusion: formulations, solution methods and qualitative effects, *Hydrogeology Journal*, *6*(1), 178–190, doi:10.1007/s100400050143.

Carslaw, H. S., and J. C. Jaeger (1947), *Conduction of Heat in Solids*, vol. 36, 386 pp., Oxford University Press, Oxford, doi:10.2307/3610347.

Chechkin, A. V., R. Gorenflo, and I. M. Sokolov (2005), Fractional diffusion in inhomogeneous media, *J. Phys. A*, *38*, L679–L684.

Codling, E. a., M. J. Plank, and S. Benhamou (2008), Random walk models in biology., *Journal of the Royal Society, Interface / the Royal Society*, *5*(25), 813–34, doi:10.1098/rsif.2008.0014.

Condamin, S., O. Bénichou, V. Tejedor, R. Voituriez, and J. Klafter (2007), First-passage times in complex scale-invariant media., *Nature*, *450*(7166), 77–80, doi:10.1038/nature06201.

Cortis, A. (2004), Numerical simulation of non-Fickian transport in geological formations with multiple-scale heterogeneities, *Water Resources Research*, *40*(4), doi:10.1029/2003WR002750.

Cortis, A., and C. Knudby (2006), A continuous time random walk approach to transient flow in heterogeneous porous media, *Water Resources Research*, *42*(10), 1–5, doi:10.1029/2006WR005227.

Crank, J. (1975), *The Mathematics of Diffusion*, Oxford University Press.

Dagan, G. (1993), Higher-order correction of effective permeability of heterogeneous isotropic formations of lognormal conductivity distribution, *Transport in Porous Media*, *12*(3), 279–290, doi:10.1007/BF00624462.

de Dreuzy, J.-R., P. Davy, J. Erhel, and J. de Brémond dâĂŹArs (2004), Anomalous diffusion exponents in continuous two-dimensional multifractal media, *Physical Review E*, *70*(1), 1–6, doi:10.1103/PhysRevE.70.016306.

de Dreuzy, J.-R., P. de Boiry, G. Pichot, and P. Davy (2010), Use of power averaging for quantifying the influence of structure organization on permeability upscaling in on-lattice networks under mean parallel flow, *Water Resources Research*, *46*(8), 1–11, doi:10.1029/2009WR008769.

Dean, D. S., I. T. Drummond, and R. R. Horgan (2004), Effective diffusion constant in a two-dimensional medium of charged point scatterers, *Journal of Physics A: Mathematical and General*, *37*(6), 2039–2046, doi:10.1088/0305-4470/37/6/005.

Dean, D. S., I. T. Drummond, and R. R. Horgan (2007), Effective transport properties for diffusion in random media, *Journal of Statistical Mechanics*, (07), P07,013, doi:10.1088/1742-5468/2007/07/P07013.

Delay, F., and J. Bodin (2001), Time domain random walk method to simulate transport by advection-diffusion and matrix diffusion in fracture networks, *Geophys. Res. Lett.*, *28*, 4051–4054.

Delay, F., G. Porel, and P. Sardini (2002), Modelling diffusion in a heterogeneous rock matrix with a time-domain {L}agrangian method and an inversion procedure, *C. R. Geoscience*, *334*, 967–973.

Delay, F., P. Ackerer, and C. Danquigny (2005), Simulating Solute Transport in Porous or Fractured Formations Using Random Walk Particle Tracking, *Vadose Zone Journal*, *4*(2), 360, doi: 10.2136/vzj2004.0125.

Delay, F., A. Kaczmaryk, and P. Ackerer (2008), Inversion of a {L}agrangian time domain random walk {(TDRW)} approach to one-dimensional transport by derivation of the analytical sensitivities to parameters, *Adv. Water Resour.*, *31*, 484–502.

Delleur, J. W. (1999), *The Handbook of Groundwater Engineering*, 992 pp., CRC Press.

Dentz, M., and B. Berkowitz (2003), Transport behavior of a passive solute in continuous time random walks and multirate mass transfer, *Water Resources Research*, *39*(5), 1–20, doi:10.1029/2001WR001163.

Dentz, M., and D. M. Tartakovsky (2006), Delay mechanisms of non-Fickian transport in heterogeneous media, *Geophysical Research Letters*, *33*(16), 1–5, doi:10.1029/2006GL027054.

Dentz, M., A. Cortis, H. Scher, and B. Berkowitz (2004), Time behavior of solute transport in heterogeneous media: transition from anomalous to normal transport, *Adv. Water Resour.*, *27*(2), 155–173.

Dentz, M., P. Gouze, A. Russian, J. Dweik, and F. Delay (2012), Diffusion and trapping in heterogeneous media: An inhomogeneous continuous time random walk approach, *Advances in Water Resources*, *49*, 13–22, doi:10.1016/j.advwatres.2012.07.015.

Diersch, H.-J., and O. Kolditz (2002), Variable-density flow and transport in porous media: approaches and challenges, *Advances in Water Resources*, *25*(8-12), 899–944, doi:10.1016/S0309-1708(02)00063-5.

Drummond, I. T., and R. R. Hogan (1987), The effective permeability of a random medium, *J. Phys. A: Math. Gen.*, *20*, 4661–4672.

Duffy, C. J. (2010), Dynamical modelling of concentration-age-discharge in watersheds, *Hydrological Processes*, *24*(12), 1711–1718, doi:10.1002/hyp.7691.

Duffy, C. J., and J. Cusumano (1998), A low-dimensional model for concentration-discharge dynamics in groundwater stream systems, *Water Resources Research*, *34*(9), 2235, doi:10.1029/98WR01705.

Duffy, C. J., and L. W. Gelhar (1985), A Frequency Domain Approach to Water Quality Modeling in Groundwater: Theory, *Water Resources*, *21*(8), 1175–1184.

Duffy, C. J., and D.-H. Lee (1992), Base flow response from nonpoint source contamination: Simulated spatial variability in source, structure, and initial condition, *Water Resour. Res.*, *28*(3), 905.

Dvoretskaya, O., and P. Kondratenko (2009), Anomalous transport regimes and asymptotic concentration distributions in the presence of advection and diffusion on a comb structure, *Physical Review E*, *79*(4), 1–6, doi:10.1103/PhysRevE.79.041128.

Dykhne, a. M., I. L. Dranikov, P. S. Kondratenko, and a. V. Popov (2005), Anomalous diffusion in regular heterogeneous media, *Journal of Hydraulic Research*, *43*(2), 213–216, doi: 10.1080/00221686.2005.9641239.

Dykhuizen, C. R. (1987), Transport of Solutes Through Unsaturated Fractured Media, *Water Resources*, *21*(12), 1531–1539.

Dykhuizen, R. C. (1990), New coupling term for dual porosity models, *Water Resources Research*, *26*(2), 351–356, doi:10.1016/0148-9062(90)92852-6.

Erskine, A. D., and A. Papaioannou (1997), The use of aquifer response rate in the assessment of groundwater resources, *Journal of Hydrology*, *202*, 373–391.

Fiori, a., D. Russo, and M. Di Lazzaro (2009), Stochastic analysis of transport in hillslopes: Travel time distribution and source zone dispersion, *Water Resources Research*, *45*(8), W08,435, doi: 10.1029/2008WR007668.

Fourier, J. B. J. (1822), *Theorie Analytique de la Chaleur*, Paris.

Freeze, R. A. (1975), A stochastic-conceptual analysis of one-dimensional groundwater flow in nonuniform homogeneous media, *Water Resources Research*, *11*(5), 725–741.

Gelhar, L. (1974), Stochastic Analysis of Phreatic Aquifers, *Water Resources Research*, *10*(3), 539–545.

Gelhar, L. W., and J. L. Wilson (1974), Ground-Water Quality Modeling, *Ground Water*, *12*(6), 399–408.

Gelhar, L. W., C. Welty, and K. R. Rehfeldt (1992), A Critical Rewiev of Data on Field-Scale Dispersion in Aquifers, *Water Resour. Res.*, *28*(7), 1955–1974.

Gouze, P., T. Le Borgne, R. Leprovost, G. Lods, T. Poidras, and P. Pezard (2008a), Non-Fickian dispersion in porous media: 1. Multiscale measurements using single-well injection withdrawal tracer tests, *Water Resources Research*, *44*(6), 1–15, doi:10.1029/2007WR006278.

Gouze, P., Y. Melean, T. Le Borgne, M. Dentz, and J. Carrera (2008b), Non-Fickian dispersion in porous media explained by heterogeneous microscale matrix diffusion, *Water Resources Research*, *44*(11), 1–19, doi:10.1029/2007WR006690.

Goychuk, I. (2004), Quantum dynamics with non-{M}arkovian fluctuating parameters, *Phys. Rev. E*, *70*, 16,109.

Gutjahr, A., L. W. Gelhar, B. Adel, and J. R. MacMillan (1978), Stochastic Analysis of Spatial Variability in Subsurface Flows. Evaluation and Application, *Water Resources Research*, *14*(5).

Haggerty, R., and S. M. Gorelick (1995), Multiple-rate mass transfer for modeling diffusion and surface reactions in media with pore-scale heterogeneity, *Water Resources Research*, *31*(10), 2383–2400.

Haggerty, R., S. A. McKenna, and L. C. Meigs (2000), On the late time behavior of tracer test breakthrough curves, *Water Resour. Res.*, *36*(12), 3467–3479.

Haggerty, R., C. F. Harvey, C. von Schwerin, and L. C. Meigs (2004), What controls the apparent timescale of solute mass transfer in aquifers and soils? {A} comparison of experimental results, *Water Resour. Res.*, *40*, W01,510.

Harvey, C. F., and S. M. Gorelick (1995), Temporal moment-generating equations: Modeling transport and mass transfer in heterogeneous aquifers, *Water Resources*, *31*(8), 1895–1911.

Haus, J. W., and K. W. Kehr (1987), Diffusion in regular and disordered lattices, *Phys. Rep.*, *150*, 263–406.

Havlin, S., and D. Ben-Avraham (2002a), Diffusion in disordered media, *Advances in Physics*, *51*(1), 187–292, doi:10.1080/00018730110116353.

Havlin, S., and D. Ben-Avraham (2002b), Diffusion in disordered media, *Adv. Phys.*, *51*, 187–292.

Hollenbeck, K. J. (1998), INVLAP.M: A matlab function for numerical inversion of Laplace transforms by the Hoog algorithm.

Hu, X., and J. H. Cushman (1994), Nonequilibrium statistical mechanical derivation of a noniocal Darcy' s Law for unsaturated / saturated flow, *Stochastic Hydrology and Hydraulics*, *8*, 109–116.

Hughes, B. D. (1995), *Random Wlaks and Random Environments*, 631 pp., Clarendom Press, Oxford.

Hurst, H. E. (1951), *Long Term Storage Capacity of Reservoirs*, 770–799 pp., American Society of Civil Engineers, 119.

Indelman, P., and B. Abramovich (1994), nonlocal properties of nonuniform averaged flows in heterogeneous media, *Water Resources Research*, *30*(12), 3385–3393.

Indelman, P., and Y. Rubin (1996), Average flow in heterogeneous media of trending hydraulic conductivity, *Journal of Hydrology*, *183*, 57–68.

Iomin, A. (2011), Subdiffusion on a Fractal Comb, *Phys. Rev. E*, *052106*, 1–4.

James, S. C., and C. V. Chrysikolpoulos (2001), An efficient particle tracking equation with a specified spatial step for the solution of the diffusion equation, *Chem. Eng. Sci.*, *56*, 6535ï£¡6543.

Jiménez-Martínez, J., L. Longuevergne, T. L. Borgne, P. Davy, A. Russian, and O. Bour (2012), A frequency domain analysis to characterize heterogeneity and recharge mechanisms in fractured crystalline-rock aquifers, *Water Resour. Res.*

Juki, D., and V. Denijuki (2004), A frequency domain approach to groundwater recharge estimation in karst, *Journal of Hydrology*, *289*(1-4), 95–110, doi:10.1016/j.jhydrol.2003.11.005.

Kantelhardt, J. W., D. Rybski, S. a. Zschiegner, P. Braun, E. Koscielny-Bunde, V. Livina, S. Havlin, and A. Bunde (2003), Multifractality of river runoff and precipitation: comparison of fluctuation analysis and wavelet methods, *Physica A: Statistical Mechanics and its Applications*, *330*(1-2), 240–245, doi:10.1016/j.physa.2003.08.019.

Kantelhardt, J. W., E. Koscielny-Bunde, D. Rybski, P. Braun, A. Bunde, and S. Havlin (2006), Long-term persistence and multifractality of precipitation and river runoff records, *Journal of Geophysical Research*, *111*(D1), 1–13, doi:10.1029/2005JD005881.

Kaviany, M. (1995), *Heat transfer in porous media*, 2 ed., University of Michigan, New York.

Keller, J. B. (2001), Flow in Random Porous Media, *Transport in Porous Media*, *43*, 395–406.

Kenkre, V. M., E. W. Montroll, and M. F. Shlesinger (1973), Generalized Master Equations for Continuous-Time Random Walks, *J. Stat. Phys.*, *9*(1), 45–50.

King, P. R. (1987), The use of field theoretic methods for the study of flow in a heterogeneous porous medium, *J.Phys. A: Math*, *20*, 3935–3947.

Kinzelbach, W. (1987), The random walk method in pollutant transport simulation, in *Advances in analytical and numerical groundwater flow and quality modelling*, *C*, vol. 224, edited by E. Custodio, p. 227ï£¡246, NATO ASI.

Kitanidis, P. K. (1990), Kitanidis-flow.pdf, *Water Resources Research*, *26*(6), 1197–1208.

Koscielny-Bunde, E., J. W. Kantelhardt, P. Braun, A. Bunde, and S. Havlin (2006), Long-term persistence and multifractality of river runoff records: Detrended fluctuation studies, *Journal of Hydrology*, *322*(1-4), 120–137, doi:10.1016/j.jhydrol.2005.03.004.

Labat, D., A. Mangin, and R. Ababou (2002), Rainfall-runoff relations for karstic springs: multifractal analyses, *Journal of Hydrology*, *256*, 176–195.

Labat, D., J. Masbou, E. Beaulieu, and a. Mangin (2011), Scaling behavior of the fluctuations in stream flow at the outlet of karstic watersheds, France, *Journal of Hydrology*, *410*(3-4), 162–168, doi:10.1016/j.jhydrol.2011.09.010.

Law, J. (1944), A Statistical Approach to the Interstitial Heterogeneity of Sand Reservoirs, *Americal Institute of Mining, Metallurgical, and Petroleum Engineers, Technical Publication*, *7*(3), 202–221.

Le Borgne, T. (2004), Equivalent mean flow models for fractured aquifers: Insights from a pumping tests scaling interpretation, *Water Resources Research*, *40*(3), 1–12, doi:10.1029/2003WR002436.

Le Borgne, T., and P. Gouze (2008), Non-Fickian dispersion in porous media: 2. Model validation from measurements at different scales, *Water Resources Research*, *44*(6), 1–10, doi:10.1029/2007WR006279.

Lewandowska, J. (2004), Modélisation de l'écoulement dans les sols non saturés avec inclusions très perméables, *Comptes Rendus Mecanique*, *332*(1), 91–96, doi:10.1016/j.crme.2003.10.012.

Little, M. A., and J. P. Bloomfield (2010), Robust evidence for random fractal scaling of groundwater levels in unconfined aquifers, *Journal of Hydrology*, *393*(3-4), 362–369, doi:10.1016/j.jhydrol.2010.08.031.

Livina, V., Z. Kizner, P. Braun, T. Molnar, a. Bunde, and S. Havlin (2007), Temporal scaling comparison of real hydrological data and model runoff records, *Journal of Hydrology*, *336*(1-2), 186–198, doi:10.1016/j.jhydrol.2007.01.014.

Lods, G. (2004), WTFM, software for well test analysis in fractured media combining fractional flow with double porosity and leakance approaches?, *Computers & Geosciences*, *30*(9-10), 937–947, doi:10.1016/j.cageo.2004.06.003.

Lods, G., and P. Gouze (2008), A generalized solution for transient radial flow in hierarchical multifractal fractured aquifers, *Water Resources Research*, *44*(12), 1–17, doi:10.1029/2008WR007125.

Manga, M. (1999), On the timescales characterizing groundwater discharge at springs, *Journal of Hydrology*, *219*(1-2), 56–69, doi:10.1016/S0022-1694(99)00044-X.

Margolin, G., M. Dentz, and B. Berkowitz (2003), Continuous time random walk and multirate mass transfer modeling of sorption, *Chem. Phys.*, *295*, 71–80.

Matheron (1967), Composition des Permeabilites en Milieu Poreux Heterogene Methode de Schwydler et Regles de Ponderation, *Revue de l'institut Française du Pétrol*, *XXII*(3), 443–466.

McCarthy, J. (1993), Continuous-time random walks on random media, *J. Phys. A: Math. Gen.*, *26*, 2495–2503.

Metz, B., D. Ogunlade, H. de Coninck, M. Loos, and L. Meyer (2005), Carbon Dioxide Capture and Storage, *Tech. rep.*, Intergovernmental Panel on Climate Change, Cambridge University Press.

Metzler, R., and J. Klafter (2000), The Random Walk's Guide to Anomalous Diffusion: a Fractional Dynamic Approach, *Physics Reports*, *339*, 1–77.

Molenat, J., P. Davy, C. Gascuelodoux, and P. Durand (1999), Study of three subsurface hydrologic systems based on spectral and cross-spectral analysis of time series, *Journal of Hydrology*, *222*(1-4), 152–164, doi:10.1016/S0022-1694(99)00107-9.

Molenat, J., P. Davy, and P. Durand (2000), Spectral and Cross-Spectral Analysis of Three Hydrological Systems, *Phys. Chem. Earth (B)*, *25*(4), 391–397.

Montroll, E. W., and G. H. Weiss (1965), Random Walks on Lattices, 2., *J. Math. Phys.*, *6*(2), 167.

Neuman, S. P. (1990), Universal Scaling of Hydraulic Conductivities and Dispersivities in Geologic Media, *Water Resources Research*, *26*, 1749–1758.

Neuweiler, I., S. Attinger, and W. Kinzelbach (2001), Macrodispersion in a radially diverging flow field with finite Peclet Numbers: 1. Perturbation theory approach, *Water Resources Research*, *37*(3), 481, doi:10.1029/2000WR900313.

Noetinger, B. (1994), The effective permeability of a heterogeneous porous medium, *Transport in Porous Media*, *15*(2), 99–127, doi:10.1007/BF00625512.

Noetinger, B., and T. Estebenet (2000), Up-Scaling of Double Porosity Fractured Media Using Continuous-Time Random Walks Methods, *Transp. Porous Media*, *39*, 315–337.

Noetinger, B.Estebenet, T., and M. Quintard (2001), Up-scaling Flow in Fractured Media : Equivalence Between the Large Scale Averaging Theory and the Continuous Time Random Walk Method, *Transport in Porous Media*, *43*, 581–596.

Pabitra, S. (2004), Time-dependent diffusion coefficient as a probe of geometry, *Concepts in Magnetic Resonance Part A*, *23A*, 1–21.

Patankar, S. H. (1980), *Numerical Heat Transfer and Fluid Flow*, Taylor and Francis.

Peszynska, M., and R. E. Showalter (2007), Multiscale elliptic-parabolic systems for flow and transport Âť, *Electronic Journal of Differential Equations*,, *2007*(147), 1–30.

Peters, R. R., and E. A. Klavetter (1988), A Continuum Model for Water Movement in an Unsaturated Fractured Rock Mass, *Water Resources Research*, *24*(3), 416–430.

Reimus, P. W., and S. C. James (2002), Determining the random time step in a constant spatial step particle tracking algorithm, *Chem. Eng. Sci.*, *57*(21), 4429–4434, doi:10.1016/S0009-2509(02)00396-2.

Renard, P., and G. de Marsily (1997), Calculating equivalent permeability: a review, *Advances in Water Resources*, *20*(5-6), 253–278.

Risken, H. (1989), *The Fokker-Planck Equation*, vol. 98, 1–472 pp., Springer, doi: 10.1521/prev.2011.98.3.419.

Risken, H. (1996), *The Fokker-Planck Equation*, Springer Heidelberg New York.

Rovey, C. W., and D. S. Cherkauer (1995), Scale Dependency of Hydraulic Conductivity Measurements, *Ground water*, *33*, 769–780.

Russian, A., M. Dentz, and J. Carrera (2012), Sub-diffusive Anomalous Scaling Modeled by Double- and Multi-Continuum Models, *Unpublished*.

Sanchez Vila, X., J. Carrera, and J. Girardi (1996), Scale effects in transmissivity, *Journal of Hydrology*, *183*, 1–22, doi:10.1016/S0022-1694(96)80031-X.

Sanchez-Villa, X., A. Guadagnini, and J. Carrera (2006), Representative hydraulic conductivities in saturated groundwater flow, *Rev. Geophys.*, *44*(RG3002).

Scanlon, B. R., R. W. Healy, and P. G. Cook (2002), Choosing appropriate techniques for quantifying groundwater recharge, *Hydrogeology Journal*, *10*, 18–39, doi:10.1007/s10040-0010176-2.

Scher, H., and M. Lax (1973), Stochastic transport in a disordered solid. {I}. {T}heory, *Phys. Rev. B*, *7*(1), 4491–4502.

Schulze-Makuch, D., Douglas, A. Carlson, Douglas, S. Cherkauer, Malik, P. (1999), Scale Dependency of Hydraulic Conductivity in Heterogeneous Media, *Ground Water*, *37*(6), 904–919.

Schumer, R. (2003), Multiscaling fractional advection-dispersion equations and their solutions, *Water Resources Research*, *39*(1), 1022, doi:10.1029/2001WR001229.

Tartakovsky, D. M., and S. P. Neuman (1998a), Transient flow in bounded randomly heterogeneous domains 2. Localization of conditional mean equations and temporal nonlocality effects, *Water Resources Research*, *34*(1), 13–20.

Tartakovsky, D. M., and S. P. Neuman (1998b), Transient flow in bounded randomly heterogeneous domains 1 . Exact conditional moment equations and recursive approximations, *Water Resources Research*, *34*(1), 1–12.

Teodorovich, E. (2002), An improved perturbation theory method for describing the effective permeability of a randomly heterogeneous medium, *J. Appl. Maths Mechs*, *66*(3), 439–446, doi: 10.1016/S0021-8928(02)00053-9.

Tessier, Y., D. Schertzer, P. Hubert, and S. Pecknoldl (1996), Multifractal analysis and modeling of rainfall and river flows and scaling, causal transfer functions, *Journal of Geophysical Research*, *101*(D21), 26,427–26,440.

Turcotte, D. L., and L. Greene (1993), A scale-invariant approach to flood-frequency analysis, *Stochastic Hydrology and Hydraulics*, *7*(1), 33–40, doi:10.1007/BF01581565.

Warren, J. E., and P. Root (1963), The Behavior of Naturally Fractured Reservoirs, *The Soc. Petrol. Eng. J.*, *3*(3), 245–255.

Weiss, G. H. (1994), *Random Materials and Processes*, north-holl ed., Elsevier Science, Amsterdam, London, New York, Tokyo.

Wiener, N. (1949), *Extrapolation, Interpolation, and Smoothing of Stationary Time Series*, wiley ed., MIT Press, New York.

Willmann, M., J. Carrera, and X. Sanchez-Vila (2008), Transport upscaling in heterogeneous aquifers : What physical parameters control memory functions ?, *Water Resources Research*, *44*(12), 1–45.

Wittebroodt, C., S. Savoye, and P. Gouze (2008), Influence of initial iodide concentration on the iodide uptake by the argillite of Tournemire, *Physics and Chemistry of the Earth*, *33(14-16)*, 943–948.

Zhang, D., and A. Y. Sun (2000), Stochastic analysis of transient saturated flow through heterogeneous fractured porous media: A double-permeability approach, *Water Resources Research*, *36*(4), 865, doi: 10.1029/2000WR900003.

Zhang, Y.-K. (2004), Temporal scaling of hydraulic head and river base flow and its implication for groundwater recharge, *Water Resources Research*, *40*(3), 1–9, doi:10.1029/2003WR002094.

Zhang, Y.-K. (2005), Temporal scaling of hydraulic head fluctuations: Nonstationary spectral analyses and numerical simulations, *Water Resources Research*, *41*(7), 1–10, doi:10.1029/2004WR003797.

Zhang, Y.-K., and X. Yang (2010), Effects of variations of river stage and hydraulic conductivity on temporal scaling of groundwater levels: numerical simulations, *Stochastic Environmental Research and Risk Assessment*, *24*(7), 1043–1052, doi:10.1007/s00477-010-0437-5.

Zumofen, G., and J. Klafter (1993), Scale-invariant motion in intermittent chaotic systems, *Phys. Rev. E*, *47*, 851–863.